Modelling of Unsteady Aerodynamic Characteristics for Aircraft Dynamics Applications at High Incidence Flight.

by

Nikolay Abramov

Faculty of Computing Science and Engineering,
De Montfort University,
Leicester.

A dissertation submited
in partial fulfillment for the
degree of Doctor of Philosophy
at De Montfort University.

June 2005

Abstract

A traditional representation of aerodynamic characteristics based on the concept of aerodynamic derivatives fails to be accurate at high angles of attack due to significant dynamic effects generated from separated and vortical flow. As the possibility of performing controlled flight at high angles of attack has already become a common requirement for modern combat aircraft, the problem of an adequate model for aerodynamic loads at high incidences is the issue of the day.

This thesis presents a phenomenological approach to modelling of unsteady aerodynamic characteristics at high angles of attack. In this approach aerodynamic characteristics are considered as a combination of two components having different characteristic time scales which describe the contribution to the total aerodynamic load from the different flow structures. It is assumed that all dynamic properties of the flow are amassed in the "slow" component. To describe its behaviour specially designed nonlinear differential equations are used. Depending on the parameters, this model can reproduce both "weak" and "strong" nonlinear effects including static hysteresis. A special identification technique has been developed for the estimation of the model parameters using dynamic wind tunnel test data.

To verify the proposed technique, mathematical models of unsteady aerodynamic loads of a 65^o delta wing and a high aspect ratio rectangular wing which has hysteresis in the static dependence of its normal force have been developed. These models demonstrate good quantitative and qualitative coincidence with the experimental data.

The limitations of a conventional aerodynamic model based on the aerodynamic derivatives concept are analyzed considering the longitudinal motion of a hypothetical aircraft with the 65^o delta wing and thrust vectoring control. A dynamic unsteady aerodynamic model approximating the vortical and separated flow time lag effects is considered along with a conventional aerodynamic model and their impact on aircraft dynamics and control law design is discussed.

Acknowledgments

I would like to thank my first supervisor Professor Mikhail Goman and second supervisor Professor Gwynne Evans for the support and encouragement which they gave me during my work. Their guidance, constructive criticism, advice and discussions significantly helped me to accomplish this work. I am also thankful to Professor Hussein Zedan who sheltered me in STRL and provided an excellent academic environment.

The wind tunnel tests which furnished me with extremely valuable and important experimental data would not be possible without the facilities and expertise of the Central Aerohydrodynamic Institute (TsAGI, Russia). I would like to express my gratitude to the head of the unsteady aerodynamic division of TsAGI Dr. Alexander Khrabrov and his colleagues Dr. Konstantin Kolinko, Dr. Yuriy Vinogradov, Dr. Oleg Miatov and Mr. Anatoly Zhuk and all technical staff of the T-103 wind tunnel. I am grateful to them for their highly qualified work and tutorship during the tests.

I want also to express my thanks to Professor Jonathan Blackledge, who was my supervisor during the first year at DMU, Mr. Brian Foxon, Mr. Grahame Hudson, Ms. Charlotte Kitson and Mrs. Tracey Gosling from the International Research Office for their tremendous support of the collaborative programme between DMU and Russian universities. I deeply appreciate the financial support provided by DMU within this programme.

Special thanks should be tendered to Dr. Douglas Greenwell, Dr. Yoge Patel, Dr. Phill Smith, Mr. Nicholas Swain, Mr. Anton Gibbs and Mr. George Nichols from DERA/QinetiQ Ltd. My research work was a part of a seven years collaborative project between DERA/QinetiQ, TsAGI and DMU, and I am very indebted to DERA/QinetiQ for their encouragement and financial support.

I gratefully acknowledge support from my colleagues Dr. Andrew Khramtsovsky, Dr. Maria

Sidoriuk, Mr. Sergey Usoltsev and Mr. Eugene Kolesnikov with whom I have the honour of working in the Flight Dynamics and Control Department in TsAGI and to be a companions for almost ten years.

Finally I pay tribute to my Alma Mater, the Faculty of Aeromechanics in the Moscow Institute of Physics and Technology, which did open me the way to the world of Science and Aviation.

Nikolay Abramov
De Montfort University

June 2005

List of notations

α	Angle of attack, deg or rad
β	Sideslip angle, deg or rad
δ_k	Deflection of k-th control surface
ϕ	Roll angle, deg or rad
Φ	Cost function
ψ	Heading angle, deg or rad
θ	Pitch angle, deg or rad
ρ	Air dencity, kg/m^3
τ_i	Characteristic time constant
$\omega = \frac{2\pi f \bar{c}}{2V}$	Non-dimensional frequency of oscillations
b	Wing span, m
$\bar{c}$	Mean aerodynamic chord, m
C_D	Drag force coefficient
C_L	Lift coefficient
C_N	Normal force coefficient
C_Y	Side force coefficient
C_l	Rolling moment coefficient
C_m	Pitching moment coefficient
C_n	Yawing moment coefficient
$C_{i_{att}}$	Aerodynamic force/moment coefficient on attached flow conditions
$C_{i_{st}}$	Static dependence of i-th aerodynamic force/moment coefficient
$C_{i_{dyn}}$	Dynamic component of the mathematical model
f	Frequency of oscillations, Hz

g	Gravity acceleration, m/sec^2
H	Altitude, m
I_{XX}	X body-axis moment of inertia, kg m^2
k_i	Parameter of the model
l_T	Engine trust arm, m
M	Mach number
$\mathbf{p}$	Vector of unknown parameters of the model
p	X body-axis angular velocity component, rad/sec
$\bar{p} = \frac{pb}{2V}$	Non-dimensional X body-axis angular velocity component, rad/sec
q	Y body-axis angular velocity component, rad/sec
$\bar{q} = \frac{q\bar{c}}{2V}$	Non-dimensional Y body-axis angular velocity component, rad/sec
r	Z body-axis angular velocity component, rad/sec
$\bar{r} = \frac{rb}{2V}$	Non-dimensional Z body-axis angular velocity component, rad/sec
$Re = \frac{\rho V l}{\nu}$	Reynolds number
S	Wing arear, m^2
$Sh = \frac{l}{Vt}$	Strouhal number
t	Time, sec
$\bar{t} = \frac{2V}{\bar{c}}$	Non-dimensional time
T_{aft}	Normalized afterburning thrust
T_{max}	Normalized normal thrust
T_A	Maximum afterburning thrust, kgf
T_M	Maximum normal thrust, kgf
V	Velocity, m/s
$\mathbf{x}$	State vector
x_{cg}	Centre of gravity location
x_T	Throttle position, $[0, 2]$

Subscript

mod	Result of modelling
exp	Experimental result

Contents

1 Introduction 1

2 Experimental investigation of unsteady aerodynamic characteristics 9

2.1 Experimental setups for dynamic tests 10

2.1.1 Dynamic Plunge-Pitch-Roll rig in Virgina Polytechnic Institute . . . 10

2.1.2 Small amplitude forced oscillation rig in DRA 10

2.1.3 Rotary balance rig in DLR 10

2.1.4 ONERA-IMFL dynamic tests rigs 11

2.1.5 Pendulum support rig 11

2.1.6 TsAGI forced oscillation test rig 12

2.1.6.1 Configuration for small amplitude oscillations 12

2.1.6.2 The rig configuration for large amplitude oscillations 14

2.1.6.3 The rig configuration for static and slow sweep motion tests 15

2.2 Typical results of the dynamic tests 15

2.2.1 Motion frequency/amplitude effects 16

2.2.2 Slow sweep motion 16

2.2.3 Large amplitude motion 17

2.2.4 Free to roll motion 17

2.3 Summary 19

3 Review of unsteady aerodynamic modelling approaches 27

3.1 Aerodynamic derivative concept 27

3.2 Linear indicial functions 29

3.3 Nonlinear indicial functions 31
3.4 Fourier functional analysis 34
3.5 Volterra series 37
3.6 State-space representation 38
3.7 Discussion 42

4 Modelling of high incidence aerodynamic loads using dynamic systems 45
4.1 Aerodynamic loads partitioning 46
4.2 Linear model analysis 52
4.2.1 Oscillation frequency effect on the aerodynamic derivatives 52
4.2.2 Identification of the characteristic time scales 54
4.2.3 Identification of the attached flow parameters 54
4.3 Nonlinear model 57
4.3.1 Parameter identification technique 57
4.3.2 Analysis of mathematical model sensitivity to parameter variation . 60
4.3.3 Model validation 60
4.4 Comparison with alternative modelling techniques 61
4.5 Summary 63

5 Delta wing nonlinear unsteady aerodynamic models 65
5.1 Longitudinal aerodynamic characteristics of the 65^o delta wing 67
5.1.1 Normal force coefficient C_N 67
5.1.2 Pitch moment coefficient C_m 69
5.1.3 Comparison of the characteristic time constants for the normal force and pitch moment coefficients 76
5.2 Lateral aerodynamic characteristics of the 65^o delta wing 78
5.2.1 Rolling moment coefficient C_l 78
5.2.1.1 Identification of the linear model using small amplitude oscillatory data in yaw 81
5.2.1.2 Identification of the linear model using small amplitude oscillatory data in roll 82

5.2.1.3 Comparison of the models estimated using small amplitude oscillatory data in roll and yaw 86
5.2.1.4 Identification of the nonlinear model using large amplitude oscillatory data in yaw 87
5.3 Comparison with the conventional aerodynamic derivative model 92
5.4 Unsteady aerodynamic models for the 70^o delta wing 95
5.4.1 Normal force coefficient for pitch motion at constant sideslip. 95
5.4.2 Normal force and rolling moment coefficients for yaw motion at constant angle of attack. 96
5.5 Comparison of the characteristic time scales for different delta wings 98
5.6 Summary 102

6 Modelling of static aerodynamic hysteresis 103
6.1 Physical aspects of static aerodynamic hysteresis 103
6.2 Bifurcational model of static aerodynamic hysteresis 107
6.3 Design of the nonlinear dynamic system 111
6.3.1 Internal region of the static hysteresis loop 111
6.3.2 External region of the static hysteresis loop 112
6.4 Mathematical model of C_N for the high aspect ratio wing 113
6.5 Validation of identified aerodynamic model with static hysteresis 115
6.5.1 Quasi-steady motion 115
6.5.2 Large amplitude oscillatory motion 116
6.6 Summary 116

7 Aircraft dynamics with account of unsteady aerodynamics effects 119
7.1 Frequency dependence effect in the time domain 120
7.2 Longitudinal motion dynamics 122
7.2.1 Trim in horizontal flight 124
7.2.2 The open-loop system eigenvalues analysis 124
7.2.3 Stabilizing control law 125
7.2.4 Closed-loop system analysis 127
7.2.4.1 Eigenvalues analysis 127

7.2.4.2 Stability regions analysis 129
7.3 Summary 130

8 Aerodynamic model development tools **137**
8.1 ADDB - experimental data storage and processing tool 138
8.1.1 Program interface 140
8.1.2 Database objects 141
8.1.3 Experimental data processing 144
8.1.4 Data fusion tool 145
8.1.5 Electronic digitizer - DIGIT 145
8.1.6 Flight-test data processing 146
8.1.7 Linear regression tool 147
8.1.8 Automatic generation of an aerodynamic model 147
8.2 PIIMTM- dynamic system identification tool 148

9 Conclusions and suggestions for future research **149**
9.1 Summary 149
9.2 Suggestions for future research 150

A Linear regression technique **163**
A.1 Least squares estimates 163
A.2 Stepwise regression 165
A.3 Principal components regression 166

B Aerodynamic derivatives estimation **169**

C Example of dynamic system implementation in ADDB **171**

D Example of the model implementation in PII **173**

E Experimental and predicted aerodynamic responses **177**

Chapter 1

Introduction

The problem of aerodynamic modelling is one of the most important and difficult challenges in modern flight dynamics. An adequate description of the aerodynamic forces and moments acting on an airplane in an arbitrary motion is required in flight dynamics for many tasks such as analysis of aircraft stability and dynamic properties, control law design, flight simulation, etc. A reasonably accurate description of the unsteady aerodynamic loads even at high angles of attack with a complex flow structure can be reached by means of advanced computational methods. Since the direct application of these methods jointly with the equations of aircraft motion complicates the solution of flight dynamics problems considerably, simplified mathematical models of aerodynamic forces and moments are commonly used.

When elaborating the mathematical model two, somewhat contradictory requirements must be taken into account. At first, the model has to encompass as many phenomena as possible to provide reasonable accuracy. But on the other hand it should have a simple, easy to handle structure, which leaves the equations of motion in a form suitable for analytical consideration.

From the beginning of aviation the most accepted formulation of aerodynamic loads in motion equations was the so called aerodynamic derivative approach (see Chapter 3). The aerodynamic loads in this case are considered as functions of instantaneous values of aircraft incidence, angular rates, control surfaces deflection, etc. The assumption that the aerodynamic loads and aircraft motion are described by analytical functions allows

the aerodynamic forces and moments to be represented in the form of a Taylor series expansion along kinematic parameters and control functions, with the terms higher than linear normally neglected. Thus the corresponding first derivatives totally define increments in the aerodynamic loads in response to variation of kinematic parameters and deflection of control surfaces. Moreover, it was found that these derivatives, called the aerodynamic derivatives, are invariant for some range of variation of the parameters which allows a rather simple representation of aerodynamic loads at various flight conditions.

In the case of small perturbations near the trim point such a representation of aerodynamic loads makes possible numerous simplifications of the equations of motion. The most important ones are linearization and splitting the full system into subsystems describing the longitudinal and lateral/directional modes of motion. All the modes defined by these subsystems correspond to characteristic frequencies of a rigid body dynamics. As the classical theory of ordinary differential equations provides a large number of techniques for analysis of such systems a set of simple criteria and methods has been proposed for assessment of aircraft stability, dynamic properties, controllability, performance, etc on the basis of the aerodynamic derivatives.

There are two main approaches for determining the aerodynamic derivatives for flight dynamics applications. The first one is based on the application of computational methods using simplified aerodynamical codes (vortex lattice, panel methods, etc) and advanced CFD methods. The second approach relies on experimental tests in wind tunnels. In spite of significant progress in computational methods the experimental methods still remain the most reliable instrument in real engineering practice, especially for high angles of attack conditions. A long practice of using of the aerodynamic derivatives approach has proven its ability to describe aerodynamic loads rather accurately at normal flight regimes and during not very intensive manoeuvering.

The classical dynamics of atmospheric flight considers an aircraft as a rigid body with characteristic frequency of the motion $0.2 \ldots 1\,\mathrm{Hz}$. Under these conditions a prehistory of motion does not significantly affect aerodynamics and the quasi-steady model of aerodynamic loads turns out to be acceptable. Beside this case there is a classical unsteady aerodynamic theory dealing with the structural dynamics of an elastic aircraft. At high frequencies corresponding to structural elastic modes ($5 \ldots 20\,\mathrm{Hz}$) the aerodynamic loads

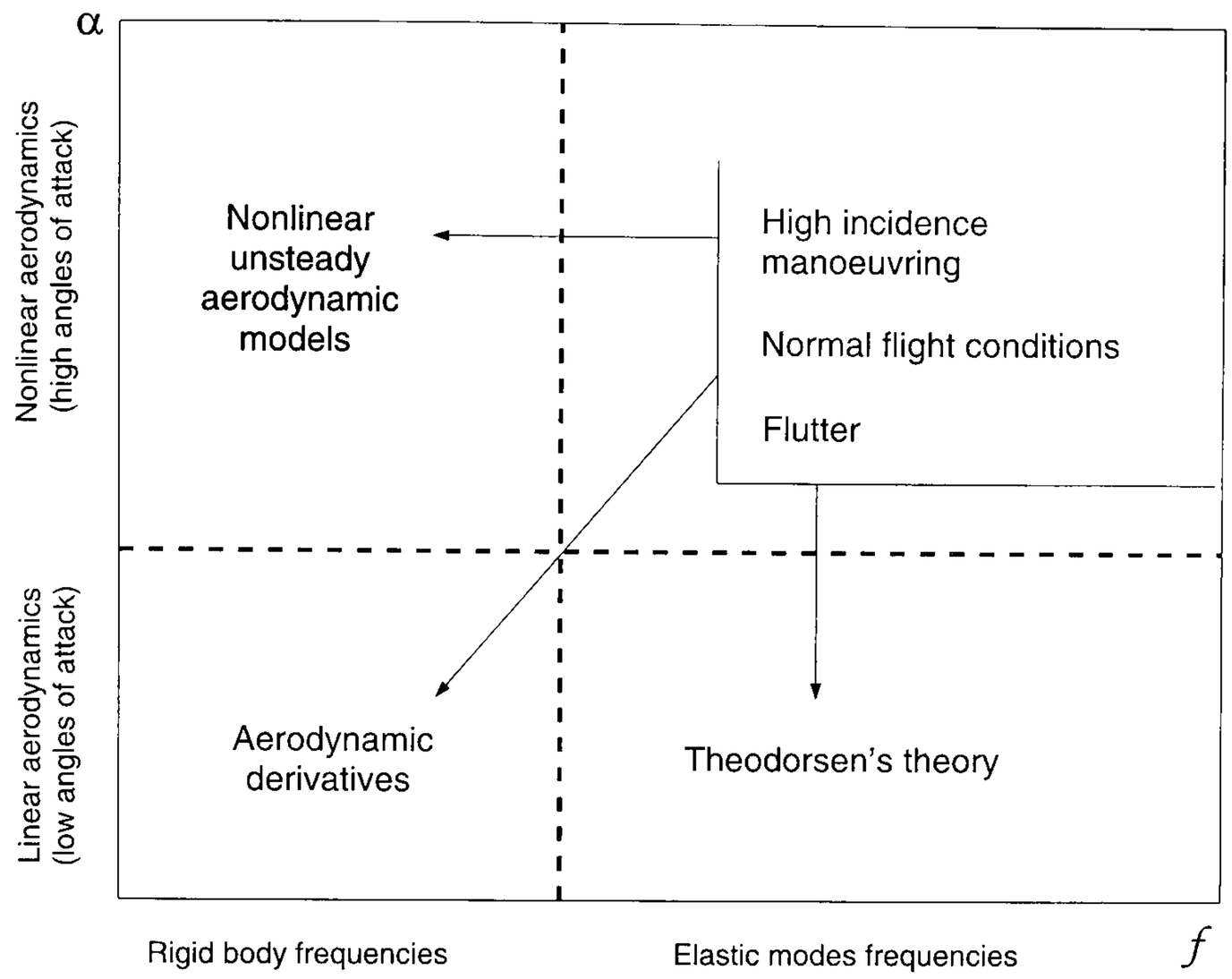

Figure 1.1: Approaches to unsteady aerodynamics modelling and their scopes of applicability.

become sensitive to prehistory of motion therefore an unsteady aerodynamic model is required. A typical application of such a kind of aerodynamic model is for the analysis of unstable flexural-and-torsional vibration of aircraft wing consoles in a stream known as flutter. The mathematical description of aerodynamic loads acting on an oscillating aerofoil was proposed by Theodorsen in 1930s within the framework of the potential flow and a thin aerofoil theory. Fundamental studies of an airfoil lift due to abrupt change of angle of attack (indicial response) and sharp-edge gust were performed by Wagner and Küssner respectively, [14]. These works underlay the classical approach to unsteady aerodynamic modelling at low angles of attack. The theoretical results obtained for the frequency dependence of the aerodynamic loads are widely used for simulation and analysis of flutter and gust alleviation problem. The scope of the discussed modelling techniques covering the linear aerodynamic region is schematically shown in Fig. 1.1 in the angle of attack vs. frequency plane.

During the last two decades a high emphasis has been placed on the problem of flight at high angles of attack. The ability to fly and perform controllable manoeuvres at critical

and post-critical incidences is highly requested for modern fighter aircraft. The so called super manoeuvrability in many cases enables an aircraft to get significant advantage over its rivals especially in a close air combat [20]. These advanced manoeuvres cannot be designed and simulated in the absence of an adequate aerodynamic model which is valid at high incidence flight (see the hatched region in Fig. 1.1).

The extension of the angle of attack range is also useful for common airplanes as this increases safety during manoeuvering at normal flight regimes. An adequate aerodynamic model in this case is required for design of the control system, which would suppress the onset of critical processes, for example, due to careless pilot behavior or action of strong gusts.

Due to the loss of lateral directional stability at a high angle of attack an aircraft encounters stall and enters spin motion. This happens due to changes in aerodynamic loads resulting from onset of complex vortical and separated flow. For example, the interaction between a rigid body motion and vortical flow results in complicated large amplitude oscillations in roll known as "wing rock". Again, an adequate mathematical model of aerodynamic loads is important for analysis, simulation and suppression of these critical flight regimes.

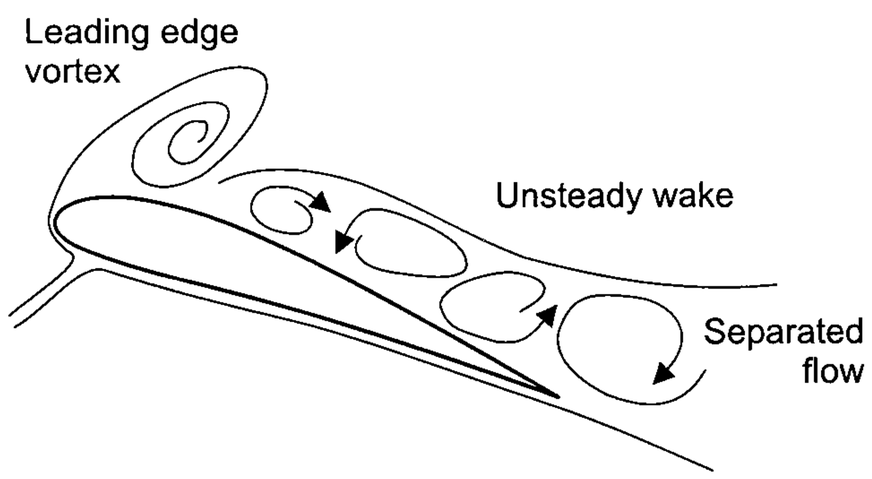

Figure 1.2: Flow around an aerofoil.

Experimental investigations of aerodynamic characteristics at high angles of attack presented in Chapter 2 demonstrate a complicated nonlinear behavior of aerodynamic loads resulting from flow separation processes over an aircraft. During aircraft manoeuvering the complex flow is subject to readjustment processes, which have their own dynamics leading to delays in aerodynamic responses to a variation of the kinematic parameters. Theodorsen's theory becomes inaccurate in these case as it was developed under the assumption of the attached potential flow without any account of vortical and separated flow effects.

The main problem peculiar to airplanes with a high aspect ratio wing at high angles of attack is separation of flow from the upper surface of the wing consoles (Fig. 1.2). Usually,

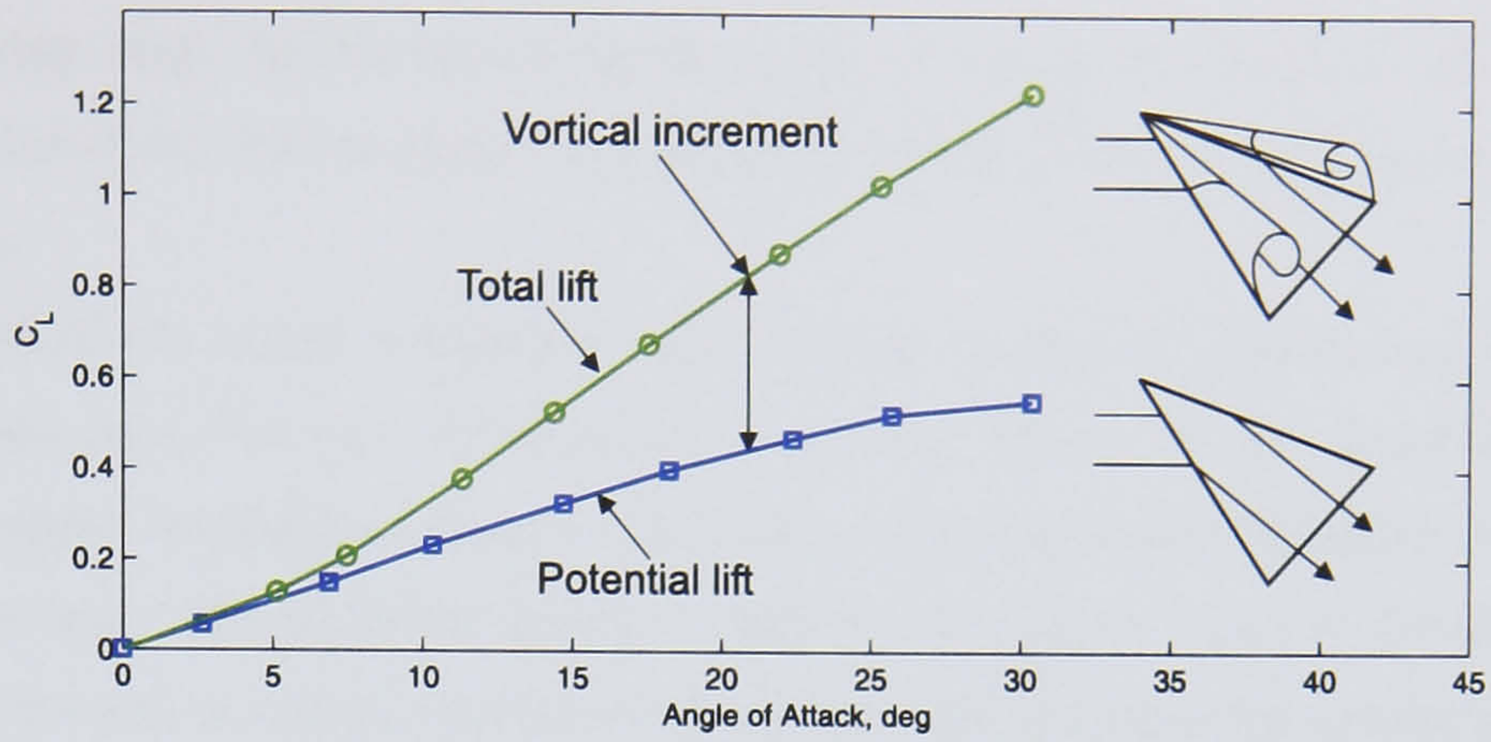

Figure 1.3: Vortex induced increment of the lift in case of delta wing.

when increasing incidence, the stalled flow starts from the trailing edge and develops towards the leading edge covering the entire wing surface. This results in a lift force decrement compared to attached (potential) flow conditions and is accompanied by dangerous aircraft behaviors.

In the case of swept wings, which are typical of modern manoeuvrable aircraft, separation starts at the leading edge and rolls up into a vortex sheet (Fig. 1.4). This results in a decrease of pressure over the upper surface leading to a significant increase of the lift in a nonlinear manner compared to potential flow case (Fig. 1.3). This effect can be calculated by applying modern CFD methods, but a simplified empirical method proposed by Polhamus [76] is widely used for the estimation of this vortical lift. The Polhamus method states that the extra normal force produced by a highly swept wing at high angles of attack is equal to the loss of the leading edge suction associated with the separated flow.

Figure 1.4: Vortical flow around the fighter at high angle of attack.

Starting with some angle of attack the vortices begin to break over the wing. A further increase in incidence leads to propagation of the vortex bursting points from the trailing

to the leading edges. In this case a significant loss of the vortex generated lift takes place and the value of this loss strongly depends on the extent of the development of the vortex breakdown.

Location of the vortex breakdown points during incidence variation was investigated in [39] based on a flow field visualization in a water tunnel. It was found that the location of vortex breakdown points in unsteady conditions essentially differ from that in static conditions. The same conclusion is valid for the instant value of the lift. Thus, a proper mathematical model of aerodynamic loads at high incidence has to take into account dynamic processes occurring in unsteady vortical or stalled flow and resulting in complex nonlinear behavior of aerodynamic characteristics.

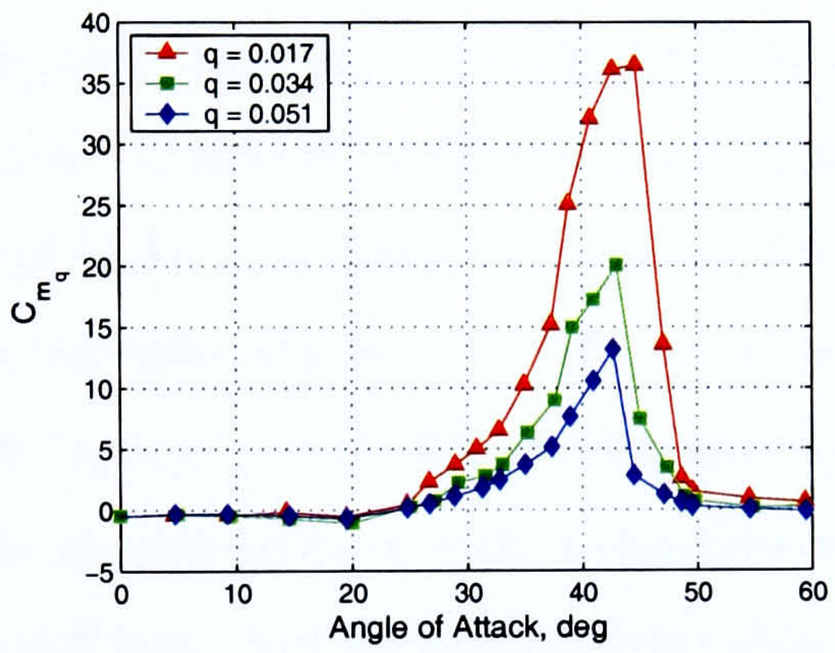

Figure 1.5: Typical dependence of aerodynamic derivatives on angle of attack and reduced frequencies of forced oscillations.

Analysis of the experimental aerodynamic derivatives provides a rather accurate evaluation of angles of attack where dynamic properties of flow around an aircraft are essential. Typical experimental dependence of the C_{m_q} derivative is presented in Fig. 1.5. One can see that at low angles of attack ($\alpha \leq 25^o$) the value of C_{m_q} remains the same at all frequencies of oscillations while at high angles of attack ($\alpha = 25^o \ldots 50^o$) there is a strong dependence on the reduced frequency, which disappears again at higher ($\alpha \geq 50^o$) angles of attack. The frequency dependency of aerodynamic derivatives significantly complicates the application of the conventional model in the time domain and may result in an incorrect prediction of dynamic characteristics (see Chapter 7). Although the model still may be used for small amplitude manoeuvers at high angles of attack provided that the frequency of oscillations is known, it totally fails for maneuvers with large amplitude (see Chapter 5).

The above mentioned problems associated with high incidence flight clearly demonstrate the need for a more adequate technique for the mathematical description of aerodynamic loads acting on intensively manoeuvering aircraft. Several main requirements can be for-

mulated for such a model. At first, it should reproduce aerodynamic responses to kinematic parameters variation as accurately as possible within the required flight envelope. Special emphasis should be made on a qualitative similarity to experimentally measured loads. The second requirement is that this model should inherit the conventional aerodynamic derivatives model at low incidence. In the end, the structure of the model should be consistent with the equations of motion in order to leave it suitable for classical methods of analysis and simulation.

Due to the complexity of the problem and the lack of effective theoretical solutions for high incidence flight conditions (see the hatched region in Fig. 1.1), the only way to develop the mathematical model is based on the analysis of the experimentally obtained aerodynamic responses. The identification of the model structure and the estimation of the model parameters require a comprehensive set of experimental data covering the whole range of flight conditions and motion parameters. Fortunately, a huge amount of wind tunnel test data obtained in TsAGI both in static and dynamic conditions have provided a reliable background for the development of such an empirical modelling technique.

The maintenance of such a database which normally can contain hundreds of lookup tables is a very time consuming and tiring work. Apparently, a special software is required for keeping, visualizing, correcting and processing all the experimental data used for the identification of the aerodynamic model. Such a software also has to be able to produce a standalone aerodynamic model in a form suitable for postprocessing and coupling with the other software for the flight simulation and analysis.

This thesis summarises the cycle of works devoted to unsteady aerodynamic modelling carried out in TsAGI and DMU under the support of QinetiQ Ltd, UK (former DERA). The personal contributions of the author to this project were to develop and validate an adequate technique for the unsteady aerodynamic modelling for high incidence flight conditions, to analyze the impact of this modelling approach on typical flight dynamics problems and to develop a software for facilitation of the aerodynamic modelling.

There are three logical parts in the thesis. The first one which includes Chapters 2, 3 and 8 gives a review of experimental investigations carried out both in TsAGI and worldwide, discusses the existing approaches and software developed by the author to support the process of aerodynamic modelling. The second part, which is the major one, describes

the developed technique for high incidence aerodynamic modelling using nonlinear dynamical systems (see Chapter 4) and a method for the identification of model parameters using wind tunnel experimental data. Chapter 5 presents the results of the practical application and validation of the proposed technique to the modelling of the longitudinal and lateral aerodynamic characteristics of the 65^o and 70^o delta wings. A comparison with the conventional aerodynamic derivatives model is performed to estimate at what conditions the application of the developed aerodynamic model is indispensable. The extension of the modelling technique to the case of static aerodynamic hysteresis taking into account the bifurcational character of the flow is given in Chapter 6. Finally, Chapter 7 is dedicated to a comparison of aircraft dynamic properties obtained using the conventional and the proposed unsteady aerodynamic models. This comparison is performed in terms of stability analysis of the open- and the closed-loop system, their transient processes and regions of attraction.

Chapter 2

Experimental investigation of unsteady aerodynamic characteristics

The ability to fly at high angles of attack and perform rapid and large amplitude manoeuvers is an essential requirement for modern fighters. Such manoeuvers result in a highly nonlinear dependence of aerodynamic characteristics on the kinematic parameters mainly due to complicated vortical and separated flow structures around the aircraft. In order to accurately describe aircraft dynamics at these regimes it is required to develop an adequate aerodynamic model. In spite of significant progress in CFD methods, experimental investigations are still the most reliable and accurate source of information about flow structures and aerodynamic loads. Therefore, a large number of experimental facilities have been developed in aeronautical research centers such as NASA (USA), DRA[1] (UK), DLR (Germany), ONERA (France), IAR (Canada), TsAGI (Russia), etc to support high incidence dynamic tests. These rigs are able to perform free and forced angular oscillations with small and large amplitudes at different frequencies, translational and rotary motion, etc. In order to outline the principles of dynamic testing in wind tunnels a brief review of several test rigs and typical results are presented in this chapter. Further information about the dynamic test facilities can be found in [2, 17, 1, 8, 37, 7]. The main emphasis is made on TsAGI's

[1] Currently QinetiQ

forced oscillation test rig because all data which are used in the thesis for aerodynamic modelling were obtained using this rig.

2.1 Experimental setups for dynamic tests

2.1.1 Dynamic Plunge-Pitch-Roll rig in Virgina Polytechnic Institute

The DyPPiR [25] installed in Virginia Tech's Stability Wind Tunnel is shown in Fig. 2.1. It combines three hydraulic actuators to plunge a model through a 1.5 m range vertically, pitch the model through $\pm 45^o$ range, and roll the model through a $\pm 140^o$ range. Maximum model weight is about 45 kg, plunge rate is up to 9 m/s and pitch rate is over 90 deg/s. The DyPPiR is digitally controlled by a personal computer, so it is capable of performing arbitrary pre-programmed manoeuvers. The model is mounted on an internal six-component strain-gauge balance, which in turn is mounted on one end of the sting.

2.1.2 Small amplitude forced oscillation rig in DRA

The oscillatory rig used in DRA [2] is shown in Fig. 2.2. The model is fixed on the rig which can be oscillated with five degrees of freedom, i.e. pitch, plunge, yaw, sideslip or roll. Forces acting on the model are measured by the strain gauge balance mounted in the sting. The flared downstream sting end is mounted on a swinging arm assembly which provides oscillatory harmonic motion. The amplitude of translational and rotational motion is about 50 mm and 2^o, respectively. The mean angle of attack may be set up to 42^o. The rig is mounted in the $4 \times 2.7\,m^2$ Low Speed (up to 90 m/s) Wind Tunnel at DRA, Bedford.

2.1.3 Rotary balance rig in DLR

The rotary balance rig mounted in the working section of the $3.25 \times 2.8\,m^2$ low speed wind tunnel in DLR, Braunschweig [2] is shown in Fig. 2.3. The pitch angle may be set from 10^o to 90^o and remotely controlled within 30^o range. The experiment can be conducted at Reynolds numbers up to 5.5×10^6 per meter at a rate of rotation up to 300 rpm in either clockwise or counterclockwise directions. The rate is kept constant by an electro-hydraulic control system. Due to the horizontal orientation of the rotation axis the model is subject

to periodic gravity loads superimposed on the steady aerodynamic and inertia loads.

2.1.4 ONERA-IMFL dynamic tests rigs

The oscillatory test setup used in France [2] is shown in Fig. 2.4. It allows kinematic representation of the Euler degrees of freedom. The heading angle ψ and roll angle ϕ are fixed during the test while the pitch angle θ is changing in time according to a specified programme such as pitch oscillations, plunging motion or any arbitrary manoeuver meeting the rig constraints. The following angles may be achieved: $\psi \in [-20^o, 15^o]$, $\phi \in [-180^o, 180^o]$ $\theta \in [-90^o, 100^o]$ $|\dot{\theta}| \in 500\,\mathrm{deg/s}$ and $|\ddot{\theta}| \in 5000\,\mathrm{deg/sec^2}$. The system is mounted in a 2.4 m diameter horizontal wind tunnel providing a flow speed up to 50 m/s.

The rotary balance (Fig. 2.5) used in ONERA is installed in the vertical wind tunnel that makes possible direct simulation of developed steady spin. The advantage of this approach is elimination of variable mechanical loads due to gravity which occurs in horizontally oriented balances.

2.1.5 Pendulum support rig

The above mentioned experimental rigs are mainly able to perform only specific type of a single degree of freedom motion due to kinematic features or preprogrammed motion. Although dynamic rigs are designed to meet real flight conditions such as characteristic frequencies of oscillations or steady spin rotation rates they are unable in many cases to reproduce free flight effects. For example, due to the immobility of the aircraft center of mass many rigs are unable to separate effects of angular and translational motion on aerodynamic derivatives. Known attempts of development of multiple degree of freedom rigs resulted in complicated and very expensive facilities [1].

A novel low-cost approach to dynamic wind tunnel testing proposed in [36] has been recently implemented in the University of Bristol, UK [64]. The movable aircraft model is suspended in a wind tunnel on a pendulum strut providing three angular and two translational degrees of freedom (Fig. 2.6). The model is controlled remotely through control surface deflections rather than support motion that significantly extends the set of possible aircraft manoeuvers.

2.1.6 TsAGI forced oscillation test rig

The whole set of experimental data which are used in this work for mathematical modelling has been obtained in the TsAGI low speed wind tunnel T-103 in 1999-2001. The wind tunnel has a closed circuit and elliptical open jet test section $2.3 \times 4\,\mathrm{m}^2$, the flow speed range is $5 \div 70\,\mathrm{m/s}$ at continuous type operation. Dynamic tests are usually conducted at speeds of $25 \div 50\,\mathrm{m/s}$ that corresponds to Reynolds number $Re \approx 10^6$ per meter.

The forced oscillation rig OVP-102B is mounted on the rotating floor of the wind tunnel test section, which provides sideslip in the range $-90^o \div 20^o$. The rig is used for static and dynamic tests with small and large amplitudes in pitch, yaw and roll. The frequency and amplitude of oscillations is in the ranges $f = 0.2 \div 2.5\,\mathrm{Hz}$, and $\Delta\Theta = 0.5^o \div 26^o$, respectively. To produce yaw oscillations the model is mounted in the vertical plane with a 90^o bank angle. The angle of attack, in this case, is changed using the rotating floor. Oscillatory motion of the model is excited by the oscillating vertical rod driven by an electric motor/gearbox unit placed on the rotating floor of the wind tunnel test section.

The aerodynamic loads acting on the model are measured by the five component internal strain gauge balance placed on the sting tip, which is mounted on the vertical and L-shaped rotated struts of the rig. The sting has a very small thickness ($\varnothing \approx 33\,\mathrm{mm}$) leaving a very small size for the docking adapter for the strain gage balance. The signals from the strain gauge balance are measured by a high speed analogue-to-digital converter and collected on a PC as time histories of aerodynamic loads, angles and wind tunnel flow parameters. After that the records are filtered and reduced to one period of oscillation.

2.1.6.1 Configuration for small amplitude oscillations

Small amplitude oscillations are used for extracting aircraft aerodynamic derivatives depending on the angle of attack and frequencies. The following derivatives and combinations can be obtained as a result of oscillations along the appropriate degree of freedom:

Pitch	Yaw	Roll
$C_{Z_\alpha},\ C_{m_\alpha}$	$C_{Y_\beta}\cos\alpha,\ C_{Y_r}-C_{Y_{\dot{\bar{\beta}}}}\cos\alpha$	$C_{Y_\beta}\sin\alpha,\ C_{Y_p}+C_{Y_{\dot{\bar{\beta}}}}\sin\alpha$
$C_{Z_q}+C_{Z_{\dot{\bar{\alpha}}}}$	$C_{n_\beta}\cos\alpha,\ C_{n_r}-C_{n_{\dot{\bar{\beta}}}}\cos\alpha$	$C_{n_\beta}\sin\alpha,\ C_{n_p}+C_{p_{\dot{\bar{\beta}}}}\sin\alpha$
$C_{m_q}+C_{m_{\dot{\bar{\alpha}}}}$	$C_{l_\beta}\cos\alpha,\ C_{l_r}-C_{l_{\dot{\bar{\beta}}}}\cos\alpha$	$C_{l_\beta}\sin\alpha,\ C_{l_p}+C_{l_{\dot{\bar{\beta}}}}\sin\alpha$

Sketches of the rig configurations reproducing these degrees of freedom are shown in Fig. 2.7.

The derivatives are extracted from the time histories of loads using the following linear regression model. For example, during small amplitude pitch oscillatory motion with mean angle of attack α_0 the aerodynamic force/moment coefficient may be presented as the following Taylor series expansion:

$$C(t) = C(\alpha_0) + C_\alpha(\alpha_0)\alpha(t) + (C_q(\alpha_0) + C_{\dot{\bar{\alpha}}}(\alpha_0))\frac{\bar{c}}{2V}\dot{\alpha}(t), \tag{2.1}$$

where $\alpha(t)$ and $\dot{\alpha}(t)$ are considered as independent values. Applying the regression technique described in Appendix B one can estimate values of the regressors C, C_α and $C_q + C_{\dot{\bar{\alpha}}}$ at each α_0.

During the test the dependence $\alpha(t)$ is measured by a sensor fitted between the vertical and L-shaped rotated struts. The signal $\dot{\alpha}(t)$ may be measured by a model sensor if it is available or obtained by means of differentiation of the $\alpha(t)$ dependance. Due to the presence of noise in the experimental records, direct differentiation using, for example, a finite difference algorithm will lead to incorrect results. To overcome this problem, the original signal is filtered by means of a low pass Butterworth digital filter. Zero phase shift is reached by applying the filter in forward and reverse directions. The order of the Butterworth filter and cut-off frequency are chosen as a result of signal spectrum analysis.

After has been filtered the signal is differentiated using the polynomial of the best approximation. If $z(t) = \dot{u}(t)$ and u is the equally spaced vector $u_1, u_2, \ldots, u_N$ with sample interval Δt then the first derivative can be found as follows [56]:

$$z_i = \frac{1}{12\Delta t}(3u_{i+1} + 10u_i - 18u_{i-1} + 6u_{i-2} - u_{i-3}). \tag{2.2}$$

This technique has been included in the ADDB toolset (see section 8.1.3) and applied to the experimental data processing.

2.1.6.2 The rig configuration for large amplitude oscillations

The forced oscillations experimental setup configured for pitch motion is shown in Fig. 2.8(a). The angle of attack which is equal in this case to the pitch angle is assigned by means of the sting inclination, while the sideslip angle is set by a rotating floor. The aircraft model is installed in a horizontal flight with zero bank angle.

In order to produce the large amplitude oscillations in yaw the model is rotated to 90^o in roll as shown in Fig. 2.8(b). The pitch angle in this case is set by rotation of the working section floor and deflection of the sting results in the yaw angle variation. If the floor rotation angle is θ and the angle of the sting inclination is ψ then the angle of attack α and sideslip β are expressed as follows:

$$\begin{aligned} \tan\alpha &= \tan\theta/\cos\psi \\ \sin\beta &= \cos\theta\sin\psi. \end{aligned} \tag{2.3}$$

For a not very large sting inclination angle ψ these expressions can be presented in the simplified form:

$$\begin{aligned} \alpha &= \theta \\ \beta &= \psi\cos\theta. \end{aligned} \tag{2.4}$$

One can see that at higher angles of attack the amplitude of the sideslip variation is decreasing at the same sting variation amplitude. The relation between pitch and yaw angles provided by the experimental setup during yaw motion and the model angle of attack and sideslip is shown in Fig. 2.9.

During large amplitude oscillations in a roll a wing model is rotated about the axis coinciding with the sting axis as shown in Fig. 2.8(c). As in the case of yaw motion, pitch angle is set by rotating the flow. The rotation of the model for roll angle ϕ results in the development of a model sideslip angle. Due to the rig kinematics, a model angle of attack and sideslip are expressed as follows:

$$\begin{aligned} \tan\alpha &= \tan\theta\cos\phi \\ \sin\beta &= \sin\theta\sin\phi. \end{aligned} \tag{2.5}$$

For a not very large roll angle ϕ these expressions can be presented in the simplified form:

$$\begin{aligned} \alpha &= \theta \\ \beta &= \phi\sin\theta. \end{aligned} \tag{2.6}$$

One can see that at a smaller angle of attack, the amplitude of the sideslip variation is decreasing at the same roll variation amplitude. The transformation of the pitch and roll angles produced by the experimental setup during roll motion to angle of attack and sideslip of the model is shown in Fig. 2.10.

During the dynamic experiment, the internal strain gauge measures the total loads acting on the aircraft model namely: aerodynamic, centrifugal and inertial components. These signals are passed to a high speed 16 channel analogue-to-digital converter installed in the PC. The process is controlled by the data acquisition system based on LabView. To separate pure aerodynamic components, the tests are conducted in two stages. At first the run without wind flow is executed during which centrifugal and inertial components are measured for the current model configuration, then a series of tests with wind is performed. After that pure aerodynamic loads are extracted using results of "wind on" and "wind off" runs. Finally, the signals are filtered using the low-pass Butterworth filter with zero phase lag and reduced to one period of oscillation. As a result of the signal processing, each run in dynamic mode is represented by a time history of pitch, yaw or roll angle (depending on the setup configuration), normal and side forces, pitch, roll and yaw moments. Timing is set to provide 128 samples per period of oscillation which is typically about 1 sec. Thus, this sampling results in time step $\Delta t \sim 0.01$ sec that is enough for typical flight dynamics applications.

2.1.6.3 The rig configuration for static and slow sweep motion tests

Static and slow sweep motion tests with constant angular rate in both directions can be also conducted on the dynamic rig. The rod driving the L-shaped rotated struts is replaced in this case with a special remotely controlled expanding rod. Model angle and total loads may be registered both during continuous slow (quasi-steady) angle variation and at specified fixed angles i.e. in statics.

2.2 Typical results of the dynamic tests

Five simple wings, namely, three 70^o delta wings (two with rounded leading edges having $\bar{c} = 727\,\text{mm}$ and $494\,\text{mm}$, and one with sharp leading edges having $\bar{c} = 494\,\text{mm}$),

one 65^o delta wing ($\bar{c} = 437\,\text{mm}$) and one 60^o-80^o ($\bar{c} = 860\,\text{mm}$) double delta wing (see Fig. 2.11) have been tested in TsAGI within the joint programme with QinetiQ in 1999-2001 [56, 55, 52, 53, 51] The wings have been investigated using a wide range of pitch, roll and yaw motions including static tests, slow sweep motions, small and large amplitude oscillations, oscillatory-coning tests and pure plunging motions. These data were used for the investigation of high incidence flow properties and mathematical modelling but only results obtained for the 65^o delta wing with central body are considered in detail in the thesis. However, comparative analysis of characteristic time functions and some results of the mathematical modelling for other delta wings are also discussed in order to complete the picture.

2.2.1 Motion frequency/amplitude effects

Effects of the frequency/amplitude of oscillations in the aerodynamic derivatives are directly connected with the internal dynamics of vortical flow. The static and dynamic aerodynamic derivatives obtained by a standard harmonic analysis of the experimentally measured aerodynamic loads during small amplitude oscillations for the 65^o and 70^o delta wings are presented in Fig. 2.12. One can see that due to frequency effects, these aerodynamic derivatives may change not only in magnitude but even in sign. Significant dependence in these aerodynamic derivatives on the frequency of oscillations corresponds to the range of angles of attack and sideslip where vortex breakdown is present.

The comparison of the static and the dynamic derivatives for the 70^o delta wings with rounded and sharp leading edges given in Fig. 2.13 shows that the sharp leading edges which generate stronger vortices shift the start of the vortex breakdown to smaller angles of attack.

2.2.2 Slow sweep motion

Slow sweep motion with variations of the model attitudes over a wide range may be used to detect the critical states crossing, reflecting changes in the flow structure. These crossings are usually characterized by hysteresis loops in the dependencies of loads corresponding to slow forward and reversed attitude variations. This effect may be ascribed to delays

in vortex bursting/readjusting process that leads to some uncertainties in loads within the region of incidences where vortex breakdown takes place. Contrary to braking down vortical flow, the attached and fully separated flows are free from hysteresis type dependencies during slow sweep motion (see Fig. 2.14). This fact allows an approximate evaluation of the region in the plane of angles of attack and sideslip where the vortex burst points are above the wing.

2.2.3 Large amplitude motion

Oscillatory motions in pitch, roll and yaw covering the incidences with different flow structures have been deeply investigated for all available delta wings. The aerodynamic loads acting on a wing undergoing large amplitude oscillations reveal complicated nonlinear behaviour which can be ascribed both to the nonlinear static dependencies and the time lag effects. An example of aerodynamic responses during large amplitude oscillations in pitch at non zero sideslip $\beta = -10^o$ is given in Fig. 2.15. At low reduced frequency $\bar{\omega} = 0.0194$ the aerodynamic responses in the normal force coefficient C_N and the pitching moment coefficient C_m bear a resemblance to the shape of the static dependencies while at higher frequencies $\bar{\omega} = 0.0388, 0.0466$ they lose this memory i.e. the effect of dynamic straightening takes place.

2.2.4 Free to roll motion

With use of the "free to roll" experimental setup which is assembled on the base of the OVP-102B rig it is possible to investigate "Wing Rock" type motion [50]. A sketch of such a rig used in TsAGI [56] is shown in Fig. 2.16. A wing model is mounted on the tip of the fixed sting using a ball-bearing hinge providing free rotation in roll. The required angle of attack is set by the sting inclination angle (pitch angle). At a given angle of attack, various initial positions of roll deflection can be installed and fixed. After a model has been released by means of a remotely controlled lock, it either converges to a stable position or self-induced oscillations with a significant amplitude are developed. Under certain conditions, this one degree of freedom system can even demonstrate chaotic dynamics. Some experimental results obtained in TsAGI [51] for the 80^o-60^o double delta wing are presented in Figs. 2.17–

2.19.

To investigate the dynamics of the system, let us consider a mathematical model of the experimental setup. It can be represented as a classical torsion pendulum where the elasticity is provided by an aerodynamic rolling moment. Thus the following equation for the roll angle ϕ is valid:

$$\frac{d^2\phi}{dt^2} = \frac{\rho V^2 S b}{2 I_{xx}} C_l. \tag{2.7}$$

Friction in the hinge is neglected here due to its minor effect. Using a conventional approach to aerodynamic loads modelling, the rolling moment coefficient is represented as a nonlinear function of the kinematic parameters: $C_l = F(\alpha, \beta, p, \ldots)$. Due to the rig kinematics $\alpha = \alpha(\phi)$ and $\beta = \beta(\phi)$, therefore, $C_l = C_l(\phi, \dot{\phi})$. Thus the system (2.7) belongs to the class of autonomous second order nonlinear differential equations. According to Cauchy's theorem concerns singular solutions this system cannot have crossing phase trajectories. Moreover, it cannot demonstrate chaotic behavior.

Analysis of the experimental results presented in Figs. 2.17–2.19 leads to some conclusions about the system dynamics. For example, at $\theta = 30^o$ there are three different attractors which are reached by phase trajectories on the plane $\dot{\phi} - \phi$, with one of them being stable equilibrium. At $\theta = 35^o$ and $\theta = 50^o$ there are two and one attractors, respectively. In all cases the phase trajectories intersect each other and demonstrate irregular behavior within the regions of attractions. In some cases they even jump to adjacent attractors that makes this picture resemble the Lorenz's strange attractor.

Such a behavior can be explained if we assume that we deal with $\dot{\phi} - \phi$ projections of the phase trajectories of higher than a second order dynamic system. This means that a widely used representation of rolling moment coefficient in terms of aerodynamic derivatives becomes inconsistent as the second order system describes just rigid body dynamics while according to experimental results at least one additional dimension seems to exist. This internal dynamics of the system may be ascribed to processes taking place in vortical and/or separated flow at high incidences, which cannot be described by conventional representation of aerodynamic loads as the Taylor series expansion along kinematic parameters. That is why an adequate mathematical model of aerodynamic loads taking into account internal dynamics of a flow is required to couple the equations of aircraft motion.

2.3 Summary

A brief review of the experimental rigs which are used in different research centres for wind tunnel dynamic tests has been presented to demonstrate the basic principles, objectives and capabilities of such an experiments. In spite of the variety of designs almost all of them are aimed at providing variation of at least one degree of freedom. The dynamic rigs may be divided into two main groups according to the type of operation. The first group includes the rigs providing predefined forced motion.

Small amplitude forced oscillations are used to evaluate aerodynamic derivatives, which are very important for local stability analysis and control law design. At high angles of attack analysis of the dependence of the derivatives upon the frequency of oscillations provides valuable information about changes of the flow structure and the dynamic properties of the flow readjustment processes. The time lags of aerodynamic loads with respect to the motion parameters may be evaluated using these frequency dependency.

Large amplitude tests are indispensable for aerodynamic load analysis during manoeuvers covering regions with different flow structures. These data are used for the identification of mathematical models of the aerodynamic characteristics which are necessary for global stability analysis, adequate simulation of aircraft dynamics at high incidence, planning of extreme manoeuvers like, for example, "Cobra" when the angle of attack varies from 0^o up to 100^o and backwards for several seconds.

The second group includes rigs performing free motion or controlled by onboard effectors within constraints imposed by the rig. In this case some manoeuvers close to real flight conditions may be naturally reproduced. For example, rotary balance is usually used for the investigation of aerodynamic loads during intensive rotation at high angles of attack which is typical for spin. If a dynamically similar aircraft model is used in a vertical wind tunnel then due to the interaction between inertial (rigid body dynamics) and aerodynamic loads rotation can be developed at some conditions similar to real flight spin. Remotely controlled aerodynamic surfaces may be used in this case for perturbing the motion.

"Free to roll" rigs are capable of reproducing "Wing Rock" type motion which is peculiar to practically all modern fighters at high angles of attack in subsonic flight. The "Wing Rock" results in regular or chaotic oscillations in the lateral/directional motion with sig-

nificant amplitude. A special case of "Wing Rock" is "Wing Drop" [3] motion, which is characterized by abrupt loss of lateral stability at relatively small angles of attack at transonic speeds due to the asymmetrical development of local compression shocks. This "Wing Rock" is found to be due to the interaction of rigid body motion with vortices and separation processes having their own dynamics which is ignored in conventional aerodynamic models.

It worth mentioning that "Wing Rock" is a striking but not the only possible example of "real life" flight dynamic problems which demonstrate the need for more sophisticated technique of aerodynamic modelling than the traditional one. Flight at high angles of attack with intensive manoeuvering is still a real challenge for adequate mathematical modelling. That is why numerous papers proposing different approaches to high incidence aerodynamics modelling have been published. There have been several techniques having merits and demerits proposed, but no one is still able to solve the problem [41, 61]. Some of these developed over several decades are widely known and are discussed in the next chapter.

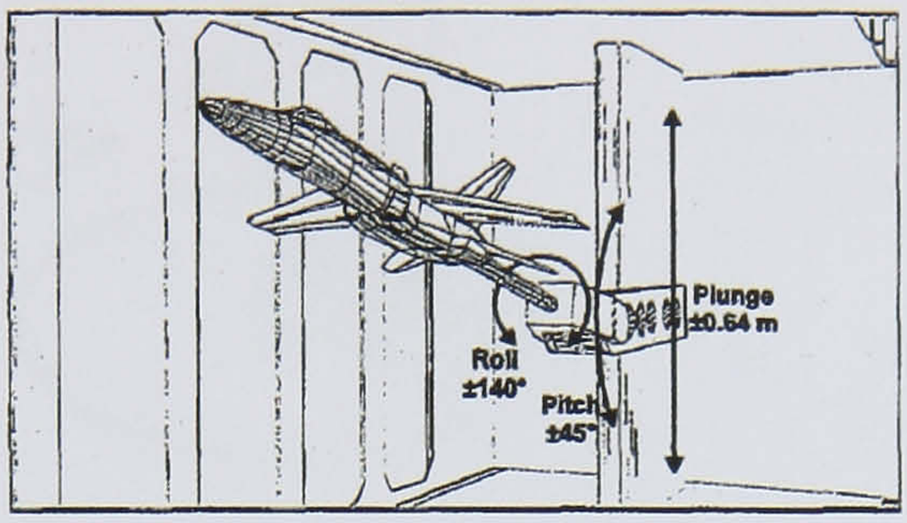

Figure 2.1: DyPPPiR: Dynamic Plunge-Pitch-Roll test mount.

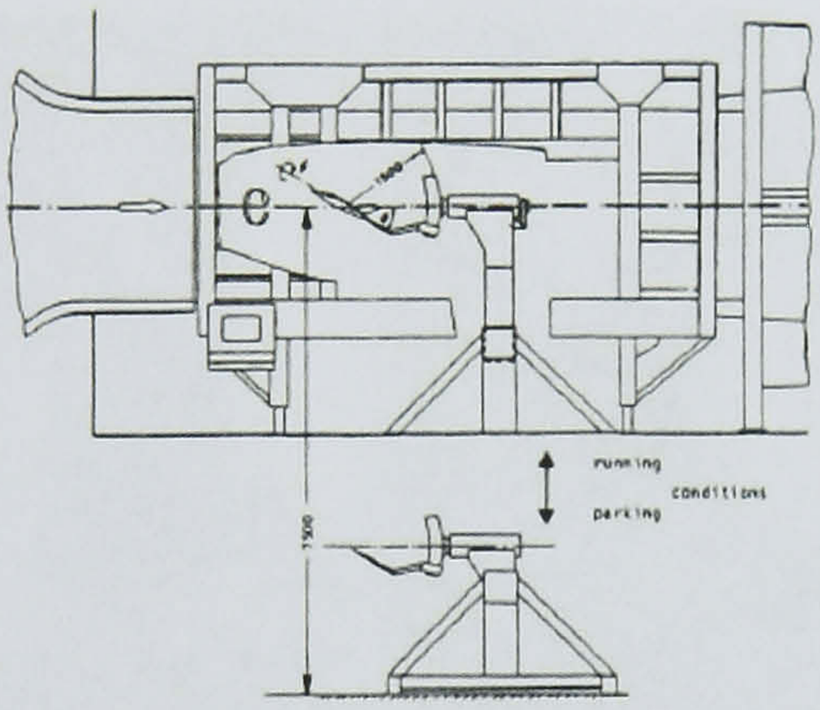

Figure 2.3: DLR rotary balance in Braunschweig $3.25 \times 2.8\,\mathrm{m}$ low speed wind tunnel.

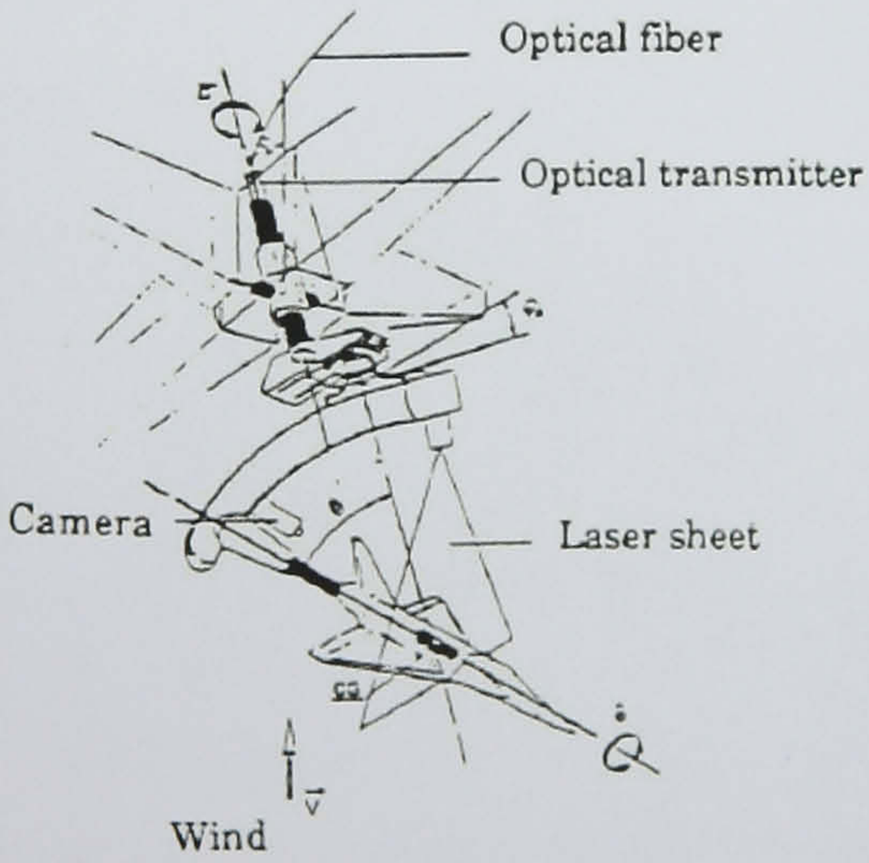

Figure 2.5: ONERA's rotary balance.

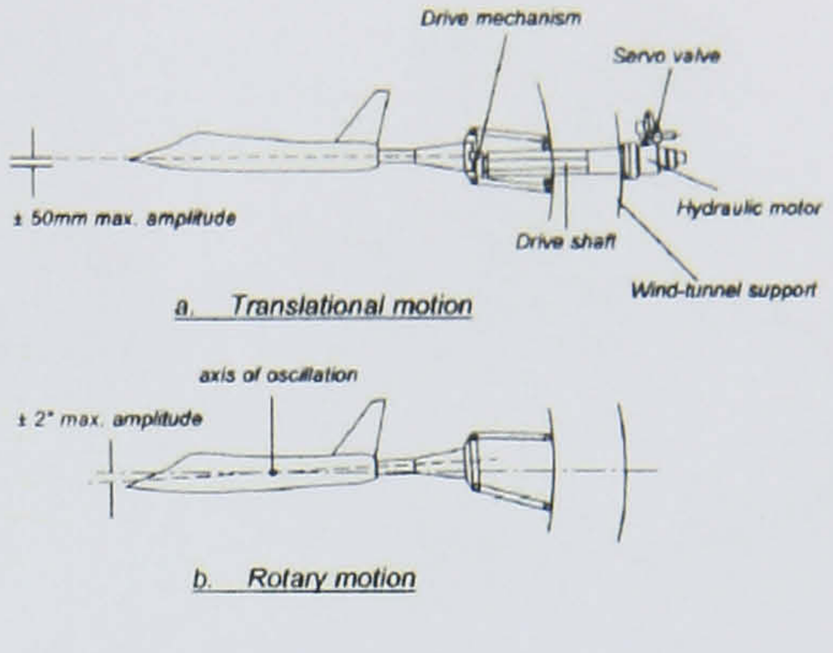

Figure 2.2: DRA's oscillatory rig.

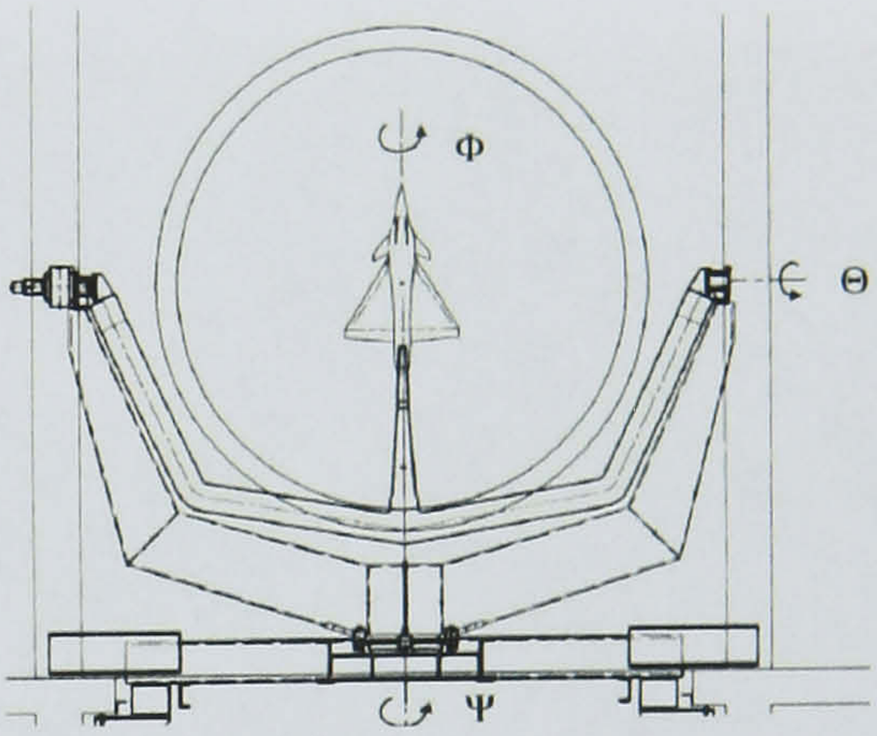

Figure 2.4: ONERA's oscillatory rig (PQR).

Figure 2.6: Pendulum Support Rig in the University of Bristol.

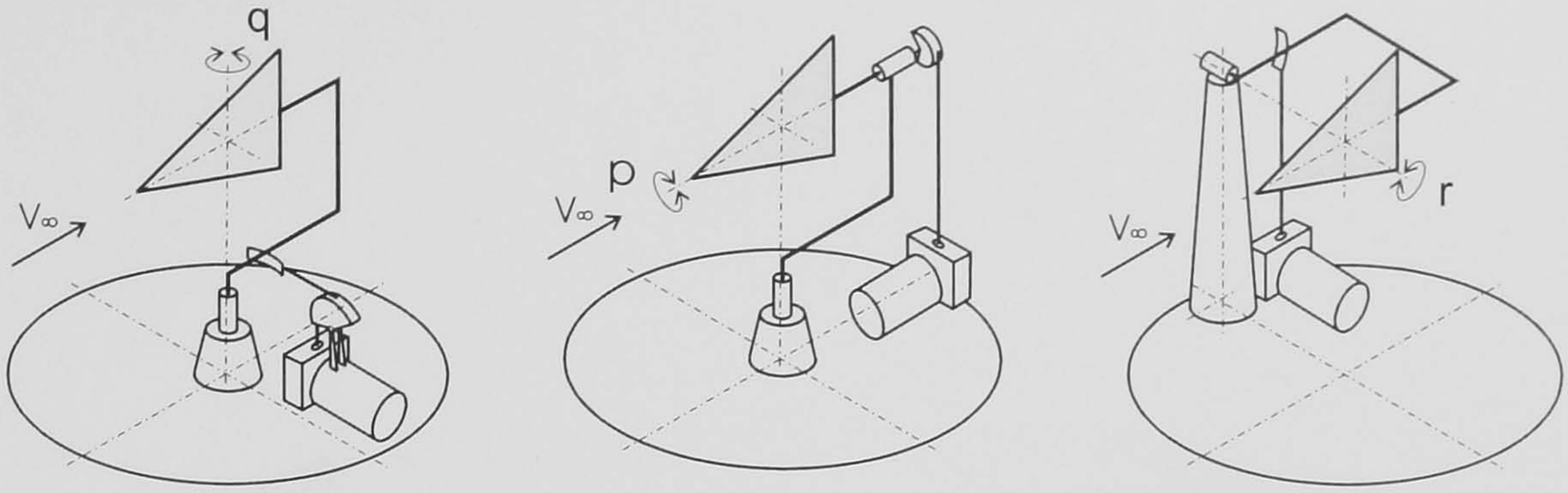

Figure 2.7: Sketch of the OVP-102B experimental setup for pitch, roll and yaw oscillations with small amplitudes.

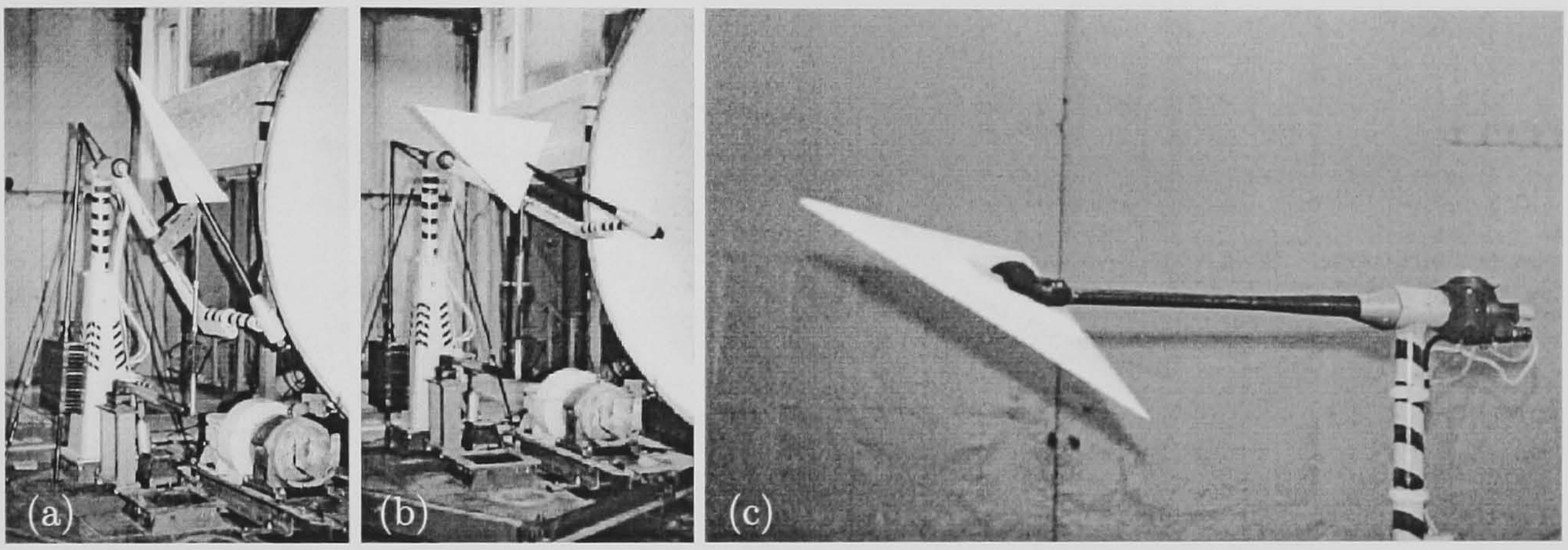

Figure 2.8: Configurations of the forced oscillation rig OVP-102B in case of large amplitude motion in pitch (a), yaw (b) and roll (c).

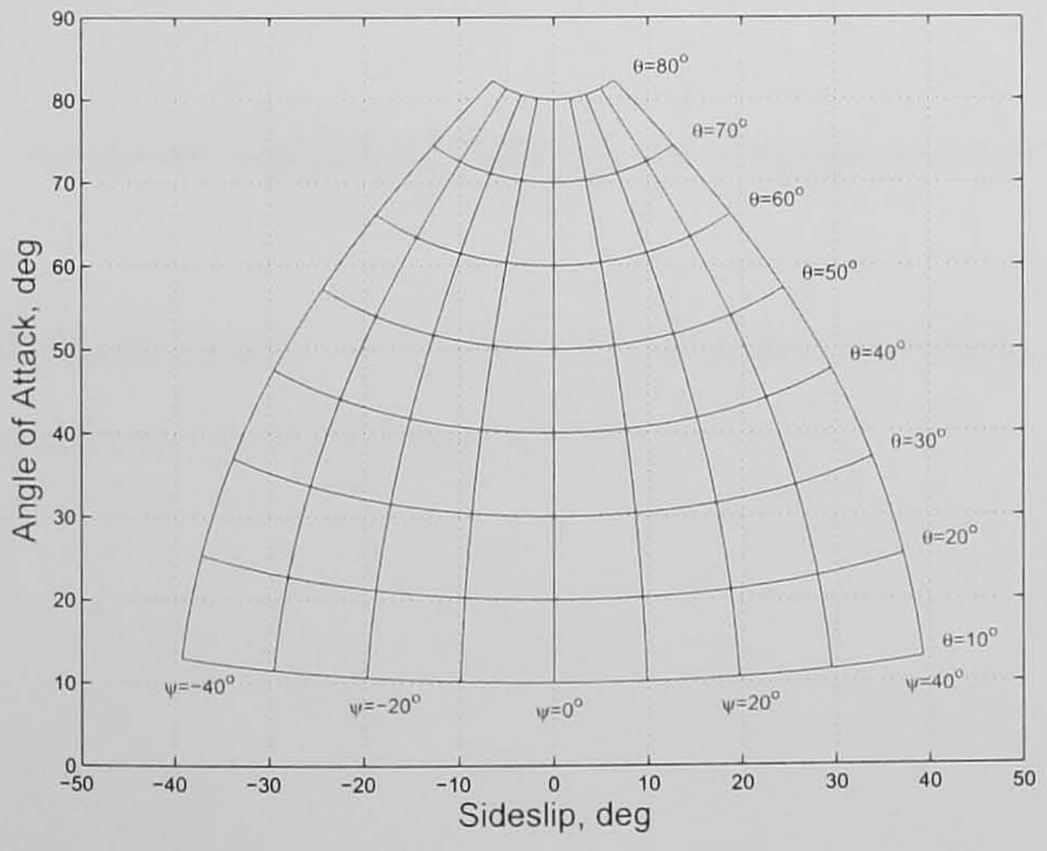

Figure 2.9: Kinematics of the OVP-102B experimental setup in yaw motion.

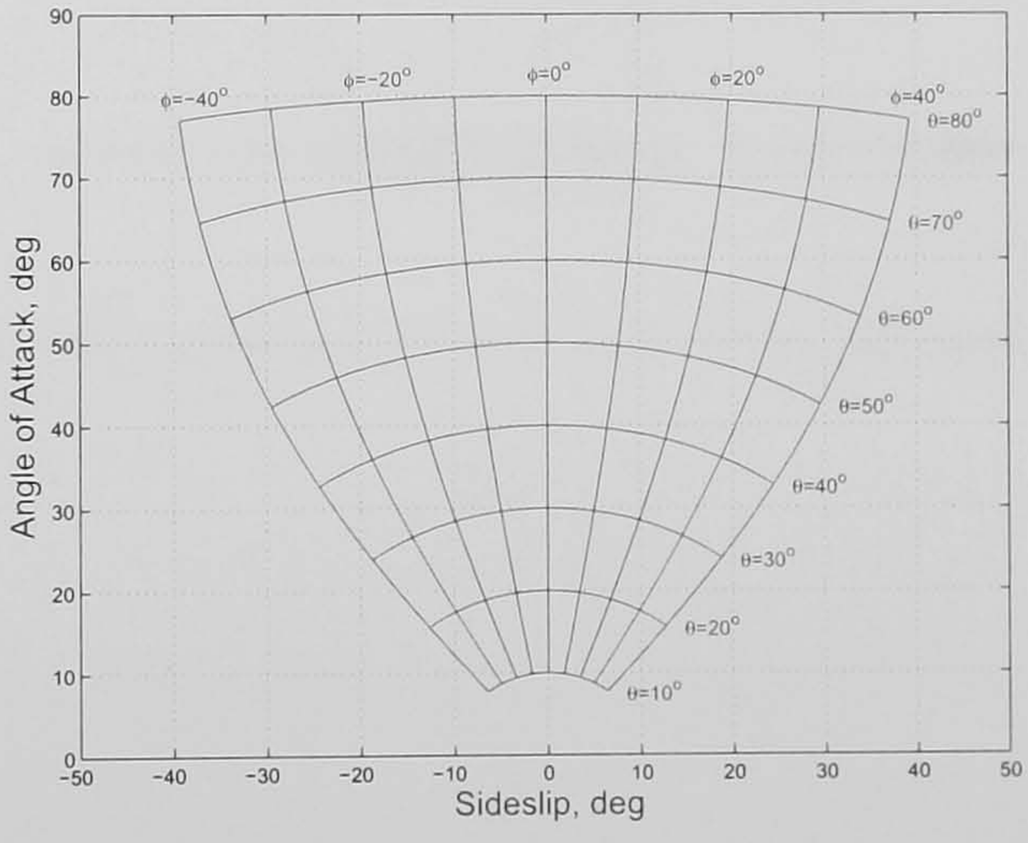

Figure 2.10: Kinematics of the OVP-102B experimental setup in roll motion.

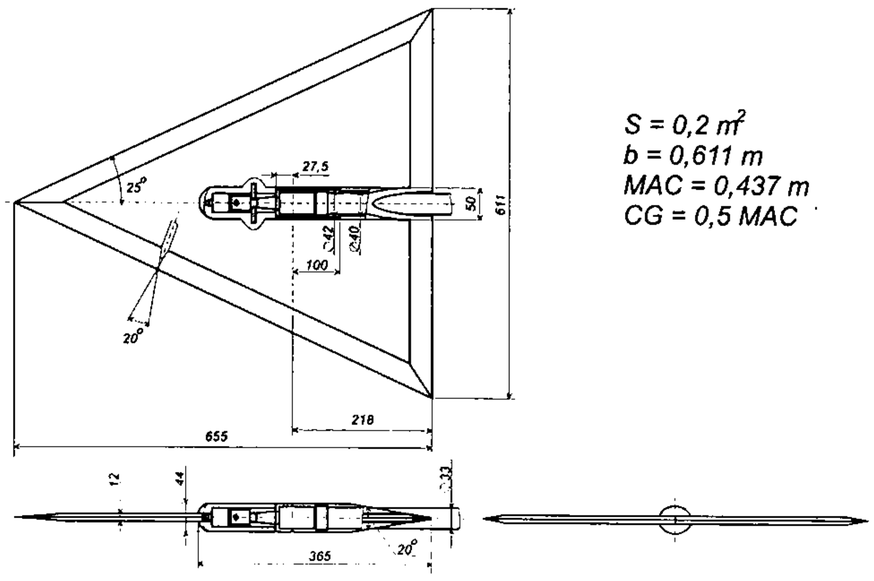

S = 0,2 m²
b = 0,611 m
MAC = 0,437 m
CG = 0,5 MAC

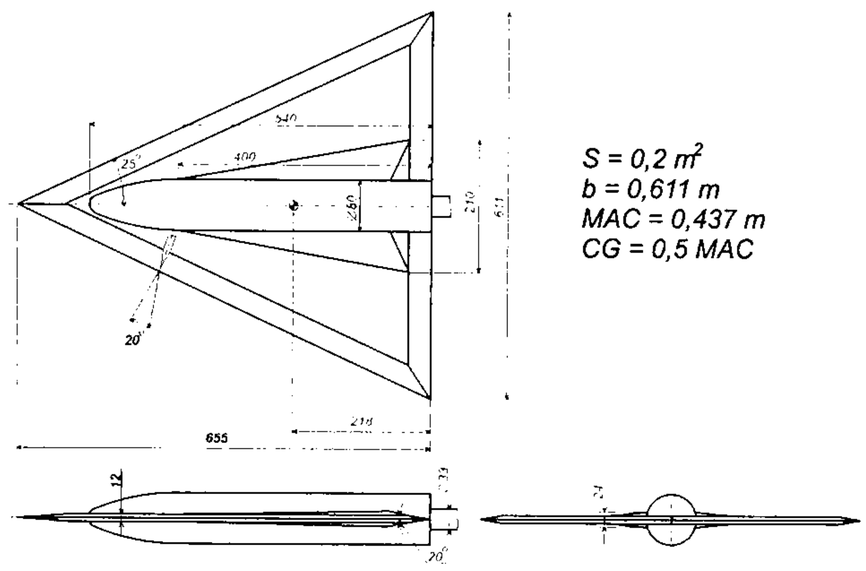

S = 0,2 m²
b = 0,611 m
MAC = 0,437 m
CG = 0,5 MAC

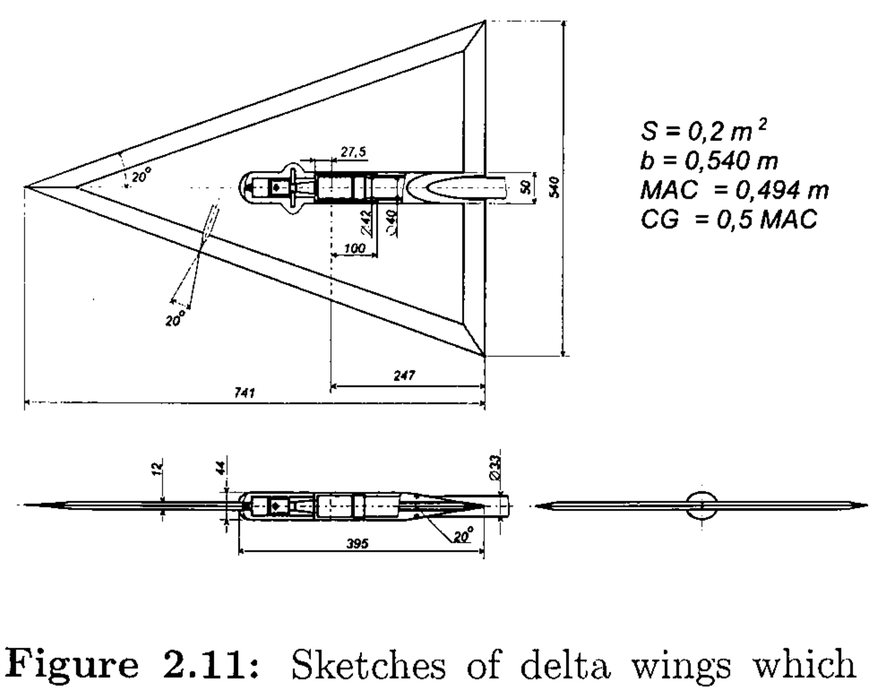

S = 0,2 m²
b = 0,540 m
MAC = 0,494 m
CG = 0,5 MAC

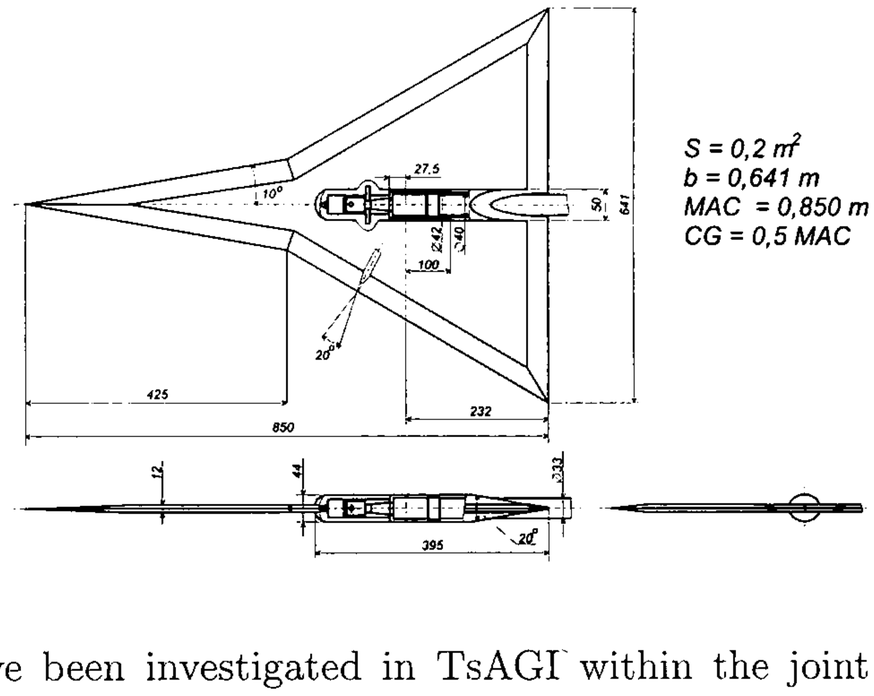

S = 0,2 m²
b = 0,641 m
MAC = 0,850 m
CG = 0,5 MAC

Figure 2.11: Sketches of delta wings which have been investigated in TsAGI within the joint programme with QinetiQ [37].

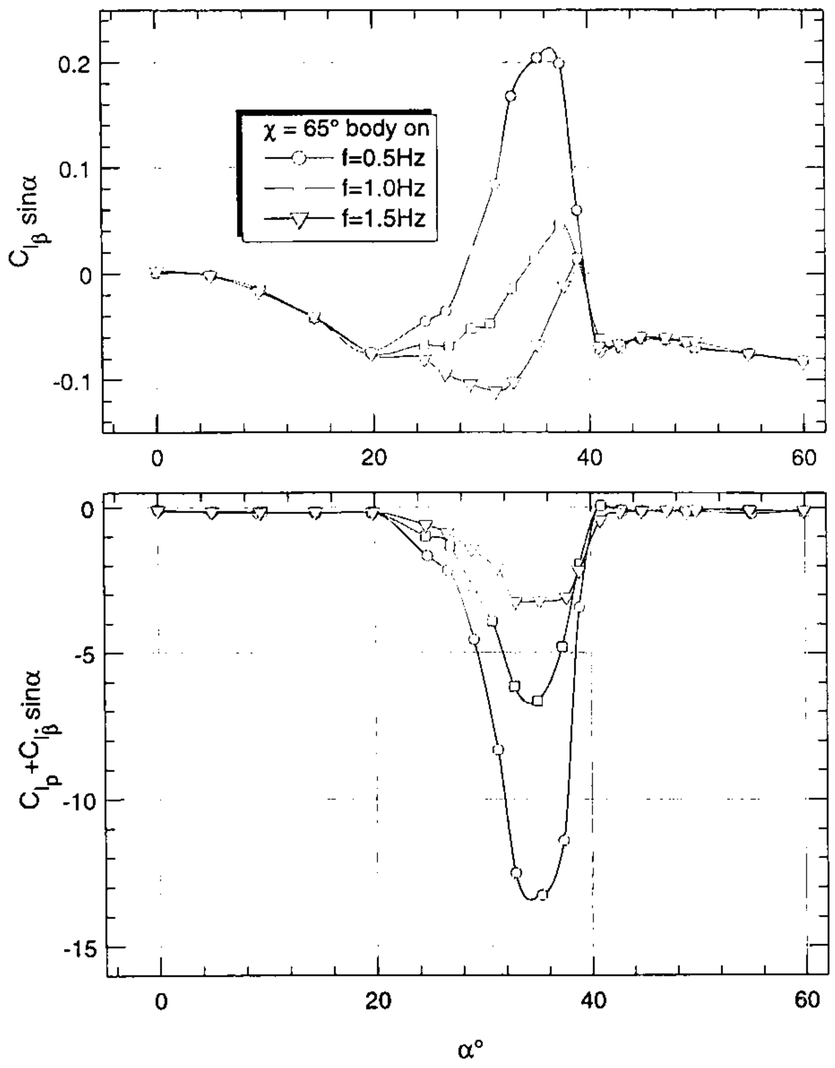

Figure 2.12: The 65^o delta wing with center body. Derivatives of rolling moment coefficient in roll motion.

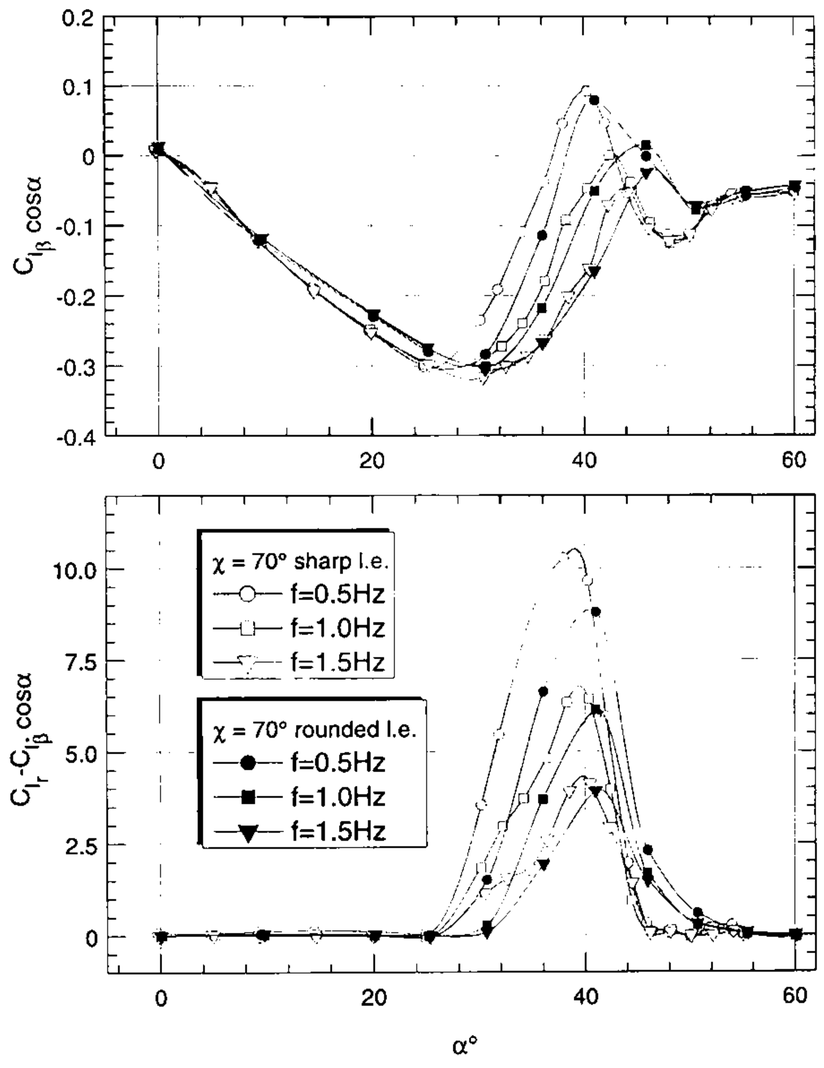

Figure 2.13: The 70^o delta wings with sharp and rounded leading edges. Derivatives of rolling moment coefficient in yaw motion.

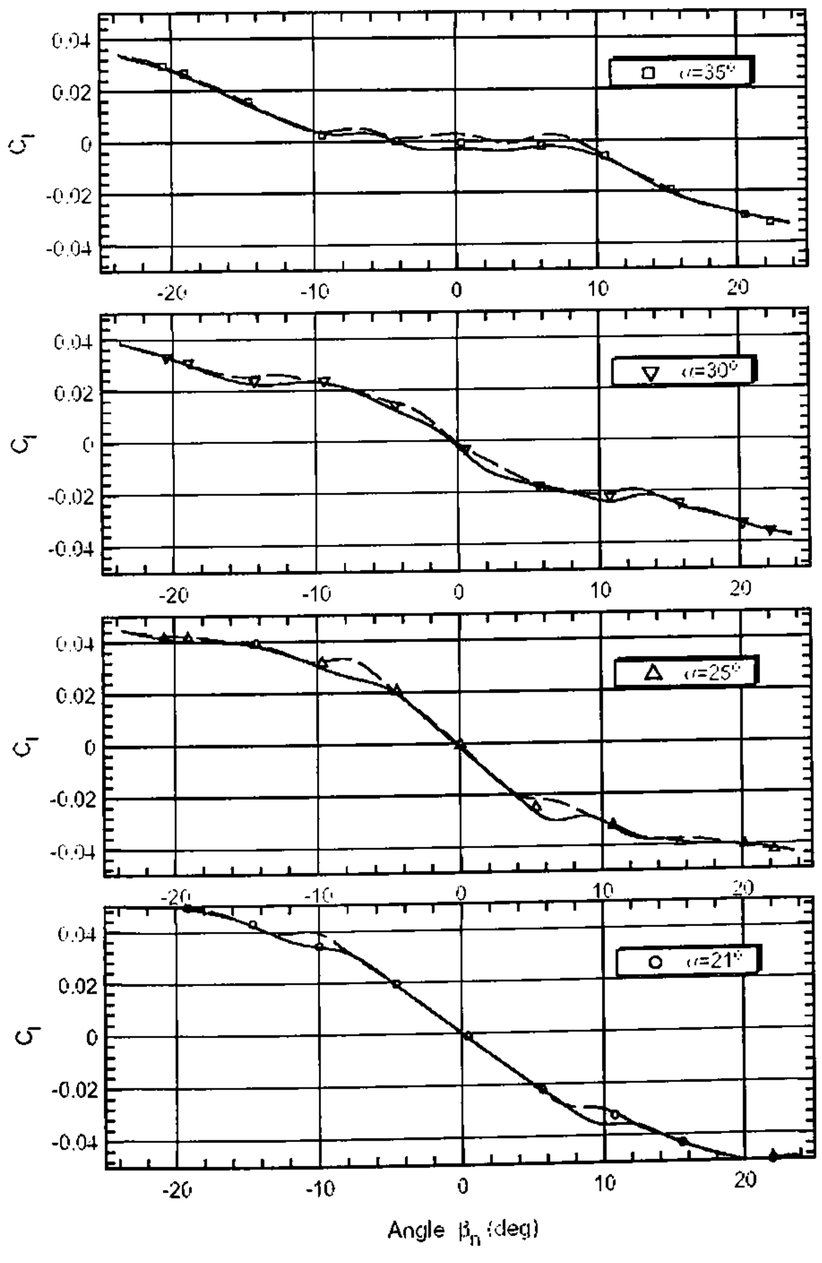

Figure 2.14: Slow sweep sideslip motion (70^o delta wing).

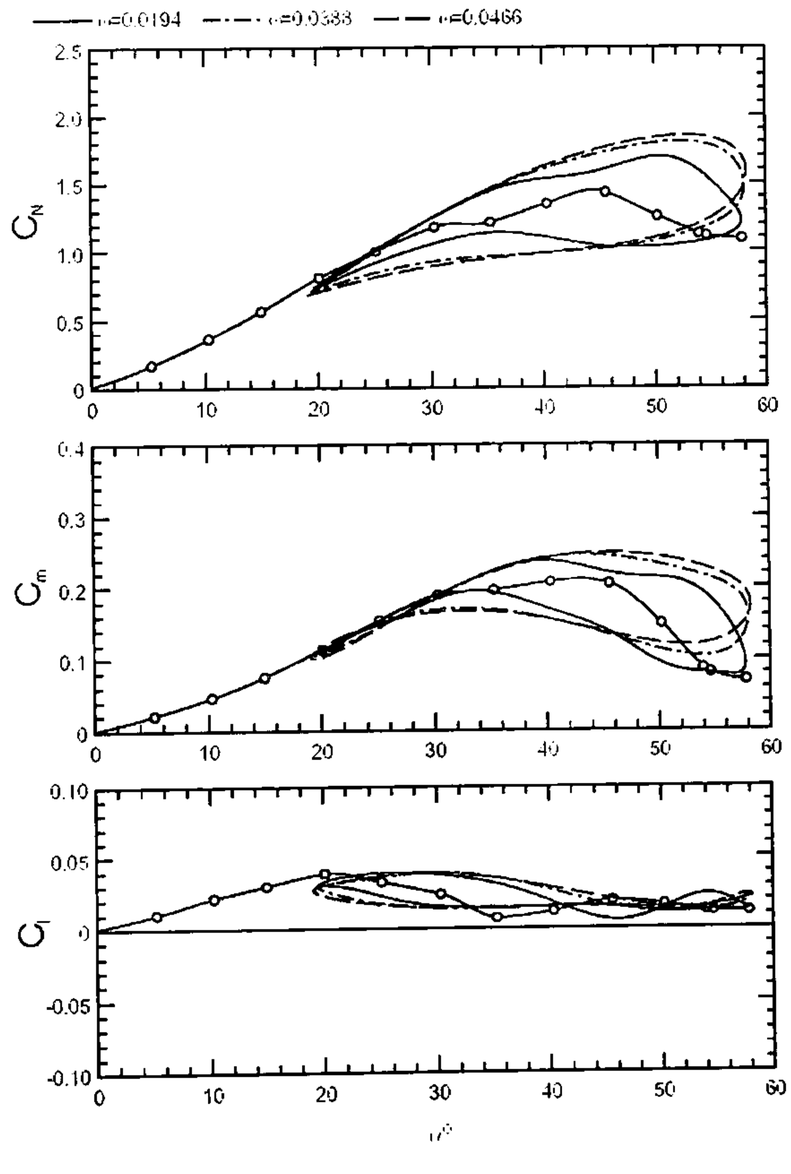

Figure 2.15: Aerodynamic loads during large amplitude pitch oscillations (70^o delta wing).

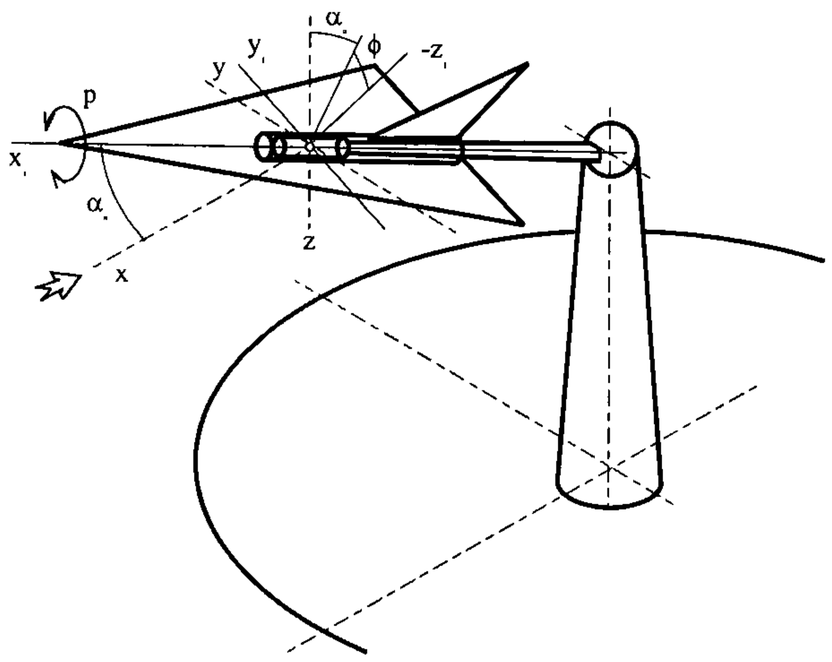

Figure 2.16: TsAGI free to roll motion experimental setup.

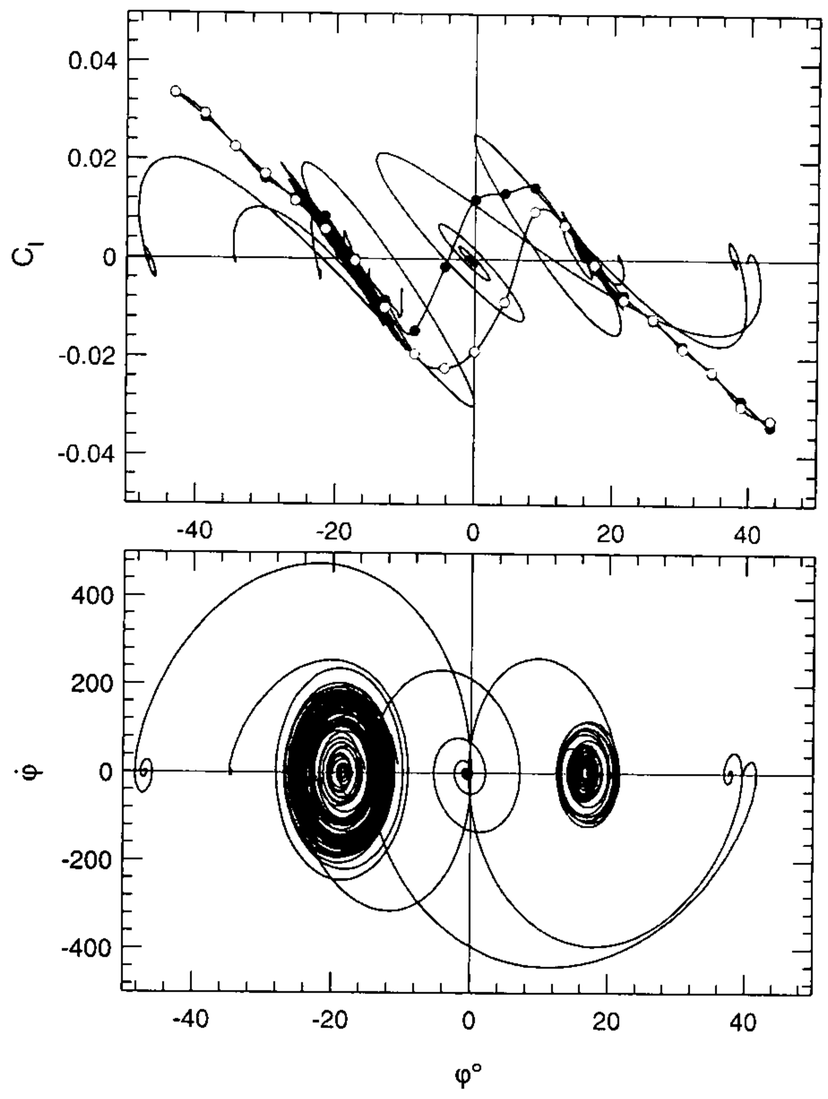

Figure 2.17: Multi-attractor dynamic of the free to roll system at $\theta = 30^o$ (80^o-60^o double delta wing).

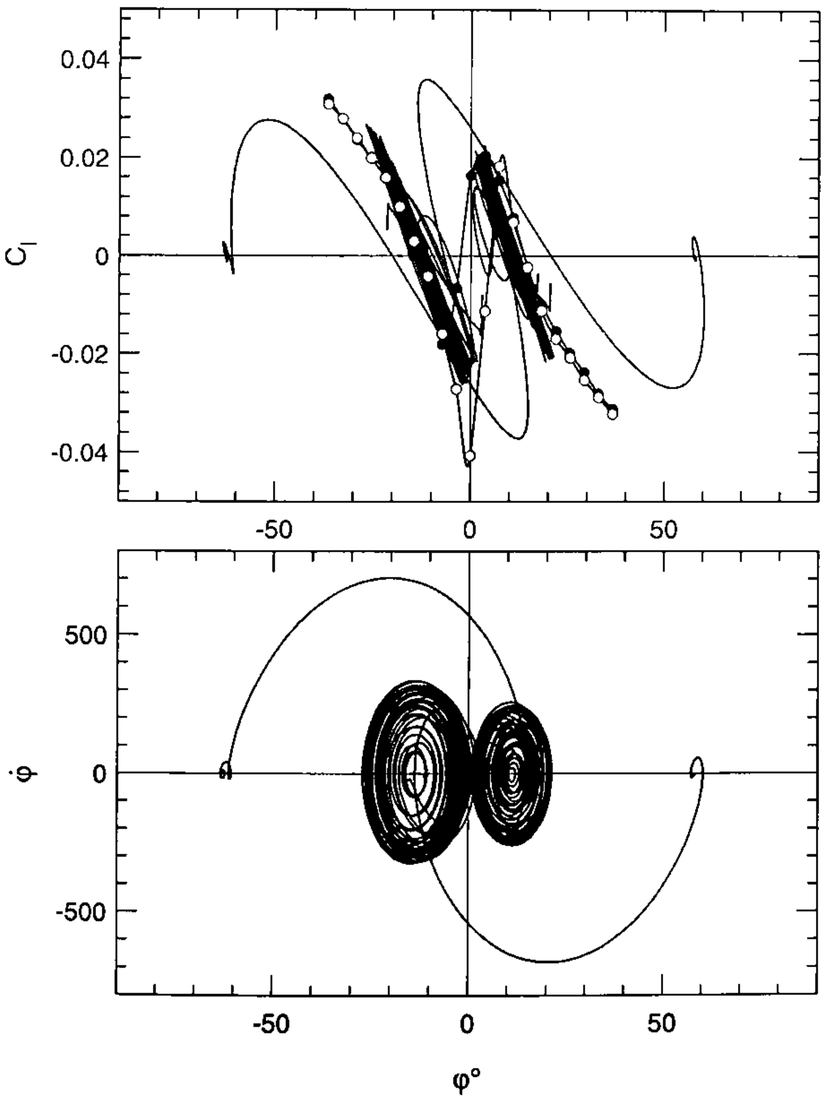

Figure 2.18: Multi-attractor dynamic of the free to roll system at $\theta = 35^o$ (80^o-60^o double delta wing).

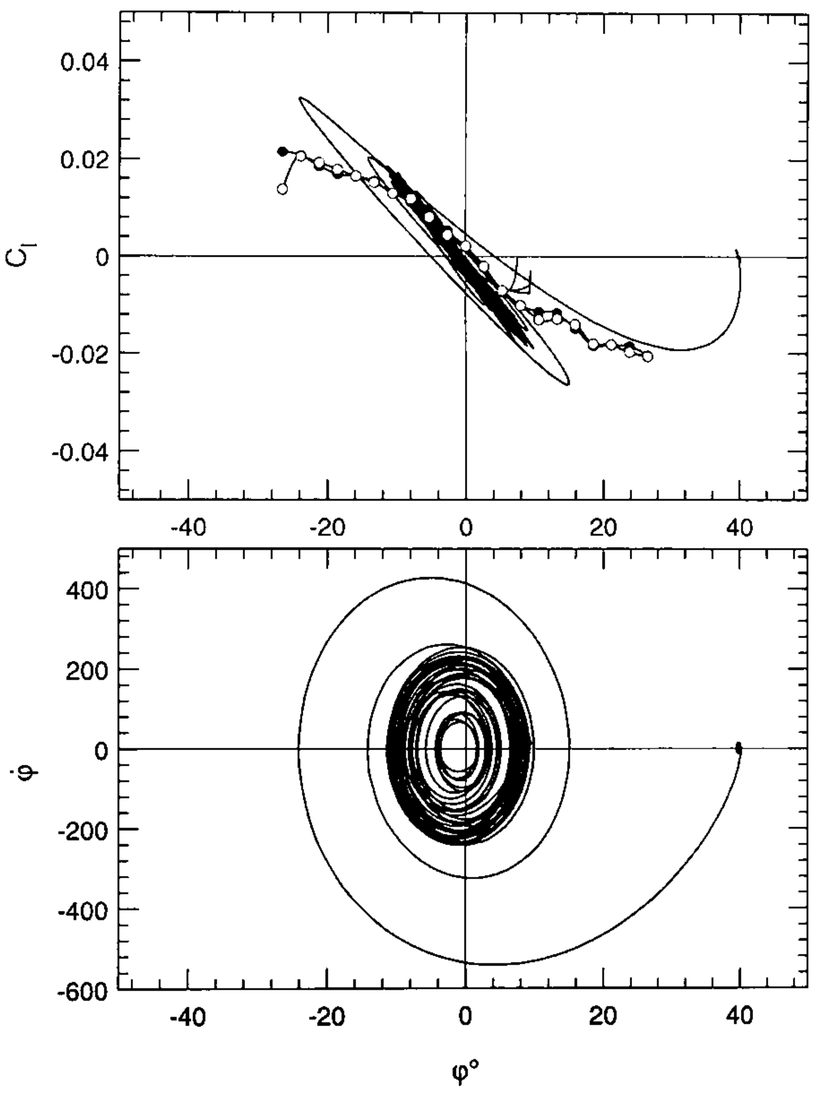

Figure 2.19: Multi-attractor dynamic of the free to roll system at $\theta = 50^o$ (80^o-60^o double delta wing).

Chapter 3

Review of unsteady aerodynamic modelling approaches

3.1 Aerodynamic derivative concept

Unsteady aerodynamic loads acting on manoeuvering aircraft are usually presented in the form of aerodynamic derivatives. Many years experience demonstrates that this approach is rather accurate for different aircraft configurations at low angles of attack and relatively slow angular motion. The conventional description of aerodynamic loads is usually based on experimental data obtained in wind tunnels using facilities for static, forced oscillations and rotary balance tests [22, 1]. In order to build an adequate mathematical model it is very important to properly combine all the available data for different flight regimes. A set of experimental facilities and computational methods have been developed to support this approach. To complement the experiment data, modern CFD methods are usually applied.

In the general case unsteady aerodynamic loads are represented as functionals of kinematic parameters and control deflections: $C_i = C_i(\alpha, \beta, p, q, r, \dot{\alpha}, \dot{\beta}, \delta_j, M, Re, Sh, ...)$, where $i = (L, D, Y, l, m, n)$ – lift, drag, side forces and rolling, pitching, yawing moment coefficients, M – Mach number, $Re = \rho V l/\mu$ – Reynolds number, $Sh = l/Vt$ – Strouhal number and δ_j – j-th control surface deflection. Assuming that the motion is an analytical function of time and aerodynamic reactions are also analytical functions of instant values of the state variables and their time derivatives, aerodynamic coefficients are expanded as Taylor

series with only the linear terms being considered. Thus, for example, the longitudinal aerodynamic coefficients ($i = L, m$) can be represented as follows:

$$C_i = C_{i_\alpha}\alpha + \frac{\bar{c}}{2V}(C_{i_q}q + C_{i_{\dot{\bar{\alpha}}}}\dot{\alpha}) + \sum_k C_{i_{\delta_k}}\delta_k. \tag{3.1}$$

This representation of the aerodynamic coefficients is correct only when they can be presented by a linear function of angular rates. The effect of frequency and amplitude on the aerodynamic derivative is negligible as well. Such an approach is able to describe the aerodynamic loads rather accurately at relatively low incidences.

This approach has been later adapted to high incidence regimes by means of introducing nonlinear dependencies on the angle of attack. The longitudinal aerodynamic coefficients in this case are represented as follows [46]:

$$\begin{aligned} C_L &= C_{L_0}(\alpha) + \frac{\bar{c}}{2V}C_{L_q}(\alpha)q + C_{L_{\delta_{e,l}}}(\alpha)\delta_{e,l} + C_{L_{\delta_{e,r}}}(\alpha)\delta_{e,r} \\ C_m &= C_{m_0}(\alpha) + \frac{\bar{c}}{2V}C_{m_q}(\alpha)q + C_{m_{\delta_{e,l}}}(\alpha)\delta_{e,l} + C_{m_{\delta_{e,r}}}(\alpha)\delta_{e,r}. \end{aligned} \tag{3.2}$$

where C_{L_0} and C_{m_0} are the static dependencies of normal force and pitch moment coefficients.

Intensive rotation at high angles of attack considerably influences the vortical and separated flow structure which results in a nonlinear dependency of aerodynamic coefficients on the coning rate. In this case, in particular, during spin or stall motion, the body-axis force and moment coefficients can be represented as functions of the wind-body angular velocity components, and results of rotary balance tests are directly taken into account. The following example, borrowed from [35], demonstrates this representation in case when disturbances of the pure conical motion are small:

$$\begin{aligned} C_i &= C_{i_{RB}}\left(\alpha, \beta, \frac{p_w b}{2V}, \boldsymbol{\delta}\right) + C_{i_{q_w}}\frac{q_w\bar{c}}{2V} + C_{i_{\dot{\bar{\alpha}}}}\frac{\dot{\alpha}\bar{c}}{2V} + C_{i_{r_w}}\frac{r_w b}{2V} + C_{i_{\dot{\bar{\beta}}}}\frac{\beta b}{2V} \\ &= C_{i_{RB}}\left(\alpha, \beta, \overline{p}_w, \boldsymbol{\delta}\right) + \left(C_{i_{q_w}} + C_{i_{\dot{\bar{\alpha}}}}/\cos\beta\right)\frac{q_w\bar{c}}{2V} + \left(C_{i_{r_w}} - C_{i_{\dot{\bar{\beta}}}}\right)\frac{r_w b}{2V} - \\ &\quad C_{i_{\dot{\bar{\alpha}}}}\frac{q_{w_{sp}}\bar{c}}{2V\cos\beta} + C_{i_{\dot{\bar{\beta}}}}\frac{r_{w_{sp}}b}{2V}. \end{aligned} \tag{3.3}$$

Here the roll rate in wind-body axes

$$\begin{aligned} p_w &= (p\cos\alpha + r\sin\alpha)\cos\beta + q\sin\beta \\ q_w &= -(p\cos\alpha + r\sin\alpha)\sin\beta + q\cos\beta \\ r_w &= r\cos\alpha - p\sin\alpha \end{aligned}$$

define both the unsteadiness and spirality of motion: $\dot{\alpha} = (q_w - q_{w_{sp}})/\cos\beta$, $\dot{\beta} = -r_w + r_{w_{sp}}$. The values of $q_{w_{sp}}$, $r_{w_{sp}}$ are the wind-body angular rates in steady state spiral motion and their nondimensional values are usually very small.

The aerodynamic derivative concept has been using for the representation of aerodynamic loads in the equations of motion since the infancy of aviation. It gives good results for conventional aircraft at relatively low incidences but this approach can not be already adequate for high angles of attack conditions in the presence of flow separation and vortex breakdown. The unsteady aerodynamic derivatives in such conditions depends both on the amplitude and on the frequency of oscillations and, therefore, can not be implemented for simulation in a time domain. Some theoretical and practical failings of the aerodynamic derivative concept have been also observed in [42]. In particular, it has been shown that normally neglected angular acceleration effects can be significant for combat aircraft. Nevertheless, the conventional concept is still used in flight dynamics because more adequate alternative methods are now only under construction and are yet unable to satisfy all practical requirements.

3.2 Linear indicial functions

A fundamental study of the unsteady lift on an aerofoil due to abrupt changes in the angle of attack was made by Wagner [90]. The work was extended by Theodorsen who calculated the forces and moments acting on an oscillating aerofoil. Their works made in the 1920s-1930s became classical ones. They have been described in detail in numerous textbooks on aerodynamics [14, 13].

The indicial approach is based on the concept that a characteristic variable $f(t)$, which describes the state of the flow can be linearized with respect to its boundary condition $\epsilon(t)$ if the variation of $f(t)$ is a smooth function of $\epsilon(t)$. In this case $f(t)$ can be represented as the Taylor series expansion about some value of $\epsilon = \epsilon_0$:

$$f(t) = f(0) + \Delta\epsilon \frac{\partial f}{\partial \epsilon}|_{\epsilon=\epsilon_0} + \dots \tag{3.4}$$

If $f(0)$ is zero then

$$f(t) = \Delta\epsilon \frac{\partial f}{\partial \epsilon}|_{\epsilon=\epsilon_0} \tag{3.5}$$

This approximation becomes more accurate at $\Delta\epsilon \to 0$ and is exact when $f(t)$ is a linear function of $\epsilon(t)$. If the response $\frac{\partial f}{\partial \epsilon}$ depends only on the elapsed time as in the case of linear time invariant response than the formal solution for $f(t)$ is

$$f(t) = \tilde{f}(t)\epsilon(0) + \int_0^t \frac{d\epsilon}{d\tau}\tilde{f}(t-\tau)d\tau, \tag{3.6}$$

where $\tilde{f}(t) = \frac{\partial f}{\partial \epsilon}|_{\epsilon=\epsilon_0}$ is the so called "indicial function". If $\tilde{f}(t)$ is known from some computation or experiment then Eq. 3.6 defines the value of $f(t)$ for any schedule of the boundary condition function $\epsilon(t)$.

Following the above mentioned concept, aerodynamic characteristics can be formulated as [59]

$$C_a(t) = C_a(0) + \int_0^t C_{a_\xi}(t-\tau)\frac{d\xi(\tau)}{d\tau}\tau, \tag{3.7}$$

where $a = (X, Y, Z, l, m, n)$, ξ is a vector of aircraft state variables, C_{a_ξ} – the indicial function that can be defined as a transient aerodynamic reaction to a step change in the angle of attack.

In [58] the indicial functions have been identified by means of a procedure, which consists of a combination of the stepwise regression and the maximum likelihood methods. The identification scheme was applied to wind tunnel oscillatory data in pitch for a tailless aircraft and the F-16XL aircraft. Aerodynamic model equations for the longitudinal motion of an aircraft with a horizontal tail were developed in [57] using linear indicial functions. These functions represent responses in the lift for a wing and tail alone and also the interference between these surfaces.

The power of linear indicial theory is in the fact that if a system can be approximated by a linear time-invariant system then knowledge of only indicial functions of this system makes possible to determine its response to any arbitrary variation of boundary conditions (or forcing function). This leads to a significant reduction of computations. Furthermore, in [62] it has been shown that if the indicial function can be approximated by exponential fits than the problem of unsteady aerodynamic prediction is reduced to solving a system of inhomogeneous first order ordinary differential equations. The shortcoming of the linear indicial theory is that it is valid at small perturbations and away from points where the flow structure is changed. Moreover, the aerodynamic model being used together with the flight

dynamic equations leads to an integro-differential system describing the aircraft motion, which is not convenient for classical methods of analysis.

3.3 Nonlinear indicial functions

The nonlinear approach for aerodynamic modelling was formulated by Tobak and his colleagues in [85] and has been under development since the 1980s [83]. The linear indicial response method was modified by introducing the concept of a nonlinear indicial response and a generalized superposition integral, which is a generalization of the linear convolution model (Duhamel convolution integral). The indicial response $\tilde{f}$ is now taken to be a functional $\tilde{f}(\epsilon(\xi), t, \tau)$, where $\epsilon(\xi)$ denotes the dependence on the entire motion history. Thus, Eq. (3.6) is transformed to the following form:

$$f(t) = \tilde{f}(t, \epsilon(0)) + \int_0^t \frac{d\epsilon}{d\tau} \tilde{f}(\epsilon(\xi), t, \tau) d\tau. \tag{3.8}$$

In this formulation the nonlinear indicial function $\tilde{f}(\epsilon(\xi), t, \tau)$ is defined as the following derivative [78]:

$$\tilde{f}(\epsilon(\xi), t, \tau) = \lim_{\Delta\epsilon \to 0} \frac{\Delta f(t)}{\Delta\epsilon} = \lim_{\Delta\epsilon \to 0} \left[\frac{f(\epsilon(\xi) + H(\xi - \tau)\Delta\epsilon) - f(\epsilon(\xi))}{\Delta\epsilon} \right], \tag{3.9}$$

where the step in boundary condition $\Delta\epsilon$ is applied at time $t = \tau$ and H is the Heaviside step function.

Thus, linear (3.6) and nonlinear (3.8) indicial approaches have fundamental distinctions. The nonlinear indicial function $\tilde{f}(\epsilon(\xi), t, \tau)$ has a separate dependence on t and τ and also depends on $\epsilon(\xi)$ rather than linear function which depends only on elapsed time $t - \tau$. This signifies that the nonlinear indicial function can depend on all the past history of the boundary conditions (memory effect).

In practice, in place of $\tilde{f}$ might usually be aerodynamic loads $C_L, C_m, \ldots$ while the boundary conditions $\epsilon(t)$ might be angle of attack, aeroelastic model amplitude, etc. When angle of attack is treated as a boundary condition it is possible to describe a full dependence of $C_L, C_m, \ldots$ by means of Eq. (3.8) for any arbitrary schedule of $\alpha(t)$. It is worth mentioning that this approach is not valid for bifurcation points where the function is not differentiable according to Eq. (3.9).

In order to get round this problem the theory was modified by Tobak [84]. Bifurcation points are considered as discrete points during the aircraft motion at which differentiability is lost. Due to the loss of stability at these points the solution is changing to a new stable equilibrium. If the jump to a new equilibrium occurs in time τ_0, then the integral in (3.8) is split as follows:

$$f(t) = f(t, \epsilon(0)) + \int_0^{\tau_0} \frac{d\epsilon}{d\tau} \tilde{f}(\epsilon(\xi), t, \tau) + \Delta f(t, \epsilon(\tau_0)) + \int_{\tau_0}^{t} \frac{d\epsilon}{d\tau} \tilde{f}(\epsilon(\xi), t, \tau), \tag{3.10}$$

where $\Delta f(t, \epsilon(\tau_0)) = f(\epsilon(\xi), t, \tau_0 + \delta\tau) - f(\epsilon(\xi), t, \tau_0 - \delta\tau)$ at $\delta\tau \to 0$. This representation permits the critical states like bifurcation transitions in static hysteresis to be taken into account. To substantiate the approach, it was shown that it can be derived directly from the Navier-Stokes equations [89].

The nonlinear indicial response theory supposes that the indicial functions should be obtained from numerical computations, experimental tests or by analytical means. A nonlinear indicial response model of the lift coefficient in the case of 1-DOF pitch motion was developed by Reisenthel [78]. The model was based on functional interpolation of the parameterized responses. In this work Eq. (3.8) for the lift coefficient was reduced to the following form:

$$C_L(t) = C_L(0) + \int_0^t \left[\frac{\delta C_L(t-\tau)}{\delta\alpha}\right]_\tau \frac{d\alpha}{d\tau} d\tau. \tag{3.11}$$

where $\left[\frac{\delta C_L}{\delta\alpha}\right]_\tau$ is the local approximation of the indicial function around $\alpha = \alpha_M(\tau)$, where $\alpha_M(t)$ is the reference motion, which was used to determine the indicial response. In this case time partition $[t_{k-1}, t_k)$ is assigned one representative indicial function $\left[\frac{\delta C_L}{\delta\alpha}\right]_k$. A finite number of indicial responses was determined in nodes during the aircraft motion trajectory $\alpha_M(t)$. To determine indicial function at every time instant τ, zero-order, linear, quadratic and spline interpolation schemes were considered. In general, all the considered schemes can be expressed as

$$\left[\frac{\delta C_L}{\delta\alpha}\right]_\tau = \sum_{k=1}^{+\infty} \left[\sum_{p=1}^{+\infty} \left[\sum_{n=1}^{n=N} d_{pnk}(\tau) \left[\frac{\delta C_L}{\delta\alpha}\right]_p^n\right]\right] (H(\tau - t_{k-1}) - H_{\tau - t_k}). \tag{3.12}$$

The development, testing and validation of the nonlinear indicial prediction model require a large amount of unsteady aerodynamic data. Up to that time only a limited number

of experimental investigations were performed. These data unfortunately are not sufficient for generating the required indicial functions and/or critical state responses. Therefore, to calculate indicial functions Reisenthel used the state-space mathematical model which was developed by Goman and Khrabrov [31].

In [48], the Taylor series expansion was applied to approximate the indicial function for a thin aerofoil. Away from the bifurcation points, the indicial function was expressed about zero angle of attack as follows:

$$\begin{aligned} C_{L_\alpha}[\alpha(\xi), t-\tau] &\approx C_{L_\alpha}[\alpha(\tau), t-\tau] = C_{L_\alpha}(0,\infty) + 0.5\frac{\partial^2}{\partial\alpha^2}C_{L_\alpha}(0,\infty)\alpha^2(\tau) - \\ &- F_0(0, t-\tau) - 0.5F_2(0, t-\tau)\alpha^2(\tau) + ..., \end{aligned} \tag{3.13}$$

In order to calculate F_0 and F_2 the Jones' [27] approximation was used:

$$\begin{aligned} F_0 &\approx a_1 e^{-a_2\tau_1} + (\pi - a_1)e^{-a_3\tau_1}, \\ F_2 &\approx b_1(1 - e^{-b_2\tau_1})e^{-b_3\tau_1}, \end{aligned} \tag{3.14}$$

where $\tau_1 = t - \tau$. Coefficients a_i and b_i were defined by fitting experimental (numerically calculated in this paper) data.

It was shown that if a serial expansion approximation of the indicial response is given then the generalized superposition integral can be approximated by an asymptotic expansion, valid for sufficiently slow motions. Finally, a representation for the lift response to an arbitrary motion is given by the equation

$$\begin{aligned} C_L &= C_{L\,am}\dot{\alpha}(t) + C_{L_\alpha}(0,\infty)\alpha(t) + C_{L_{\alpha\alpha\alpha}}\frac{\alpha^3(t)}{6} + \\ &+ \sum_{n=0}^{\infty}\left(I_{n+1}(0)\left[\frac{d\dot{\alpha}}{dt}(t)\right] - I_{n+1}(t)\left[\frac{d\dot{\alpha}}{dt}(0)\right]\right) + \\ &+ 0.5\sum_{n=0}^{\infty}\left(J_{n+1}(0)\left[\frac{d^n(\alpha^2\dot{\alpha})}{dt^n}n(t)\right] - J_{n+1}(t)\left[\frac{d^n(\alpha^2\dot{\alpha})}{dt^n}n(0)\right]\right), \end{aligned} \tag{3.15}$$

where $C_{L\,am}$ is an apparent mass term which accounts for the noncirculatory part of the lift response, $I_n = I_{0n}$ and $J_n = I_{2n}$, $I_{in}(t) = \int_{n\,\overbrace{times}} \int F_i(\tau_1)d\tau_1...d\tau_1|_{\tau_1=t}$.

In [44], Jenkins and Hsia used experimental data for the 65^o delta wing, which was forced harmonically in roll to determine the indicial functions. This interpretation of the nonlinear indicial response approach resulted in a reasonable practically realizable technique, which is valid for sufficiently slow motion. For harmonic motion this series representation diverges for frequencies greater then the slowest varying exponential involved in the corresponding indicial function.

3.4 Fourier functional analysis

One more simplification of the nonlinear indicial function approach was proposed in [15]. The Fourier transformation is used to relate the aerodynamic response to a step change in angle of attack of a wing with aerodynamic loads obtained in large-amplitude forced oscillations at high angles of attack with different frequencies.

As shown in [85] unsteady aerodynamic lift for arbitrary planar motion can be presented as the following integral:

$$C_L(t) = C_L(0) + \int_0^t C_{L_\alpha}\left[\alpha(\xi), q(\xi), t, \tau\right] \frac{d\alpha}{d\tau} d\tau + \frac{l}{V_\infty} \int_0^t C_{L_q}\left[\alpha(\xi), q(\xi), t, \tau\right] \frac{dq}{d\tau} d\tau, \quad (3.16)$$

where $\xi \in [0, \tau]$.

To be used in practice, the integrals in Eq. (3.16) need to be simplified. Assuming that α and q are analytical functions in the vicinity of $\xi = \tau$ they are expanded in the Taylor series at $\xi = \tau$ with only zero and first order terms being considered. For further simplification the indicial response is considered as a function of the elapsed time $t - \tau$. Furthermore, when in wind tunnel testing the pitch axis coincides with the center of gravity, the q effect cannot be separated from the $\dot{\alpha}$ effect. That is why $\dot{\alpha}$ is used instead of q. The effect of $\ddot{\alpha}$ is included in the response without lag like the apparent mass effect in 2D incompressible flow. Thus (3.16) is reduced to

$$\begin{aligned} C_L(t) &= C_L(0) + C_{L_{zlr}} + \int_0^t C_{L_\alpha}[t-\tau, \alpha(\tau), \dot{\alpha}(\tau)] \frac{d\alpha}{d\tau} d\tau \\ &+ \frac{l}{V_\infty} \int_0^t C_{L_q}[t-\tau, \alpha(\tau), \dot{\alpha}(\tau))] \frac{d\dot{\alpha}}{d\tau} d\tau, \end{aligned} \quad (3.17)$$

where $C_{L_{zlr}}$ includes the effect of apparent mass, which does not depend on the past history of motion [13] and, therefore, was moved out from the time integral.

The main problem in calculation of the integrals in Eq. (3.17) is to find a form of the analytical representation of the indicial responses C_{L_α} and C_{L_q} and relate them to responses in the forced oscillation tests. In the frame of linear theory of 2D incompressible flow Theodorsen (see [14]) found that the unsteady lift of a slender aerofoil undergoing small amplitude oscillatory motion can be presented as a sum of two parts: non-circulation and circulation lifts. The last component is presented as a product of amplitude $A(\alpha, \dot{\alpha})$ and phase $\Phi(k)$ functions. The amplitude function depends only on α and $\dot{\alpha}$ while the phase

function defines lag between response and excitation and depends only on the reduced frequency k. It is the phase function which considers the past history of the motion.

$$C_L = C_{L_0} + C_1\{\underbrace{E_{11}\dot{\alpha}_1 + E_{21}\ddot{\alpha}_1}_{\text{noncirculation lift}} + \underbrace{A(\alpha,\dot{\alpha})\Phi(k)}_{\text{circulation lift}}\}. \tag{3.18}$$

For large amplitude oscillations Eq. (3.18) is unable to describe the nonlinear behaviour of the response because of dynamic effects in the flow structure changing. These effects can be considered by introducing high order terms of the same structure as in the linear case:

$$C_L = C_{L_0} + \sum_{j=1}^{M} A_j(\alpha,\dot{\alpha})\Phi_j(k). \tag{3.19}$$

Taking into account Eq. (3.18) and (3.19) Lan suggested the following approximation for response due to large amplitude motion:

$$C_L = A_0(k) + \sum_{j=1}^{M} C_j\left(E_{1j}\dot{\alpha} + E_{2j}\ddot{\alpha}\right) + \sum_{j=1}^{M}\sum_{m=0}^{j} C_j\left(H_{(m+1),j}\dot{\alpha}^m\alpha^{(j-m)}\right)(1 - PD_j) \tag{3.20}$$

where PD_j – 2nd order Pade approximation, $\dot{\alpha}_j = ik\Delta\alpha^j e^{-ijk\bar{t}}$ and $\ddot{\alpha}_j = -k^2\Delta\alpha^j e^{-ijk\bar{t}}$.

Equation (3.20) is the general form of the nonlinear unsteady lift model. It interpolates a set of experimental relations during large amplitude oscillatory motion with different frequencies. At $M = 1$, Eq. (3.20) reduces to the classical dependence, and each parameter of this dependence can be expressed analytically, but high order terms are semi-empirical approximations. To determine the amplitude and phase functions, Fourier functional analysis is used. The motion is considered to be harmonic oscillations. Then, using complex notation, experimentally measured responses to the variation of $\alpha(\bar{t}) = \Delta\alpha e^{ik\bar{t}}$ are presented by the Fourier series

$$C_L(t) = A_0 + \sum_{j=1}^{M}(A_j - iB_j)e^{ijk\bar{t}}, \tag{3.21}$$

which coefficients are related to those in (3.20) by means of some kind of regression technique.

For the case of arbitrary motion, Lan obtains the following representation for the re-

sponse in the time domain:

$$\begin{aligned} C_L(\bar{t}) \;=\; & C_{av} + \sum_{j=1}^{M} C_j A(\alpha,\dot{\alpha})(1 - a_{1j}e^{-a_{3j}\bar{t}} - a_{2j}e^{-a_{4j}\bar{t}}) + \sum_{j=1}^{M} C_j \left(E_{1j}\dot{\alpha}_j + E_{2j}\ddot{\alpha}_j\right) + \\ & \sum_{j=1}^{M} C_j \int_0^{\bar{t}} \frac{dA(\alpha,\dot{\alpha})}{d\alpha}(1 - a_{1j}e^{-a_{3j}(\bar{t}-\tau)} - a_{2j}e^{-a_{4j}(\bar{t}-\tau)})\frac{d\alpha}{d\tau}d\tau + \\ & \sum_{j=1}^{M} C_j \int_0^{\bar{t}} \frac{dA(\alpha,\dot{\alpha})}{d\dot{\alpha}}(1 - a_{1j}e^{-a_{3j}(\bar{t}-\tau)} - a_{2j}e^{-a_{4j}(\bar{t}-\tau)})\frac{d\dot{\alpha}}{d\tau}d\tau, \end{aligned} \tag{3.22}$$

where $A(\alpha,\dot{\alpha}) = \sum_{m=0}^{j}\left(H_{(m+1),j}\dot{\alpha}^m\alpha^{(j-m)}\right)$ – the amplitude function and

$C_{av} = \frac{1}{M}\sum_{m=1}^{M}(a_1 k_{eq}(\tau|_{\alpha=\alpha_0}) + a_0)$ – the contribution of the zero term $A_0(k)$ of the Fourier expansion. Thus, in this representation a nonlinear response to large amplitude motion is fully determined by a set of constant coefficients E_{ij} and H_{ij}.

Since the amplitude functions are determined in the frequency domain using complex algebra, an arbitrary motion is locally represented by a cosine function $\alpha_1(\tau) = \alpha_0 + \Delta\alpha\cos(k_{eq}\tau + \phi_{eq})$ at any time, where α_1 describes an arbitrary motion, α_0 and $\Delta\alpha$ – the mean angle and amplitude of the oscillations that were used for the determination of the unknown model parameters. Having calculated the equivalent frequency k_{eq} and the phase ϕ_{eq} the lift response to arbitrary motion can be calculated using Eq. (3.22).

This approach was applied in [45] for the representation of the drag, lift and pitch moment coefficients of the F-18 aircraft. Also, the method was utilized in [5] for the representation of unsteady lift of a 70^o delta wing. The results demonstrate that this method is capable of modelling nonlinear responses with a large hysteresis effect. Aerodynamic models identified using the large amplitude oscillation test data predict rather well the responses to small amplitude oscillations and to a ramp-type motion.

The nonlinear indicial response method is the most rigorous approach to unsteady aerodynamic modelling. However, in practical applications it presents a considerable challenge because special experimental or theoretical techniques for determining the nonlinear indicial responses are required. Analysis of existing works in this area reveals that numerous simplifying assumptions are made that lead to the lack of accuracy and reduce the scope of applicability of such models. The final flight dynamics model is formulated in the class of integro-differential equations, which leads to significant complications in the motion simulation, stability analysis and control law design. This fact really limits the applicability of

the approach only on calculation of responses to predefined incidence variation.

3.5 Volterra series

In [77, 69] the Volterra theory of nonlinear systems was applied to describe unsteady aerodynamic effects. The theory asserts that a time invariant nonlinear system can be modelled as an infinite sum of multidimensional convolution integrals. Let $y(t)$ be the output (response) of the system to input $x(t)$. Then the Volterra series expansion of $y(t)$ with respect to $x(t)$ is given by

$$y(t) = \sum_{n=1}^{\infty} \underbrace{\int_0^t \dots \int_0^t}_{n} K_n(t-\tau_1, \dots, t-\tau_n) x(\tau_1) \dots x(\tau_n) d\tau_1 \dots d\tau_n, \tag{3.23}$$

where K_n is the n-th order Volterra kernel. The Volterra series approach provides a mathematically rigorous approximation technique to describe nonlinear systems but known attempts of practical application faced the challenge of kernel identification.

Some progress in kernel identification using experimental data was achieved in [69] where a Neural Network model equivalent to a discrete time Volterra series truncated to 2nd order was used. In [77] the unknown kernels were expanded using some known basis function set $\mu_k^{(n)}$ as follows:

$$K_n(t_1, t_2, \dots, t_n) = \sum_{k=1}^{N} c_k^{(n)} \mu_k^{(n)}(t_1, t_2, \dots, t_n), \tag{3.24}$$

The unknown coefficients $c_k^{(n)}$ of the basis function were identified then using multiple time histories $\{x(t), y(t)\}$ describing the system behavior.

This method was used to identify the first and second order Volterra kernels for the aerodynamic loads acting on a wing during pitch oscillations. A set of functions consisting of nine decaying exponentials was considered as the base functions for the first order kernel. For the two-dimensional kernel this set was extended to a 10×10 matrix. Identification of the higher order terms presents too many difficulties and seems unlikely to be achieved in practice.

The fact that the identification procedure was developed only for kernels up to the second order restricts possible applications only to systems with weak nonlinearities. Similar

to the indicial functions approach, the Volterra series aerodynamic model having been coupled with equations of motion will result in an integro-differential system, which is extremely complicated for analysis.

3.6 State-space representation

The approximate approach based on the application of nonlinear dynamic systems for unsteady aerodynamic modelling at high angles of attack was proposed in [39, 31]. In order to describe the dynamic flow effects affecting the integrated aerodynamic loads internal state variables are introduced. The behaviour of these variables is governed by a nonlinear dynamic system, which is designed in such a way to reproduce the physical properties of the flow. In some cases, a physical meaning is ascribed to the state vector, for example, the coordinate of the vortex burst point or flow separation point. It was shown that their positions during changing of incidence can be described rather accurately by a first order differential equation.

The state-space approach postulates [39, 31] that in general case the internal flow dynamics can be approximated by the following n-dimensional system:

$$\frac{d\mathbf{x}}{dt} = \mathbf{g}(\mathbf{x}, \xi, \dot{\xi}), \tag{3.25}$$

where the vector $\mathbf{x} \in \mathbf{R}^n$ describes the state of separated and vortex flow about an aircraft and the vector $\xi = (\alpha, \beta, p, q, r, \delta)^T$ is composed of the aircraft motion kinematical parameters and aerodynamic controls. The aerodynamic coefficients $\mathbf{C} = (C_X, C_Y, C_Z, C_l, C_m, C_n)^T$ depend not only on the aircraft motion parameters ξ, $\dot{\xi}$ but also on the internal state variables $\mathbf{x}$:

$$\mathbf{C} = \mathbf{f}(\mathbf{x}, \xi, \dot{\xi}). \tag{3.26}$$

The state-space representation (3.25) – (3.26) is more appropriate for flight dynamics problems since it retains the state-space form of the aircraft motion equations. There is only an increase in dimension of the mathematical model, while the possibility of numerical simulation and stability analysis by means of classical methods is retained contrary to the case of the indicial functions approach, which results in the equations of motion being represented by a set of integro-differential equations. The state-space representation can

naturally model bifurcations [4] in flow equilibrium states for outlining the static hysteresis, model self oscillation flow regimes, involve different physical considerations like interference effects between different aerodynamic surfaces [54], etc.

The determination of the system (3.25) structure and the definition of the aerodynamic coefficients representation (3.26) presents a serious challenge. But it is possible to take into account experimentally observed flow dynamics processes, qualitative solutions resulting from simple analytical models, etc. For example, analysis of the vortex breakdown point behaviour above the triangular wing, visualized in a water tunnel, showed that vortex breakdown dynamics can be described by a very simple first order linear differential equation [39]. A similar model can be applied to the process of trailing edge flow separation above an aerofoil and a large aspect ratio wing.

Recently a number of works utilizing modifications of the state-space approach for high incidence unsteady aerodynamics modelling has been published. Thus in [31, 32, 33], the simple form for the mathematical model (3.25) – (3.26) implementation was proposed. Since two vortices arising on the apex of a highly swept delta wing dominate in aerodynamic load formation, the coordinates x_L and x_R of vortex breakdown points were considered as state variables. In the case of symmetrical flow structure, the vortices burst position is described by a single coordinate x which is governed by the first order linear differential equation

$$\tau_1 \dot{x} + x = x_0(\alpha - \tau_2 \dot{\alpha}), \tag{3.27}$$

where the nonlinear function x_0 is a static position of vortex breakdown that depends on the angle of attack, parameters τ_1 and τ_2 are characteristic time constants. These constants may be different for different flow structures, therefore, they can be functions of the angle of attack α.

The general representation for the normal force coefficient (3.26) (here $\dot{\alpha} \equiv q$ due to dynamic rig kinematics) is simplified supposing that dependency on the internal variable x can be separated by introducing the normalized weight function $0 \leq g(x) \leq 1$:

$$C_N = \left(C_{N_1}(\alpha) + \frac{\bar{c}}{V} C_{N_{q_1}} q\right) g(x) + \left(C_{N_0}(\alpha) + \frac{\bar{c}}{V} C_{N_{q_0}} q\right)(1 - g(x)), \tag{3.28}$$

where the functions $C_{N_1}(\alpha)$, $C_{N_0}(\alpha)$ are analogues to static dependencies of the normal force coefficient for fixed flow structures corresponding to $x = 1$ (unburst vortex flow) and

$x = 0$ (fully separated flow), respectively. The unknown model parameters were identified using small and large amplitude oscillation experimental data for the 70^o delta wing. Rather accurate prediction of the aerodynamic derivatives as well as responses to small and large amplitude variations of angle of attack was reached.

In [8, 4] linear equation (3.27) was extended to the third order polynomial form

$$\frac{dx}{dt} = k_0 + k_1(\alpha)x + k_2(\alpha)x^2 + k_3(\alpha)x^3 \tag{3.29}$$

that introduced a capability to model static hysteresis typical for many separated flows. It is seen that using the N^{th} order polynomial as the right hand side function results in the possibility of multiple (up to N) equilibrium points at each angle of attack. A technique capable of building the right hand side function, which reproduces the experimental static dependence was proposed. The model was verified using large amplitude oscillatory data for a high aspect ratio wing with NACA-0018 aerofoil. It was assumed that the flow separation starts from the trailing edge and extends to the leading edge with an increase in the angle of attack. The state variable x was considered as the position of the upper boundary of the separated flow region. The results of simulation demonstrated good agreement with experimental data both in static and in dynamic conditions.

In [23], Fan and Lutze used the following first order equation in order to describe the dynamics of the flow separation point:

$$\tau_1 \frac{dx}{dt} + x = x_0 \left(\alpha - \tau_2 \dot{\alpha} - \tau_3 q(\alpha - \alpha^*)\right), \tag{3.30}$$

where $x_0(\alpha) = \dfrac{1}{1 + e^{\sigma(\alpha - \alpha^*)}}$ is the approximation of the static dependence of the flow separation or vortex breakdown position on the angle of attack, and parameter σ is used to vary the shape of x_0. Contrary to Eq. (3.27), the additional term $\tau_3 q(\alpha - \alpha^*)$ is included to take into account the effect of pitch up (down) rate, which causes the local angles of attack to increase (decrease) along the chord. The lift coefficient is presented as the Taylor series expansion with respect to the kinematic parameters:

$$C_L(x, \alpha, q) = C_{L_0} + \frac{\partial C_L}{\partial \alpha}\alpha + \frac{\partial C_L}{\partial q}q + \frac{1}{2}\left[\frac{\partial^2 C_L}{\partial \alpha^2}\alpha^2 + \frac{\partial^2 C_L}{\partial q^2}q^2 + 2\frac{\partial C_L}{\partial \alpha \partial q}\alpha q\right] + \ldots \tag{3.31}$$

For a full aircraft configuration consisting of different elements which generate both vortical (highly swept strakes, fore-bodies, leading-edge wing extensions) and separated

(moderately swept wings and tail surfaces) flow fields, the model was extended to take into account interaction between these two flow types [24, 25]:

$$\begin{aligned} \tau_{x_1}\frac{dx}{dt}+x &= x_0(\alpha-\tau_{x2}\dot{\alpha}) \\ \tau_{y_1}\frac{dy}{dt}+y &= \mu x+(1-\mu)y_0(\alpha-\tau_{y2}\dot{\alpha}) \\ C_L(x,\alpha,q) &= C_{L_0}+C_{L_\alpha}(x,y)\alpha+C_{L_q}q+ \\ &+ \frac{1}{2}\left[C_{L_{\alpha\alpha}}(x,y)\alpha^2+C_{L_{qq}}(x,y)q^2+2C_{L_{\alpha q}}(x,y)\alpha q\right]. \end{aligned} \tag{3.32}$$

The mathematical model (3.30)-(3.31) was identified using experimental data for a NACA-0015 aerofoil pitching up at a constant rate and for the 70^o delta wing in sinusoidal pitch oscillation. The model (3.32) for the F-18 aircraft was identified using constant rate pitch up and down experimental dependencies. The results of the modelling presented in [23, 24, 25] show that these models are able to predict aerodynamic responses with a rather good accuracy but it seems that the experimental data set consisting of a few responses for each model was used for identification therefore it is difficult to appreciate the quality of modelling at more extensive ranges of manoeuvers.

In [80] the state-space model was applied for identification of the lateral-directional behavior of the C-160 aircraft from the flight test data at stall and post-stall regimes. Nonlinear behaviour of the lift and drag coefficients was approximated using Kirchhoff's theory of flow separation:

$$\begin{aligned} C_L &= C_{L_\alpha}\left[(1+\sqrt{x})/2\right]^2\sin\alpha \\ \Delta C_D &= C_{L_\alpha}\left[(1-\sqrt{x})/2\right]^2\sin\alpha\tan\alpha. \end{aligned} \tag{3.33}$$

The position of the flow separation point was described by the first order differential equation

$$\begin{aligned} \tau_1\frac{dx}{dt}+x &= x_0(\alpha-\tau_2\dot{\alpha}) \\ x_0(\alpha) &= \frac{1}{2}\left[1-\tanh(\sigma(\alpha-\alpha^*))\right]. \end{aligned} \tag{3.34}$$

Here the parameters have the same sense as in (3.30). The asymmetry of flow separation on two wing panels was accounted in the model as follows:

$$\begin{aligned} C_l &= C_{l0}+C_{l\beta}\beta+C_{lp}p+C_{lr}r+C_{l\delta_r}\delta_r+C_{l\delta_a}\delta_a+\frac{1}{2b}\left(C_{N_L}-C_{N_R}\right) \\ C_n &= C_{n0}+C_{n\beta}\beta+C_{np}p+C_{nr}r+C_{n\delta_r}\delta_r+C_{n\delta_a}\delta_a+\frac{1}{2b}\left(C_{c_L}-C_{c_R}\right). \end{aligned} \tag{3.35}$$

The results demonstrated that the model (3.35) was able to identify the longitudinal and lateral dynamics in stall.

3.7 Discussion

The state-space approach was recently evaluated by a number of researchers and was successfully applied to some practical flight dynamics problems. It was confirmed that the application of dynamic systems provides a rather simple and accurate tool for the time domain modelling and prediction of arbitrary aerodynamic responses at high angles of attack conditions with flow separation and vortex breakdown.

For the identification of unsteady aerodynamic models at high angles of attack a large amount of experimental data covering the whole range of possible aircraft manoeuvers is required. Such data is available now both for simple configurations such as delta wings and for full aircraft configurations. Using this data a number of unsteady aerodynamic models have been developed applying variations of these technique.

The main problem in the implementation of the nonlinear dynamic system method is caused by an uncertainty of dynamical model structure, the dimension of the internal state vector and a nonlinear transformation for the aerodynamic coefficients. An other problem arises in case of complex configurations when a lot of separation zones and vortices exist. To describe complex dynamics of such a hybrid flow, the state vector of higher dimension is required. Moreover, nowadays it is not clear how to describe the interaction between these components. Physical analysis sometimes can significantly help to select dominating components and simplifying factors. Ascribing a meaningful sense to the state variables is simultaneously a merit and a demerit of this approach because it requires "low-level" consideration. It can help in relatively simple cases and overload the system in the case of complex configurations. Thus, in the case of delta wing non-planar motion at least two state variables are required for the description of the breakdown dynamics of two vortices that results in additional difficulties in the model parameter/structure identification. Sometimes it is better to decompose total aerodynamic loads into several parts with different characteristic times [71, 8] of flow adjustment, for example, loads generated by unburst vortex flow and loads generated by vortex breakdown processes, which can be described by a differential equation.

The method, which takes into account flow dynamic properties dealing with "higher" level effects such as integral loads is considered in this thesis as a baseline for aerodynamic

modelling. On the basis of physical consideration, the aerodynamic loads are assumed to be partitioned into components having different dynamic properties and consequently different characteristic time constants. These components result from different flow structures contribution to the entire loads, for example, attached, separated, attached vortical flow or flow with partially broken vortices. To describe their dynamics, nonlinear differential equations which are able to reproduce both "weak" and "strong" nonlinearities and bifurcation points crossing are used. The general form of this approach and identification procedure is considered in Chapter 4. Its practical applications are discussed in Chapter 5 for the case of weak nonlinearities and in Chapter 6 for the case when static hysteresis exists. The validity of the proposed approach is verified by comparison with the experimental data.

Chapter 4

Modelling of high incidence aerodynamic loads using dynamic systems

Aerodynamic forces and moments acting on an aircraft at high angles of attack and at high angular rates due to vortical and separated flow adjustment processes depend on all motion history. Vortical and separated flow, rearranging during the motion, interacts with the aircraft that results in complicated flow dynamics and consequently in vagueness in the aerodynamic loads. The frequency and amplitude dependence of the aerodynamic derivatives also result from the internal vortical flow dynamics. Analysis of experimental data shows that the dynamic effects due to vortical flow adjustment processes are significant in the frequency range of aircraft rigid body dynamics. Under these conditions, the conventional representation dealing with the instantaneous values of the state variables becomes invalid. That is why the representation of the aerodynamic loads model by means of the dynamic system has been found more appropriate in the presence of vortex breakdown processes. Moreover, dynamic representation of the aerodynamic model is very suitable for aircraft dynamics simulation and stability analysis.

This chapter is devoted to the problem of mathematical modelling of aerodynamic characteristics at vortical and separated flow conditions. The model structure, the method of identification of the characteristic time constants and other unknown parameters are

suggested. To verify the approach, mathematical models of aerodynamic force and moment coefficients are developed and discussed in the subsequent chapters. Comparisons of the experimental data and the results of simulation both for the longitudinal and lateral motion are then presented to demonstrate the models' capabilities.

4.1 Aerodynamic loads partitioning

The influence of oscillation frequency and amplitude on aerodynamic derivatives is directly related to the internal dynamics of vortical flow. The example of the "in-phase" and "out-of-phase" aerodynamic derivatives for the 65^o delta wing with central body is given in Fig. 4.1. These derivatives were obtained using experimental data in pitch oscillations with different frequencies and amplitude $\Delta\Theta = 3^o$. One can see a strong dependence of aerodynamic derivatives on the frequency resulting even in a change of their sign. This effect usually occurs in the region of angles of attack and sideslip where the process of vortex breakdown takes place.

In order to estimate the influence of dynamic flow properties on resulting aerodynamic

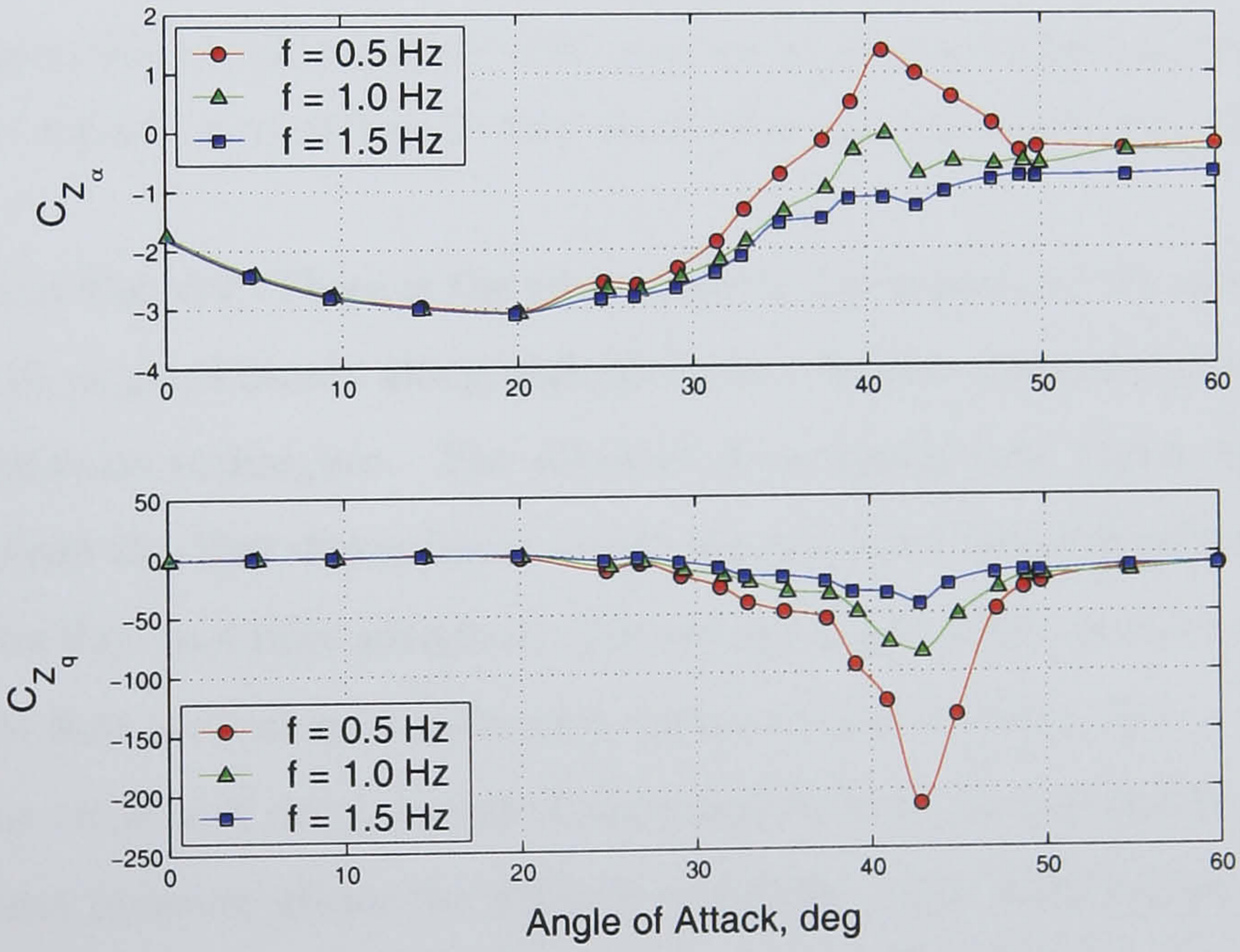

Figure 4.1: Example of aerodynamic derivatives obtained from small amplitude pitch oscillations.

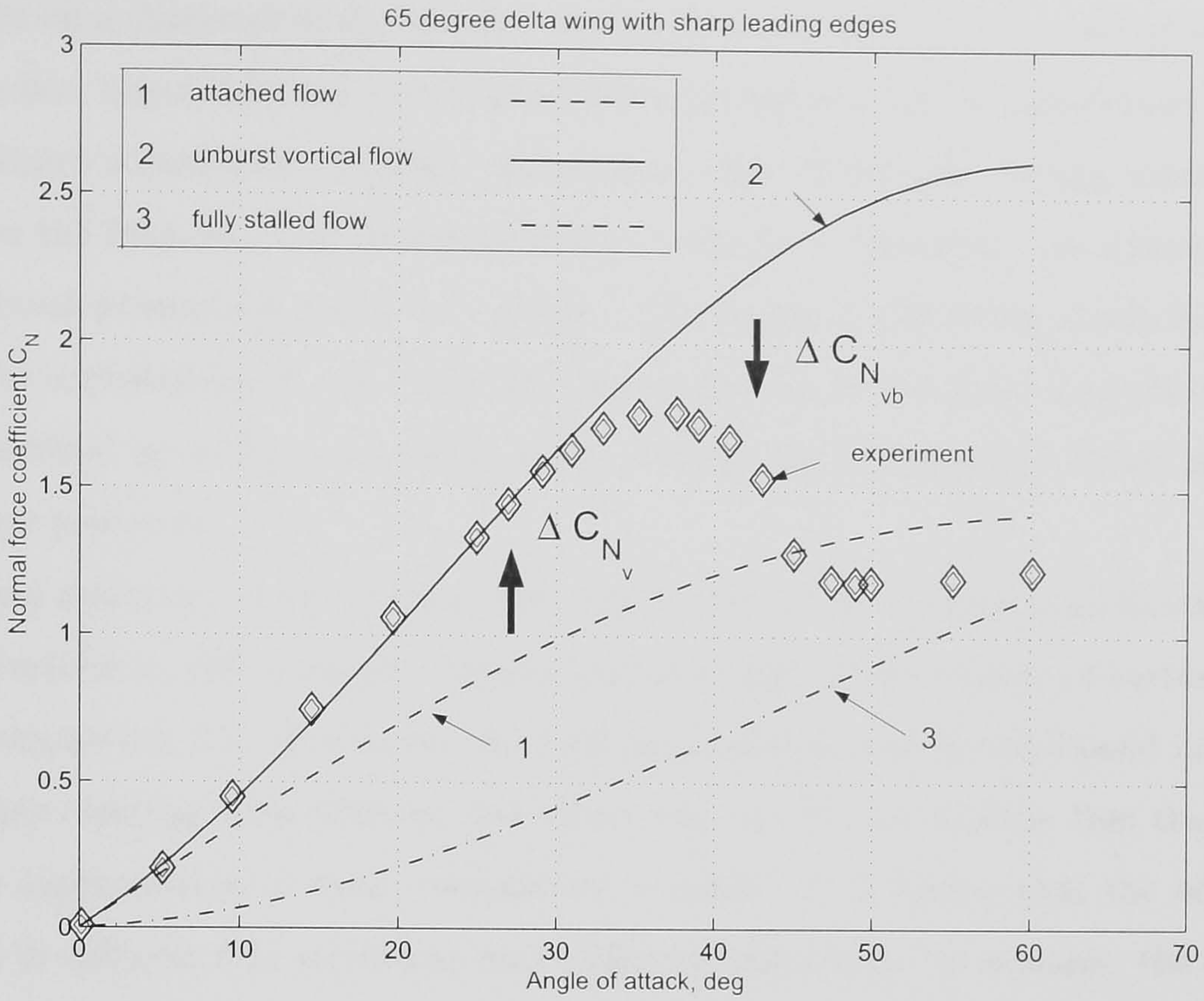

Figure 4.2: Normal force coefficient of 65^o delta wing corresponding to different flow structures: 1 - attached flow, 2 - unburst vortical flow, 3 - fully stalled flow and experimental statics - "diamonds".

loads one looks at Fig. 4.2. There is the experimental dependence of the normal force coefficient C_N on the angle of attack along with the static dependencies of C_N calculated using different approximate techniques. The attached flow model (the vortex lattice method) was used to obtain the first dependence, which characterizes the normal force that would be present if the flow was fully attached. The second dependence would take place in the unburst vortical flow according to Polhamus vortex suction analogy theory [76]. The third dependence was computed using a conical approximation of the Kirchhoff model with the region of constant pressure above the wing. It would be in the fully stalled flow.

The vortices generated by a delta wing leading edge produce the increment ΔC_{N_v} in the normal force in comparison with the attached flow model (case 1). The vortex breakdown processes, which start at approximately 30^o results in the normal force decrement $\Delta C_{N_{vb}}$ in comparison with the unburst vortical flow. Finally, when the vortices are fully broken (at $\alpha \geq 45^o$) the aerodynamic loads tend to the fully stalled case (3). This simple model

sheds light on a character of the aerodynamic loads variation due to flow structure change. Since the flow separation and vortex breakdown processes result in considerable delays in flow structure adjustment, unsteady aerodynamic derivatives are strongly nonlinear and depend on the frequency and amplitude of the oscillations. Relatively low dynamics of the vortices burst points lead to the time delay in the change of the aerodynamic loads. That is why the contribution of the vortex breakdown process to the total force/moments has to be described by a dynamic system which reflects the characteristic times of the flow adjustment processes.

Internal dynamics of the vortical flow can be described without consideration of the internal variable x with a definite physical meaning like the coordinate of vortex burst or the flow separation [31]. To do this, the total aerodynamic load is partitioned into several components resulting from different flow structures, and the assumption that the resulting load is a superposition of these components is made. It is known that the adjustment processes in different flow structures have different time scales, for example, the dynamics of vortex breakdown is much slower than the dynamics of unburst vortical flow or vortex-free attached flow. Taking into account these facts the following empirical model structure is postulated in the thesis: a total aerodynamic load can be represented as the sum of the "fast" and "slow" components, namely, the component for the attached vortical flow and the component describing the vortex breakdown dynamics, respectively. The first one is treated as an inertialess component while the second one is dynamic. All unsteady and nonlinear behaviour is amassed in variation of the dynamic component C_{dyn}. Thus, for example, in the case of longitudinal motion the force/moment coefficients can be represented by the following equation:

$$C(t) = C_{att}(\alpha, \beta) + C_{\bar{\dot{\alpha}}_{att}}(\alpha, \beta)\frac{\bar{c}}{2V}\dot{\alpha} + C_{dyn}, \tag{4.1}$$

where $C_{att}(\alpha, \beta)$ is the force coefficient which would be in the case of unburst vortical flow, $C_{\dot{\alpha}_{att}}(\alpha)$ is the complex of unsteady aerodynamic derivatives.

To describe the behaviour of the dynamic component, which is the result of vortex breakdown processes, the following nonlinear dynamic equation is used:

$$\frac{dC_{dyn}}{dt} = \frac{2V}{\bar{c}}\sum_{i=0}^{n} k_i \left(\Delta C(\alpha, \beta) - C_{dyn}\right)^i, \tag{4.2}$$

where $\Delta C(\alpha, \beta) = C_{st}(\alpha, \beta) - C_{att}(\alpha, \beta)$, k_i are coefficients of the expansion and n is the number of terms in the right hand side polynomial function. Typical dependencies of the mathematical model components as well as the experimental and simulated responses are shown in Fig. 4.3.

Static dependence of the force/moment coefficient is measured during the experiment, the unburst vortical flow component $C_{\alpha_{att}}(\alpha, \beta)$ can be calculated using numerical methods such as the vortex lattice, the Polhamus vortex suction analogy method or it can be parameterized and identified as in [33]. This dependence is the analogy of the envelope function, which was used in [33] to represent the normal force coefficient value at $x = 1$ corresponding to the attached vortical flow conditions.

If we consider only the first term in (4.2) we will have the same equation as was used in [39, 31, 32] to describe the behaviour of the internal variable x. The additional second and third terms allow the modelling equation to take into account the nonlinear effects of

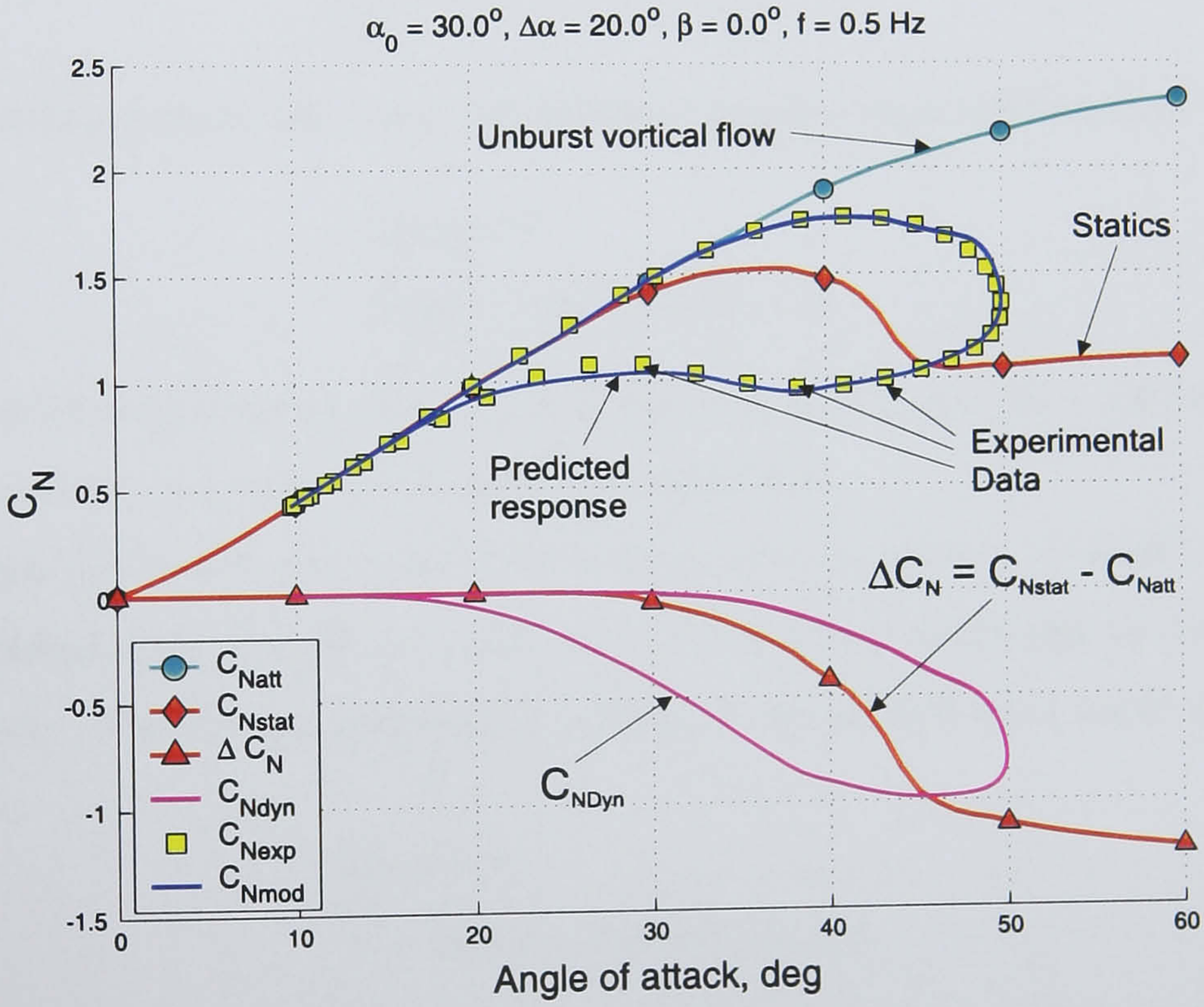

Figure 4.3: Typical experimental and predicted aerodynamic responses.

the amplitude of oscillation. In order to represent bistable static hysteresis, it is required to keep four terms ($n = 3$) in equation (4.2) at least in the non-uniqueness region. The technique for the specification of the unknown parameters in equation (4.2) is suggested in this thesis both for the case of unique static dependence (this Chapter) and bistable static hysteresis (Chapter 6). It is shown there that model (4.1)–(4.2) is suitable both for dynamic and for static hysteresis simulation.

The nonlinear terms in (4.2) allow the simulation of changes of the characteristic time constant $\tau_1 = 1/k_1$ subject to the distance from stable state (third order term) and the different convergence rate from different sides of the stable state (second term). This may be useful to describe the convergence from regions with qualitatively different flow structures, for example, from the deep stall or from the region with unburst vortical flow.

When coefficients k_i in (4.2) are being determined the static condition has to be fulfilled:

$$\sum_{i=0}^{n} k_i \left(\Delta C(\alpha,\beta) - C_{dyn}\right)^i = 0 \,. \tag{4.3}$$

If there is no hysteresis in the static dependence the following condition must be met:

$$\begin{aligned} &k_0(\alpha) = 0 \\ &k_2(\alpha)^2 - 4k_3(\alpha)k_1(\alpha) < 0 \,. \end{aligned} \tag{4.4}$$

The first condition guarantees that the (4.3) has solution $C_{dyn}(\alpha,\beta) = \Delta C(\alpha,\beta)$ and the second one assures that there are no other real solutions.

The terms $k_2(\alpha) \neq 0$ and $k_3(\alpha) \neq 0$ while $k_0(\alpha) = 0$ produce a "weak" nonlinearity which transforms only the effective time scale (local slope) depending on the amplitude of the motion. The strong nonlinearity leading to static hysteresis needs the following conditions:

$$\begin{aligned} &k_0(\alpha) \neq 0 \\ &D = k_2^2(\alpha) - 4k_3(\alpha)k_1(\alpha) \geq 0 \,. \end{aligned} \tag{4.5}$$

The slope of the curve $\frac{d\Delta C}{dt}(\Delta C)$ in the equilibrium point C_0 (Fig. 4.4) defines the characteristic time scale τ: $\tan\phi = -k_1 = -1/\tau$. In the case of a "strong" nonlinearity an additional stable equilibrium ΔC_1 can appear, signifying the onset of static hysteresis. It is clearly seen from the sketch that the effective time scale depends on the distance between a stable state and a current value of C_{dyn}.

In contrast to the described case, the internal state variable x in [39, 31, 32] was driven by a linear dynamic equation while a nonlinearity was introduced in the model through the dependance of total load on the internal state variable. Such an approach was unable to reproduce possible changes in the time constants and the variation of rates of convergence to the static state. It was implied that the characteristic time constant at any x is the same as at $x = x_{stat}$. This fact is illustrated by thin line in Fig. 4.4.

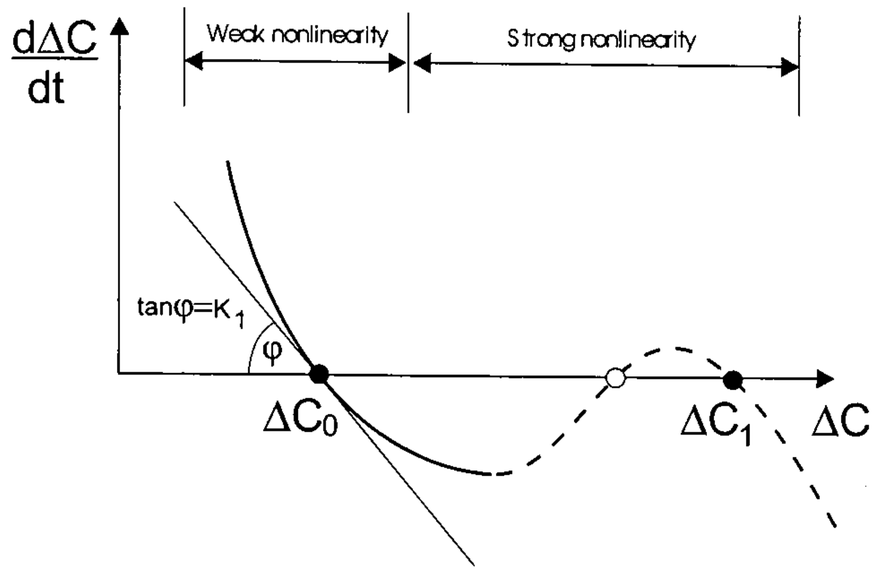

Figure 4.4: Nonlinear dynamic equation and characteristic time scales.

The mathematical model (4.1)–(4.2) includes a set of unknown functions of the angle of attack and sideslip such as $k_i(\alpha, \beta)$ or $C_{att}(\alpha, \beta)$. During the research, different strategies of the model parameters identification were sampled. For example, in the beginning, when a limited amount of experimental data for the 70^o delta wing was available, all unknown functions were parameterized at several nodes, and identified using the whole set of time responses. In this case, the identification procedure consisted in the direct minimization of the value of the discrepancy Φ between the experimental and predicted responses:

$$\Phi(\mathbf{p}) = \frac{1}{NM} \sum_{k=1}^{M} \sum_{i=1}^{N} \left[C_k^{exp}(t_i) - C_k^{mod}(t_i, \mathbf{p}) \right]^2, \tag{4.6}$$

where $\mathbf{p}$ is the vector of unknown parameters, N is the number of experimental dependencies, M is the number of sampling points. A set of experimental responses during small amplitude ($\Delta\alpha = 3^o$) oscillations was used for the preliminarily identification of $k_1(\alpha)$ dependence. The function $C_{att}(\alpha)$ was estimated using the Polhamus method, $k_2(\alpha) \equiv 0$ and $k_3(\alpha) \equiv 0$ were fixed. After determining $k_1(\alpha)$ providing a minimum to the cost function, the large amplitude experimental responses were added, and all other functions were released. Then the cost function defined using the whole set of experimental data was minimized again.

Normally, the model contained 20 to 30 unknown parameters, and the final identification of the unknown functions required significant effort and time even being equipped with

such a powerful dynamic system identification tool as PIIMTM [34]. The minimization procedure for the cost function (4.6) is complicated by the fact that its surface can have a complex geometry, containing multiple local minimums, ravines, etc. As a result, the process of minimization may strongly depend on the initial conditions, which were usually taken based on some physical consideration. Nevertheless, it was successfully accomplished each time, and obtained parameters providing good coincidence between the experimental and simulated data [8].

The main difficulty for identification in this manner was the estimate of the characteristic time scale $\tau(\alpha)$ from small amplitude responses. In order to make the identification procedure more robust and reliable, a systematic identification technique, which would separate the influence of particular data sets on specific parameters was required. Since the characteristic time scale $\tau(\alpha)$ defines the dynamic properties of the system in the vicinity of the statics, the linear aerodynamic model can be used for its estimate. Analysis of the linearized mathematical model presented in the next section underlies the technique able to provide a reasonable estimate of the characteristic time scales using corresponding aerodynamic derivatives. The advantage of this approach is that it is based on a linear regression technique, which makes it possible to obtain a result instantly and avoid the direct minimization of the cost function (4.6).

4.2 Linear model analysis

4.2.1 Oscillation frequency effect on the aerodynamic derivatives

Let us consider identification of the linearized aerodynamical model using small amplitude longitudinal oscillations in pitch. According to equation (4.1) the model for force/moment coefficients C can be written as follows:

$$C(t) = C_{att}(\alpha) + C_{\bar{\dot{\alpha}}_{att}}(\alpha)\frac{\bar{c}}{2V}\dot{\alpha} + C_{dyn}. \tag{4.7}$$

For a small amplitude variation of the angle of attack with respect to its mean value equation (4.2) for the dynamic component $C_{N_{dyn}}$ may be reduced to the following first order form:

$$\tau\frac{dC_{dyn}}{d\bar{t}} = \Delta C(\alpha) - C_{dyn}, \tag{4.8}$$

where $\bar{t} = \frac{2V}{c}t$ – the non-dimensional time, $\tau = 1/k_1$ – the characteristic time constant and

$$\Delta C(\alpha) = C_{st}(\alpha) - C_{att}(\alpha). \tag{4.9}$$

Has been linearized with respect to the mean angle of attack α_0 equation (4.8) becomes

$$\tau \frac{d\,\delta C_{dyn}}{d\bar{t}} + \delta C_{dyn} = \Delta C_\alpha(\alpha_0)\,\delta\alpha, \tag{4.10}$$

where $\delta\alpha$ and δC_{dyn} are the small variations of angle of attack and the force/moment coefficient, respectively. After rewriting this equation in the form of a transfer function we obtain:

$$\frac{\delta C_{dyn}}{\delta\alpha} = \frac{\Delta C_\alpha(\alpha_0)}{1+\tau s}. \tag{4.11}$$

During forced oscillation tests, the angle of attack varies with a small amplitude $\Delta\alpha$ around a mean angle of attack α_0:

$$\alpha(t) = \alpha_0 + \Delta\alpha \sin\omega t$$

$$\dot{\alpha}(t) = \Delta\alpha\omega \cos\omega t,$$

where ω is the frequency of oscillations. Thus, the variation of the dynamic component $\delta C_{dyn}(t)$ is described in the time domain as follows:

$$\delta C_{dyn}(t) = \left(\frac{\Delta\alpha \sin\omega t}{1+\omega^2\tau^2} - \frac{\Delta\alpha\omega\tau \cos\omega t}{1+\omega^2\tau^2} + \frac{\Delta\alpha\omega\tau e^{-\bar{t}/\tau}}{1+\omega^2\tau^2} \right) \Delta C_\alpha(\alpha_0), \tag{4.12}$$

where the last term in parentheses tends to zero in steady harmonic oscillations.

An aerodynamic response to a small amplitude harmonic variation of the angle of attack can be represented by the first term of the Fourier series expansion:

$$C(t) = C_0(t) + C_\alpha(\alpha_0,\omega)\Delta\alpha \sin\omega t + C_{\dot{\alpha}}(\alpha_0,\omega)\omega\Delta\alpha \cos\omega t, \tag{4.13}$$

where C_0 is the mean value of the aerodynamic coefficient, C_α and $C_{\dot{\alpha}}$ are "in-phase" and "out-of-phase" aerodynamic derivatives, which can depend on the frequency of oscillation.

Substituting (4.12) into (4.7) and comparing the respective terms with 'sin' and 'cos' in (4.7) and (4.13) we find that

$$\begin{aligned} C_\alpha(\alpha_0,\omega) &= C_{\alpha_{att}}(\alpha_0) + \frac{\Delta C_\alpha(\alpha_0)}{1+\omega^2\tau^2} \\ C_{\dot{\alpha}}(\alpha_0,\omega) &= C_{\dot{\alpha}_{att}}(\alpha_0) - \frac{\tau\Delta C_\alpha(\alpha_0)}{1+\omega^2\tau^2}. \end{aligned} \tag{4.14}$$

Thus, we have a representation of the measured aerodynamic derivatives as a sum of the potential (attached unburst vortical flow) and dynamic contributions.

4.2.2 Identification of the characteristic time scales

"In-phase" and "out-of-phase" derivatives $C_\alpha(\alpha_0,\omega)$ and $C_{\dot\alpha}(\alpha_0,\omega)$ are calculated using experimental data obtained in a wind-tunnel at small amplitude forced oscillations and, consequently, can be considered as experimentally measured functions. Multiplying the first equation in (4.14) by τ and adding the second one, we have:

$$C_{\dot\alpha}(\alpha_0,\omega) = -\tau C_\alpha(\alpha_0,\omega) + (C_{\dot\alpha_{att}}(\alpha_0) + \tau C_{\alpha_{att}}(\alpha_0)). \tag{4.15}$$

Denoting $a_0 = C_{\dot\alpha_{att}}(\alpha_0)+\tau C_{\alpha_{att}}(\alpha_0)$ we obtain a linear dependence between the "in-phase" and "out-of-phase" aerodynamic derivatives:

$$C_{\dot\alpha}(\alpha_0,\omega) = -\tau C_\alpha(\alpha_0,\omega) + a_0, \tag{4.16}$$

which can be considered as a linear regression equation with independent variable $C_\alpha(\alpha_0,\omega)$, dependent variable $C_{\dot\alpha}(\alpha_0,\omega)$ and two unknown constants τ and α_0 for each experimental angle of attack α_0. Usually there are several different frequencies for each mean angle α_0 available from the experiment. To obtain the estimates for a_0 and τ with their standard square deviations, the number of tested frequencies has to be at least three, but it is desirable to have five–six for more reliable results [59].

Using this data set, one can estimate the unknown parameters in (4.16). Details of the linear regression technique are given in Appendix E. The result of an application of this regression technique to estimate the time scales from aerodynamic derivatives for the X-31 aircraft is presented in Fig. 4.5 [7]. One can see that the linear functions fit the experimentally measured dependencies of $C_{\bar{\dot\alpha}}(\alpha_0,\omega)$ on $C_\alpha(\alpha_0,\omega)$ rather accurately at a wide range of angles of attack.

4.2.3 Identification of the attached flow parameters

After an estimate of characteristic time functions τ, equations (4.14) can be considered as a linear regression system for the unknown parameters $C_{\alpha_{att}}(\alpha_0)$, $C_{\dot\alpha_{att}}(\alpha_0)$ and $\Delta C_\alpha(\alpha_0)$ for different mean angles of attack, with the constraint (4.9) being taken into account.

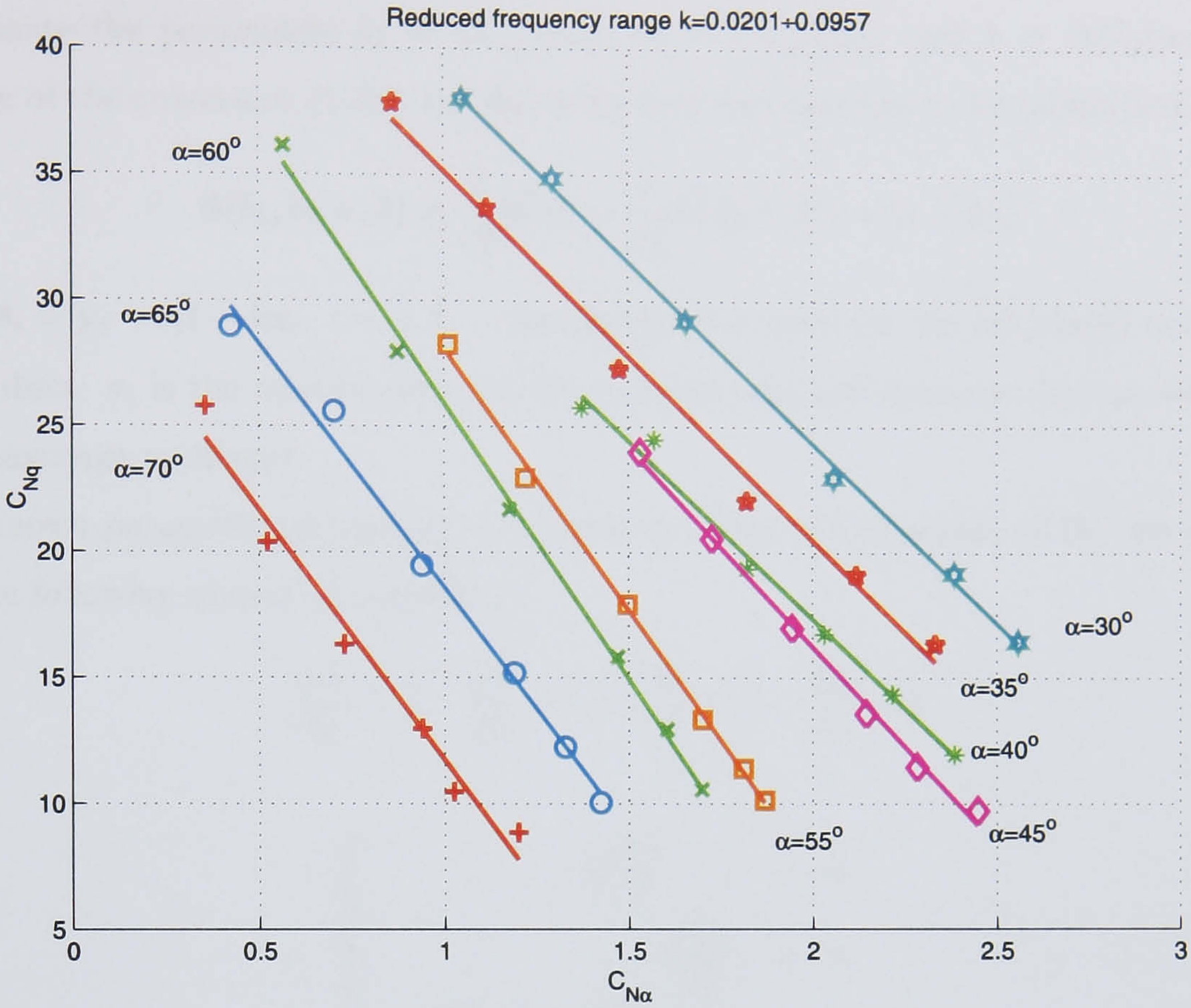

Figure 4.5: The linear regression results for C_N oscillatory data for the X-31 aircraft.

Normally, there are several dependencies of the "in-phase" and "out-of-phase" aerodynamic derivatives on angles of attack corresponding to different frequencies ω_i, $(i = 1, \ldots, N)$ obtained as a result of the small amplitude oscillation tests. Hence, at each angle of attack α_0 equations (4.14) can be presented in the following vector-form:

$$\begin{cases} \mathbf{y_1} &= b_1\mathbf{I} + k\mathbf{x_1} \\ \mathbf{y_2} &= b_2\mathbf{I} + k\mathbf{x_2} \end{cases} \tag{4.17}$$

where $\omega = (\omega_1, .., \omega_N)^T$ is the vector of tested frequencies and $\mathbf{I} = (\underbrace{1, \ldots, 1}_{N})^T$ is the vector with all components equal to one. All other vectors are defined through their components as follows: $x_{1i} = \dfrac{1}{1+\omega_i^2\tau^2}$, $x_{2i} = -\dfrac{\tau}{1+\omega_i^2\tau^2}$, $y_{1i} = C_\alpha(\alpha_0, \omega_i)$ and $y_{2i} = C_{\dot\alpha}(\alpha_0, \omega_i)$. The constraint equation similar to (4.9) can be written for aerodynamic derivatives:

$$z \equiv C_{\alpha_{st}}(\alpha_0) = b_1 + k. \tag{4.18}$$

To estimate the parameters $b_1 = C_{\alpha_{att}}(\alpha_0)$, $b_2 = C_{\dot{\alpha}_{att}}(\alpha_0)$ and $k = \Delta C_\alpha(\alpha_0)$ in the presence of the constraint (4.18), the following cost function has to be minimized:

$$\Phi(b_1, b_2, k, \lambda) = \frac{1}{\sigma_1^2}\boldsymbol{\delta}_1^T\boldsymbol{\delta}_1 + \frac{1}{\sigma_2^2}\boldsymbol{\delta}_2^T\boldsymbol{\delta}_2 + \lambda(z - b_1 - k), \tag{4.19}$$

where $\boldsymbol{\delta}_i = \mathbf{y}_i - b_i\mathbf{I} - k\mathbf{x}_i$, $i = 1, 2$ – the discrepancy between the calculated and experimental data, σ_i is the relative error for the experimental aerodynamic derivatives, and λ is the Lagrange multiplier.

Unknown parameters providing an extremum to the cost function (4.19) can be found from the following system of equations:

$$\frac{\partial\Phi}{\partial b_1} = 0, \quad \frac{\partial\Phi}{\partial b_2} = 0, \quad \frac{\partial\Phi}{\partial k} = 0, \quad \frac{\partial\Phi}{\partial\lambda} = 0 \tag{4.20}$$

or

$$\begin{cases} -2\dfrac{\boldsymbol{\delta}_1^T\mathbf{I}}{\sigma_1^2} - \lambda = 0 \\ -2\dfrac{\boldsymbol{\delta}_2^T\mathbf{I}}{\sigma_2^2} = 0 \\ -2\dfrac{\boldsymbol{\delta}_1^T\mathbf{x}_1}{\sigma_1^2} - 2\dfrac{\boldsymbol{\delta}_2^T\mathbf{x}_2}{\sigma_2^2} - \lambda = 0 \\ z - b_1 - k = 0. \end{cases} \tag{4.21}$$

Rewriting equations (4.21) in matrix form one can obtain the following linear system for the sought parameters:

$$\begin{Vmatrix} N & 0 & \boldsymbol{x}_1^T\boldsymbol{I} & \frac{\sigma_1^2}{2} \\ 0 & N & \boldsymbol{x}_2^T\boldsymbol{I} & 0 \\ \frac{\boldsymbol{I}^T\boldsymbol{x}_1}{\sigma_1^2} & \frac{\boldsymbol{I}^T\boldsymbol{x}_2}{\sigma_2^2} & \frac{\boldsymbol{x}_1^T\boldsymbol{x}_1}{\sigma_1^2} + \frac{\boldsymbol{x}_2^T\boldsymbol{x}_2}{\sigma_2^2} & -1/2 \\ 1 & 0 & 1 & 0 \end{Vmatrix} \begin{vmatrix} b_1 \\ b_2 \\ k \\ \lambda \end{vmatrix} = \begin{vmatrix} \boldsymbol{y}_1^T\boldsymbol{I} \\ \boldsymbol{y}_2^T\boldsymbol{I} \\ \frac{\boldsymbol{y}_1^T\boldsymbol{x}_1}{\sigma_1^2} + \frac{\boldsymbol{y}_2^T\boldsymbol{x}_2}{\sigma_2^2} \\ z \end{vmatrix} \tag{4.22}$$

This system can be solved analytically but in order to avoid cumbersome formulas, it seems better to do it numerically using, for example, MATLAB.

Thus, system (4.22) provides an estimate of the aerodynamic derivatives for the potential (inertialess) flow components and the vortex breakdown flow contribution $\Delta C_{\alpha_{st}}(\alpha_0)$. With a characteristic time scale τ known from the first step of the linear regression, there is now a full set of relations to estimate all the parameters of the linear mathematic model (4.7)–(4.8).

4.3 Nonlinear model

The linear mathematical model (4.7)–(4.8) provides rather good agreement with experimental data during small ($\Delta\alpha \sim 3^o$) and medium ($\Delta\alpha \sim 10^o$) amplitudes of oscillation while it significantly loses accuracy during large amplitude oscillations (Figs. 5.11 and 5.20). Also, this model will be unable to describe static hysteresis adequately. To reconcile the model with this condition a higher order equation for the dynamic component is to be used. If there is only one stable branch in the static dependence of the aerodynamic coefficient, it is sufficient to use the dynamic equation (4.2) with $N = 3$ and $k_0 = 0$:

$$\frac{\bar{c}}{2V}\frac{dC_{dyn}}{dt} = k_1\left(\Delta C(\alpha) - C_{dyn}\right) + k_2\left(\Delta C(\alpha) - C_{dyn}\right)^2 + k_3\left(\Delta C(\alpha) - C_{dyn}\right)^3. \quad (4.23)$$

In order to produce only a "weak" nonlinearity which transforms the effective time scale for an increase of the amplitude of motion, conditions (4.4) have to be satisfied at every angle of attack. The case of strong nonlinearity leading to static hysteresis appearance is considered later in Chapter 6.

4.3.1 Parameter identification technique

One of the most important points for the wide practical application of the nonlinear mathematical model (4.1)–(4.2) is the availability of a reliable identification procedure. Success in the identification of the unknown parameters providing the best representation of all experimental responses strongly depends on the adequacy of the initial guesses. Therefore, the initial estimates obtained using the linearized model significantly help to reduce ambiguity due to the complicated multiextremum geometry of the cost function for the nonlinear model. The block diagram of the nonlinear model identification algorithm, which was drawn up and applied during the course of the research is presented in Fig. 4.6.

The experimental data set usually contains aerodynamic forces and moments time responses during forced oscillations in pitch, yaw, roll with small and large amplitude at different frequencies and mean angles of attack and sideslip. At first, the "in-phase" and "out-of-phase" aerodynamic derivatives are calculated using small amplitude experimental data according to the technique described in Chapter 2. The obtained experimental derivatives are used as the input data in the first step of the linear regression method, which

provides estimates for the characteristic time constant τ and the parameter a_0. Then, these two parameters, along with the aerodynamic derivatives are considered as inputs for the second step of the linear regression procedure. As a result of this step estimates for the aerodynamic derivatives of the "potential" flow components $C_{\alpha_{att}}(\alpha_0)$, $C_{\dot{\alpha}_{att}}(\alpha_0)$ and $\Delta C_\alpha(\alpha_0)$ are obtained.

At some angles of attack, the standard square deviation for the estimated parameters of the mathematical model is reasonably small, however, at some point they turned out to be very high (see Fig. 5.21, top plot). The consistency of the results of identification can be improved if an increased number of the aerodynamic derivatives obtained for a more extensive set of the frequencies are used (see Fig. 5.21, bottom plot). Unfortunately, during this study the aerodynamic derivatives were available only for three different frequencies which was found to be insufficient under some conditions. Therefore, all results obtained from the regression analysis of the linearized model were considered only as a first approximation. After smoothing and some corrections according to the physical meaning, these results were used for the nonlinear model identification.

The technique for the mathematical model development accepted in this study implies that all experimental and calculated aerodynamic dependencies are kept in the same

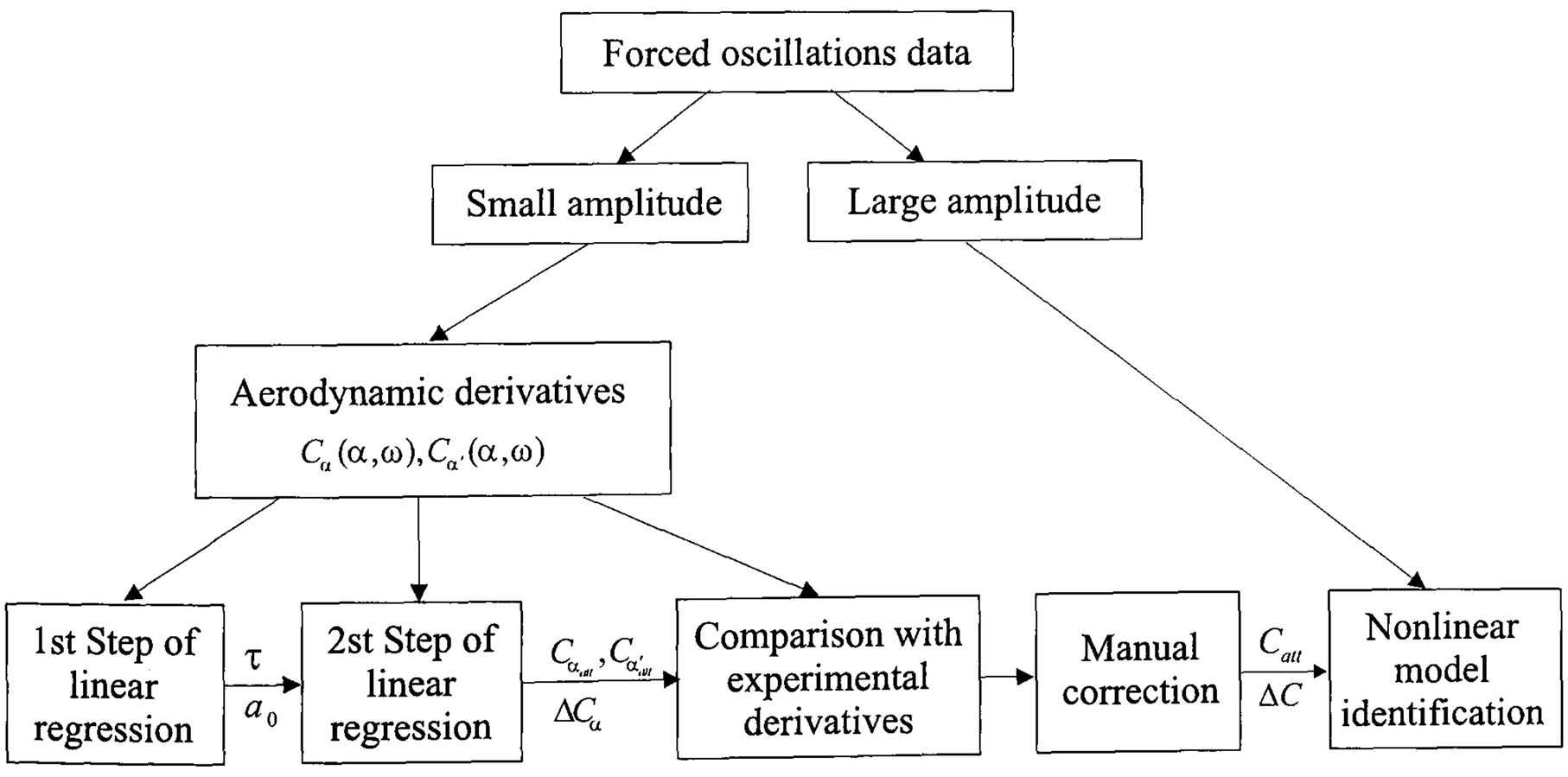

Figure 4.6: Model identification procedure.

database in the ADDB program [9] which makes all data available in the MATLAB environment and provides necessary tools for aerodynamic data processing. This approach significantly facilitates gathering all data relevant to the mathematical model identification and effective manipulation of them, avoiding programming and lookup data table processing.

The final stage of the identification process is the full nonlinear model parameters estimation. After the initial steps have been completed, we have estimates for the characteristic time constants and functions associated with the attached flow. All these dependencies are then included into the full nonlinear model either "as is" or with some correction factor. Unknown functions $k_2(\alpha, \beta)$, $k_3(\alpha, \beta)$, etc are defined by a set of values in nodes (α_i, β_i), and linear or cubic interpolation is used to calculate the values at intermediate points.

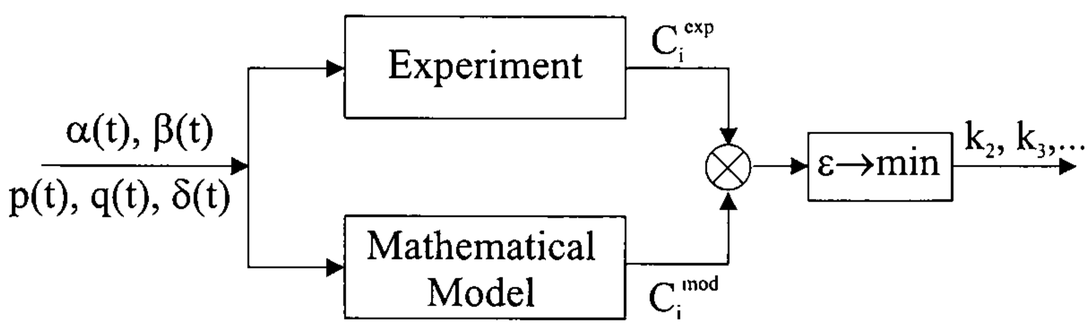

Figure 4.7: Nonlinear model identification.

The identification of the full nonlinear mathematical model is performed using the large amplitude experimental data (See Fig. 4.7). Inputs to the mathematical model are time histories of an aircraft model attitude and angular rates measured in time points $t_i,\ i = 0, \ldots, N-1$ while the outputs are the variation of the force/moment coefficients having the same time sampling. To eliminate the dependence of the responses on the initial conditions, two periods are simulated but only the second one, corresponding to steady oscillations, is taken into account. Then the following cost function is used to compare experimentally measured and simulated aerodynamic force/moment coefficients:

$$\Phi(\mathbf{p}) = \frac{1}{NM} \sum_{k=1}^{M} \sum_{i=1}^{N} \left[C_k^{exp}(t_i) - C_k^{mod}(t_i, \mathbf{p}) \right]^2, \tag{4.24}$$

where M is a number of aerodynamic responses, N is a number of sample points. All unknown parameters are determined as a result of the cost function (4.24) minimization, after that the identification procedure is considered to be accomplished.

In order to facilitate the process of dynamic system identification the PIIMTM software is used. It implements descent, gradient and conjugate gradient methods for extremum seeking and provides a user-friendly interface to observe and interactively control the cost

function minimization process.

4.3.2 Analysis of mathematical model sensitivity to parameter variation

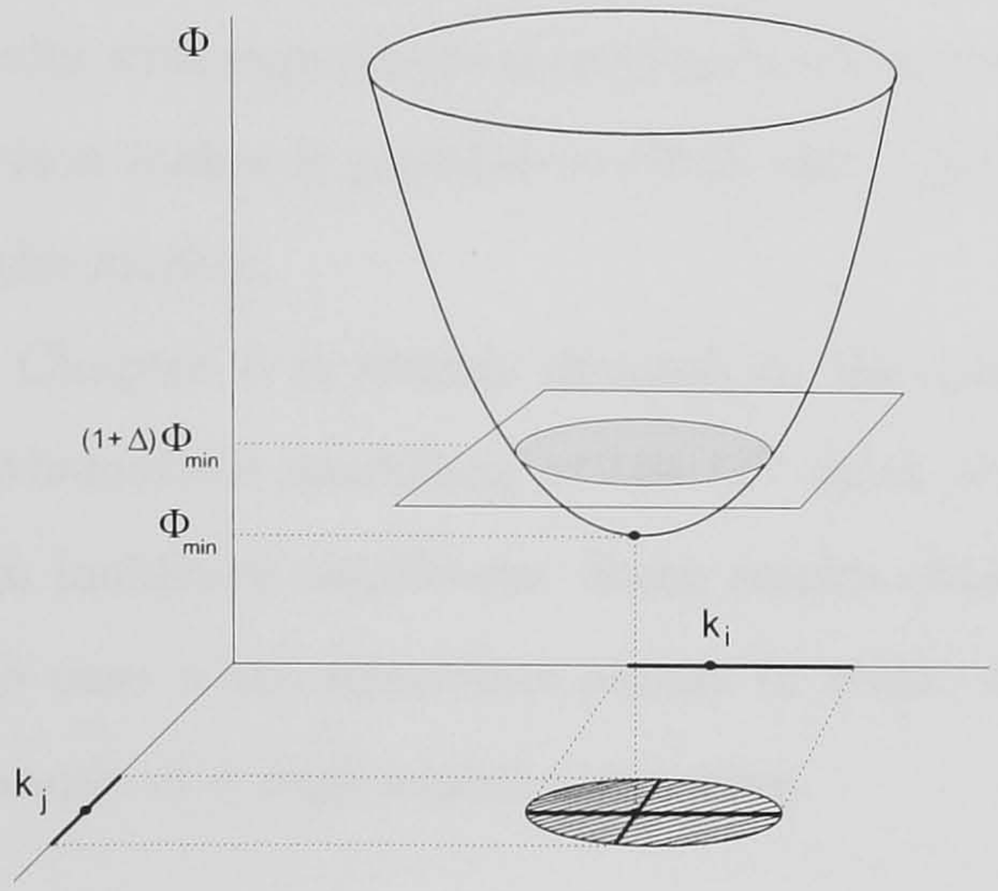

Figure 4.8: Sensitivity of the cost function to uncertainty of model parameters.

The identified parameters are obtained using the least square method by means of minimization of the cost function Φ. The local minimum for this function provides the magnitudes for the mathematical model parameters and its shape in the vicinity of this minimum reveals the level of parameter sensitivity. To formalize the parameter sensitivity analysis, the following procedure is used. Some level of the cost function exceeding its local minimum value is selected: $\Phi_\Delta = (1 + \Delta)\Phi_{min}$. After that possible variations of the parameters are calculated for the condition, when $\Phi \leq \Phi_\Delta$, see Fig. 4.8. The obtained dispersion of the parameters will demonstrate the sensitivity of the mathematical model to a variation of its different parameters and the tendency of other local extremum to exist. Such information is also very valuable for the further improvement of the mathematical model structure, for example, identifying more and less important parameters. If a parameter scatter is small one can say that the mathematical model is very sensitive to this parameter and, therefore, consistent to it. Otherwise, either additional experimental data should be used to make the result more consistent or the impact of such a parameter on the model may be admitted as inessential for some range of incidences.

4.3.3 Model validation

The outlined technique was validated many times being applied to experimental data analysis and mathematical model identification for different wings and aircraft models [8, 29, 37, 7]. The quality of the mathematical model is mainly evaluated by comparison of the simulated and experimental responses at all available mean angles of attack and sideslip, amplitudes and reduced frequencies that allows one to reveal the domain of

applicability for the model. Special emphasis is made on the ability of the technique to reproduce the qualitative effects and physical meanings of the estimated parameters. Usually an extensive set of available experimental data such as statics, small and large amplitude oscillations, etc is used for identification but it is also important to compare the simulated results with experimental responses which were not involved in the identification. This comparison makes it possible to check the "interpolational" and "extrapolational" capabilities of the models.

Chapter 5 is mainly devoted to the practical application of the above technique for mathematical modelling of the 65^o delta wing aerodynamic force/moment coefficients at high incidence conditions. Some results obtained for the 70^o delta wing are also discussed. The case when hysteresis occurs in static dependence is considered in Chapter 6 in the example of a high aspect ratio wing.

4.4 Comparison with alternative modelling techniques

Let us consider model (4.1)–(4.2) in the linear form:

$$\begin{cases} C_N(\alpha) &= C_{N_{att}}(\alpha) + C_{N_{\dot{\bar{\alpha}}_{att}}}(\alpha)\dot{\bar{\alpha}} + C_{N_{dyn}} \\ \frac{dC_{N_{dyn}}}{dt}\frac{\bar{c}}{2V} &= k_1\left(\Delta C_N - C_{N_{dyn}}\right). \end{cases} \tag{4.25}$$

Add and subtract the $\Delta C_N = C_{N_{st}} - C_{N_{att}}$ function in the first equation of the system above.

$$C_N(\alpha) = \underbrace{C_{N_{att}}(\alpha) + \Delta C_N(\alpha)}_{C_{N_{st}}(\alpha)} + C_{N_{\dot{\bar{\alpha}}_{att}}}(\alpha)\dot{\bar{\alpha}} + C_{N_{dyn}} - \Delta C_N(\alpha). \tag{4.26}$$

Assuming that the variation of the angle of attack with respect to the static position is small and applying the Laplace transformation, the second equation for the dynamic component can be written in terms of transfer functions as follows:

$$C_{N_{dyn}} = \frac{1}{\tau s + 1}\Delta C_N, \tag{4.27}$$

where $\tau = 1/k_1$. Substituting equation (4.27) to (4.26) and linearizing the static dependence ΔC_N with respect to the angle of attack we obtain the following expression for the normal force coefficient:

$$C_N = C_{N_{st}}(\alpha) + \left[C_{N_{\dot{\bar{\alpha}}_{att}}}(\alpha_0)s - \frac{s}{s+k_1}\left(C_{N_{\alpha_{st}}}(\alpha_0) - C_{N_{\alpha_{att}}}(\alpha_0)\right)\right]\alpha. \tag{4.28}$$

Aerodynamic derivatives

It is known that the conventional unsteady aerodynamic modelling approach is unable to capture the dynamic flow properties because it deals only with instantaneous values of the aerodynamic derivatives. This situation could take place in an inertialless flow where the characteristic time constant of the flow readjustment processes τ is equal to zero. Taking into account that $k_1 = \frac{1}{\tau} \to \infty$ equation (4.28) is reduced to the conventional aerodynamic derivatives form:

$$C_N = C_{N_{st}}(\alpha) + C_{N_{\bar{\dot{\alpha}}_{att}}}(\alpha_0)\bar{\dot{\alpha}}. \tag{4.29}$$

From the other side, equation (4.28) turns into (4.29) at $C_{N_{\alpha_{st}}}(\alpha) = C_{N_{\alpha_{att}}}(\alpha)$ or $C_{N_{st}}(\alpha) = C_{N_{att}}(\alpha)$ i.e. in the range of angles of attack where the flow is fully attached or vortices are not broken down. Thus one can conclude that models (4.1)–(4.2) and the conventional aerodynamic derivative model are equivalent at low incidences.

Linear Indicial Functions Approach (V.Klein)

The mathematical model of the normal force coefficient based on the linear indicial response (LIR) approach [86, 87, 88] is presented in the following form [59]:

$$C_L(t) = C_{L_\alpha}\alpha(t) - \int_0^t F_\alpha(t-\tau)\frac{d}{d\tau}\alpha(\tau) + \frac{l}{V}C_{L_q}(\infty)q(t). \tag{4.30}$$

For obtaining a model with a limited number of parameters the indicial function is assumed in the simple exponential form:

$$C_{L_\alpha}(t) = C_{L_\alpha}(\infty) - ae^{-b_1 t}. \tag{4.31}$$

Finally, an expression for C_L is obtained by substitution of (4.31) into (4.30) and applying the Laplace transformation to (4.30).

$$C_L(s) = C_{L_\alpha}(\infty)\alpha + \left[-\frac{as}{s+b_1} + \frac{l}{V}C_{L_q}s\right]\alpha. \tag{4.32}$$

Comparing (4.32) with (4.28) one can see that these equations are equivalent, with b_1 being equal to k_1 and $a = C_{N_{\alpha_{st}}} - C_{N_{\alpha_{att}}}$. The only difference is that equation (4.28) describes the total value of C_N while equation (4.32) is that for the increment with respect to the static value.

Volterra Series Approach (P.Reisenthel)

In order to accurately describe nonlinear unsteady aerodynamic effects, the application of the Volterra Series has been proposed in [77]. This approach provides a mathematically rigorous technique for the modelling of time-invariant nonlinear systems expressed as a series of multidimensional convolution integrals:

$$\begin{aligned} C_L(t) &= h_0 + \int_0^t h_1(t-\tau_1)\alpha(\tau_1)d\tau_1 + \int_0^t\int_0^t h_2(t-\tau_1,t-\tau_2)\alpha(\tau_1)\alpha(\tau_2)d\tau_1 d\tau_2 + \dots \\ &\quad \underbrace{\int_0^t \dots \int_0^t}_{n} h_n(t-\tau_1,\dots,t-\tau_n)\prod_{i=1}^{n}\alpha(\tau_i)d\tau_i. \end{aligned} \tag{4.33}$$

Avoiding any discussion about the implementation of this method and difficulties of kernel identification, it is worth mentioning that the general idea of this approach is to introduce higher order terms capturing nonlinear effects. One can clearly notice some similarity to the nonlinear differential systems approach:

$$\frac{dC_{N_{dyn}}}{dt}\frac{\bar{c}}{2V} = k_1\left(\Delta C_N - C_{N_{dyn}}\right) + k_2\left(\Delta C_N - C_{N_{dyn}}\right)^2 + \dots + k_n\left(\Delta C_N - C_{N_{dyn}}\right)^n. \tag{4.34}$$

4.5 Summary

- The nonlinear unsteady aerodynamic modelling approach based on the nonlinear differential equations and aerodynamic loads partitioning on components with different time scales has been proposed.

- It is shown that the suggested model structure is able to reproduce both the "weak" and "strong" nonlinearities typical for high incidence flight. The "weak" nonlinearity produces amplitude dependence of the time scale while the "strong" one leads to static hysteresis.

- The regular technique for identification of unknown parameters has been developed for the linear mathematical model providing reasonable initial estimates for the nonlinear model, which is then identified by means of the least square error method.

- The relation of the proposed technique to conventional aerodynamic derivatives, linear indicial response (LIR) and Volterra series approaches is considered. It is shown that under the attached and unburst vortical flow conditions the mathematical model can be reduced to the aerodynamic derivative one. At a small incidence variation with respect to the static conditions, the identity of the LIR and the proposed models is revealed. The similarity of the proposed nonlinear modelling technique and the Volterra series approach to modelling of the nonlinear effects is also noted.

Chapter 5

Delta wing nonlinear unsteady aerodynamic models

In the framework of the research collaborative programme between DERA and TsAGI, a systematic experimental study of high angle of attack unsteady aerodynamics of several delta wings has been carried out in 1998-2001 [56, 55, 52, 53, 51]. As a result a substantial database of static, slow sweep motion and unsteady aerodynamic characteristics of the 65^o delta wing with and without a central body, two 70^o delta wings of different sizes and the $80^o/60^o$ double delta wing has been collected. The majority of the tests have been conducted in the TsAGI low speed wind tunnel T-102 using the forced oscillations rig OVP-102B, which is able to perform oscillatory motion with small and large amplitudes in pitch, yaw and roll. The main attention in the experiments was given to the dynamic properties of the vortical flow with vortex breakdown at high incidences.

The experiments revealed a strong dependence of the aerodynamic derivatives extracted from small amplitude oscillatory tests on the frequency of oscillations at the range of incidences where the vortex breakdown effects take place [52]. The large amplitude oscillatory motion shows a complicated nonlinear behaviour of the aerodynamic loads, which is due to static nonlinearities and the time lag effects [53]. Thus, the results obtained provide excellent material for the analysis of the structure and dynamic properties of flow near a highly swept wing. The extensive set of time histories of aerodynamic loads for several delta wings in motion with different amplitudes and frequencies can be used to perform identification

of mathematical models of unsteady aerodynamic loads at wide range of incidences for any tested wings.

During the 1990s the USA Air Force Research Laboratory and Canadian Institute for Aerospace Research carried out a comprehensive cycle of investigations of the 65^o delta wing having a central body at high angles of attack [74, 11]. This wing was considered as a baseline for the land-based high performance, low observable fighter investigated in the frame of the innovative control effectors (ICE) program, sponsored by both the Wright Laboratory and Naval Air Warfare Center [18]. The concept of a low observable agile fighter forces the flight envelope to be extended to high angles of attack conditions and to consider a low signature configuration without a vertical tail and equipped with innovative control effectors such as trailing and leading edge flaps, movable wing tips, etc. (see Fig. 5.1). Following the ICE program, the 65^o delta wing with central body has been chosen for development of the aerodynamic mathematical model (Fig. 5.2). After that the developed models of the normal force and pitch moment coefficients are coupled with the aircraft longitudinal motion equations in order to evaluate the contribution of the unsteady aerodynamic model to the aircraft dynamics at high angles of attack and to compare it with conventional model (see Chapter 7).

This chapter is mainly focused on the development of unsteady aerodynamic models for the 65^o delta wing with a central body for pitch and yaw motion at high incidences

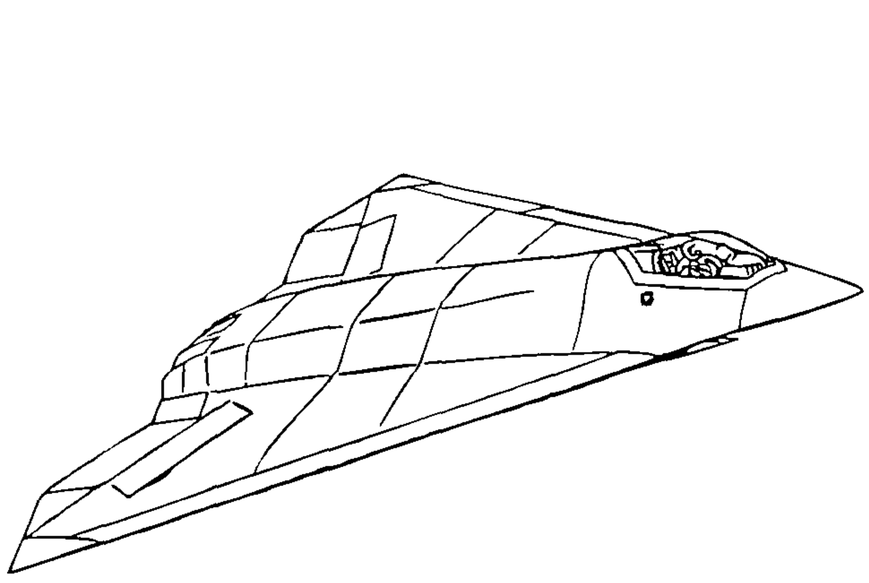

Figure 5.1: Land-based baseline configuration: an all-wing tailless concept employing a 65^o sweep delta wing [18].

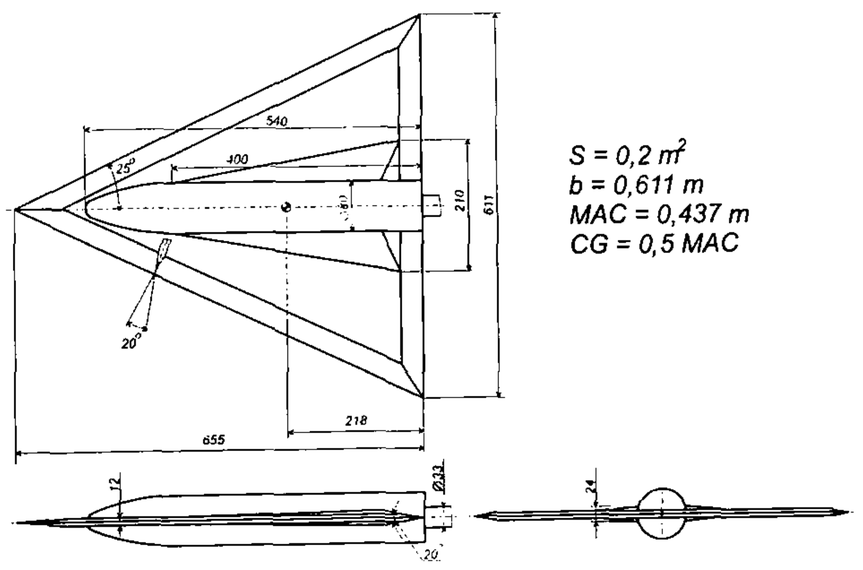

Figure 5.2: The 65^o delta wing tested in TsAGI low speed wind tunnel [8, 37, 7].

according to the approach described in the previous chapter. A similar mathematical model previously developed for the 70^o delta wing [55] makes possible more advanced verification of the aerodynamic loads partitioning and identification techniques. This also allows one to compare the characteristic time scales for different platforms.

The conventional aerodynamic derivative approach to aerodynamic loads modelling is compared with the proposed one. It is shown that the aerodynamic derivatives approach becomes inadequate for simulation of the aerodynamic forces/moments at angles of attack where the effect of internal flow dynamics is essential while the proposed unsteady aerodynamic model turns out to be able to capture nonlinear behavior of the loads.

5.1 Longitudinal aerodynamic characteristics of the 65^o delta wing

5.1.1 Normal force coefficient C_N

According to the aerodynamic loads partitioning technique described in Chapter 4 the mathematical model for the normal force coefficient C_N can be written in the following form:

$$C_N(t) = C_{N_{att}}(\alpha,\beta) + C_{N_{\bar{\dot{\alpha}}_{att}}}(\alpha,\beta)\frac{\bar{c}}{2V}\dot{\alpha} + C_{N_{dyn}}, \tag{5.1}$$

where the behaviour of the dynamic component is governed by the third order dynamic equation

$$\frac{\bar{c}}{2V}\frac{dC_{N_{dyn}}}{dt} = k_1\left(\Delta C_N(\alpha) - C_{N_{dyn}}\right) + k_2\left(\Delta C_N(\alpha) - C_{N_{dyn}}\right)^2 + k_3\left(\Delta C_N(\alpha) - C_{N_{dyn}}\right)^3. \tag{5.2}$$

The "in-phase" and "out-of-phase" aerodynamic derivatives for the normal force coefficient C_N at three different frequencies of small amplitude pitch oscillations are presented in Fig. 5.3. It is seen that at low incidence there is no dependence on the frequency of oscillations but in the range of angles of attack $\alpha = 22^o \ldots 48^o$ it is significant. Thus, the characteristic time scales can be evaluated in this region using the linear regression technique (4.16). The estimated dependencies $\tau(\alpha)$ and $a_0(\alpha)$ are shown in Fig. 5.4 with their standard deviations. Comparison of the experimental aerodynamic derivatives (markers) with those one predicted by the linearized version of the model (5.1)–(5.2) (solid lines) is

presented in Fig. 5.5 in $C_{N_\alpha} - C_{N_{\dot{\alpha}}}$ coordinates for different angles of attack. It is seen that the linear mathematical model fits experimental points rather accurately in most cases and there is clear dependence between the magnitude of the error bars and the proximity of experimental points to the line. Thus, for example, the linear model demonstrates an excellent result at $\alpha = 43^o$ and fails at $\alpha = 35^o$. Possible reasons for this are insufficiently accurate experimental data, a low number of tested frequencies or more complex flow properties, which could not be captured by the first order phenomenological model.

The upper plot in Fig. 5.6 contains α derivatives for the attached flow component $C_{N_{\alpha_{att}}}$ of the normal force coefficient and the difference of static and potential components ΔC_{N_α}, which have been estimated during the second step of the linear regression. The function $C_{N_{\alpha_{st}}}$, which has been obtained from differentiation of the steady experimental dependence of the normal force coefficient is also presented on the same plot. The lower plot contains the estimated function $C_{N_{\dot{\alpha}}}$.

In order to validate the obtained results, the dependencies of the aerodynamic derivatives on the frequencies of oscillations are calculated according to the linear model (4.14). These results are shown in Fig. 5.7 by solid lines in comparison with corresponding experimental aerodynamic derivatives denoted by markers. The "in-phase" and the "out-of-phase" aerodynamic derivatives are shown on the upper and lower plots, respectively. It is seen that the mathematical model predicts the experimental data rather accurately but the attached flow derivatives look very rough and scattered that is most likely due small number of the tested frequencies.

At this stage we have determined all the unknown functions of the linear model but only in the range of angles of attack where the aerodynamic derivatives depend on frequency i.e. in the range where vortex breakdown takes place. In order to build the mathematical model at lower and higher incidences, the obtained derivatives should be smoothed and extended on the whole range of angles of attack.

The attached flow component $C_{N_{att}}(\alpha)$, the static dependence $C_{N_{st}}(\alpha)$ and their difference $\Delta C_N(\alpha)$ are shown in Fig. 5.8 (top plot). The smoothed "out-of-phase" derivative of the attached flow component $C_{N_{\dot{\alpha}_{att}}}(\alpha)$ is shown in Fig. 5.8 (bottom plot) in comparison with the estimated one and the experimental $\dot{\alpha}$ derivatives. All these functions are in the form used in the nonlinear mathematical model of the normal force coefficient.

The characteristic time scale $\tau(\alpha)$ was considered as an unknown function out of the incidence range with strong dependence on the frequency ($\alpha \in [22^o, 48^o]$) and was parameterized there for identification. The full range dependence of $\tau(\alpha)$ as well as the identified coefficients $k_2(\alpha)$ and $k_3(\alpha)$ are presented in Fig. 5.9. The possible variations of the $k_2(\alpha)$ and $k_3(\alpha)$ coefficients resulting in an increment of the cost function of 1% are presented in Fig. 5.10.

These results show that the sensitivity of the cost function to the parameters k_2, k_3 of the nonlinear model is rather low at $\alpha < 40^o$ and becomes considerable only at higher incidences. Comparing Fig. 5.10 with Fig. 5.7 one can see that terms with k_2, k_3 becomes significant at angles of attack where the dependence of the aerodynamic derivatives on the frequency of oscillations is pronounced. Fig. 5.11 demonstrates that nonlinear terms can significantly improve prediction in the case of large amplitude motion, especially during back swing. On the contrary, the contribution of the nonlinear term is negligible at small and medium amplitudes.

The experimental aerodynamic responses for the normal force coefficient of the 65^o delta wing during large amplitude oscillations (square markers) along with the predicted ones are presented in Figs. E.1–E.3. One can see that the predicted results (solid line) coincide with the experimental ones with very good accuracy in a wide range of the various frequencies and amplitudes.

5.1.2 Pitch moment coefficient C_m

Similar to the normal force coefficient, the same technique can be used for mathematical modelling of the pitch moment coefficient. Assuming that the dependence of $C_m(\alpha)$ is a sum of the attached (inertialess) and the dynamic components, the pitch moment coefficient model is expressed as follows:

$$C_m(t) = C_{m_{att}}(\alpha, \beta) + C_{m_{\bar{\alpha}_{att}}}(\alpha, \beta)\frac{\bar{c}}{2V}\dot{\alpha} + C_{m_{dyn}}, \tag{5.3}$$

where the dynamic component is described by the following nonlinear differential equation:

$$\frac{\bar{c}}{2V}\frac{dC_{m_{dyn}}}{dt} = k_1\left(\Delta C_m(\alpha) - C_{m_{dyn}}\right) + k_2\left(\Delta C_m(\alpha) - C_{m_{dyn}}\right)^2 + k_3\left(\Delta C_m(\alpha) - C_{m_{dyn}}\right)^3. \tag{5.4}$$

The "in-phase" and "out-of-phase" aerodynamic derivatives for the pitch moment coef-:ient C_m at three different frequencies of small amplitude pitch oscillations are presented Fig. 5.12. As in the case of normal force coefficient, there is no dependence on the equency of oscillations at low incidence. It becomes significant in the range of angles ' attack 25^o to 48^o where the linear regression technique can be effectively applied. The ıaracteristic time $\tau(\alpha)$, parameter $a_0(\alpha)$ with their standard deviations determined as a :sult of regression of (4.16) are presented in Fig. 5.13.

Comparison of the experimental aerodynamic derivatives (markers) with the predicted ıe by the linearized model (5.3)–(5.4) (solid lines) is presented in Fig. 5.14 in $C_{m_\alpha} - C_{m_{\dot\alpha}}$)ordinates for different angles of attack. One can see that similar to the normal force)efficient, the linear model of the pitch moment coefficient fits the experimental points ıther accurately in most cases.

The upper plot of Fig. 5.15 contains α derivatives of the attached flow component $C_{m_{\alpha_{att}}}$ f the pitch moment coefficient and the difference of static and potential components ΔC_{m_α}, 'hich were estimated after the second step of the linear regression. The function $C_{m_{\alpha_{st}}}$ btained by differentiation of the static experimental dependence of the pitch moment)efficient is also presented on the same plot. The lower plot in the figure contains the stimated function $C_{m_{\dot\alpha}}$.

The dependency of the aerodynamic derivatives on the frequency of oscillations calcu-ıted according to the linear model (4.14) is shown in Fig. 5.16 (solid lines) in comparison 'ith the corresponding experimental aerodynamic derivatives (markers). The "in-phase" .erivatives are shown in the upper plot and the "out-of-phase" derivatives are in the lower ne. It is seen that the mathematical model predicts the experimental results rather ac-urately but similar to the normal force coefficient the attached flow derivatives look very rratic.

Smoothed and extended attached flow component $C_{m_{att}}(\alpha)$, static dependence $C_{m_{st}}(\alpha)$ ınd their difference $\Delta C_m(\alpha)$ are shown in the top plot of Fig. 5.17. The $\dot\alpha$ derivative of he attached flow component $C_{m_{\dot\alpha_{att}}}(\alpha)$ is shown in the bottom plot of the same figure in :omparison with the identified one and the experimental "out-of-phase" derivatives. All :hese functions are presented in the same form as in the nonlinear mathematical model of :he pitch moment coefficient.

The identified dependencies $\tau(\alpha)$ and $k_2(\alpha)$, $k_3(\alpha)$ are presented in Fig. 5.18 for the angles of attack 0^o to 60^o. The ranges of the $k_2(\alpha)$ and $k_3(\alpha)$ coefficients change which results in a 1% cost function increment are presented in Fig. 5.19. One can see, that similar to C_N, the nonlinear terms considerably influence on the quality of the model prediction only at high incidences ($\alpha > 35^o$) where the dependence of the aerodynamic derivatives on the frequency of oscillations is substantial. From Fig. 5.20, one can see that the nonlinear terms significantly rectify the linear model in the case of large amplitude motion and are not essential at small and medium amplitudes.

The experimental aerodynamic responses for the pitch moment coefficient during the large amplitude oscillations (square markers) and the predicted ones using the nonlinear mathematical model are presented in Figs. E.4–E.6. It is seen that the predicted results (solid line) fit the experimental responses with very good accuracy at different frequencies and amplitudes of oscillations.

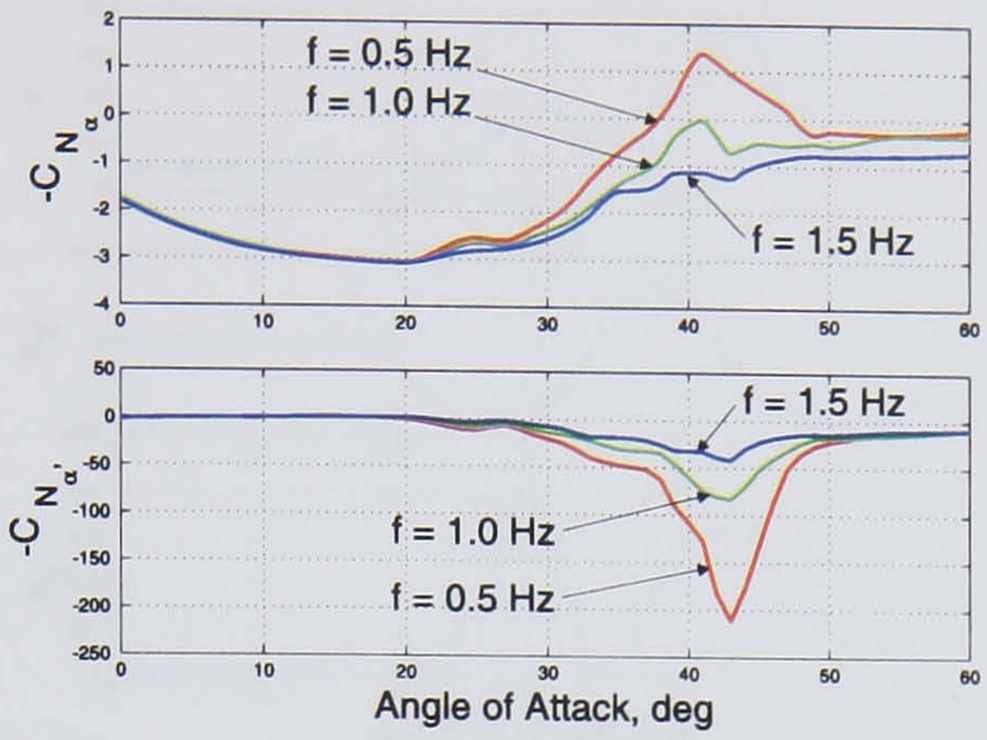

Figure 5.3: Experimental aerodynamic derivatives for the normal force coefficient C_N.

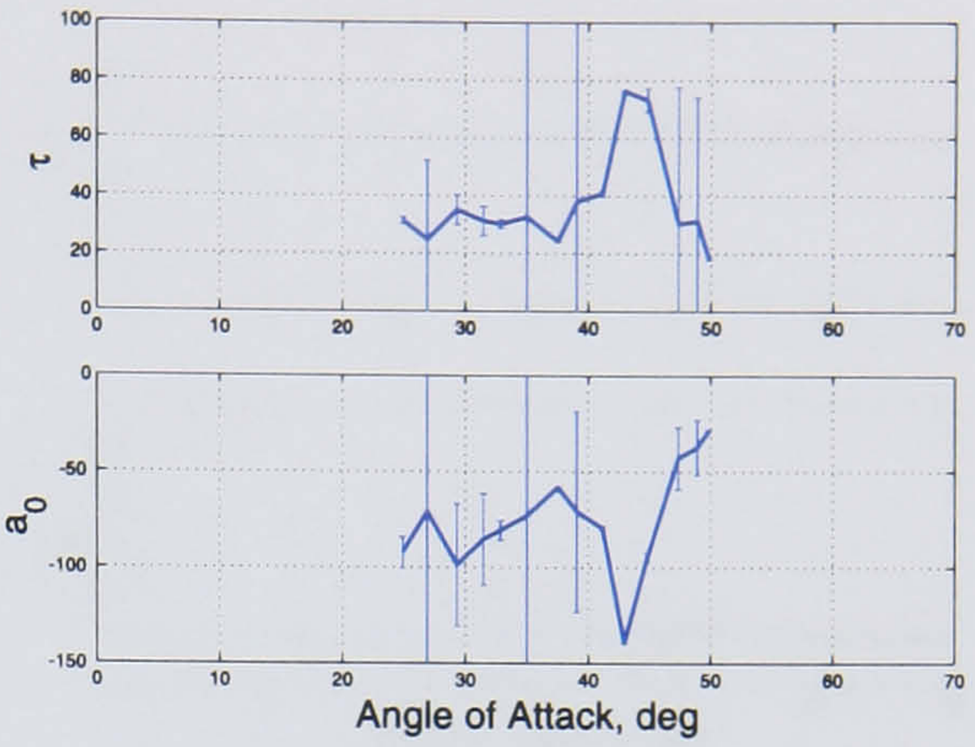

Figure 5.4: Characteristic time τ and parameter a_0 from the first step of linear regression.

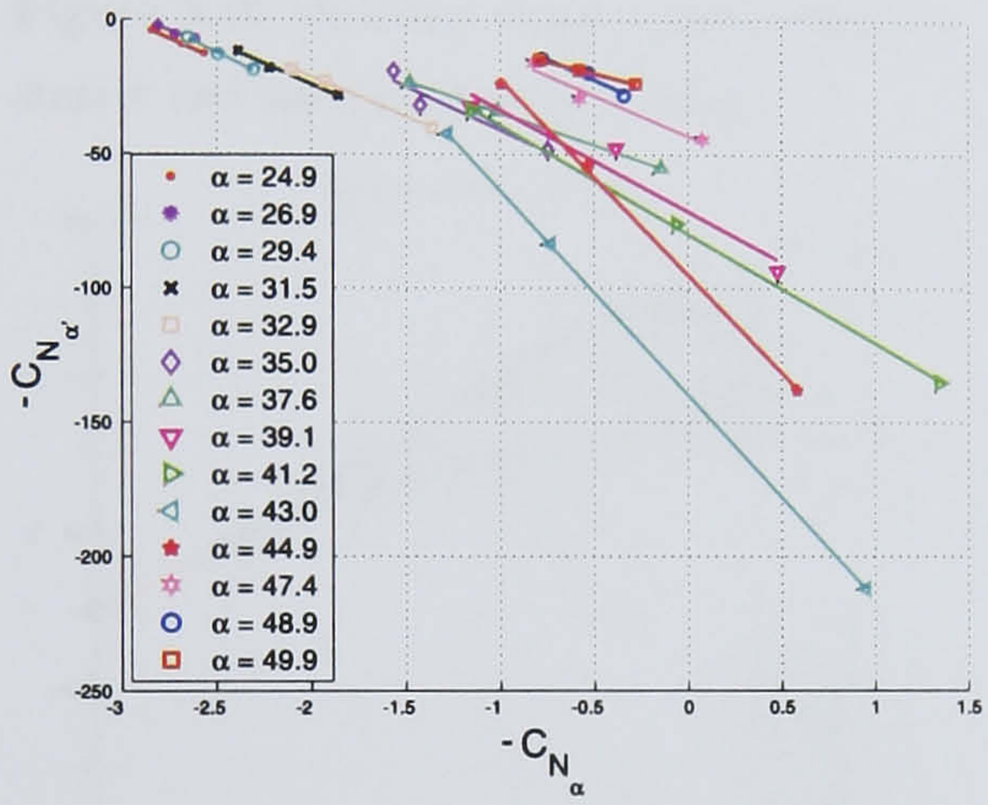

Figure 5.5: First step linear regression results for different angles of attack.

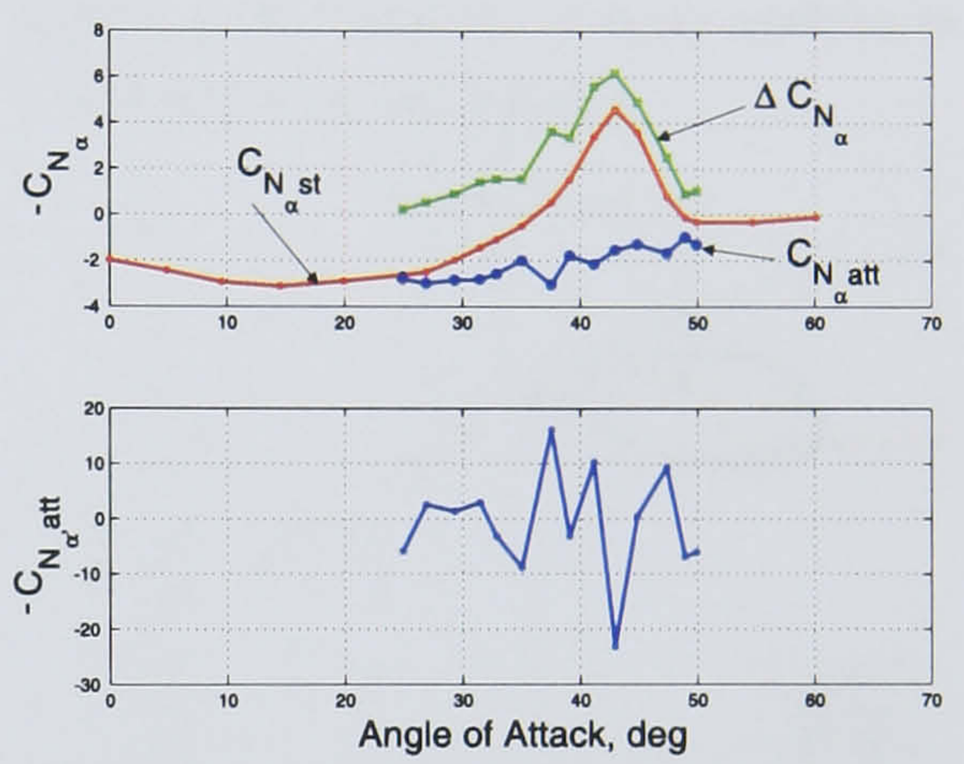

Figure 5.6: Estimated components of the linear mathematical model for C_N coefficient.

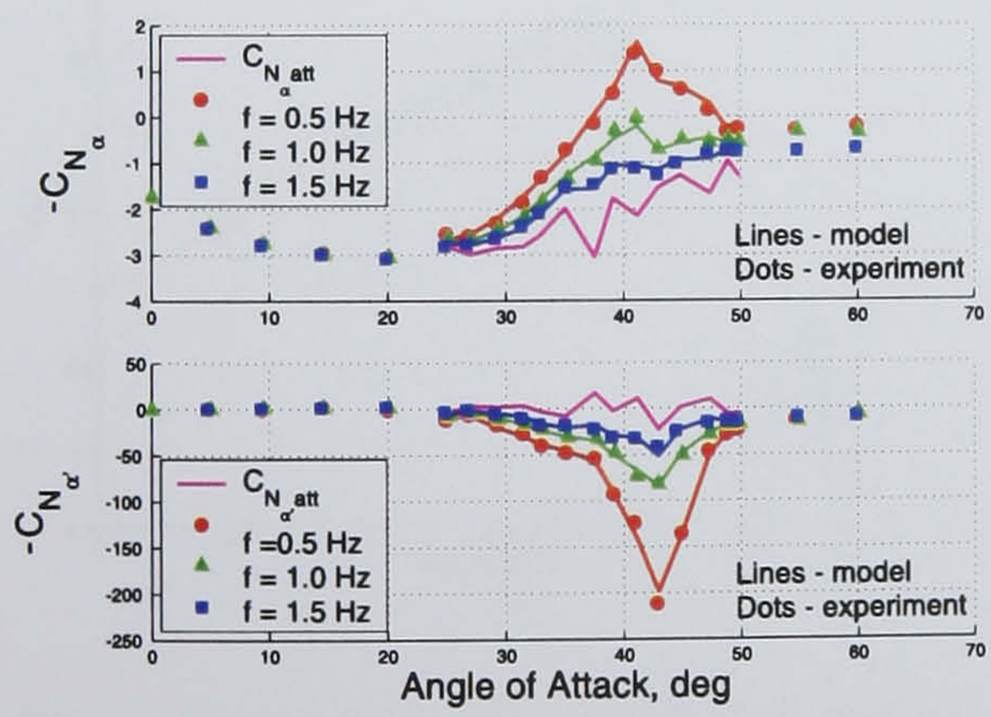

Figure 5.7: Experimental aerodynamic derivatives vs. results predicted by the linear model.

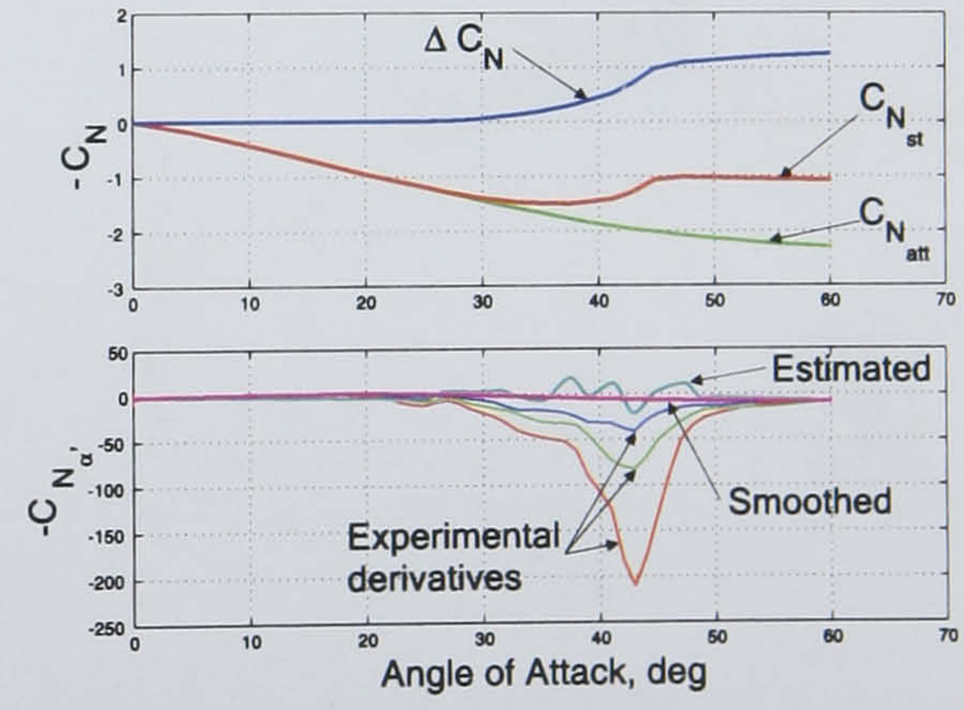

Figure 5.8: Estimated components in the form as they were included in the nonlinear model.

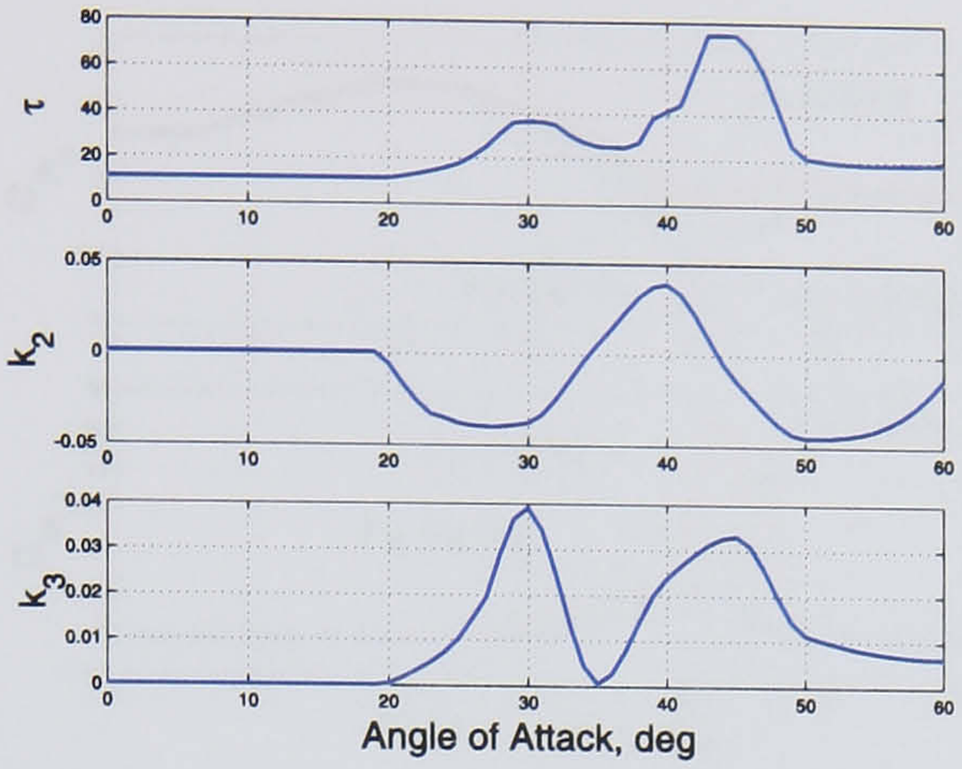

Figure 5.9: Identified characteristic time constant τ and parameters $k_2(\alpha)$, $k_3(\alpha)$.

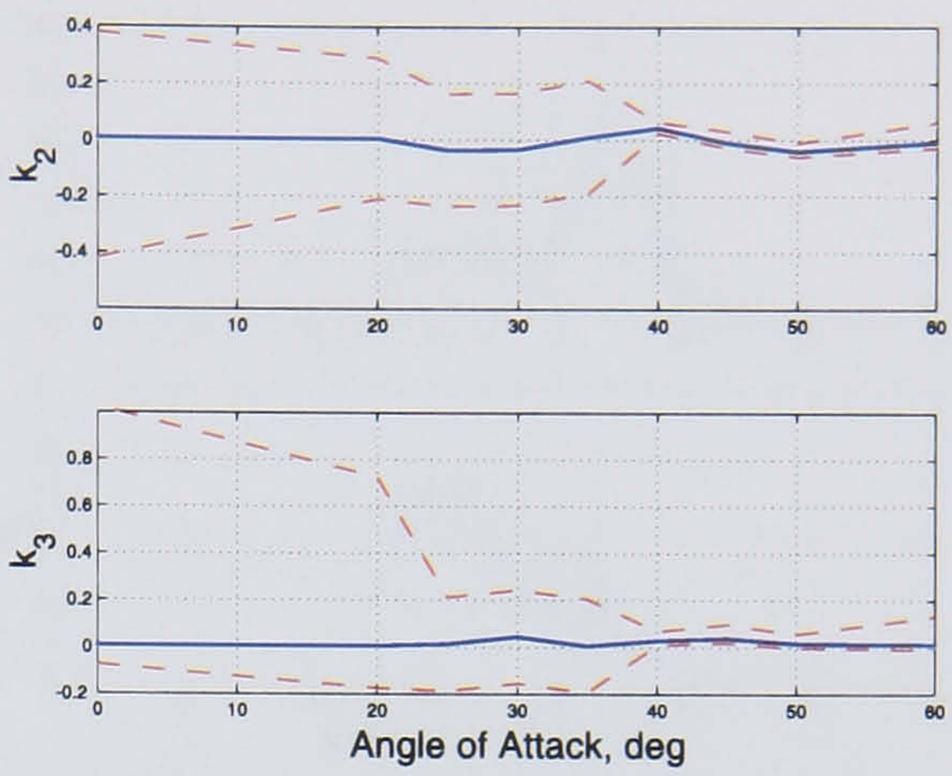

Figure 5.10: Variations of k_2, k_3 resulting in 1% change of the cost function.

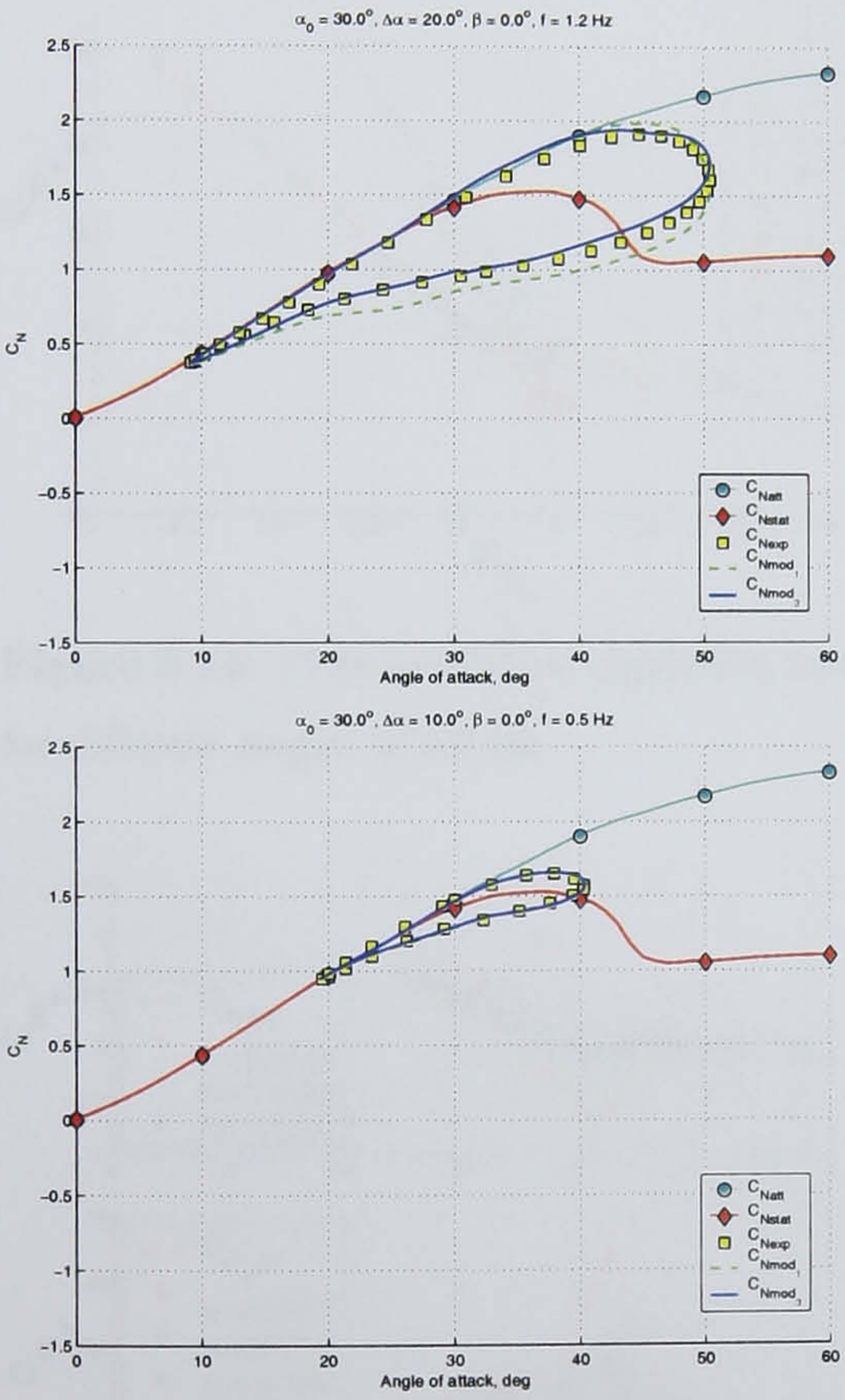

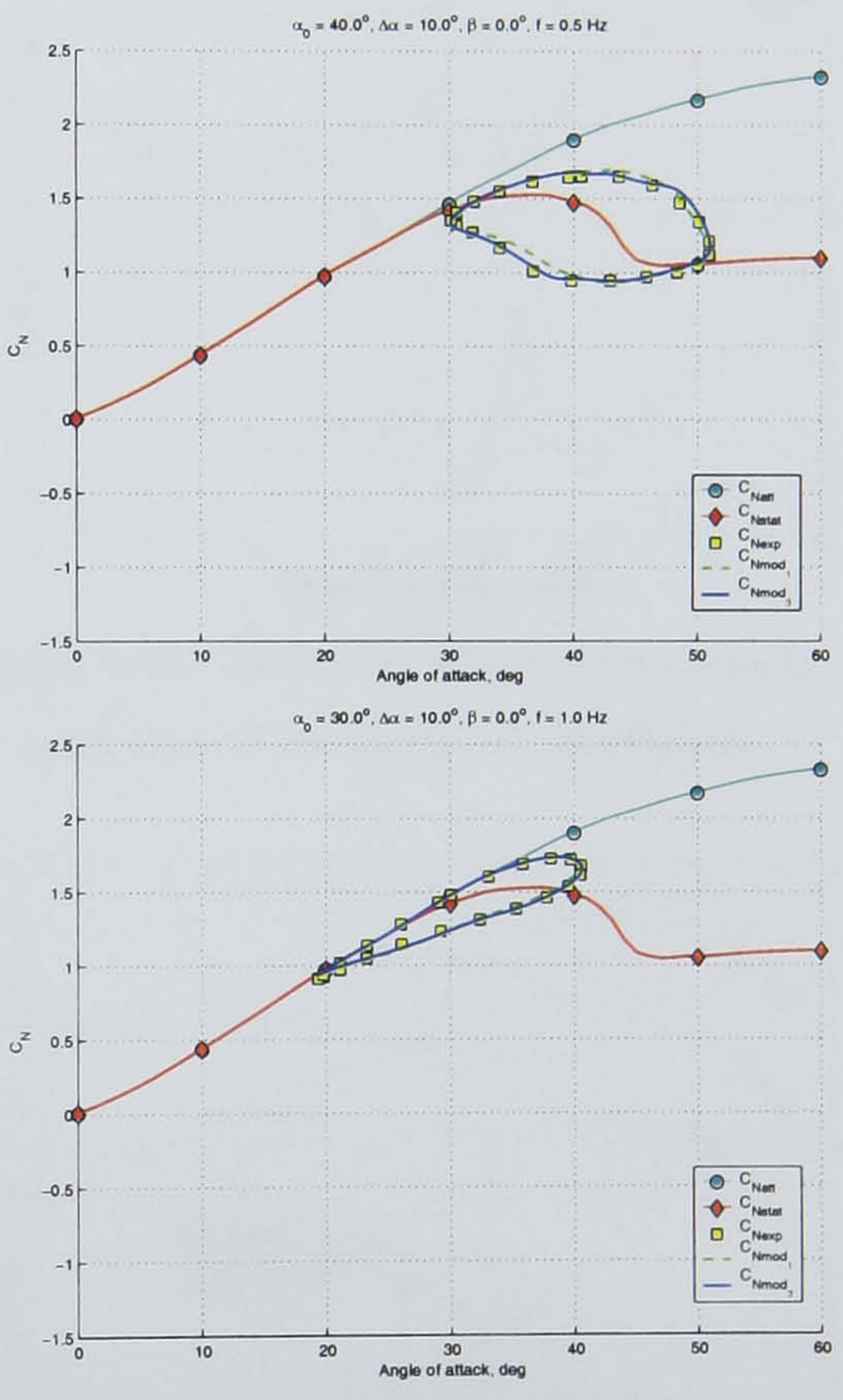

Figure 5.11: Large amplitude pitch oscillations: the experimental normal force coefficient responses (squares) in comparison with the predicted ones by the linear (dashed line) and nonlinear (solid line) mathematical models.

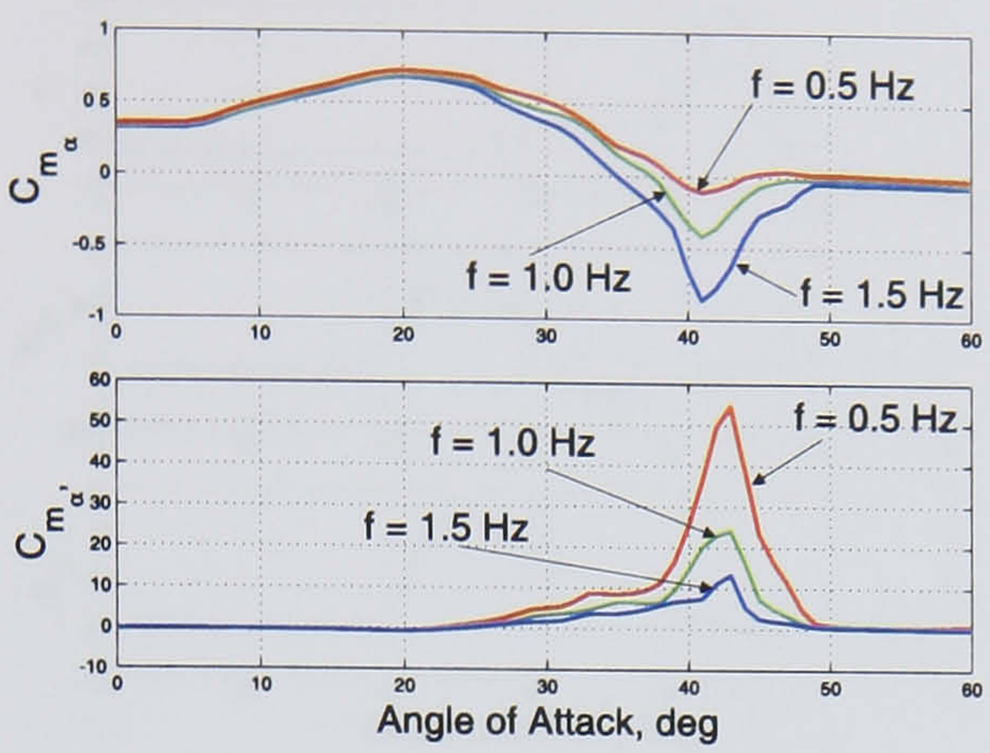

Figure 5.12: Experimental aerodynamic derivatives for the pitch moment coefficient C_m.

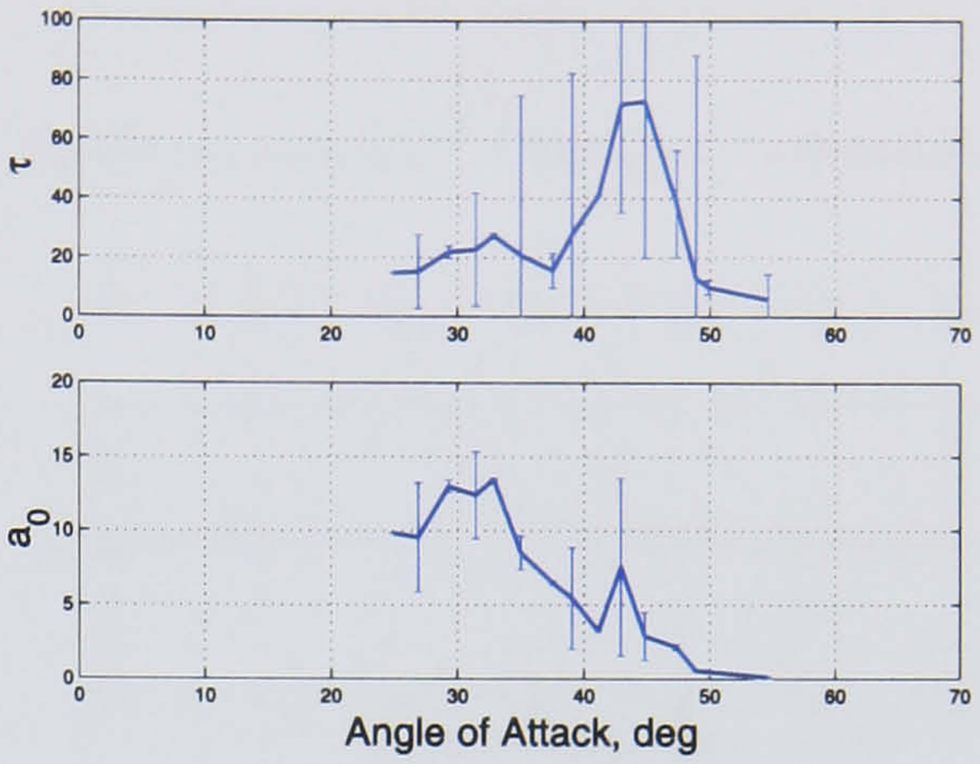

Figure 5.13: Characteristic time τ and parameter a_0 from the first step of linear regression.

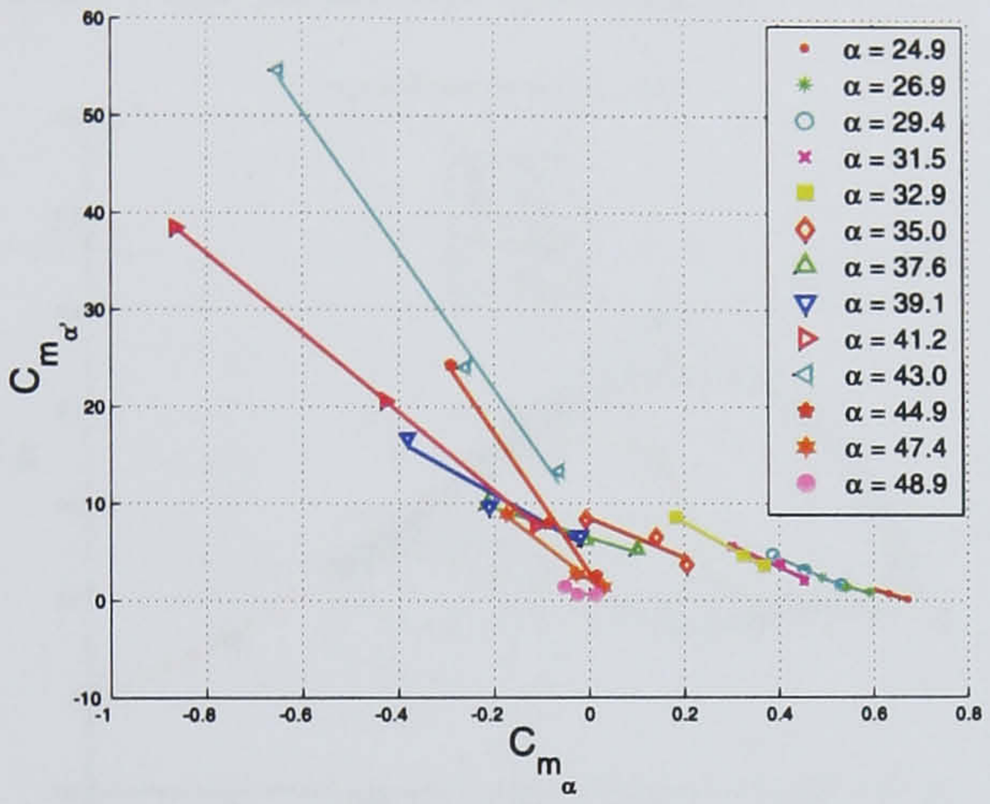

Figure 5.14: First step linear regression results for different angles of attack.

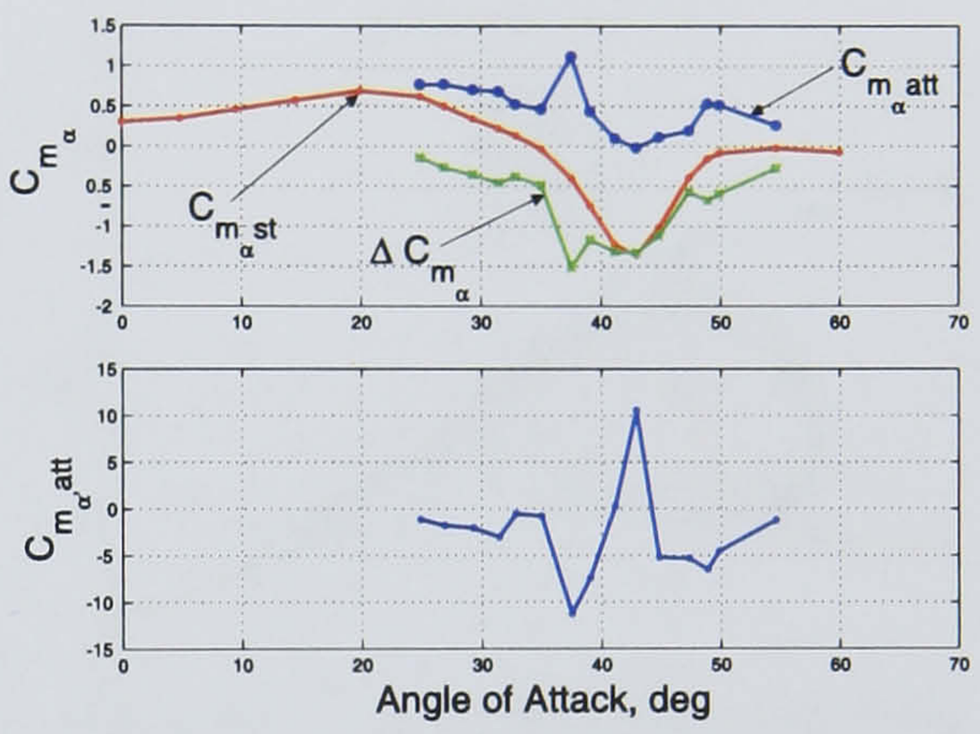

Figure 5.15: Estimated components of the linear mathematical model for C_m coefficient.

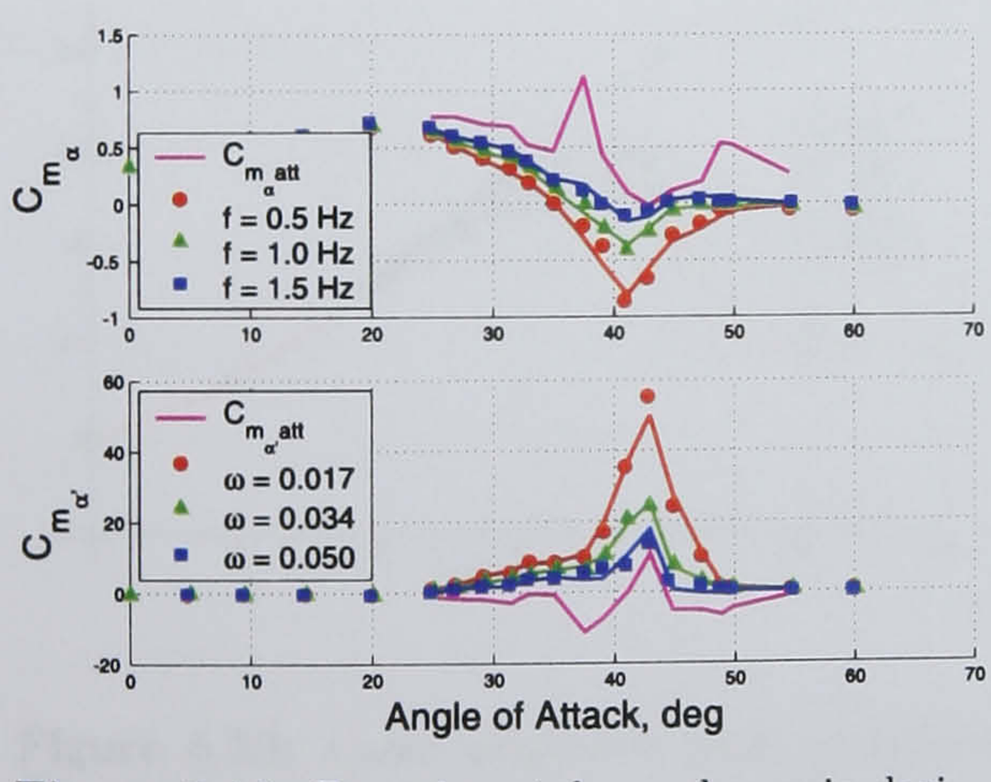

Figure 5.16: Experimental aerodynamic derivatives vs. results predicted by the linear model.

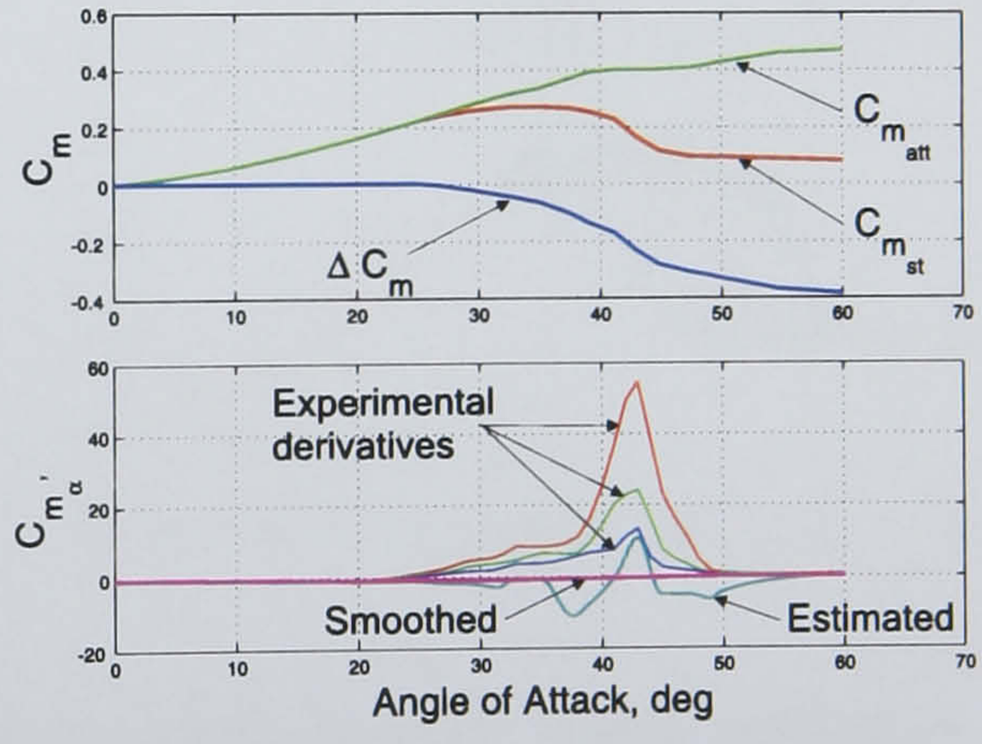

Figure 5.17: Estimated components in the form as they were included in the nonlinear model.

Figure 5.18: Identified characteristic time constant τ and parameters $k_2(\alpha)$, $k_3(\alpha)$.

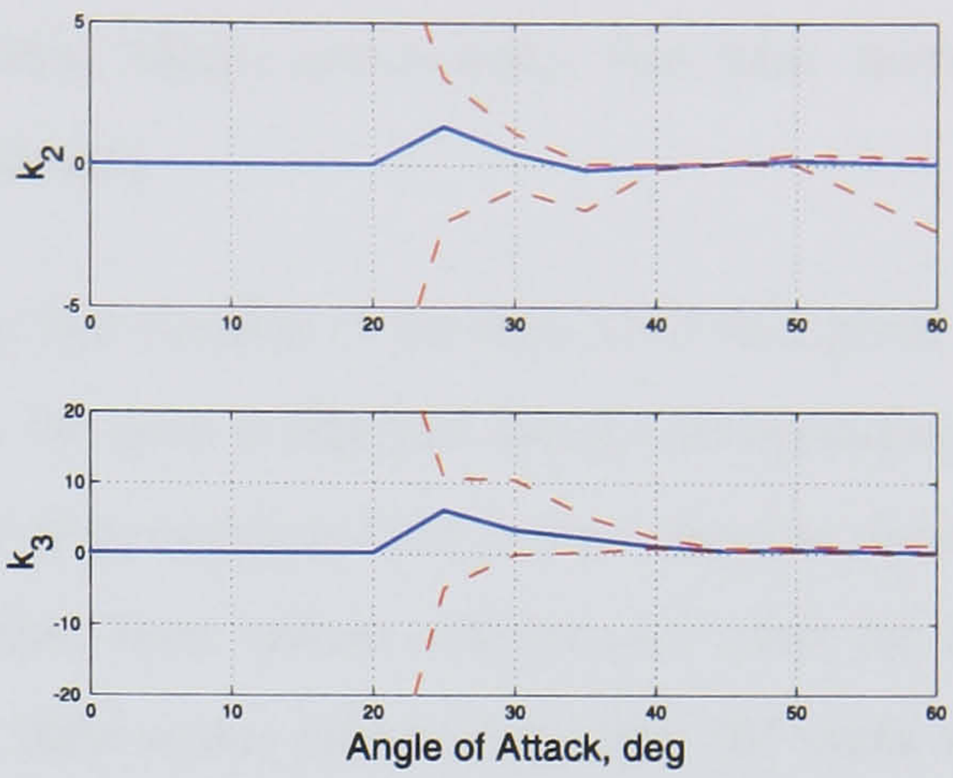

Figure 5.19: Variations of k_2, k_3 resulting in 1% change of the cost function.

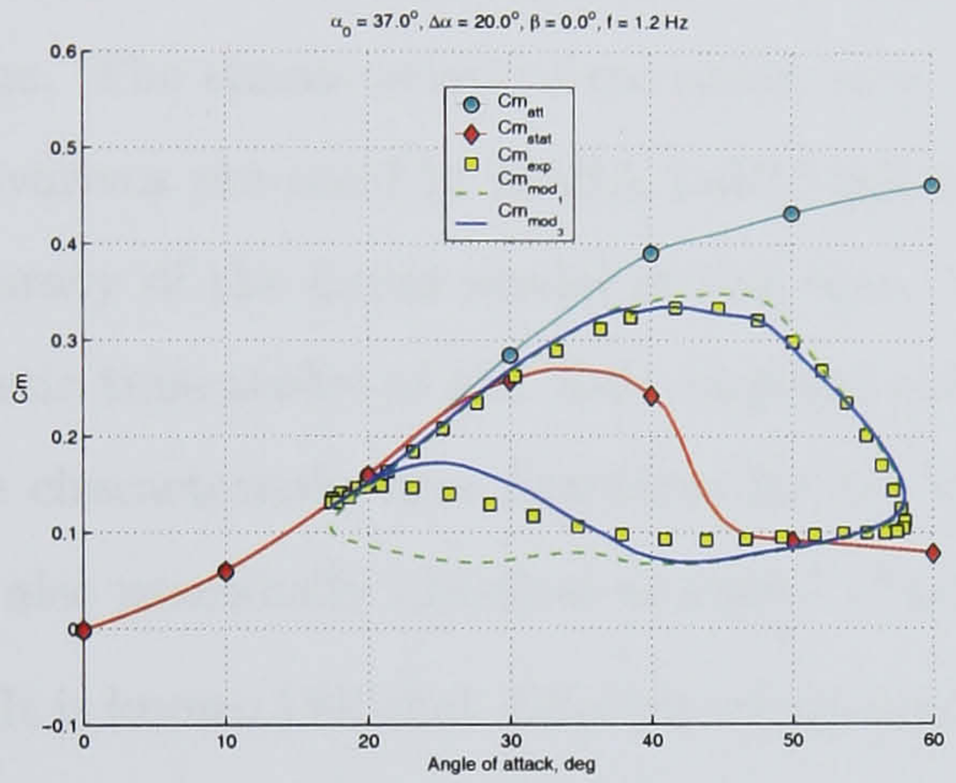

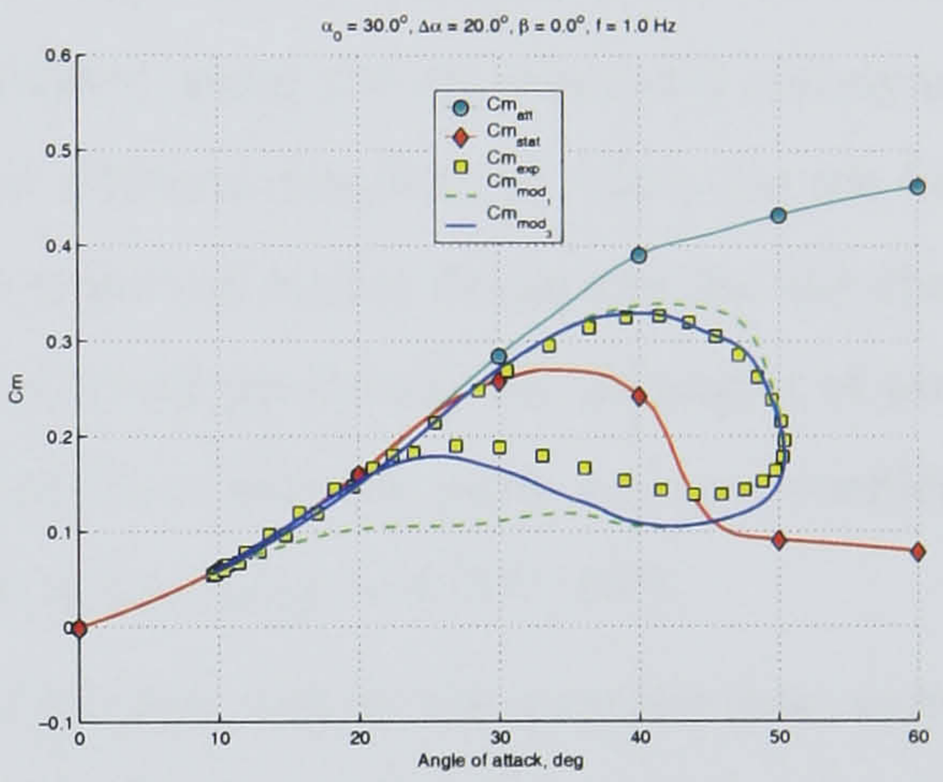

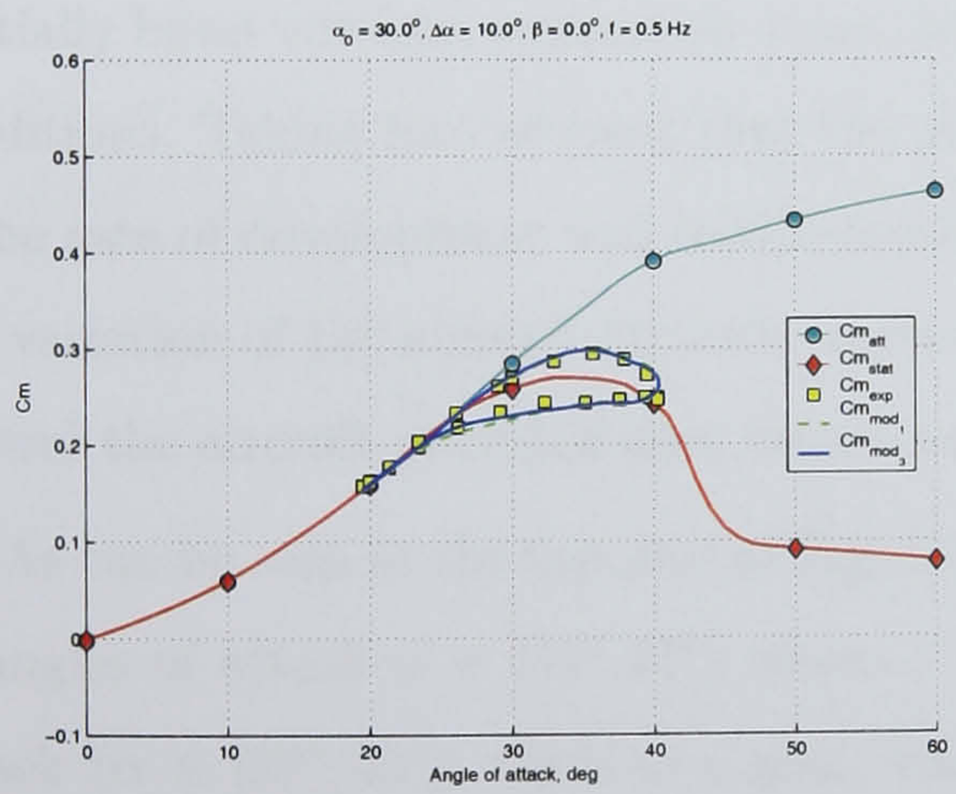

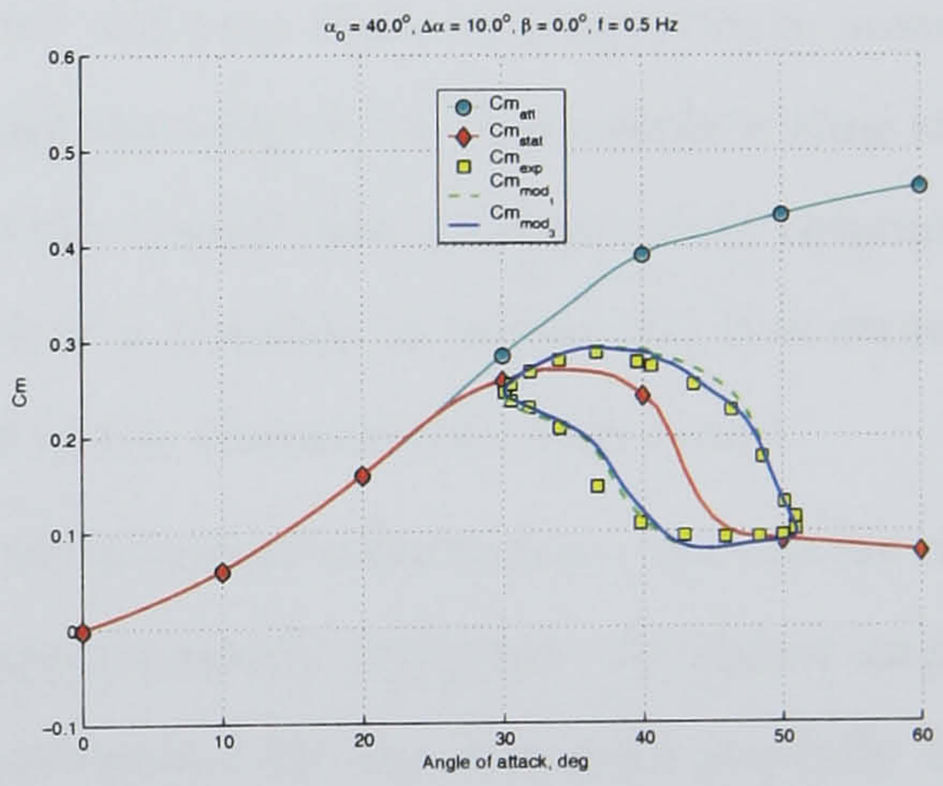

Figure 5.20: Large amplitude pitch oscillations: the experimental pitch moment coefficient responses (squares) in comparison with predicted ones using the linear (dashed line) and nonlinear (solid line) mathematical models.

5.1.3 Comparison of the characteristic time constants for the normal force and pitch moment coefficients

The characteristic time scales in the mathematical models of normal force and pitch moment coefficients were identified independently for each coefficient using corresponding experimental data. Taking into account that the characteristic time scales describe dynamic properties of the same flow, one can expect that their values will be very close for both coefficients. Comparison of the characteristic time scales obtained for the 65^o delta wing at different angles of attack is presented in Fig. 5.21 (top plot). It is seen that within the accuracy limits we deal with the same function measured by two different ways.

Similar results of identification are shown in Fig. 5.21 (bottom plot) for the X-31 airplane. The characteristic time scales were estimated using the experimental aerodynamic derivatives obtained in NASA LaRC [81] at six different frequencies. One can see better accuracy of the linear model in this case. The standard square deviations for the characteristic time scales of the X-31 airplane are very small practically for all angles of attack. The characteristic time functions for the normal force and the pitch moment coefficients are also practically identical at angles of attack in the range $\alpha \in [37^o, 65^o]$.

It is known [39] that different components of the flow such as the attached flow, vortices, partially burst vortices, separation zones, etc have different dynamic properties in unsteady conditions. Taking into account that the physical meaning of the characteristic time scales is the rate of development and readjustment of the typical flow components in response to the variation of the aircraft attitude, sometimes it is possible to outline the flow structure around the aircraft provided that we are aware of the characteristic time scales.

As can be seen in the top plot of Fig. 5.21, the attached vortical flow exists in the range of angles of attack $\alpha \in [25^o, 37^o]$ where τ is approximately constant. At higher angle of attack ($\alpha \in [37^o, 50^o]$) there is a peak which is typical for the flow with partially burst vortices. Then, this peak is followed by the region with the fully separated flow ($\alpha > 50^o$) having significantly less characteristic times.

In case of the X-31 airplane (see Fig. 5.21, bottom plot) the picture is more difficult as there are no distinct peaks like for the delta wing. Since the aircraft has more complex geometry than the wing, this can be explained by the presence of several vortical systems

arising at the nose part of the fuselage, the leading edge of the wing, etc. All these vortical systems have their own dynamic properties and interfere with each others that results in a vague dependence of the characteristic time function on angle of attack as the proposed regression technique is able to capture only the total effect.

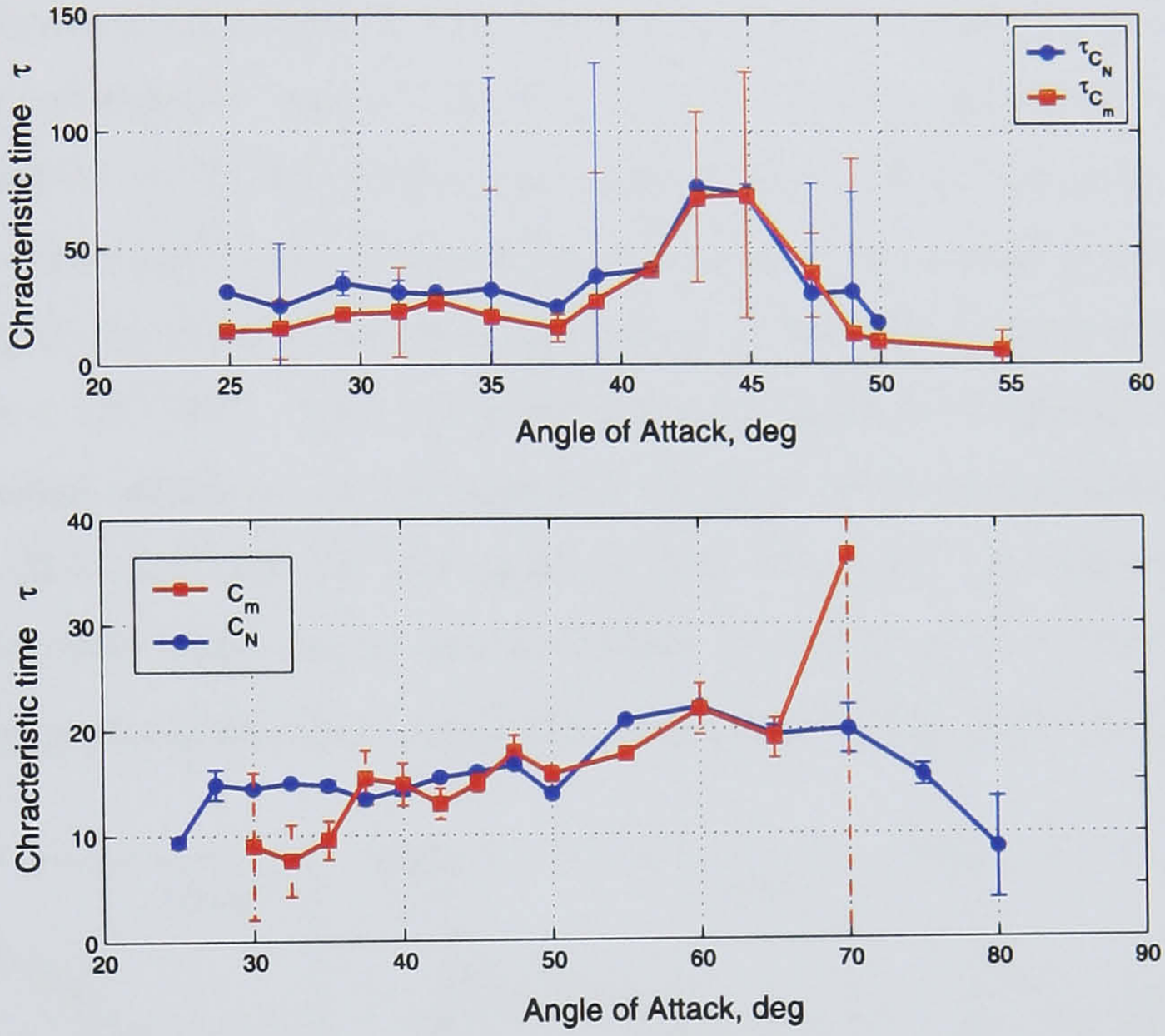

Figure 5.21: Characteristic time constants obtained using the normal force and the pitch moment data for the 65^o delta wing (top plot) and for the X-31 airplane (bottom plot).

5.2 Lateral aerodynamic characteristics of the 65^o delta wing

5.2.1 Rolling moment coefficient C_l

A mathematical model for the lateral rolling moment coefficient is developed in this section using the technique similar to that of used for the modelling of the longitudinal pitching moment and normal force coefficients. Unfortunately, static dependence of the rolling moment coefficient on sideslip was not measured in the wind tunnel tests for the whole required range of angles of attack. Therefore, the data obtained during the slow variation of the yaw angle ($r = \pm 4^o/sec$) at fixed pitch angle is used to build this static dependence. During this quasi-steady experiment two dependencies of the rolling moment coefficient corresponding to the forward and backward swings in yaw were measured for each fixed pitch angle $\gamma \in [10^o, 60^o]$. Since the pitch and yaw angles of an aircraft model on the OVP-102B forced oscillation rig are related to the angle of attack and sideslip according to equations (2.5) and that the yaw angle did not exceed 20^o, the following simplified expressions for these angles can be used for further calculations: $\alpha \approx \gamma$ and $\beta \approx \psi \cos\alpha$.

The experimental quasi-steady dependencies are given in Fig. 5.22. There is a range of

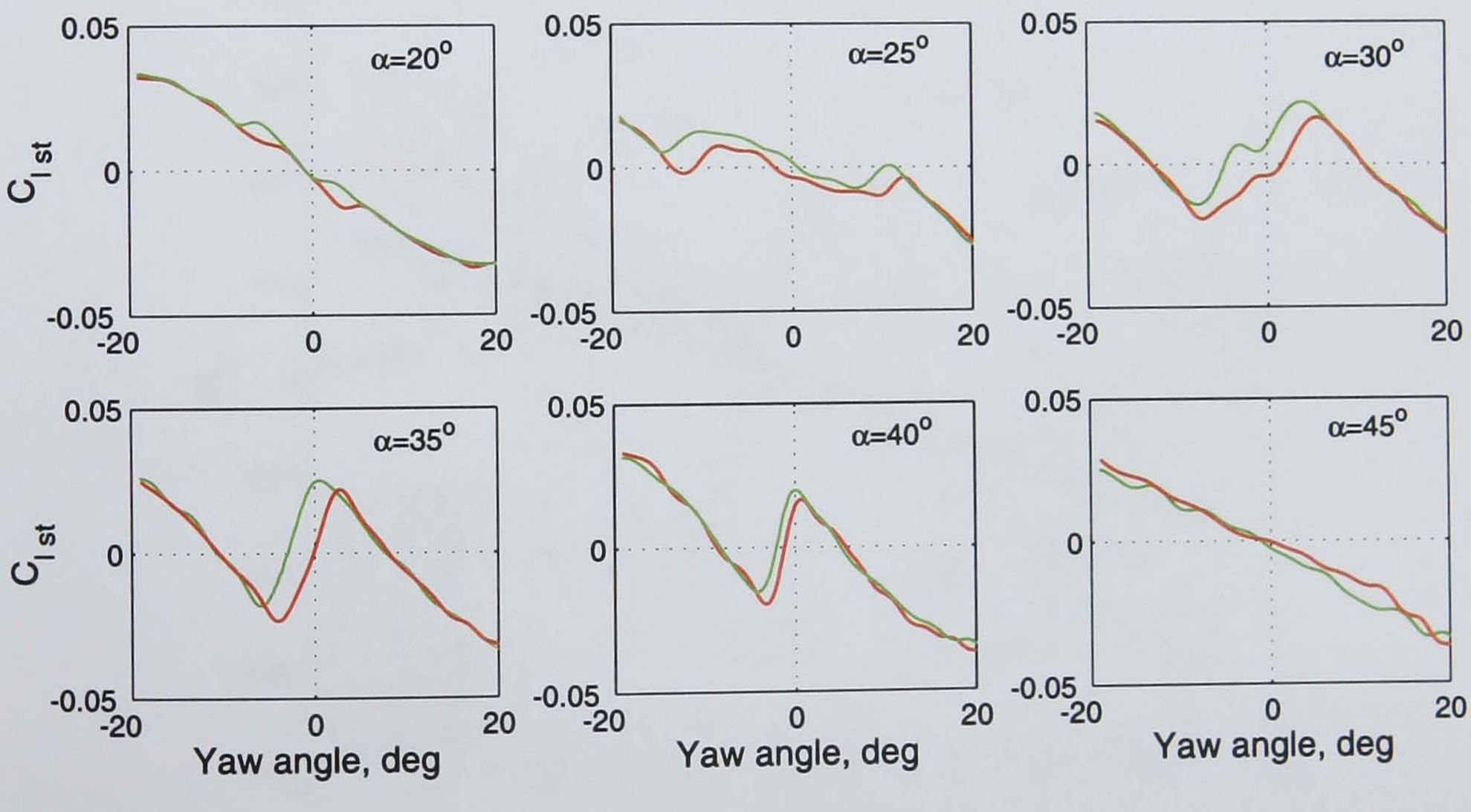

Figure 5.22: Rolling moment coefficient C_l at slow variation of yaw angle ($r = \pm 4$ deg/s) for different angles of attack (red line - $r > 0$, green line - $r < 0$)

angles of attack $\alpha \in [20^o, 40^o], \psi \approx \pm 10^o$ where the rolling moment coefficient has a strong nonlinear dependence on the angle of attack and sideslip due to the vortex breakdown processes over the wing. High sensitivity of the vortex breakdown processes to the rate of attitude variation produces the hysteresis type dependencies, and this hysteresis takes place even at a very slow change of incidence as in presented quasi-steady tests. The dynamic hysteresis loops signify the critical states crossings, for example, when the vortex breakdown point crosses the trailing edge in both directions when sideslip either increases or decreases. Based on these experimental results and the assumption that there is no static hysteresis inside these dynamic loops, the static dependence for the rolling moment coefficient on angle of attack and sideslip has been defined for further use in mathematical modelling as mean values of the corresponding dependencies (See Fig. 5.23 and Fig. 5.24).

The experimental derivatives obtained using small amplitude forced oscillation tests data for the rolling moment coefficient in yaw and roll at a fixed pitch angle and zero mean sideslip are presented in Fig. 5.25. It is seen that at angles of attack $\alpha \in [25^o, 40^o]$ they significantly depend on the frequency of oscillations f, consequently the approach discussed in Chapter 4 may be also applied for the rolling moment coefficient.

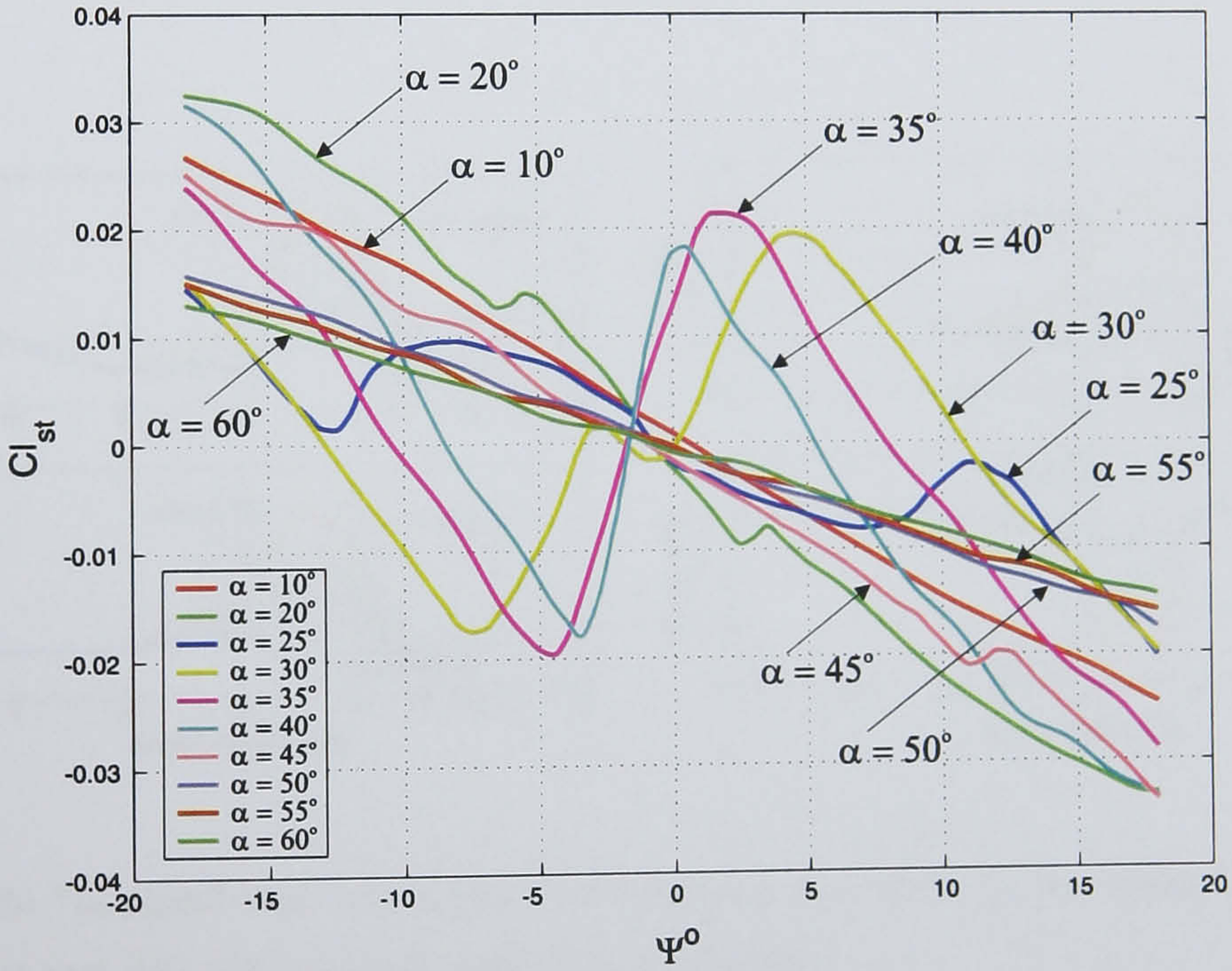

Figure 5.23: Cross-sections of static dependence of the rolling moment coefficient $C_{l_{st}}(\alpha, \psi)$.

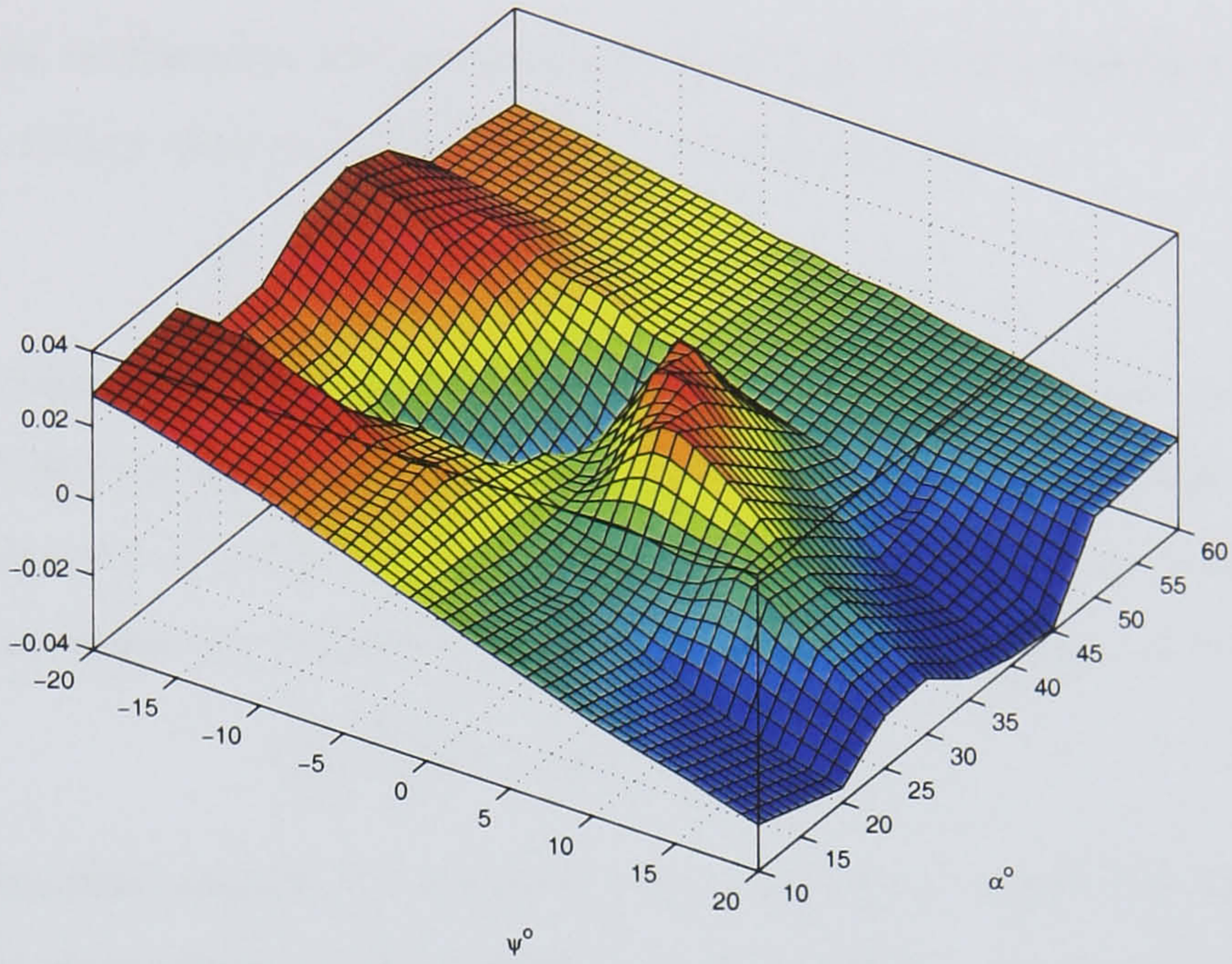

Figure 5.24: Static dependence of the rolling moment coefficient $C_{l_{st}}(\alpha, \psi)$.

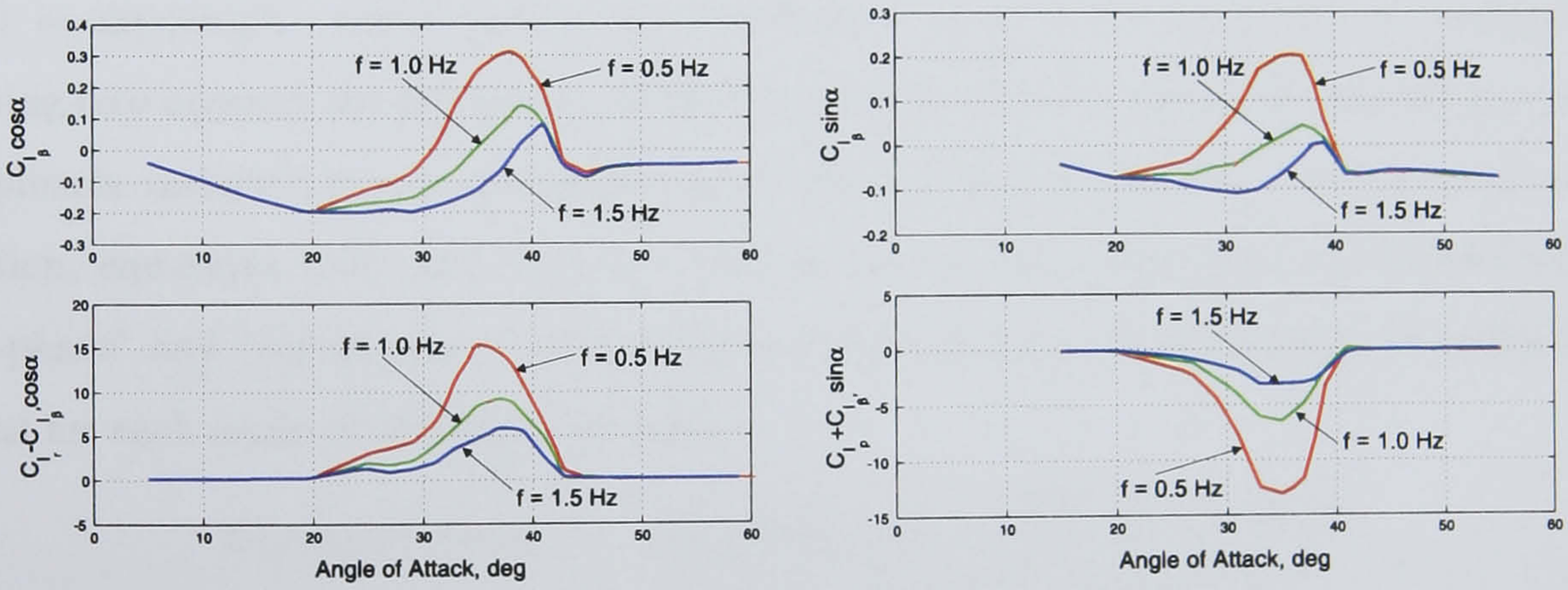

Figure 5.25: "In-phase" and "out-of-phase" aerodynamic derivatives for the rolling moment coefficient during yaw (left plot) and roll (right plot) oscillations.

5.2.1.1 Identification of the linear model using small amplitude oscillatory data in yaw

In the case of yaw oscillations, the aerodynamic loads partitioning equation (4.1) can be rewritten for the rolling moment coefficient in the following form:

$$C_l = C_{l_{att}}(\alpha, \beta) + C_{l_{dyn}} + C^*_{l_{r_{att}}}(\alpha)\dot{\psi}, \tag{5.5}$$

where $C_{l_{att}}(\alpha, \beta)$ represents a hypothetical moment and $C^*_{l_{r_{att}}}(\alpha) = \left(C_{l_r}(\alpha) - C_{l_{\dot{\beta}}}(\alpha)\cos\alpha\right)_{att}$ is the complex of derivatives, which would be in the case of unburst attached vortical flow. To describe the dynamic component $C_{l_{dyn}}$ representing the unsteady contribution from the vortical or separated flow the following linear dynamic equation similar to (4.2) is used:

$$\tau\frac{b}{2V}\frac{dC_{l_{dyn}}}{dt} = \Delta C_l(\alpha, \beta) - C_{l_{dyn}}. \tag{5.6}$$

The nonlinear function $\Delta C_l(\alpha, \beta)$ represents the difference between the experimentally determined static dependence of the rolling moment coefficient $C_{l_{st}}(\alpha, \beta)$ and hypothetical static dependence, which would be in the case of unburst attached vortical flow: $\Delta C_l(\alpha, \beta) = C_{l_{st}}(\alpha, \beta) - C_{l_{att}}(\alpha, \beta)$. Plots of these functions can be found in Fig. E.7.

During small amplitude yaw oscillations, the yaw angle ψ varies in time harmonically $\psi(t) = \Delta\psi \sin\omega t$, where $\Delta\psi$ is the amplitude and ω is the frequency of oscillations. Taking into account the kinematics of the forced oscillations rig (Eq. 2.5), assuming a small amplitude variation in yaw and applying the linearization procedure as in the longitudinal motion, equations (5.5) and (5.6) are reduced to the form describing the dependence of "in-phase" and "out-of-phase" rolling moment derivatives on the frequency of oscillations. Thus for each angle of attack α_0 we have:

$$\begin{aligned} C_{l_\beta}(\alpha_0, \omega)\cos\alpha_0 &= C_{l_{\beta_{att}}}(\alpha_0)\cos\alpha_0 + \frac{\Delta C_{l_\beta}(\alpha_0, \omega)\cos\alpha_0}{1 + \tau^2\omega^2} \\ C^*_{l_r}(\alpha_0, \omega) &= C^*_{l_{r_{att}}}(\alpha_0) + \tau\frac{\Delta C_{l_\beta}(\alpha_0)\cos\alpha_0}{1 + \tau^2\omega^2}, \end{aligned} \tag{5.7}$$

where $C^*_{l_r}(\alpha_0, \omega) = C_{l_r}(\alpha_0, \omega) - C_{l_{\dot{\beta}}}(\alpha_0, \omega)\cos\alpha_0$ is the complex of aerodynamic derivatives. Multiplying the first equation by τ and subtracting from the second one the following linear regression equation is obtained:

$$\begin{aligned} C^*_{l_r}(\alpha_0, \omega) &= a_0 + \tau C_{l_\beta}(\alpha_0, \omega)\cos\alpha_0 \\ a_0(\alpha_0) &= C^*_{l_{r_{att}}}(\alpha_0) - \tau C_{l_{\beta_{att}}}(\alpha_0)\cos\alpha_0. \end{aligned} \tag{5.8}$$

Since the values of $C^*_{l_r}(\alpha_0, \omega)$ and $C_{l_\beta}(\alpha_0, \omega)\cos\alpha_0$ are experimentally determined for three different frequencies ω at a number of fixed angles of attack α_0, the first equation in (5.8) can be applied for estimating the characteristic time scale τ in a range of angles of attack where the "in-phase" and "out-of-phase" rolling moment derivatives depend on reduced frequency of oscillations ω. Then, the second step of the linear regression technique is used to evaluate the derivatives associated with the attached flow.

The results of the application of this linear regression technique to the experimental data for the 65^o delta wing are shown in Figs. 5.26–5.28. The first figure contains the estimated characteristic time scale $\tau(\alpha)$ and the parameter $a_0(\alpha)$ with their standard deviations. One can see a very high accuracy of the estimates in the range of angles of attack $\alpha_0 \in [25^o, 40^o]$ where the aerodynamic derivatives significantly depend on frequency. Analysis of the experimental data on the $C_{l_\beta} - C^*_{l_r}$ plane (Fig. 5.26) shows that the linear dependencies fit them very well in the range $\alpha_0 \in [25^o, 40^o]$. This means that the first order dynamic model (5.5)–(5.6) is good enough to capture the unsteady aerodynamic effects.

Results of the second step of the linear regression i.e. the "in-phase" (upper plot) and "out-of-phase" (bottom plot) aerodynamic derivatives associated with the attached flow components are shown in Fig. 5.28. One can see that the obtained dependencies are rather smooth except for the leftmost and rightmost points. This is due to a singularity resulting from the weak dependence of the experimental aerodynamic derivatives on the reduced frequency ω at small and large incidences.

5.2.1.2 Identification of the linear model using small amplitude oscillatory data in roll

As can be seen from Fig. 5.25 (right plot) the experimental "in-phase" and "out-of-phase" derivatives for the rolling moment coefficient significantly depend on the frequencies of the roll oscillations. Hence, the aerodynamic load partitioning technique can be also applied in this case:

$$C_l = C_{l_{att}}(\alpha, \beta) + C_{l_{dyn}} + C^*_{l_{p_{att}}}(\alpha)\dot{\phi}, \tag{5.9}$$

where $C_{l_{att}}(\alpha, \beta)$ is the hypothetical moment and $C^*_{l_{p_{att}}}(\alpha) = \left(C_{l_p}(\alpha) + C_{l_{\dot\beta}}(\alpha)\sin\alpha\right)_{att}$ is the complex of derivatives, which would occure in the case of unburst attached vortical

flow.

To describe the dynamic component $C_{l_{dyn}}$ representing the unsteady contribution from vortical and separated flow a linear equation similar to (5.6) is used:

$$\tau \frac{b}{2V} \frac{dC_{l_{dyn}}}{dt} = \Delta C_l(\alpha, \beta) - C_{l_{dyn}}. \tag{5.10}$$

During small amplitude roll oscillations, an aircraft model roll angle ϕ varies in time harmonically: $\phi(t) = \Delta\phi \sin \omega t$, where $\Delta\phi$ is the amplitude and ω is the frequency of oscillations. Taking into account the kinematics (Eq. 2.6) of the forced oscillations rig, assuming a small amplitude variation in roll and applying a linearization procedure similar to the longitudinal motion, the equations (5.9) and (5.10) are reduced to those which describe the dependence of the "in-phase" and "out-of-phase" rolling moment derivatives on the frequency of oscillations. Thus for each angle of attack α_0 we have:

$$\begin{aligned} C_{l_\beta}(\alpha_0, \omega) \sin \alpha_0 &= C_{l_{\beta_{att}}}(\alpha_0) \sin \alpha_0 + \frac{\Delta C_{l_\beta}(\alpha_0) \sin \alpha_0}{1 + \tau^2 \omega^2} \\ C^*_{l_p}(\alpha_0, \omega) &= C^*_{l_{p_{att}}}(\alpha_0) + \tau \frac{\Delta C_{l_\beta}(\alpha_0) \sin \alpha_0}{1 + \tau^2 \omega^2}, \end{aligned} \tag{5.11}$$

where $C^*_{l_p}(\alpha_0, \omega) = C_{l_p}(\alpha_0, \omega) + C_{l_{\dot\beta}}(\alpha_0, \omega) \sin \alpha_0$ is the complex of aerodynamic derivatives. Multiplying the first equation in (5.11) by τ and subtracting from the second one the following linear regression equation is obtained:

$$\begin{aligned} C^*_{l_p}(\alpha_0, \omega) &= a_0 + \tau C_{l_\beta}(\alpha_0, \omega) \sin \alpha_0 \\ a_0(\alpha_0) &= C^*_{l_{p_{att}}}(\alpha_0) + \tau C_{l_{\beta_{att}}}(\alpha_0) \sin \alpha_0. \end{aligned} \tag{5.12}$$

As in the previous case with yaw oscillations, the values of $C^*_{l_p}(\alpha_0, \omega)$ and $C_{l_\beta}(\alpha_0, \omega) \sin \alpha_0$ have been experimentally determined for three different reduced frequencies ω at different angles of attack α_0. Thus, the first equation in (5.12) can be used for the estimation of the characteristic time scales τ at each angle of attack α_0 where the "in-phase" and "out-of-phase" rolling moment derivatives significantly depend on the reduced frequency of oscillations ω. Then the aerodynamic derivatives associated with the attached flow are evaluated during the second step of the linear regression.

The results of an application of the regression technique to the experimental data for the 65° delta wing are shown in Figs. 5.29–5.31. The first figure contains the estimated characteristic time scales $\tau(\alpha)$ and parameter $a_0(\alpha)$ with their standard deviations. One

can see a high accuracy of the estimated results in the range of angles of attack $\alpha_0 \in [20^o, 38^o]$ where the experimental aerodynamic derivatives significantly depend on frequency. Analysis of the experimental data on the $C_{l_\beta} - C^*_{l_p}$ plane (Fig. 5.29) shows that the linear dependencies fit them with very good accuracy that signifies that the first order model (5.9)–(5.10) is able to capture the internal dynamics of the flow.

The results of the second step of the regression i.e. the "in-phase" (upper plot) and "out-of-phase" (bottom plot) aerodynamic derivatives associated with the attached flow components are shown in Fig. 5.31. It is seen that the dependencies obtained are rather smooth except for some points at high incidences where the linear mathematical model fails due to a singularity resulting from the weak dependence of the experimental aerodynamic derivatives in roll on ω at large incidences.

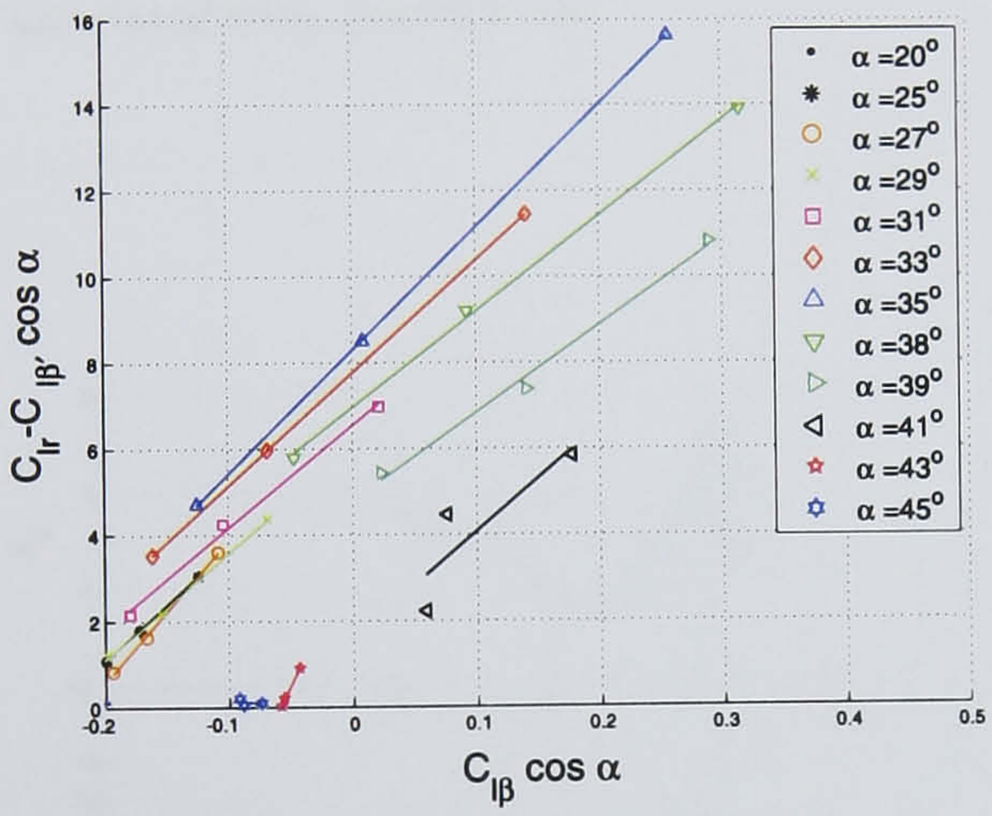

Figure 5.26: First step linear regression results for different angles of attack.

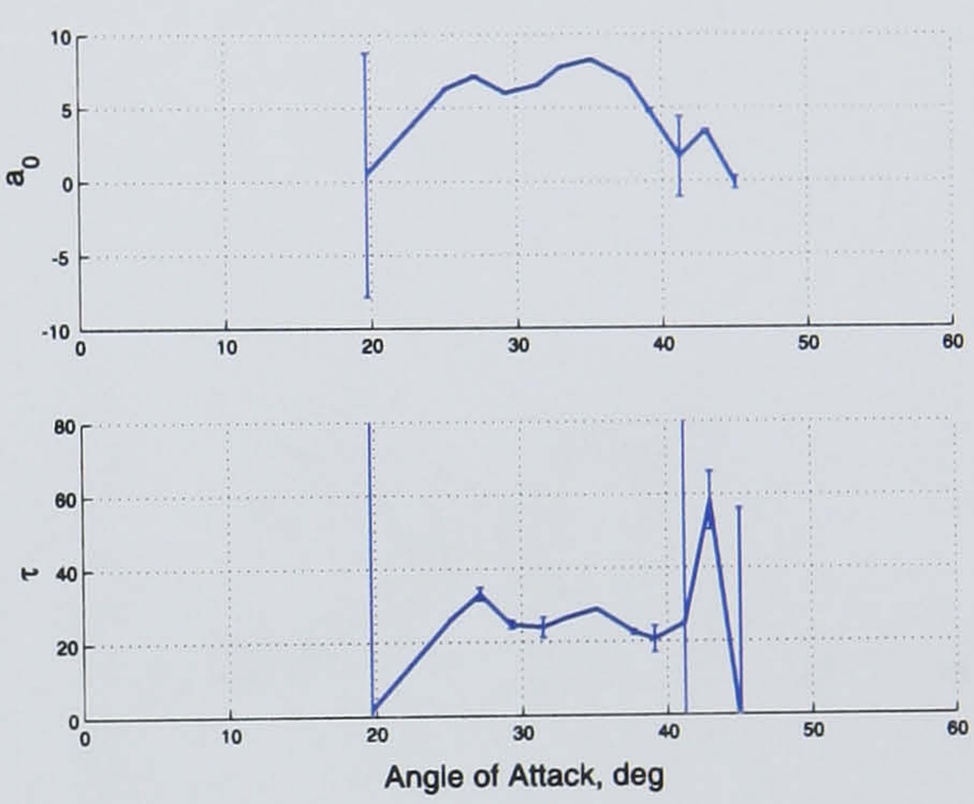

Figure 5.27: Characteristic time scale $\tau(\alpha)$ and parameter $a_0(\alpha)$ resulted from the first step of the linear regression.

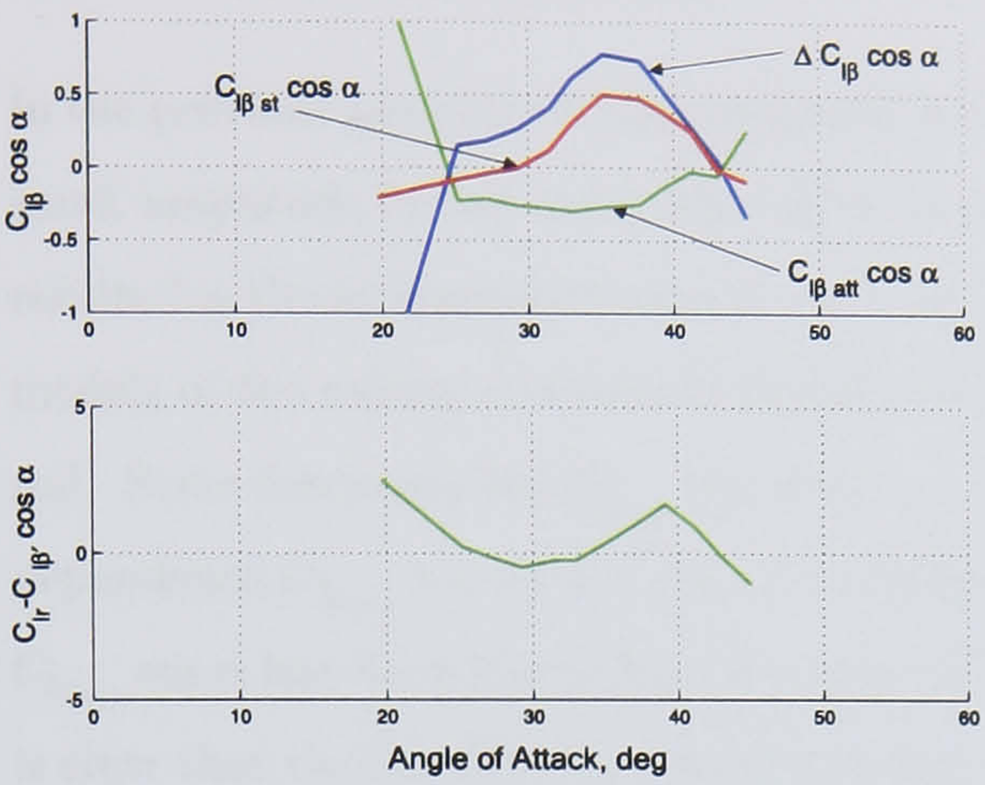

Figure 5.28: Results of second step of regression: "in-phase" and "out-of-phase" derivatives associated with attached flow.

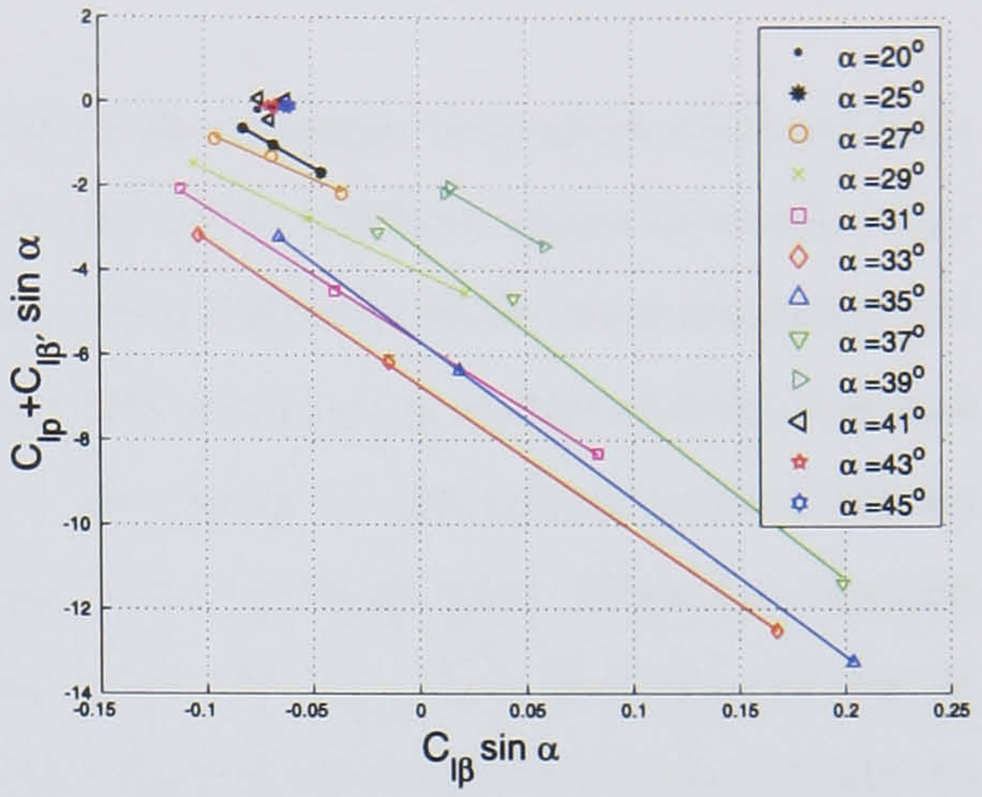

Figure 5.29: First step linear regression results for different angles of attack.

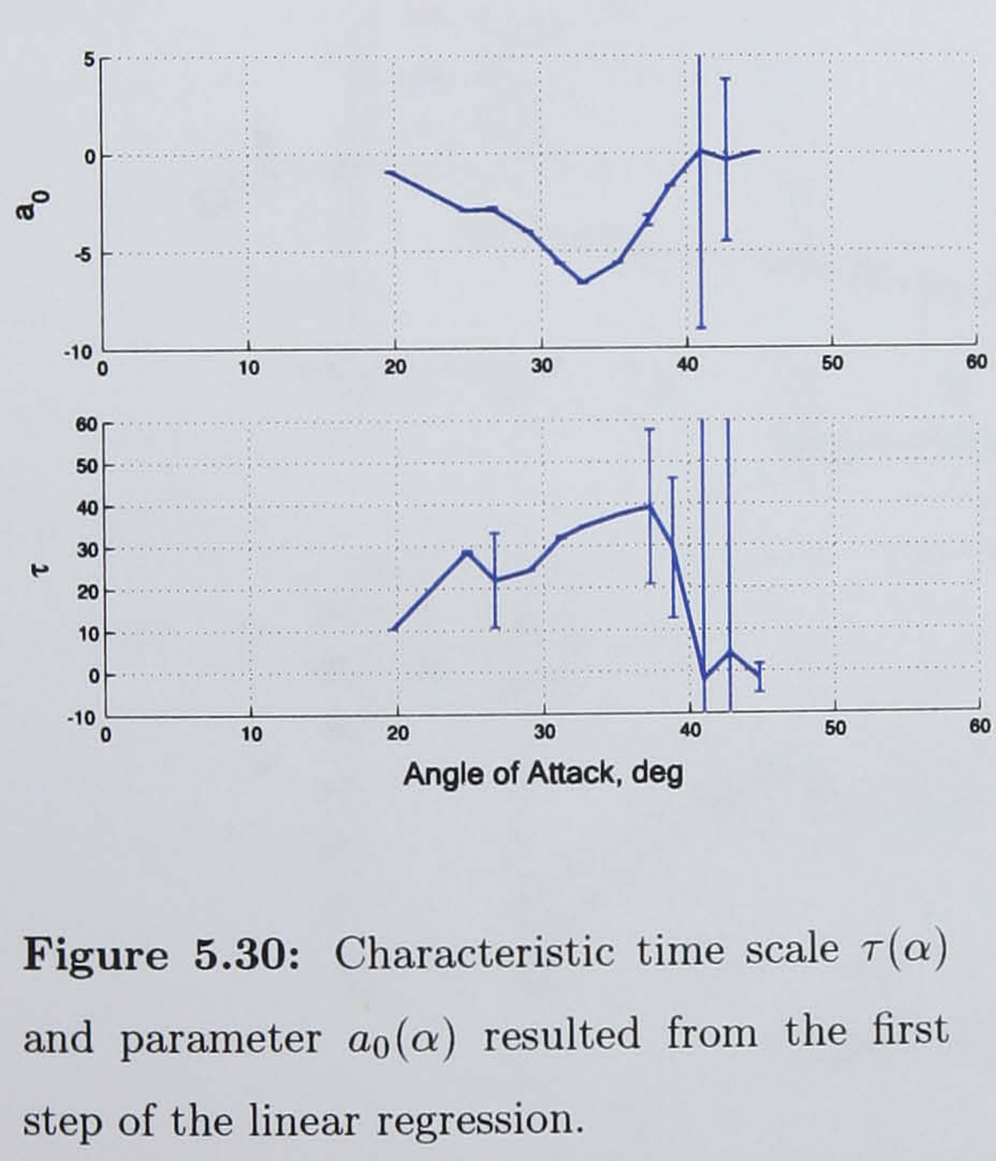

Figure 5.30: Characteristic time scale $\tau(\alpha)$ and parameter $a_0(\alpha)$ resulted from the first step of the linear regression.

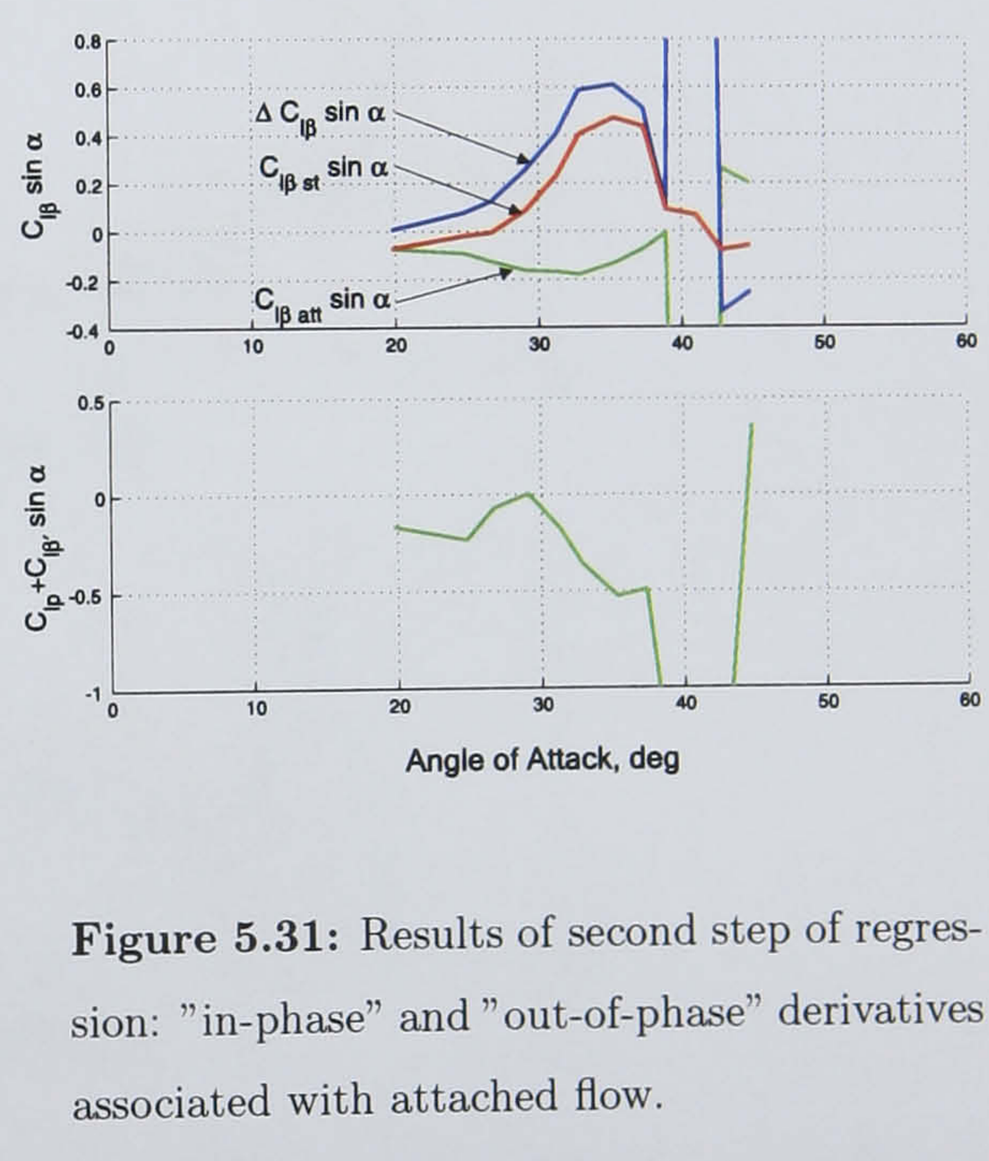

Figure 5.31: Results of second step of regression: "in-phase" and "out-of-phase" derivatives associated with attached flow.

5.2.1.3 Comparison of the models estimated using small amplitude oscillatory data in roll and yaw

In the previous sections we have analysed two sets of aerodynamic derivatives obtained from small amplitude forced oscillations tests in yaw and roll at different angles of attack. This resulted in the estimation of two sets of functions, which fully determine linear mathematical models of the rolling moment coefficient for two different types of motion namely, yaw and roll. Some functions like $C^*_{l_{r_{att}}}(\alpha)$ and $C^*_{l_{p_{att}}}(\alpha)$ are specific to the type of motion but the dependence $C_{l_{\beta_{att}}}(\alpha)$ turned out to be evaluated in two different ways. Thus, the function $C_{l_{\beta_{att}}} \cos\alpha$ has been found from the yaw motion data with $C_{l_{\beta_{att}}} \sin\alpha$ from the roll one. It is clear that the function $C_{l_{att}}(\alpha, \beta)$ specifying the static characteristic of the flow similar to $C_{l_{st}}(\alpha, \beta)$ does not depend on the type of motion. The functions $C_{l_{\beta_{att}}}(\alpha)$ estimated from roll and yaw motion data are presented in Fig. 5.32. One can see that these functions are very close in the range of angles of attack where the linear regression technique is consistent.

The characteristic time functions $\tau(\alpha)$ have been also estimated both from the yaw and roll motion experimental data. It is seen in Fig. 5.32 that they are close but not identical

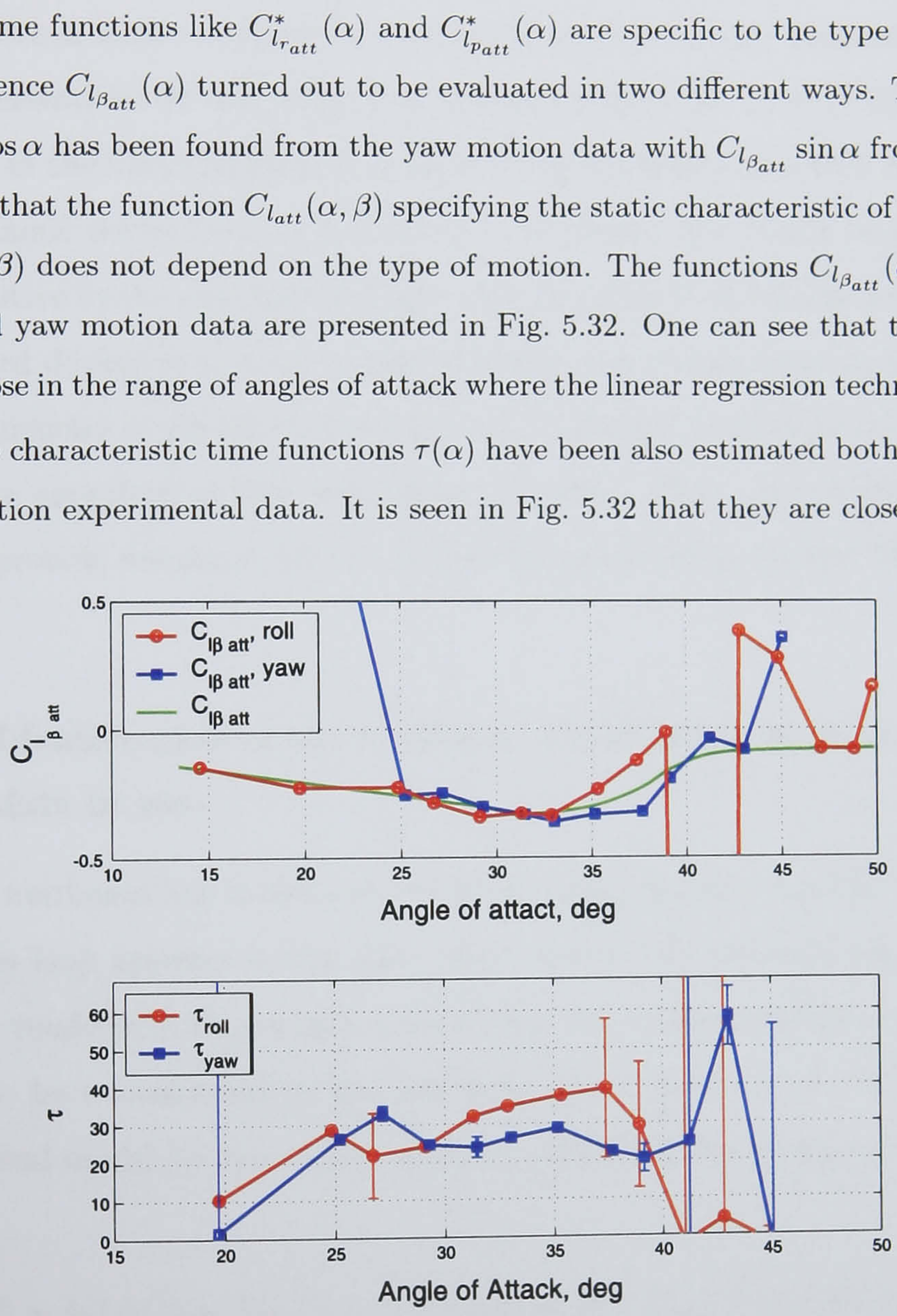

Figure 5.32: Comparison of $C_{l_{\beta_{att}}}$ derivatives (upper plot) and characteristic time functions τ (lower plot) determined using experimental oscillatory data in yaw and roll.

in the whole range of angles of attack. Thus, for example, at $\alpha \in [30^o, 37^o]$ they differ by approximately 30%, and the accuracy of the estimate is very high for this range of incidences. The most likely reason for this difference is the dependence of the characteristic time scale on the type of motion, i.e. roll or yaw, in this range of angles of attack. This fact will be discussed in Section 5.5 in connection with configurations of different wings.

An application of the described linear regression technique to the experimental data at angles of attack where vortices are not burst or flow is fully separated, e.g. where aerodynamic derivatives do not depend on frequency ($\alpha \leq 20^o$ or $\alpha \geq 40^o \ldots 45^o$) results in a singularity in the linear regression equations. At the angles of attack where the dependency of aerodynamic derivatives on frequency is moderate, the linear regression technique becomes sensitive to the experimental data that can lead to unreliable results. A high value of the standard deviation at some angles of attack can results from an insufficient number of tested frequencies or an inconsistency of the linearized mathematical model which cannot reflect more complicated flow separation processes. Thus, the analysis of standard deviations can provide estimates for the domain of applicability of the linear model regression technique.

5.2.1.4 Identification of the nonlinear model using large amplitude oscillatory data in yaw

The linear mathematical model can lose its accuracy at large amplitude oscillations or when a hysteresis loop appears in the static dependence. To reconcile the mathematical model with these conditions, the equation describing the dynamic component of an aerodynamic load has to be transformed to the nonlinear form. In this case, the dynamic part of the mathematical model for the rolling moment coefficient can be represented by the following equation:

$$\frac{b}{2V}\frac{dC_{l_{dyn}}}{dt} = k_1(\Delta C_l(\alpha,\beta) - C_{l_{dyn}}) + k_2(\Delta C_l(\alpha,\beta) - C_{l_{dyn}})^2 + k_3(\Delta C_l(\alpha,\beta) - C_{l_{dyn}})^3, \quad (5.13)$$

where $k_1 = 1/\tau$.

The attached flow component of the rolling moment coefficient $C_{l_{att}}$ is also considered as a nonlinear function of the angle of attack and sideslip:

$$C_{l_{att}}(\alpha,\beta) = C_{l_{\beta_{att}}}(\alpha) K_{C_{l_{\beta_1}}}(\alpha)\beta + C_{l_{\beta_{att_3}}}(\alpha)\beta^3, \quad (5.14)$$

where $C_{l_{\beta_{att}}}(\alpha)$ is the rolling moment coefficient derivative associated with the attached flow at zero sideslip.

This function has been estimated using small amplitude oscillatory data in yaw and roll by means of the linear regression technique. As a result, two dependencies, which are rather close in the range of angles of attack $\alpha \in [25^o, 35^o]$, have been obtained in two different ways (see Fig. 5.32). In order to be used in the nonlinear mathematical model a single dependence can be built on the basis of the estimated ones. Such a dependence, which is a smoothed combination of these two estimated functions, is shown by the green line on the same figure. Since the accuracy of the estimated dependencies $C_{l_{\beta_{att}}}(\alpha)$ is rather low at angles of attack $\alpha > 35^o$ the resulting function $C_{l_{\beta_{att}}}(\alpha)$ has to be improved in this range using additional experimental data such as the results of large amplitude oscillations in yaw. For this purpose, the correction function $K_{C_{l_{\beta_1}}}(\alpha)$ has been introduced into dependence (5.14). This correction function is parameterized in several nodes along the angle of attack and calculated at intermediate points by means of linear interpolation. Initially, the function values were set to one in all nodes and considered as free parameters during the identification. The nonlinear term $C_{l_{\beta_{att_3}}}(\alpha)\beta^3$ has been also introduced into dependence (5.14) in order to improve the prediction of aerodynamic responses in the case of large amplitude. Similar to $K_{C_{l_{\beta_1}}}(\alpha)$ the dependence $C_{l_{\beta_{att_3}}}(\alpha)$ was parameterized and initially set to zero at all nodes.

As in the case of large amplitude yaw or roll oscillations, the wing model is subject to considerable variation of sideslip β at an approximately constant angle of attack α the oscillating wing can pass through areas with different flow structures, and the model parameters reflecting these changes can vary significantly. To allow for possible variations of the flow structure in the mathematical model, a dependence on sideslip has to be introduced into the parameters k_1, k_2, k_3 in addition to that on the angle of attack.

As a result of the linear model regression, the characteristic time scale $\tau(\alpha)$ has been estimated at different angles of attack for zero sideslip. The dependence on sideslip can be introduced as a parametric function at each fixed angle of attack, and the relation $k_1(\alpha, \beta)|_{\beta=0} = 1/\tau(\alpha)$ has to be kept. Thus, a value of $k_i(\alpha, \beta), i = 1, 2, 3$ can be approxi-

mated by the following symmetrical function:

$$k_i(\alpha,\psi) = \texttt{ddspl}\left([\psi_1(\alpha),\ \psi_2(\alpha)],\ [k_{i1}(\alpha),\ k_{i2}(\alpha)],\ |\psi|\right), \tag{5.15}$$

where `ddspl` is the nonlinear function joining two constant sections with the spline, $\psi = \beta/\cos\alpha$ – an aircraft model yaw angle, functions $\psi_1(\alpha)$ and $\psi_2(\alpha)$ such that $0 \le |\psi_1| \le |\psi_2|$ are interpolation nodes, k_{i1} and k_{i2} are values of the coefficient k_i at the corresponding nodes ψ_1 and ψ_2. For $\psi \in [-\psi_1, \psi_1]$, the value of $k_i = k_{i1}$, for $\psi \ge \psi_2$ and $\psi \le -\psi_2$ the value of $k_i = k_{i2}$. A typical dependence of the characteristic time function on ψ at fixed α is shown in Fig. 5.33.

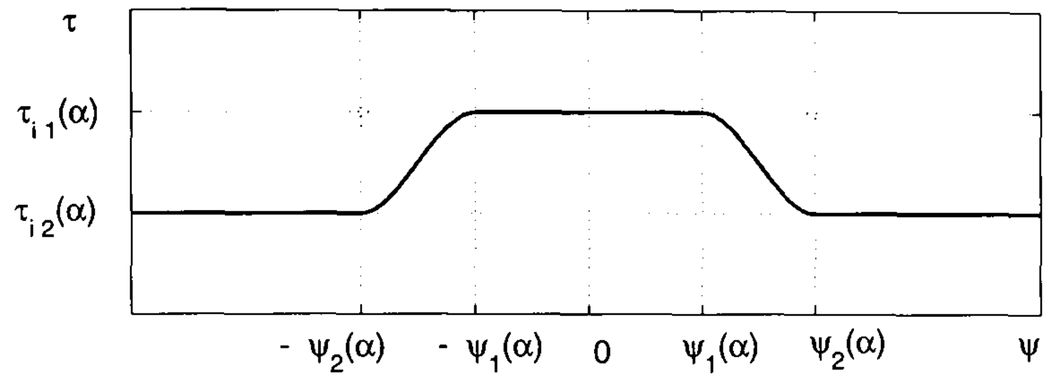

Figure 5.33: Typical dependence of characteristic time on sideslip at fixed angle of attack.

Similar to $C_{l_{\beta_{att}}}(\alpha)$ estimated using results of small amplitude oscillatory tests and the linear model, the characteristic time scale $\tau(\alpha)$ is multiplied by a correction function $K_1(\alpha)$ to improve the results of linear identification using large amplitude experimental responses, so $k_{11}(\alpha) = \dfrac{1}{\tau_1(\alpha)} K_1(\alpha)$. Initially, the values of K_1 are set to one at the interpolation nodes and determined during the identification. All other parameters k_{12}, k_{21}, k_{22}, k_{31} and k_{32} are parameterized and identified at each fixed angle of attack.

All unknown coefficients in the mathematical model are identified at this stage using experimental aerodynamic responses obtained at large amplitude yaw oscillations. This experimental data contains time records of the C_l coefficient and the ψ angle during forced oscillations in yaw with amplitudes $\Delta\psi = 10^o$ and 20^o and frequencies $f = 0.5$, 1.0 and 1.5 Hz (corresponding reduced frequencies $\omega = 0.023, 0.046$ and 0.070). The tests were conducted at several fixed angles of attack between 20^o and 45^o with a step of 5^o. This set of data covers regions with unburst vortical flow, the transient zone where vortex bursting dynamics is significant and fully stalled flow.

In order to identify the unknown parameters a procedure based on the minimization of the discrepancy (4.24) between the experimental and the predicted results was applied. Six time histories (two amplitudes at three different frequencies) were used for the parameter

identification at each fixed angle of attack between 20^o and 45^o. Totally 36 experimental records have been used for the identification. The model description for the PIIMTM program which has been used for the identification is presented in Appendix D.

One can see from Fig. 5.23 that there is a small asymmetry with respect to zero sideslip in the experimental static dependence of C_l, which is probably due to the influence of the experimental rig. To compensate this asymmetry, the following shift in sideslip is introduced: $\beta = (\psi - \psi_0)\cos\alpha$. The unknown parameter ψ_0 correlating dynamic and static data is also identified using large amplitude responses.

The identified parameters k_{12}, k_{21}, k_{22}, k_{31}, k_{32}, parameters defining the attached flow component and correction factors, which are functions of the angle of attack only, are presented in Fig. 5.34. One can see that the correction function $K_{C_{l_{\beta_1}}}(\alpha)$ is two times greater in the range of angle of attack $\alpha \in [37^o, 45^o]$, which rectifies the dependence $C_{l_{atta}}(\alpha)$ where it is ill-defined by the linear regression. Functions $C_{l_{att}}$, τ, k_2, k_3 depending on the angle of attack and yaw angle are presented in Figs. 5.35–5.38 as 3D surfaces. It is clearly seen in Fig. 5.36 that the characteristic time scales $\tau(\alpha, \psi)$ rises in the region of vortical flow and decreases in the region of fully separated flow.

A detailed comparison of the aerodynamic responses predicted by the identified mathematical model and those obtained in experiment are presented in Figs. E.7–E.12 for different angles of attack, frequencies and amplitudes of oscillations in yaw. These plots contain the

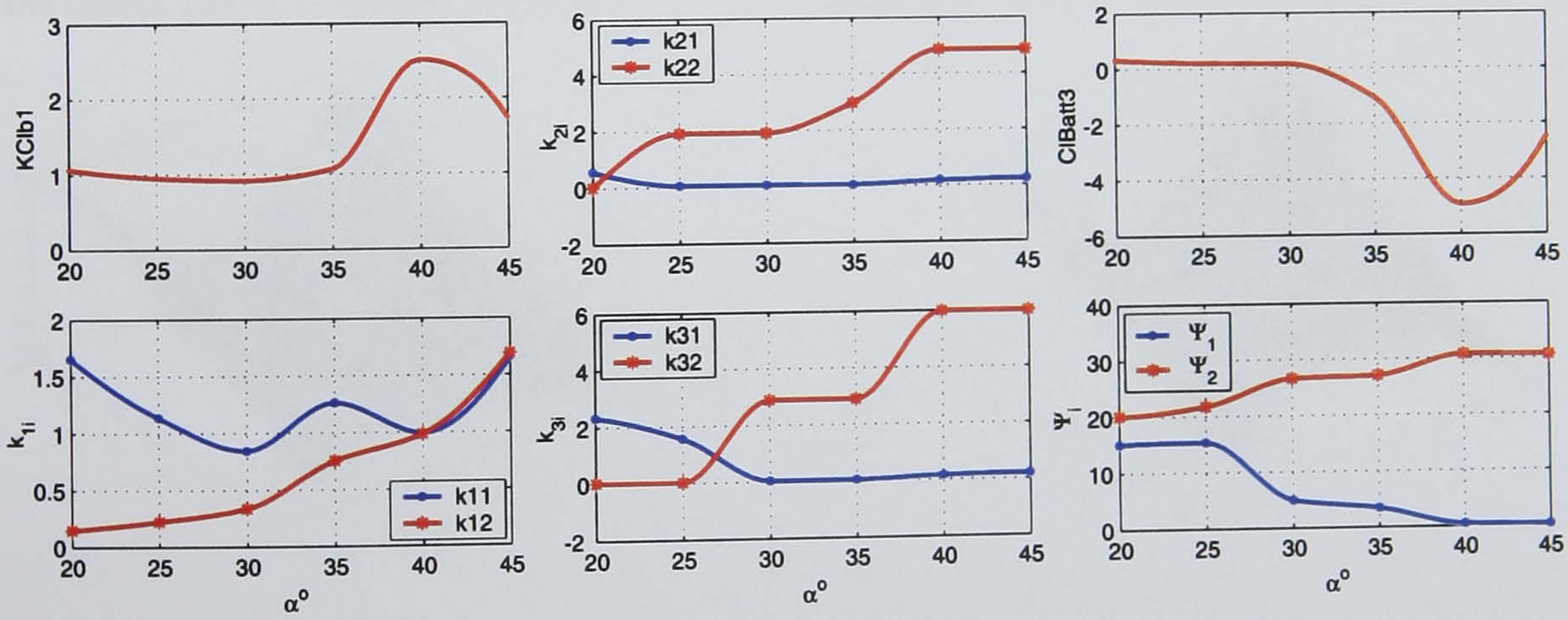

Figure 5.34: Estimated parameters of the model of rolling moment coefficient.

experimental aerodynamic response $C_{l_{exp}}(t)$ (yellow squares), the predicted aerodynamic response $C_{l_{mod}}(t)$ (blue solid line), the experimental static dependence $C_{l_{st}}$ (red line with diamonds), the attached flow contribution to the rolling moment coefficient $C_{l_{att}}$ (cyan line with circles), the function ΔC_l (red line with triangles) and the vortical dynamic contribution $C_{dyn}(t)$. It is clearly seen that the identified mathematical model rather well reflects the behaviour of the aerodynamic responses in all the considered conditions both qualitatively and quantitatively.

Unfortunately, due to the absence of large amplitude forced oscillation data in roll, it turned out to be impossible to identify a similar nonlinear mathematical model for this type of motion.

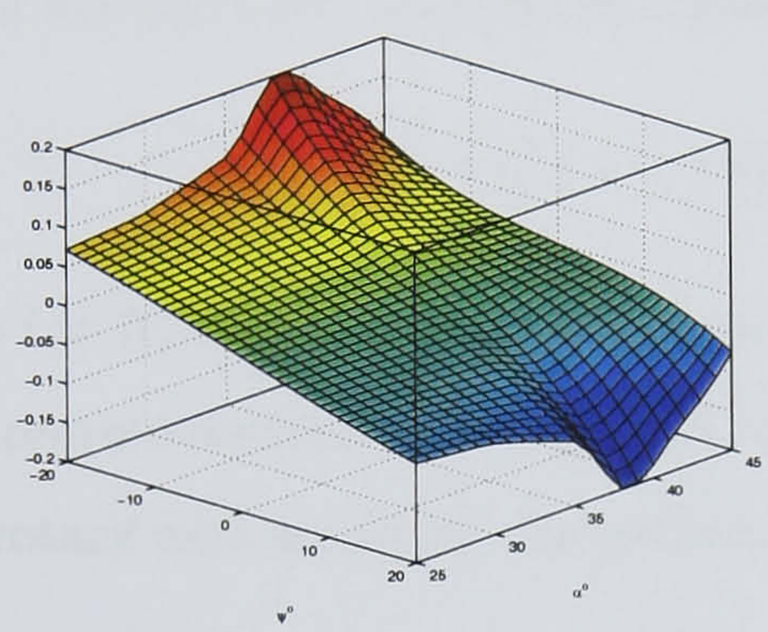

Figure 5.35: Attached flow component $C_{l_{att}}$ of the rolling moment coefficient model.

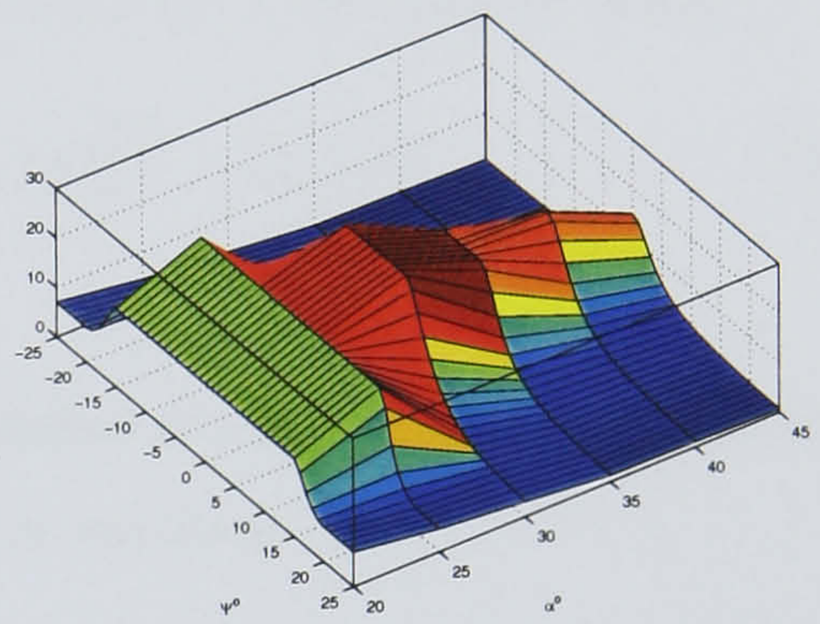

Figure 5.36: Characteristic time function for the rolling moment coefficient model in yaw.

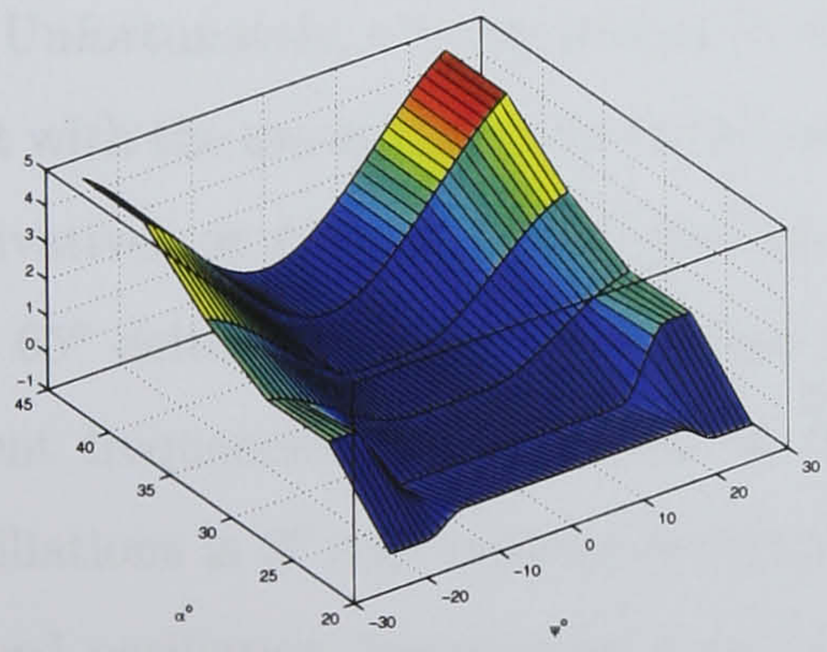

Figure 5.37: Dependence of k_2 for the nonlinear model of rolling moment coefficient.

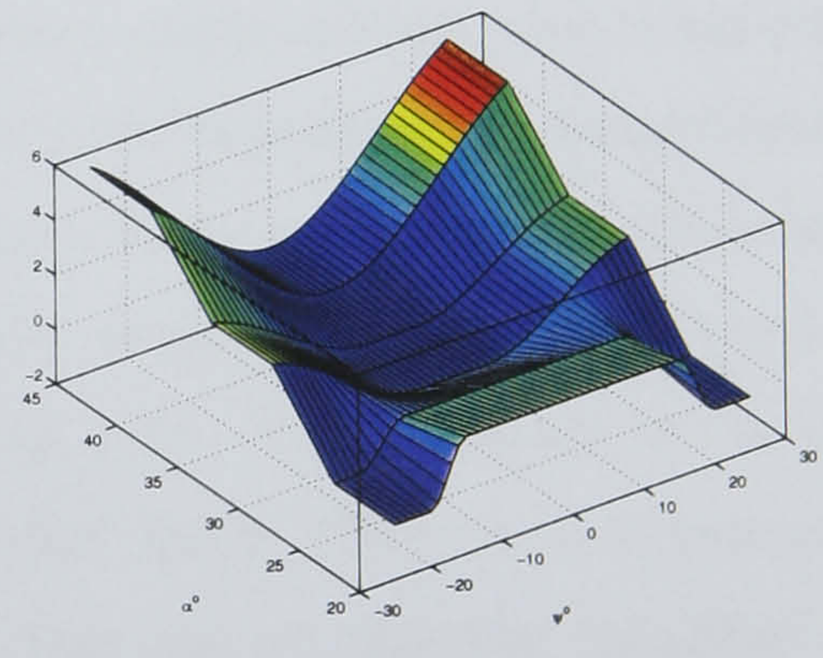

Figure 5.38: Dependence of k_3 for the nonlinear model of rolling moment coefficient.

5.3 Comparison with the conventional aerodynamic derivative model

Unsteady aerodynamic effects at low angles of attack are normally described in the form of aerodynamic derivatives, and this approximation is found to be rather accurate for different aircraft configurations. It is well supported by computational methods, wind tunnel experimental equipment and verified in many practical applications. The same aerodynamic derivative formulation has been rather formally adapted for high incidence conditions simply by including nonlinear dependencies on the angle of attack. A typical representation of longitudinal aerodynamic coefficients contains static dependency, rotary/unsteady and control aerodynamic derivatives considered now as functions of the angle of attack:

$$C_i = C_{i_{st}}(\alpha) + C_{i_q}(\alpha)\frac{q\bar{c}}{2V} + C_{i_{\dot{\alpha}}}(\alpha)\frac{\dot{\alpha}\bar{c}}{2V} + C_{i_\delta}(\alpha)\delta \tag{5.16}$$

where $i = N, m$, $\bar{c}$ is a mean aerodynamic chord.

If representation (5.16) is based on the forced oscillations experimental data, the terms with rotary and unsteady derivatives are combined in one term:

$$C^*_{i_q}\frac{q\bar{c}}{2V} = C_{i_q}(\alpha)\frac{q\bar{c}}{2V} + C_{i_{\dot{\alpha}}}(\alpha)\frac{\dot{\alpha}\bar{c}}{2V},$$

because the forced-oscillation tests are usually kinematically coupled $\dot{\alpha} = q$.

Unfortunately, representation (5.16) at high incidence flight in many cases is not consistent with the modelling tasks in the time domain due to the dependence of the aerodynamic derivatives on frequency and amplitude of oscillations. Experimental results obtained for the 65^o delta wing in dynamic wind tunnel tests with small amplitude oscillations at different frequencies are presented in Fig. 5.3 and Fig. 5.12. The amplitude of the pitch oscillations is 3^o and reduced frequencies are $\omega = 0.017, 0.034, 0.051$ which correspond to forced oscillation frequencies $f = 0.5, 1.0, 1.5\,\mathrm{Hz}$. One can see that the "in-phase" and "out-of-phase" aerodynamic derivatives both for the normal force and the pitch moment coefficients heavily depend on frequency in the range of angle of attack $\alpha \in [22, 50^o]$.

In practical applications, the frequency effect in representation (5.16) is normally voluntarily ignored as it is difficult to reconcile it with the analysis of dynamics and simulation in the time domain. Consequently, the reduced frequency ω can be considered as a free

parameter, and its improper choice can lead to a very high uncertainty in the magnitudes of the aerodynamic derivatives used in the mathematical model.

To illustrate a possible discrepancy in the aerodynamic loads, the experimental aerodynamic responses for the normal force coefficient (empty squares) are compared with responses predicted by (5.16). A number of experimental time dependencies of $\alpha(t)$ have been used as inputs to the conventional model (5.16). Since the conventional aerodynamic model (5.16) depends on a reduced frequency ω at which the aerodynamic derivatives have been obtained as on a parameter, the responses have been simulated for three different frequencies ω. The results obtained are shown in Fig. 5.39 in comparison with the experimental data. One can clearly see a very large qualitative and quantitative difference in both experimental and predicted aerodynamic responses. The only satisfactory result is shown in the upper-left plot where the aerodynamic derivative model applied at frequency $\omega = 0.051$ ($f = 1.5\,\mathrm{Hz}$) was able to reproduce the experimental response relatively accurately. The possible reason for this is a relatively low pitch rate and shallow entering of the wing model into the range of angles of attack where the vortex breakdown effect is most relevant. Opposite to the traditional aerodynamic derivative model the identified unsteady aerodynamic model reflects the joint effect of the amplitude $\Delta\alpha$ and the reduced frequency ω at large amplitude oscillations. This can be seen in Figs. E.1–E.9.

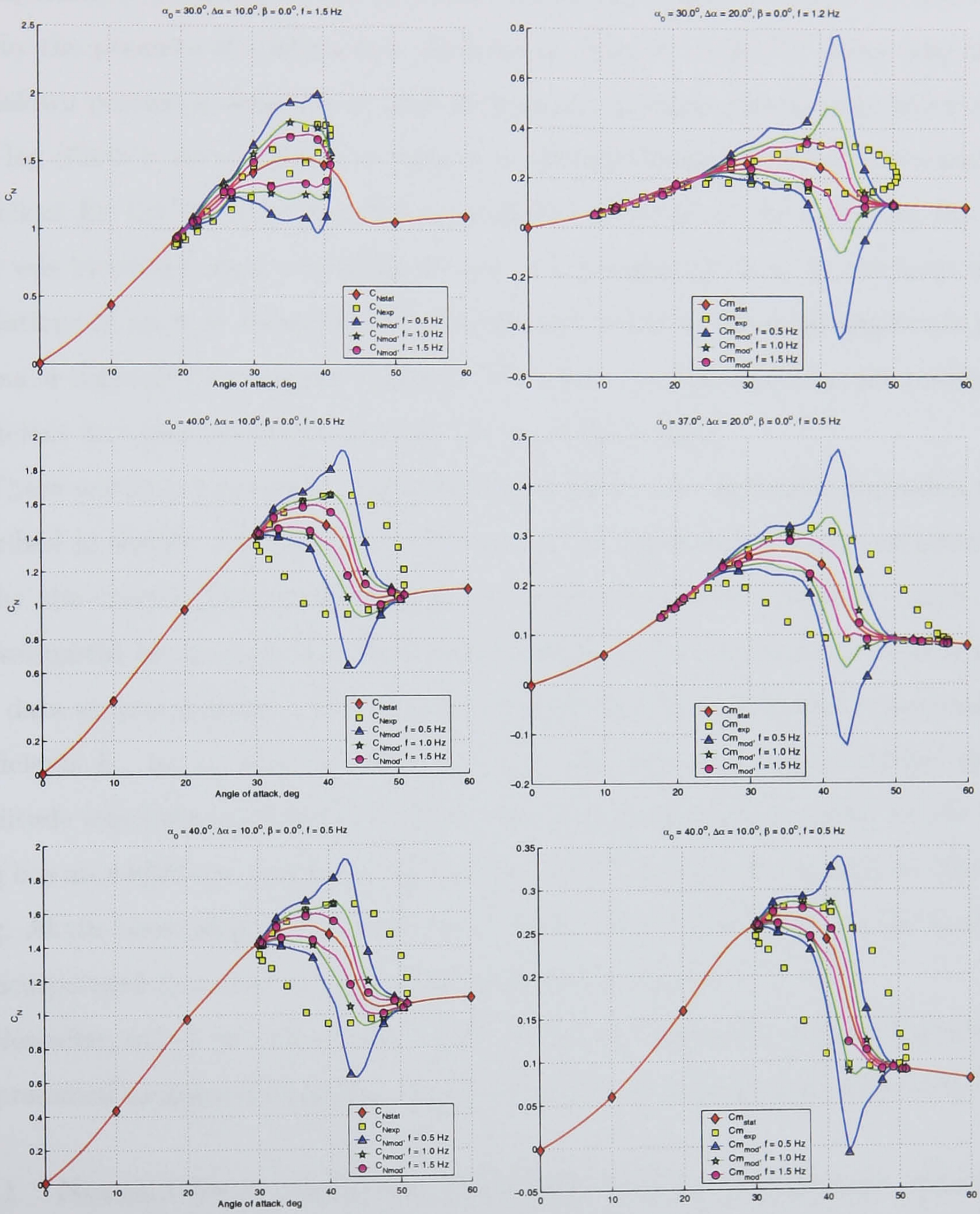

Figure 5.39: C_N (left column) and C_m (right column) predicted by conventional model depending on frequency vs. experimental response.

5.4 Unsteady aerodynamic models for the 70° delta wing

Aerodynamic loads acting on the 70° delta wing at high angles of attack are also characterized by the presence of vortical flow phenomena. Similar to the 65° delta wing the vortex breakdown processes dominate at high incidences, and their dynamics produce significant time lag effects in all aerodynamic responses. The mathematical model of the normal force coefficient for the 70° delta wing having a similar structure to the model for the 65° delta wing was identified using two different sets of experimental data: 1) the large amplitude oscillations in pitch at different fixed sideslip angles and 2) the large amplitude yaw oscillations at different fixed angles of attack. The mathematical model for the rolling moment coefficient was also identified using the yaw oscillations data.

These mathematical models were developed before the linearized regression technique described in section 4.2 was started for use on the characteristic times estimation. That is why the characteristic time functions τ were parameterized along the angle of attack and estimated by means of the direct minimization of the cost function (4.6) using oscillatory data at zero sideslip. After that the dependence on sideslip was introduced into the coefficients k_1, k_2, k_3 and the function $C_{N_{att}}$, and then they were identified using large amplitude experimental responses. Note, that the mathematical model for the 70° delta wing has an additional parameter τ_2 in comparison with the latest models for the 65° delta wing. At the latest stage of the work this parameter was found redundant as its effect could be incorporated into the "nonlinear" parameters k_2 and k_3.

Hereafter, only a brief description of the identified models and some results of simulation are presented as these models have already been published and can be found in [8].

5.4.1 Normal force coefficient for pitch motion at constant sideslip.

The mathematical model of the normal force coefficient during pitch motion according to the loads partitioning technique is presented in the following form:

$$C_N = C_{N_{v_{st}}}(\alpha, \beta) + C_{N_{dyn}} + C_{N_{\bar{\dot{\alpha}}}} \frac{c}{2V} \dot{\alpha}. \tag{5.17}$$

Dependence of the attached component on sideslip is considered by the following equation:

$$C_{N_{att}}(\alpha, \beta) = C_{N_{att}}(\alpha, 0)(1 - k_b \beta^2). \tag{5.18}$$

The dynamic contribution is described by the following nonlinear differential equation:

$$\frac{dC_{N_{dyn}}}{dt} = \frac{2V}{\bar{c}} \sum_{i=1}^{3} k_i(\alpha, \beta) \left(\Delta C_N(\alpha - \frac{\bar{c}}{2V} \tau_2 \dot{\alpha}, \beta) - C_{N_{dyn}} \right)^i . \tag{5.19}$$

Initially, the mathematical model of the lift coefficient C_N has been identified using data obtained during small and large amplitude pitch oscillations at zero sideslip. Dependencies $k_i(\alpha),\ i = 1, 2, 3$ on the angle of attack were parameterized at five nodes and were linearly interpolated at intermediate points. After unknown parameters of the mathematical model had been found at zero sideslip, this model was identified for $\beta = 5^o, 10^o, 15^o$ using corresponding experimental data for large amplitude oscillations. It was found that values of the characteristic time scales vary from approximately 10 up to 27, reflecting changes in the vortex flow dynamics along the angle of attack. It is worth mentioning that a similar increase of the time scales τ_1 for the 70^o delta wing were obtained in [42] as a result of an analysis of the aerodynamic derivatives for the rolling moment coefficient. Also, the same effect was pointed out in [58] for the F-16XL aircraft.

5.4.2 Normal force and rolling moment coefficients for yaw motion at constant angle of attack.

To describe the normal force coefficient during yawing motion at a constant angle of attack the mathematical model is presented as follows:

$$C_N = C_{N_{att}}(\alpha, \beta) + C_{N_{dyn}} + K_{bdb} \frac{b}{2V} \dot{\beta} \beta, \tag{5.20}$$

$$\frac{dC_{N_{dyn}}}{dt} = \frac{2V}{b} \sum_{i=1}^{3} k_i(\alpha, \beta) \left(\Delta C_N(\alpha, \beta - \frac{b}{2V} \tau_2 \dot{\beta}) - C_{N_{dyn}} \right)^i . \tag{5.21}$$

A similar structure of the mathematical model is used for the rolling moment coefficient but only with the first term in the dynamic equation:

$$C_l = C_{l_{att}}(\alpha, \beta) + C_{l_{dyn}} + C_{l_{\bar{\beta}}} \frac{b}{2V} \dot{\beta}, \tag{5.22}$$

$$\frac{dC_{l_{att}}}{dt} = \frac{2V}{b} k_1(\alpha, \beta) \left(\Delta C_{l_{dyn}}(\alpha, \beta - \frac{b}{2V} \tau_2 \dot{\beta}) - C_{l_{dyn}} \right) . \tag{5.23}$$

The identified characteristic time function $\tau_1(\alpha, \beta) = 1/k_1(\alpha, \beta)$ for the 70^o delta wing is shown in Fig. 5.40. It was identified only for the normal force coefficient model (5.21) and

then applied in model (5.23) for the rolling moment coefficient. This assumption was made to check the hypothesis that due to the same physical processes in the flow, the characteristic time scales should be reflected identically in both aerodynamic load components.

Some predicted results for the normal force and pitch moment coefficients during large amplitude yaw motion are shown in Figs. E.13–E.16 in comparison with the experimental data. It is seen that the results of the modelling are in good agreement with the experimental data at different angles of attack and different frequencies. This fact confirms the assumption about the coincidence of the characteristic times in the models of normal force and rolling moment coefficients for the 70^o delta wing during yaw oscillations.

Note, that only a small part of the results concerning the 70^o delta wing is presented in this section. A more detailed description of the models for unsteady aerodynamic loads and the results of simulation for the 70^o delta wing can be found in [6, 8, 29].

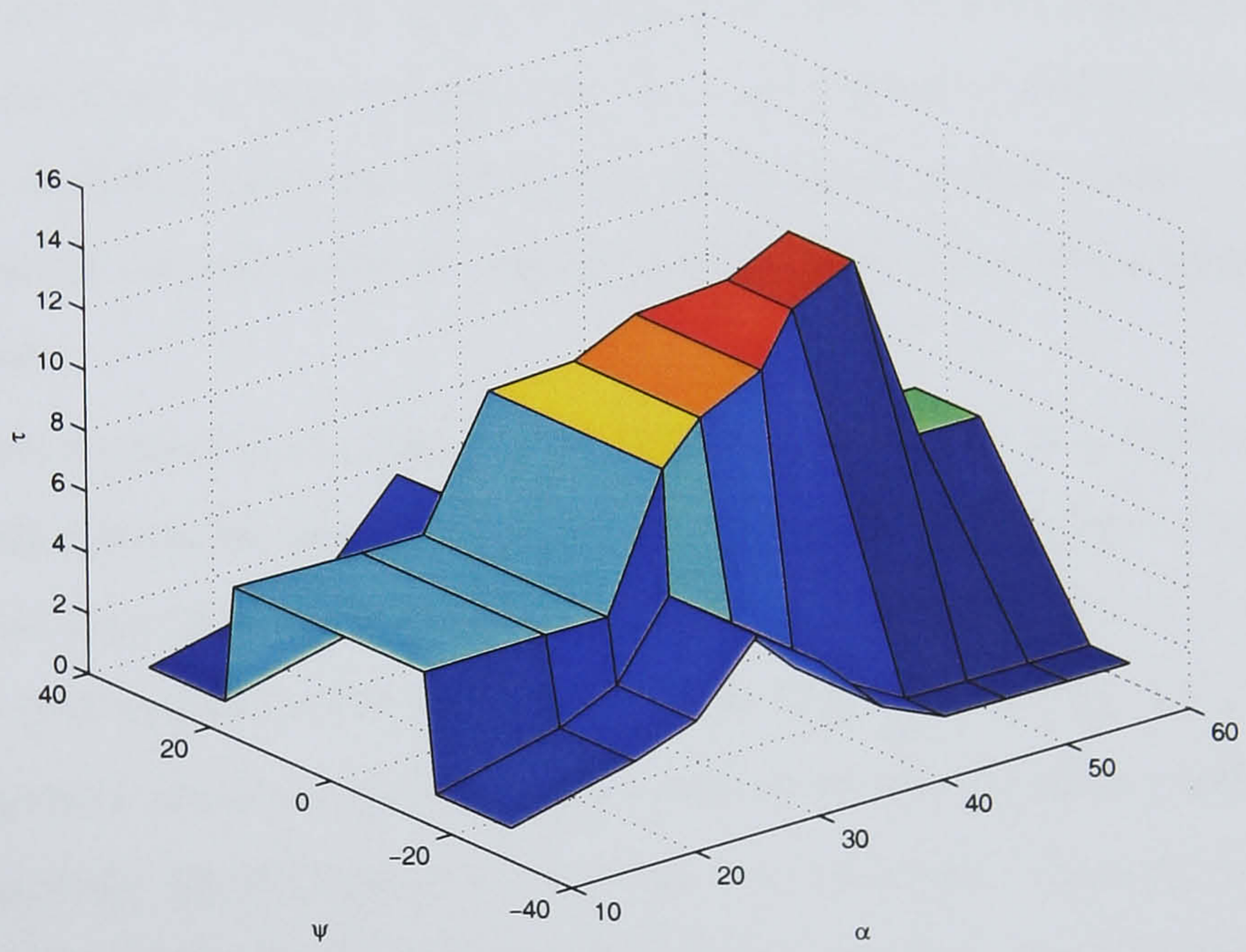

Figure 5.40: Characteristic time function for 70^o delta wing.

5.5 Comparison of the characteristic time scales for different delta wings

Characteristic time scales in the mathematical models of unsteady aerodynamic loads for the 65^o delta wing were identified independently for each aerodynamic coefficient in pitch, yaw and roll motion. Comparison of the characteristic time scales estimated from the experimental data in pitch for the normal force and pitch moment coefficients of the 65^o delta wing with central body have already been considered in section 5.1.3. The results obtained led to the conclusion that the characteristic time scales for these coefficients coincide in the case of pitch motion. In section 5.2.1.3 it was shown that the characteristic time scales can also depend on the type of motion. For example, the characteristic times in the model for the rolling moment coefficient estimated from the data in yaw, significantly differ from that of estimated from the roll motion data. Since aerodynamic derivatives for other delta wings are also available now, the comparison of the characteristic times peculiar to these wings and types of motion could be very important for the physical interpretation of the results obtained.

In [52] these characteristic time scales were calculated for five different delta wings using the linear regression technique described in section 4.2. These characteristic time scales estimated from the experimental aerodynamic derivatives of the normal force and pitch moment coefficients for the pitch motion are presented in Fig. 5.41. It is seen that within the standard deviation they are practically the same for both coefficients for each wing. Unfortunately, the dispersion is very high at some angles of attack, probably due to insufficient numbers of tested frequencies, however, in general, the dependencies obtained look rather consistent. Comparing the results obtained from the pitch oscillations data for the 65^o delta wings with and without a central body, one can conclude that the body does not significantly affect the characteristic time scales. As for the 70^o delta wings differing by shape of the leading edge (sharp and rounded), one can see some quantitative difference, but qualitatively they are close. And finally, one can note that the characteristic time scales are most subject to the influence of the wing sweep angle, which likely plays the main role in the vortical flow structure formation in case of simple wing configurations.

The characteristic time scales in the lateral/directional models have been estimated for

these five wings using experimental data obtained during small amplitude oscillations in yaw and roll. These results are presented in Fig. 5.42. The characteristic time functions in the models of the normal force and pitch moment coefficients are shown by blue and green lines, respectively. The results for the rolling moment coefficient model due to roll oscillations are shown by the red line and due to yaw oscillations – by the cyan line. One can see that the influence of the central body on the 65^o delta wing is more significant then in the longitudinal case and leads to a higher difference of the time constants determined in several ways. It is clearly seen that the characteristic time functions extracted from pitch, roll and yaw derivatives for the 65^o delta wing without a central body are very close to each other. But for the 65^o delta wing with a central body, the characteristic time scales estimated from the pitch and yaw experimental data differ from that determined from the roll oscillatory data. Thus, for example, at $\alpha \in [30^o, 38^o]$ the characteristic time function for the rolling moment coefficient due to roll motion is about two times greater than that estimated from the pitch and yaw oscillatory data. Moreover, the dispersion of the characteristic time scales estimated from the pitch and yaw data are more significant in comparison with the same wing without a central body. This result was firstly mentioned in [21, 70] for a similar 65^o American-Canadian delta wing with central body. So, one can conclude that the central body on the 65^o delta wing produces significant changes in the flow structure such as the formation of additional vortices and their interaction with the main vortices that affect the flow dynamic properties [12].

The dependence of the characteristic time scales on the type of motion poses a serious challenge to the structure of the mathematical model for arbitrary non-planar motion. A non-planar model should be, in this case, a multidimensional dynamic system with a set of eigenmodes excited by different types of motion.

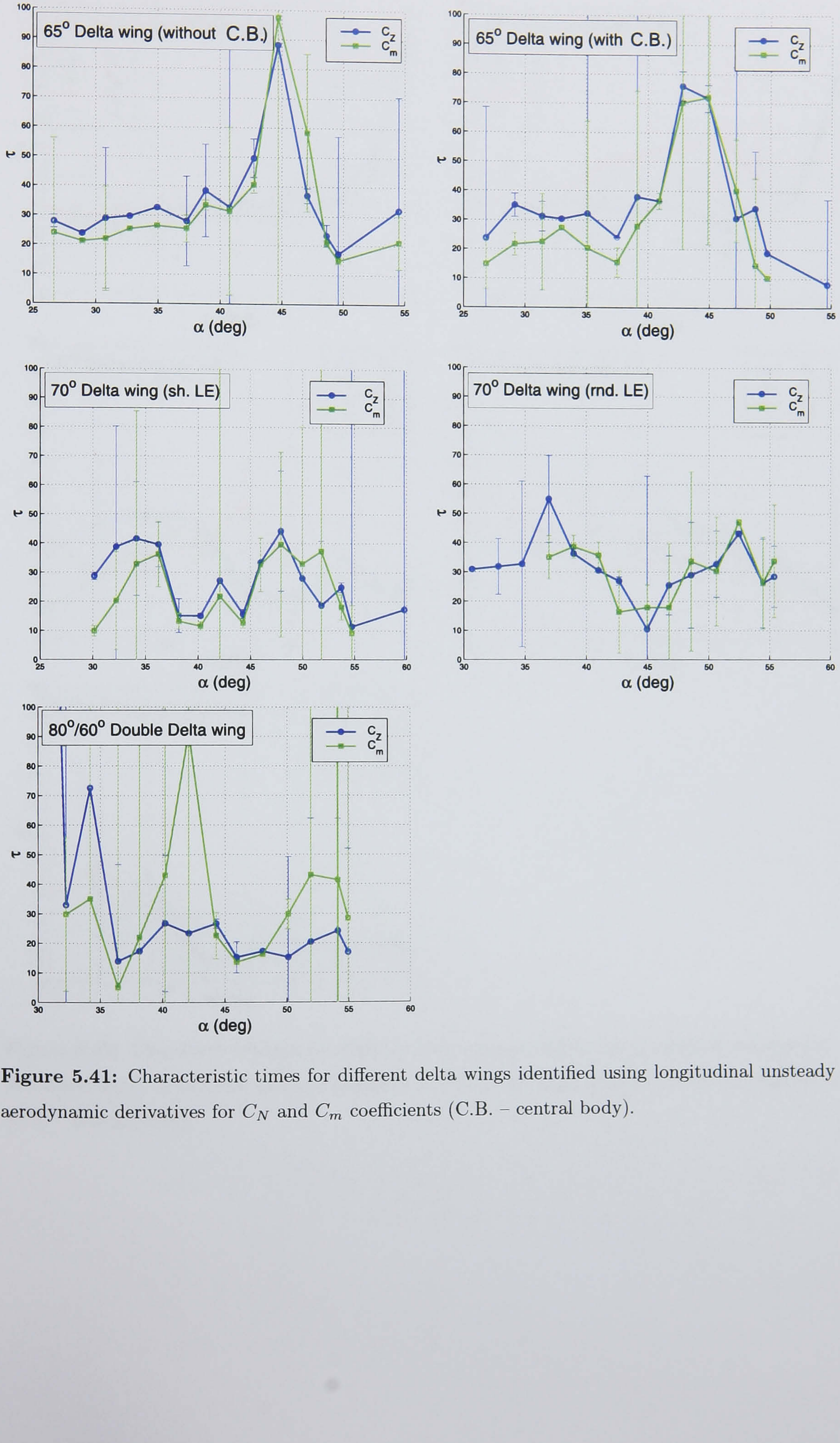

Figure 5.41: Characteristic times for different delta wings identified using longitudinal unsteady aerodynamic derivatives for C_N and C_m coefficients (C.B. – central body).

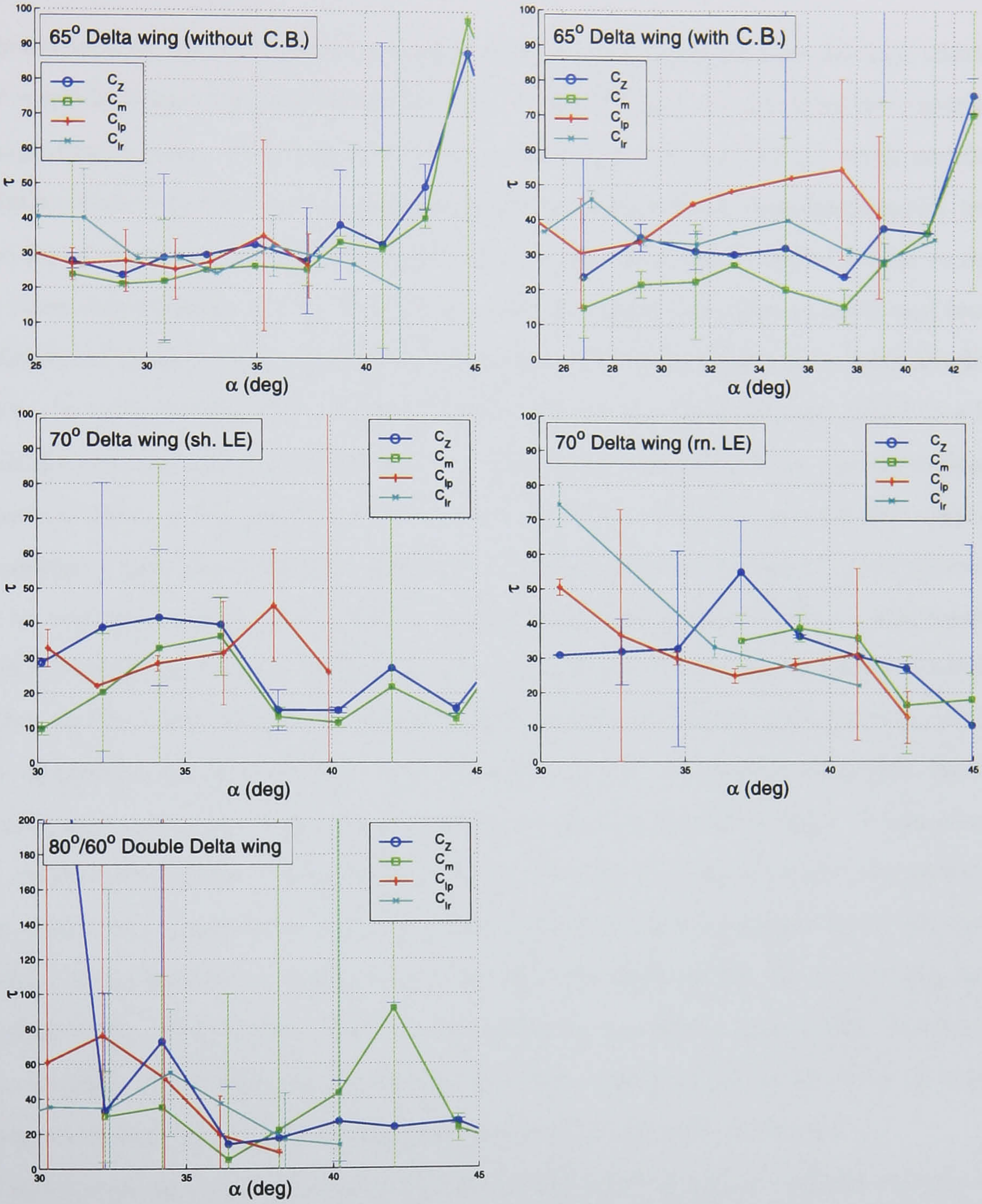

Figure 5.42: Characteristic times for different delta wings identified using unsteady aerodynamic derivatives for C_l in roll and yaw in comparison to that of for longitudinal C_N and C_m coefficients (C.B. – central body).

5.6 Summary

Mathematical models of nonlinear unsteady aerodynamic characteristics for high incidence flight conditions have been developed for the 65^o and 70^o delta wings using the experimental wind-tunnel data. Unsteady aerodynamic derivatives extracted from small amplitude oscillatory data were used for the estimation of the characteristic time functions by means of the linear regression model. It is shown that the linear dynamic model is able to reproduce these aerodynamic derivatives and the total aerodynamic loads at small and modest amplitudes of motion with high accuracy, but this model loses fidelity for a large amplitude motion. In order to extend the range of applicability of the mathematical model to a large amplitude motion nonlinear terms are introduced and identified using corresponding experimental data. A comparison of the experimental and simulated aerodynamic responses demonstrates that the technique used for the nonlinear model parameter identification is able to separate steady, and unsteady aerodynamics effects and obtain a mathematical model providing an accurate prediction of aerodynamic loads at high incidence conditions.

Due to the experimental rig kinematics, variation of a wing model sideslip at fixed angle of attack can be performed both through yaw and roll motion, therefore the same characteristic time scales were expected to be obtained in these two ways. It was revealed that characteristic time scales obtained using roll and yaw aerodynamic derivatives are equal within the accuracy to each other and to that obtained in longitudinal case for the 65^o delta wing without a central body but they are different for the same wing having a central body. This means that the mathematical model for an aircraft configuration with a fuselage could require the nonlinear unsteady aerodynamic model based on a higher dimension dynamical system providing dependence on the type of motion.

Finally, one can conclude that the proposed approach is able to simulate aerodynamic loads acting on a wing in conditions when the vortical flow dynamics is essential, and conventional methods become inadequate. The identified characteristic time scales for different delta wings provide an insight into the physical properties of separated and vortical flow at high incidences, and their behaviour can serve as a good indicator of vortex breakdown processes and changes of the flow structure.

Chapter 6

Modelling of static aerodynamic hysteresis

This chapter considers a problem of mathematical modelling of unsteady aerodynamic loads in the case of hysteresis in their static dependencies (static hysteresis). The mathematical model is based on the assumption that the total value of the unsteady aerodynamic loads can be split into the attached (potential) and dynamic components. The behaviour of the dynamic component is described by a nonlinear dynamic equation, which is constructed in such a way as to be able to reproduce the static hysteresis and dynamic properties during critical state crossing. A technique for such a system design within the mathematical modelling framework (4.1)–(4.2) is proposed. A mathematical model of the normal force coefficient has been developed and verified using wind-tunnel experimental data for the high aspect ratio wing with the NACA-0018 aerofoil. It is shown that the model reproduces experimental dependencies rather well both at attached and separated flow conditions.

6.1 Physical aspects of static aerodynamic hysteresis

The flying safety problem for passenger and general aviation airplanes is closely connected with the investigation of nonlinear unsteady aerodynamic characteristics of airplanes with high aspect ratio wings at high angles of attack. A series of experimental works were undertaken in TsAGI and worldwide to investigate aerodynamic loads acting on high aspect

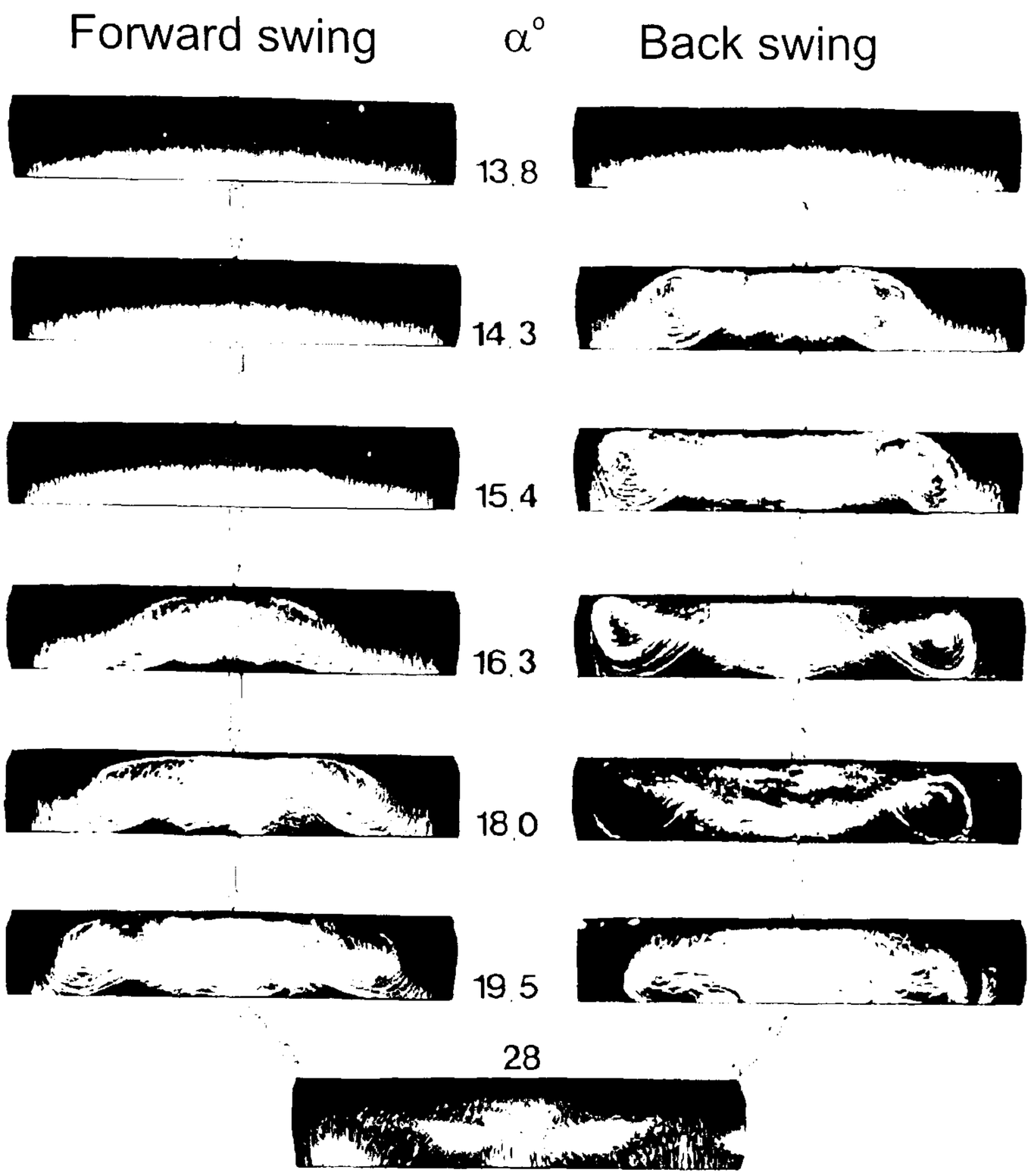

Figure 6.1: Visualization of the flow structure at forward and backward variation of angle of attack.

ratio wings at critical and post-critical angles of attack. Some experimental results obtained in static and dynamic tests for such a kind of configuration are presented in [82, 91, 79, 49]. It was shown that in addition to the dynamic effects similar to the delta wing planforms, in the case of high aspect ratio wings aerodynamic loads can even have a non-unique static dependency for some range of incidence. Physically, a static hysteresis results from the possibility of the existence of two or more different stable structures in a separated flow at the same incidence.

In most cases the flow structure is formed independently of the direction of parameters variation and their onset that results in unique dependencies of aerodynamic loads. This behaviour is typical for small and very high incidence where the flow is attached and fully

stalled, respectively.

The transient region of angles of attack is characterized by the presence of two or more stable separated flow structures at the same values of the parameters, some of these structures exist during increase while others arise during decrease of the angle of attack. In this case the flow structure and aerodynamic loads to be realized depend on the onset and/or direction of the variation of the parameters, i.e. prehistory of motion.

The results of flow visualization for a high aspect ratio wing at different incidences are shown in Fig. 6.1. At $\alpha < 15.4^o$ flow separation starts on the trailing edge of the wing and covers more and more area with an increase of the angle of attack. This attached flow structure corresponds to a practically linear monotonous rise of the lift. A further increase of the angle of attack leads to arising of a stable and well developed separated flow ($15^o \ldots 25^o$). Then after some critical value of the angle of attack ($\alpha_{cr_1} \approx 26^o$) is reached, an abrupt change of the flow structure results in an abrupt loss of the lift. The new fully stalled flow structure is stable and remains qualitatively the same with increases of incidence ($\alpha > 26^o$), and the lift dependence monotonously rises. When the angle of attack decreases the stalled flow transforms to highly separated flow and then to the flow with separation on the trailing edge only. The last transformation taking place at another critical value of the angle of attack $\alpha_{cr_2} \approx 14^o$ gives rise to an abrupt increase of the lift (see Fig. 6.2).

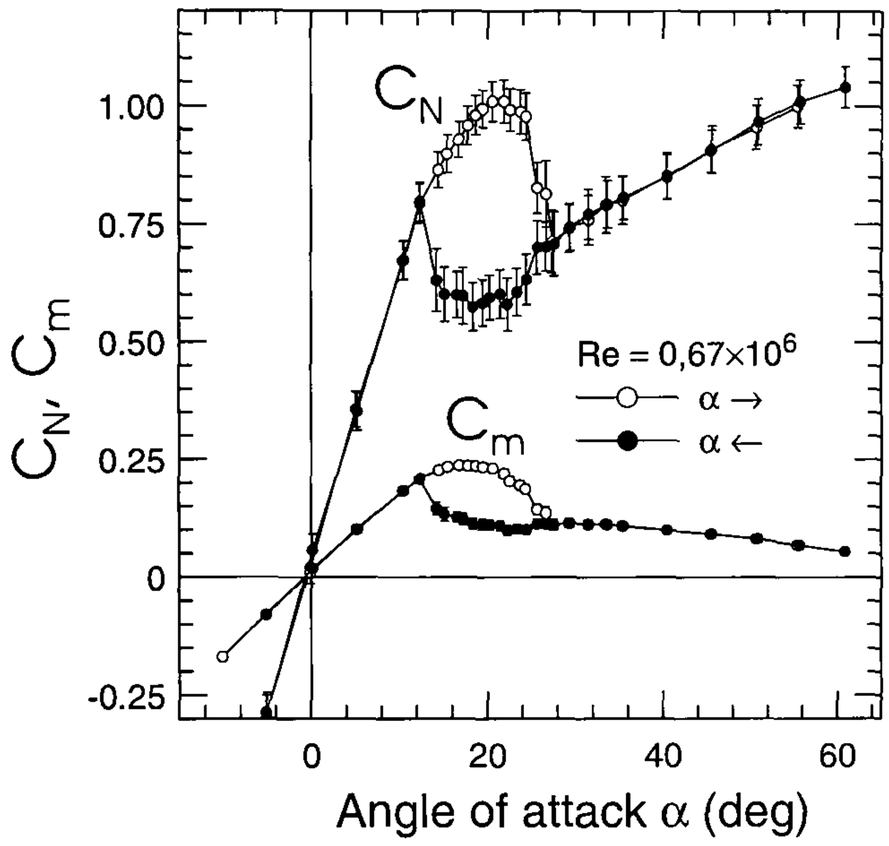

Figure 6.2: Static dependance of the normal force and pitch moment coefficients for high aspect ratio wing with NACA-0018 aerofoil.

Comparing the flow patterns in the left and right columns in Fig. 6.1 it is seen that different flow structures exist at the same angles of attack during the forward and backward incidence variation. This obviously leads to different lift values at the same angle of attack. Since $\alpha_{cr_2} < \alpha_{cr_1}$ the normal force coefficient will have hysteresis in its static dependence.

An example of the static dependence of the normal force and pitch moment coefficients

on the angle of attack obtained at forward and reversed quasi-steady swing is given in Fig. 6.2, with standard deviation [92]. One can see that there is an essential hysteresis in the $C_N(\alpha)$ and $C_m(\alpha)$ dependencies during an increase and decrease of the angle of attack. Since a difference between up and down branches is much more than the uncertainty of the measurements, one can conclude that there are two stable states at each $\alpha \in [14^o, 26^o]$.

Experimental investigations carried out in TsAGI revealed the possibility of the existence of static hysteresis with more than two stable branches or a cascade of hystereses (multiple hysteresis). Some results of this research are discussed in [60]. A very narrow intermediate branch seems to exists in the C_N dependence shown in Fig. 6.2 at $\alpha \approx 24^o$ but within the current analysis all such minor effects are neglected. The normal force dependence is considered in the form of a bi-stable hysteresis as shown in Fig. 6.3 that is sufficient to reflect the most important flow properties in the case under consideration. This dependence is accompanied by the illustrative pictures demonstrating a qualitative flow structure such as attached flow, separated flow and fully stalled flow.

The idea of using a nonlinear dynamic equation for static hysteresis modelling was proposed in [28]. To describe the nonlinear behavior of the pitch-moment coefficient C_m of a cylindric body, the nonlinear equation $\frac{dC_m}{dt} = F(C_m, \alpha)$ was used. Within the static hysteresis region, function F was made up of a cubic polynomial on C_m which has three roots at each fixed α. Outside the static hysteresis region, the righthand side function was linear. As a result, the function F was combined from three fragments and turned out to be discontinuous at the bifurcational points.

Later, in [8, 4] the state-space approach was applied to the problem of unsteady aerodynamic characteristics modelling in the presence of hysteresis in a static dependance. A nonlinear dynamic equation was used to describe the dynamic behaviour of a separation point location $x(t)$ on the aerofoil. Aerodynamic loads in this case were considered as functions of $x(t)$. The procedure for constructing a continuous equation which reflects that bifurcational flow properties has developed. The proposed approach was verified using experimental data for a high aspect ratio wing with NACA-0018 aerofoil.

6.2 Bifurcational model of static aerodynamic hysteresis

In order to describe the unsteady aerodynamic loads in the case of static hysteresis a mathematical model (4.1)–(4.2) may be used. The order of the dynamic equation is chosen such that it has the same number of stable equilibrium solutions at each angle of attack as the static dependence of the aerodynamic coefficient. Taking into account that the right hand side function in (4.2) is a polynomial, then its order n has to be at least $2m-1$, where m is the number of branches measured in experiment. For example, the experimentally measured dependence of the normal force coefficient of a high aspect ratio wing with the NACA-0018 aerofoil has two stable branches in $16^o \leq \alpha \leq 26^o$ and only one branch outside this region (see Fig. 6.3). Therefore, the dynamic equation has to be constructed in such a way as to have two stable solutions within the hysteresis region and only one solution outside. The simplest function which satisfies this requirement is a third order polynomial with coefficients depending on the angle of attack.

Thus, different static values of the C_N coefficient in the static hysteresis region which are observable in the experiment will be represented by the same number of stable equilibria of the nonlinear dynamic system while transient processes will be locally characterized by a disturbed motion near the corresponding equilibrium points. Jumps in the static dependance can be obtained in a continuous dynamic model by changing parameters (in

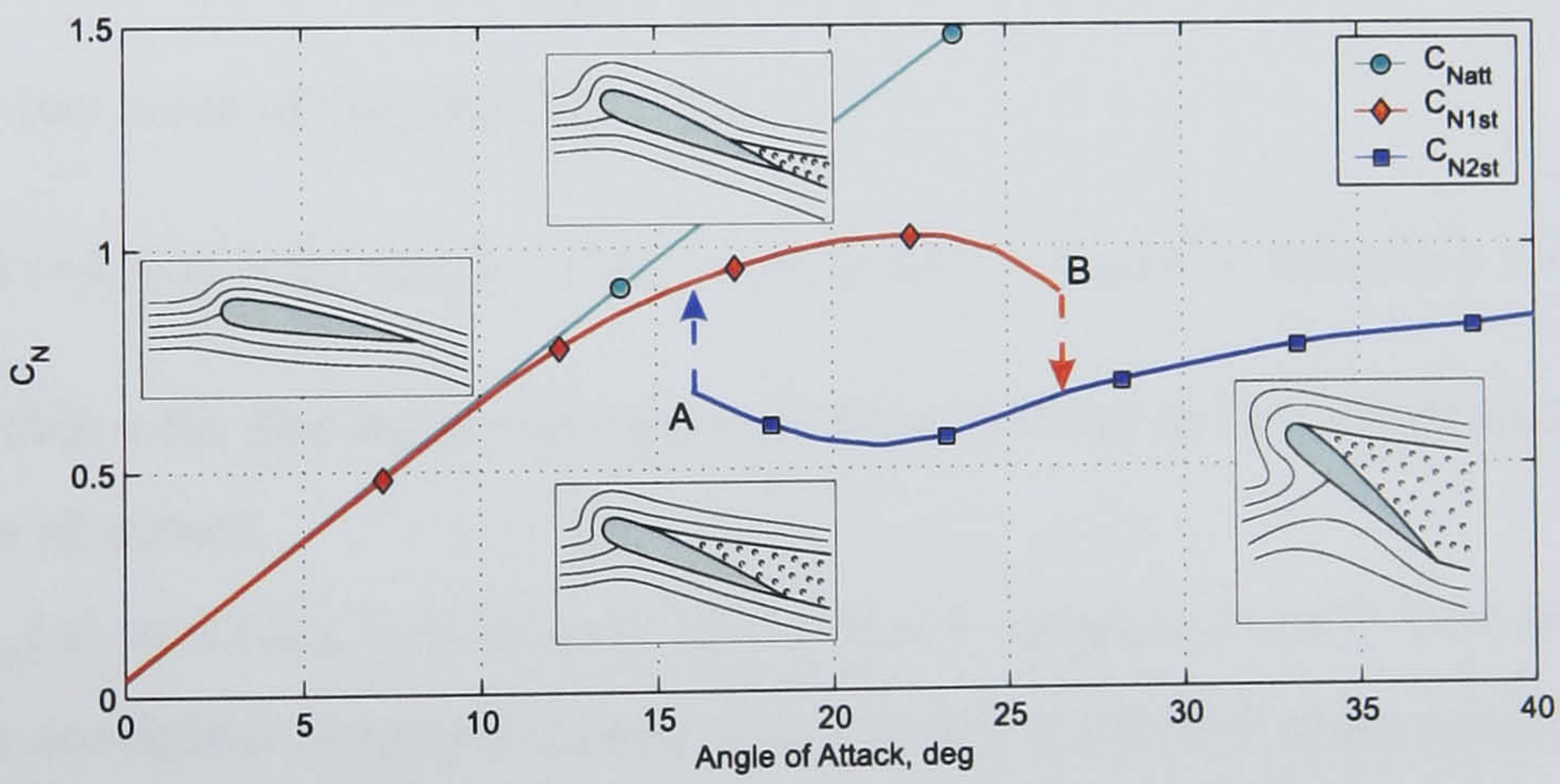

Figure 6.3: Static aerodynamic hysteresis of the normal force coefficient and corresponding flow structures.

this case the angle of attack α), which results in changing of a number of the system solutions. These critical points are in fact bifurcational points in the nonlinear dynamical model.

Taking into account all aforesaid, the mathematical model of the normal force coefficient C_N may be written as follows:

$$C_N(t) = C_{N_{att}}(\alpha) + C_{N_{\dot{\bar{\alpha}}_{att}}}(\alpha)\frac{\bar{c}}{2V}\dot{\alpha} + C_{dyn}, \tag{6.1}$$

where $C_{N_{att}}(\alpha)$ and $C_{N_{\dot{\alpha}_{att}}}(\alpha)$ are the normal force coefficient and its unsteady aerodynamic derivative which would be in the hypothetical conditions of potential and unseparated flow. The dynamic component C_{dyn} which describes the flow separation processes is governed by the following nonlinear equation:

$$\frac{\bar{c}}{2V}\frac{dC_{dyn}}{dt} = k_0 + k_1(C_0 - C_{dyn}) + k_2(C_0 - C_{dyn})^2 + k_3(C_0 - C_{dyn})^3, \tag{6.2}$$

where C_0 is an analogue of the ΔC function in equation (4.2).

Steady-state aerodynamic loads observed in the static experiment correspond to equilibrium solutions of equation (6.2) and satisfy the equation

$$\frac{dC_{dyn}}{dt} = F(\alpha, C_{dyn}) = 0. \tag{6.3}$$

Then one or two zeros of the function

$$F(\alpha, C_{dyn}) = k_0(\alpha) + k_1(\alpha)(C_0 - C_{dyn}) + k_2(\alpha)(C_0 - C_{dyn})^2 + k_3(\alpha)(C_0 - C_{dyn})^3 \tag{6.4}$$

have to coincide with the static experimental dependencies of an aerodynamic coefficient at each angle of attack.

Let $C_{N1_{st}}(\alpha)$ and $C_{N2_{st}}(\alpha)$ be the experimentally measured static dependencies of the normal force coefficient obtained during forward and backward quasi-steady motion, respectively. Then, equation (6.2) has the following stable equilibria:

$$C = \begin{cases} C_1 = C_{N1_{st}} - C_{N_{att}} \\ C_2 = C_{N2_{st}} - C_{N_{att}}. \end{cases} \tag{6.5}$$

Function $C_0(\alpha)$ in (6.4) is defined as a smooth continuous dependence which coincides with the first stable branch $C_1(\alpha)$ at $\alpha \leq \alpha_A$ and with the second stable branch $C_2(\alpha)$ at

$\alpha \geq \alpha_B$. Between the bifurcation points α_A and α_B it is represented by a cubic spline as shown in Fig. 6.4.

Let $y = C_0 - C_{dyn}$, then the right-hand side function in equation (6.2) will have the following form:

$$F(\alpha, y) = k_0(\alpha) + k_1(\alpha)y + k_2(\alpha)y^2 + k_3(\alpha)y^3. \tag{6.6}$$

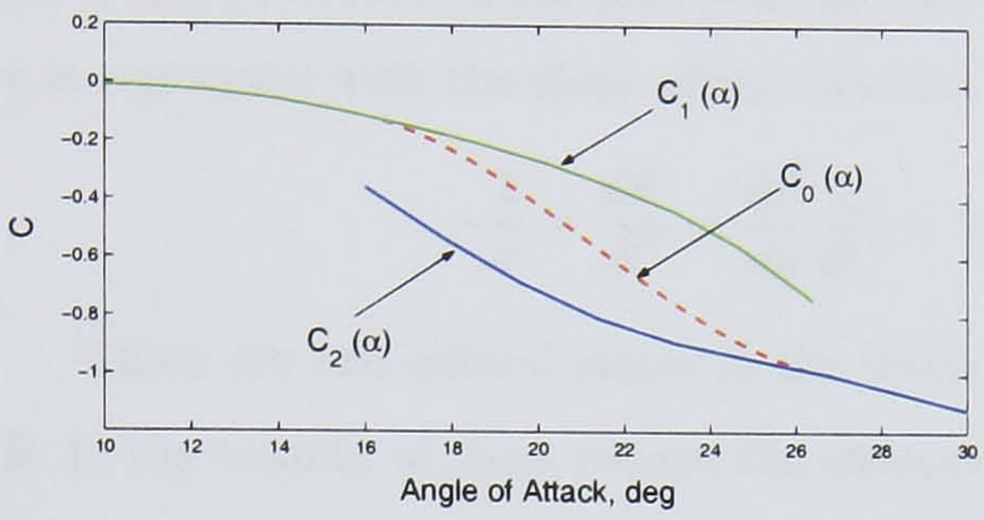

Figure 6.4: Branches of the static aerodynamic hysteresis in $\alpha - C$ coordinates.

The cross-sections of the function $F(y, \alpha)$ at different fixed angles of attack, which reveal the bifurcational character of the model are shown in Fig. 6.5. The solid lines correspond to regions with a unique flow structure and, as follows, with a single stable point (these regions exist for $\alpha \leq 16^o$ and $\alpha \geq 26^o$). The dotted line corresponds to the region with a non-unique flow structure, where there are two stable and one unstable solutions. The dashed lines correspond to boundary situations (bifurcation points). Stable solutions are marked by black circles, unstable by empty circles and bifurcational points by black-white circles. It is seen that on approaching the bifurcational points from outside of the hysteresis region, stable and unstable solutions close in and join into the same multiple root and then pass into the

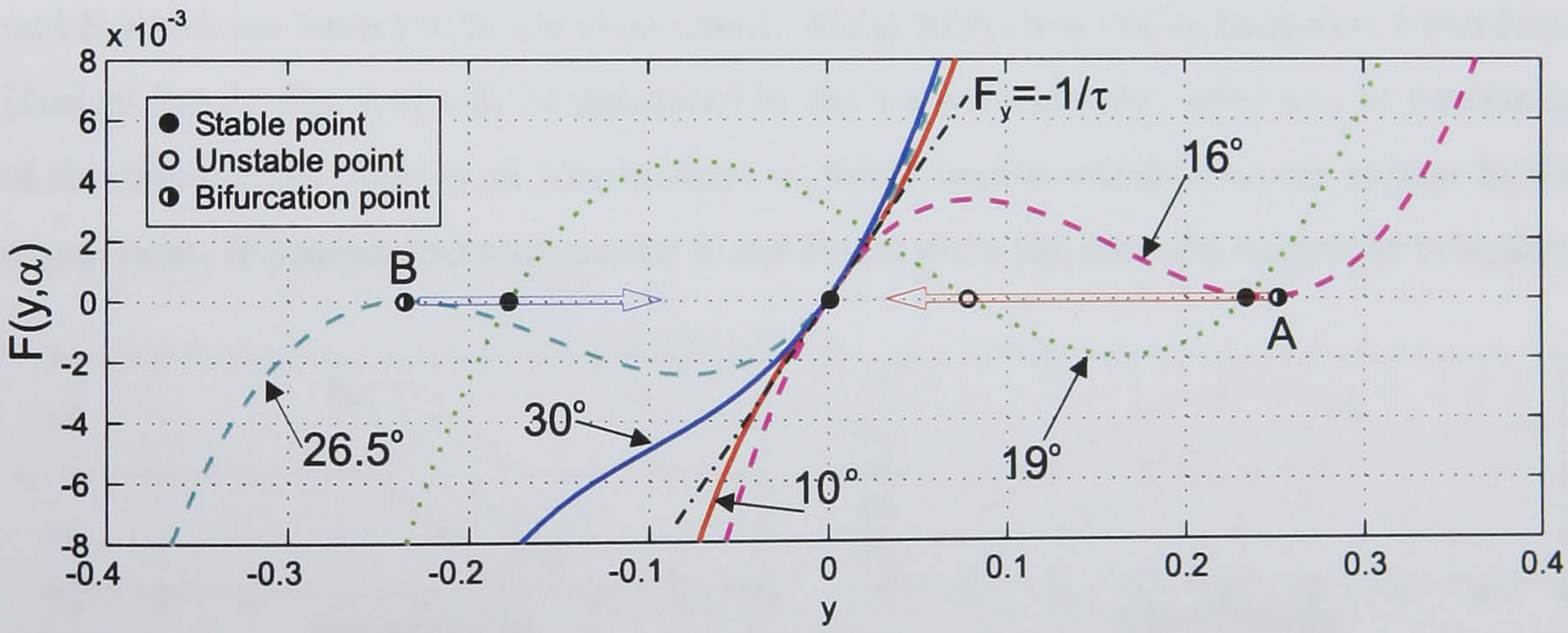

Figure 6.5: Cross-sections of the function $F(y, \alpha = fix)$ corresponding to different flow structures.

complex plane.

At every equilibrium point $\{y_e : F(\alpha, y_e) = 0\}$, the mathematical model has a characteristic time scale, defining the time lag effects in aerodynamic responses during small amplitude motion. The characteristic time scales have a physical meaning and can be identified at every stable branch from the results of small amplitude oscillations using the technique presented in the previous chapters for delta wings. The characteristic time scale τ is connected with the slope of the function F at the equilibrium points

$$-\frac{1}{\tau} = \frac{dF}{dC} = \frac{dF}{dy}\frac{dy}{dC} = -\frac{dF}{dy} \quad \Rightarrow \quad \left.\frac{dF}{dy}\right|_{y=y_e} = \frac{1}{\tau}. \tag{6.7}$$

There are two critical states in the static dependency $C_{st}(\alpha)$, marked by points A and B. In the vicinity of these points, the characteristic time scale approaches infinity ($\tau \to \infty$) because the slope of the function $F(\alpha, y)$ approaches zero ($\frac{\partial F}{\partial y} \to 0$). The crossing of the critical state points leads to a long time transient process from one branch of the static hysteresis to another one, and the duration of this process significantly exceeds the characteristic time scales τ on the branches. The bifurcational points A and B with zero slope of the function $F(\alpha, y)$ are clearly seen in Fig. 6.5.

The nonlinear function $F(\alpha, y)$ in equation (6.4) can be designed to provide all the necessary properties for unsteady aerodynamic responses observed in the presence of static hysteresis. Under static conditions, i.e. when $F(\alpha, y) = 0$, the mathematical model has to generate stable branches of the aerodynamic coefficient $C_{N_{st}}$ with bifurcational points A and B which are observed in the experiment. Along with these stable branches, a third one (dashed line in Fig. 6.6) will be generated in the static hysteresis region due to continuity of the function F. This is an intermediate unstable branch which does not appear in the experiment. It appears between points A and B and plays the role of a separatrix boundary

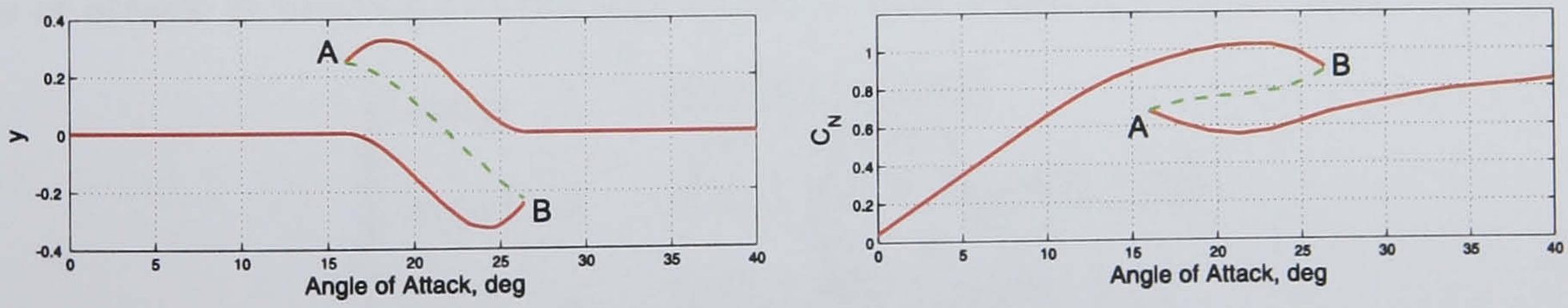

Figure 6.6: Bifurcation diagrams of system (6.2) in terms of y and C_N against parameter α.

dividing the regions of attraction of the two stable branches. Also, the condition for local stability has to be fulfilled in equation (6.3) for the experimentally observable branches:

$$\frac{\partial F}{\partial y}\Big|_{y=y_e}(\alpha) \geq 0. \tag{6.8}$$

with the equality being possible only at the bifurcation points. So, the bifurcation diagrams of the dynamic system (6.2) in terms of y and C_N with respect to angle of attack have to be as shown in Fig. 6.6.

6.3 Design of the nonlinear dynamic system

6.3.1 Internal region of the static hysteresis loop

The coefficients $k_0(\alpha), \ldots, k_3(\alpha)$ of the mathematical model inside the static hysteresis loop can be found using the conditions specified on the two observable branches of the static dependence. These conditions require that the branches provide solutions for the equation $F(\alpha, y) = 0$, and that the partial derivatives $\frac{\partial F}{\partial y}$ specify inverse values of the characteristic time scales $\tau_1(\alpha)$ and $\tau_2(\alpha)$ at each branch. As a result, at the stable branches $y_1(\alpha)$ and $y_2(\alpha)$ coefficients $k_0, \ldots, k_3$ have to satisfy the following equations:

$$\begin{cases} k_0 + k_1 y_1 + k_2 y_1^2 + k_3 y_1^3 &= 0 \\ k_0 + k_1 y_2 + k_2 y_2^2 + k_3 y_2^3 &= 0 \\ k_1 + 2k_2 y_1 + 3k_3 y_1^2 &= \frac{1}{\tau_1} \\ k_1 + 2k_2 y_2 + 3k_3 y_2^2 &= \frac{1}{\tau_2} \end{cases} \tag{6.9}$$

System (6.9) provides the following solutions for the unknown coefficients $k_0, \ldots, k_3$ at each angle of attack as functions of the characteristic time scales $\tau_1(\alpha)$ and $\tau_2(\alpha)$:

$$\begin{cases} k_0(\alpha) &= -\dfrac{y_1 y_2 (y_1\tau_1 + y_2\tau_2)}{(y_1 - y_2)^2 \tau_1 \tau_2} \\ k_1(\alpha) &= \dfrac{y_1^2\tau_1 + y_2^2\tau_2 + 2y_1 y_2(\tau_1 + \tau_2)}{(y_1 - y_2)^2 \tau_1 \tau_2} \\ k_2(\alpha) &= -\dfrac{\tau_2(y_1 + 2y_2) + \tau_1(2y_1 + y_2)}{(y_1 - y_2)^2 \tau_1 \tau_2} \\ k_3(\alpha) &= \dfrac{\tau_1 + \tau_2}{(y_1 - y_2)^2 \tau_1 \tau_2}. \end{cases} \tag{6.10}$$

Note, that $\tau_1(\alpha)$ and $\tau_2(\alpha)$ are unknown functions to be identified from the experimental data, and the condition that the characteristic time scales approach infinity at the bifurcation points has to be taken into account.

6.3.2 External region of the static hysteresis loop

Since there is only one stable branch outside the static hysteresis region, the nonlinear function $F(\alpha, y)$ has only one real and two complex roots at each angle of attack:

$$y(\alpha) = \begin{cases} y_1(\alpha) &= C_0(\alpha) - C_i(\alpha) = 0 \\ y_2(\alpha) &= a(\alpha) + jb(\alpha) \\ y_3(\alpha) &= a(\alpha) - jb(\alpha), \end{cases} \tag{6.11}$$

where the index $i = 1$ at $\alpha < \alpha_A$ and $i = 2$ at $\alpha > \alpha_B$, $a(\alpha)$ and $b(\alpha)$ are unknown functions, which can be identified from the experimental data.

In order to reproduce only one stable branch in the aerodynamic coefficient, conditions (4.4) have to be satisfied outside the static hysteresis loop. Thus, similar to the system (6.9), for the case of a single branch of the static dependence, the following conditions have to be met:

$$\begin{cases} k_1 y_i + k_2 y_i^2 + k_3 y_i^3 &= 0 \\ k_1 + 2k_2 y_i + 3k_3 y_i^2 &= \frac{1}{\tau_i}. \end{cases} \tag{6.12}$$

From equations (6.11) and (6.12) it follows that the function $F(\alpha, y) = 0$ can be represented in the following form:

$$F(\alpha, y) = \left(\frac{k_1}{k_3} + \frac{k_2}{k_3} y + y^2\right) y k_3 = (y - y_2)(y - y_3) y k_3 = 0. \tag{6.13}$$

According to the Vietta theorem we have:

$$\begin{aligned} \frac{k_2}{k_3} &= -y_3 - y_2 &&= -2a \\ \frac{k_1}{k_3} &= y_2 y_3 &&= a^2 + b^2. \end{aligned} \tag{6.14}$$

Finally, the following representation of the coefficients $k_0, \ldots, k_3$ at angles of attack outside the static hysteresis loop is obtained:

$$\begin{cases} k_0(\alpha) &= 0 \\ k_1(\alpha) &= \frac{1}{\tau_i} \\ k_2(\alpha) &= -\frac{2a}{a^2 + b^2} \frac{1}{\tau_i} \\ k_3(\alpha) &= -\frac{1}{a^2 + b^2} \frac{1}{\tau_i}, \end{cases} \tag{6.15}$$

where the index $i = 1, 2$ defines one of the two single branches of the static hysteresis.

6.4 Mathematical model of C_N for the high aspect ratio wing

The mathematical model for the normal force coefficient C_N for the high aspect ratio wing having NACA-0018 aerofoil has been developed according to the technique described in the previous section. All unknown parameters and dependencies such as $\tau_1(\alpha)$, $\tau_2(\alpha)$, $a(\alpha)$, $b(\alpha)$ were parameterized along the angle of attack and identified by means of direct minimization of the cost function (4.6). To identify the mathematical model a set of experimental responses for the rectangular wing with aspect ratio $A = 5$ in the range of angles of attack $\alpha \in [-10,\, 60^o]$ has been used. The data was obtained in TsAGI's low-speed wind-tunnel T-103 using the forced oscillation rig at different amplitudes $\Delta\alpha = 3 \ldots 25^o$ and frequencies $f = 0.2 \ldots 1.5\,\mathrm{Hz}$ ($\bar{q} = 0.01 \ldots 0.03$). The measurements were carried out using a five component strain gauge at the flow speed $V = 40\,\mathrm{m/sec}$ ($Re = 0.67 \cdot 10^6$).

The set of experimental data used for the identification consists of smoothed time dependencies of the aerodynamic loads and incidence measured during the pitch oscillations with different frequencies, amplitudes and mean angles of attack. The duration of each record is one period of oscillation. The static experimental set of data contains dependencies of aerodynamic loads at an angle of attack in the range $\alpha \in [-10^o,\, 60^o]$ which was used to determine the stable branches of the static hysteresis (see Fig. 6.4).

The static hysteresis branches which are solutions of the equation $F(\alpha, y) = 0$ are presented in Fig. 6.6 in terms of the internal variable y and the total force coefficient C_N. The identified derivatives $\left.\frac{\partial F(\alpha,y)}{\partial y}\right|_{y=y_1}$ and $\left.\frac{\partial F(\alpha,y)}{\partial y}\right|_{y=y_2}$ which are the inverse values of the characteristic time scales at corresponding stable branches are presented in Fig. 6.7. The identified dependencies $a(\alpha)$ and $b(\alpha)$ are presented in Fig. 6.8. The coefficients $k_0(\alpha), \ldots, k_3(\alpha)$, calculated using the estimated values of the characteristic time scales $\tau_i(\alpha)$, $i = 1, 2$, are given in Fig. 6.9.

The nonlinear function $F(\alpha, y)$ calculated using the identified parameters $k_0(\alpha), \ldots, k_3(\alpha)$ is shown in Fig. 6.10. Cross-sections of this function at several values of angle of attack both inside and outside of the static hysteresis loop have been presented in Fig. 6.5. It is seen that the constructed function is continuous and rather smooth in the vicinity of the static hysteresis branches. This means that one can expect the model to reproduce unsteady aerodynamic loads adequately at least at slow and moderate pitch rates.

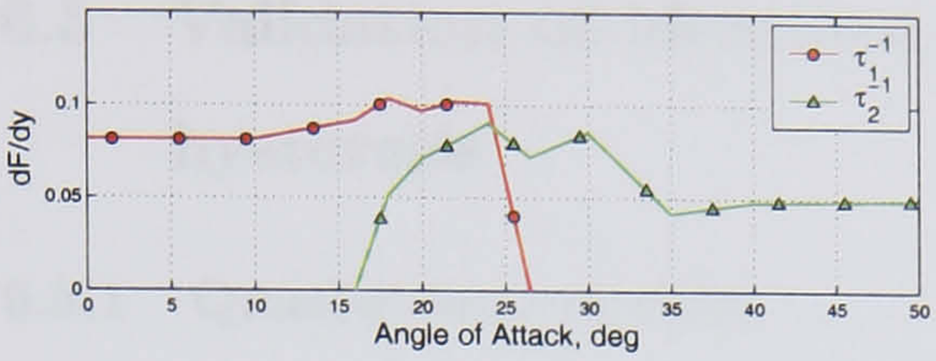

Figure 6.7: Local slope of the function $F(y, \alpha)$ at stable hysteresis branches

Figure 6.8: Coefficients $a(\alpha)$ and $b(\alpha)$

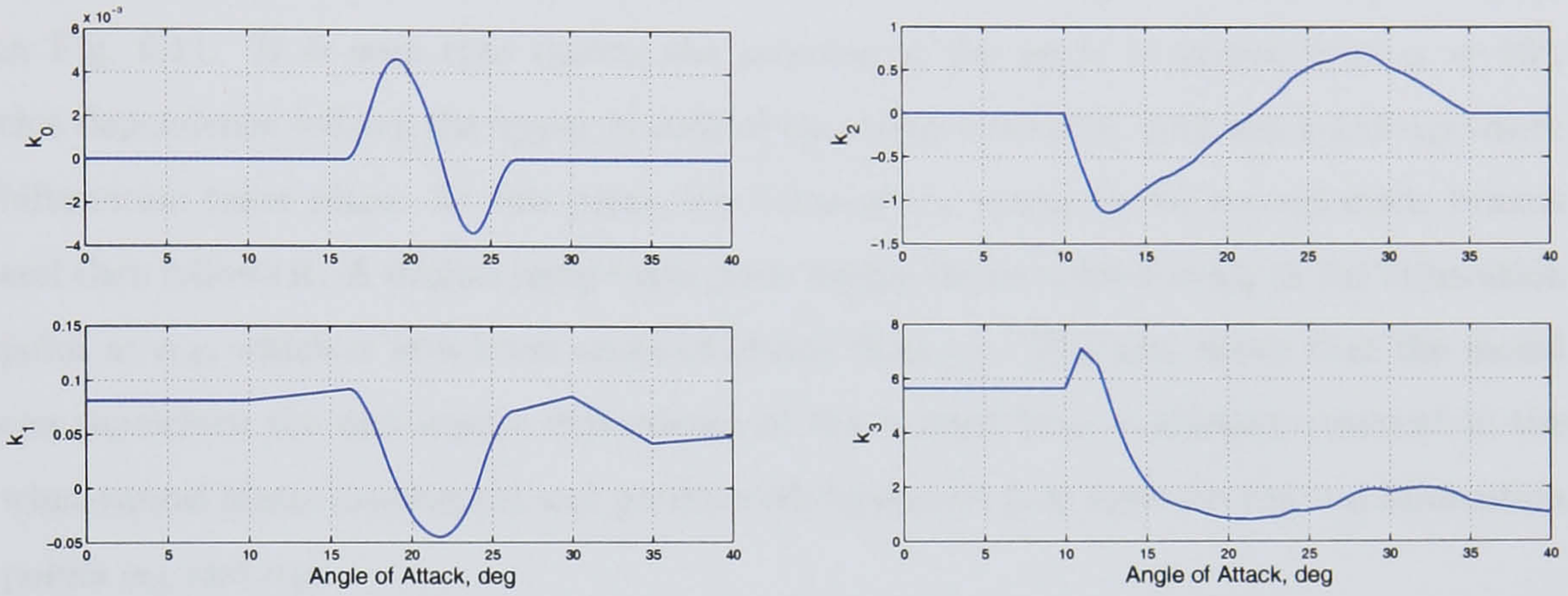

Figure 6.9: Coefficients $k_0, \ldots, k_3$ as functions of angle of attack α

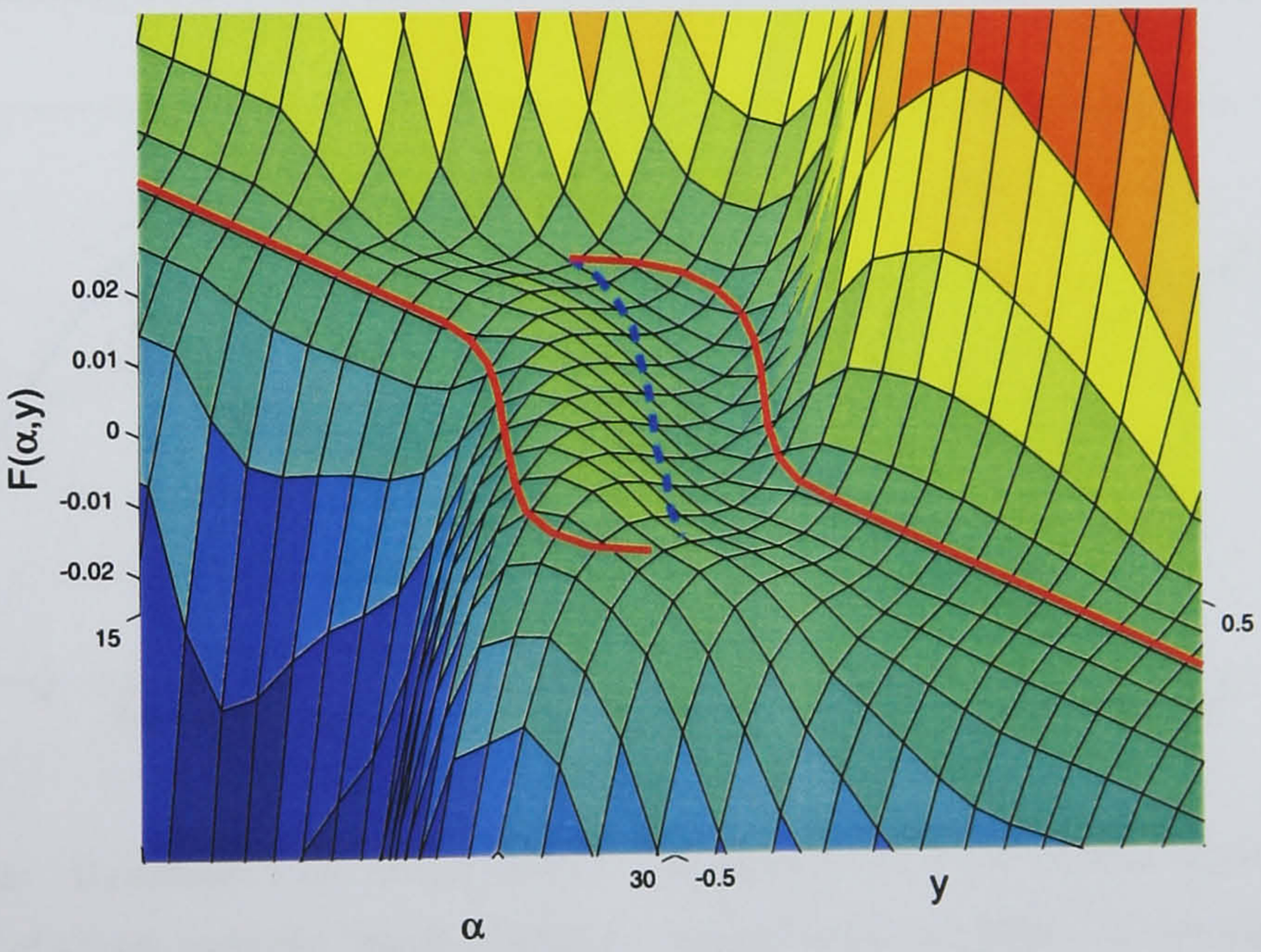

Figure 6.10: Function $F(\alpha, y)$. The solid and dashed lines correspond to the static dependency of $y(\alpha)$.

6.5 Validation of identified aerodynamic model with static hysteresis

6.5.1 Quasi-steady motion

The mathematical model which has been developed was applied to the simulation of the static hysteresis loop in the normal force coefficient during a quasi-steady variation of the angle of attack. The predicted dependence of the normal force coefficient C_N is shown in Fig. 6.11. It is seen that during the increase of the angle of attack from $\alpha = 10^o$, this dependence follows the upper branch of the static hysteresis until the point α_B where bifurcation takes place. At this point, the value of C_N jumps to the second static branch and then follows it. A similar jump takes place during the backward swing at the bifurcation point at α_A, which is at a lower angle of attack than α_B. This test shows that the model can reproduce the non-unique dependence of the normal force coefficient observed in the wind-tunnel static experiment and produce the hysteresis loop between the two bifurcation points α_A and α_B.

The bifurcation points or the critical states A and B are very sensitive to various disturbances as they have a neutral stability. These points can be strongly affected by the flow turbulence leading to a narrowing of the static hysteresis loop. Even a very slow variation

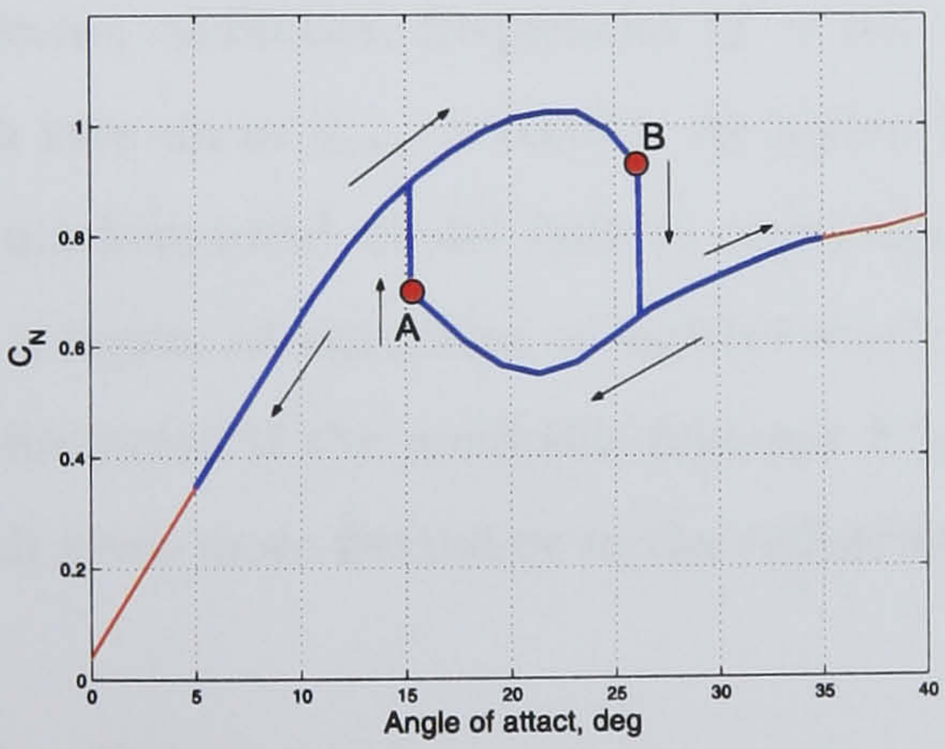

Figure 6.11: Hysteresis loop during quasi-steady angle of attack variation (result of simulation).

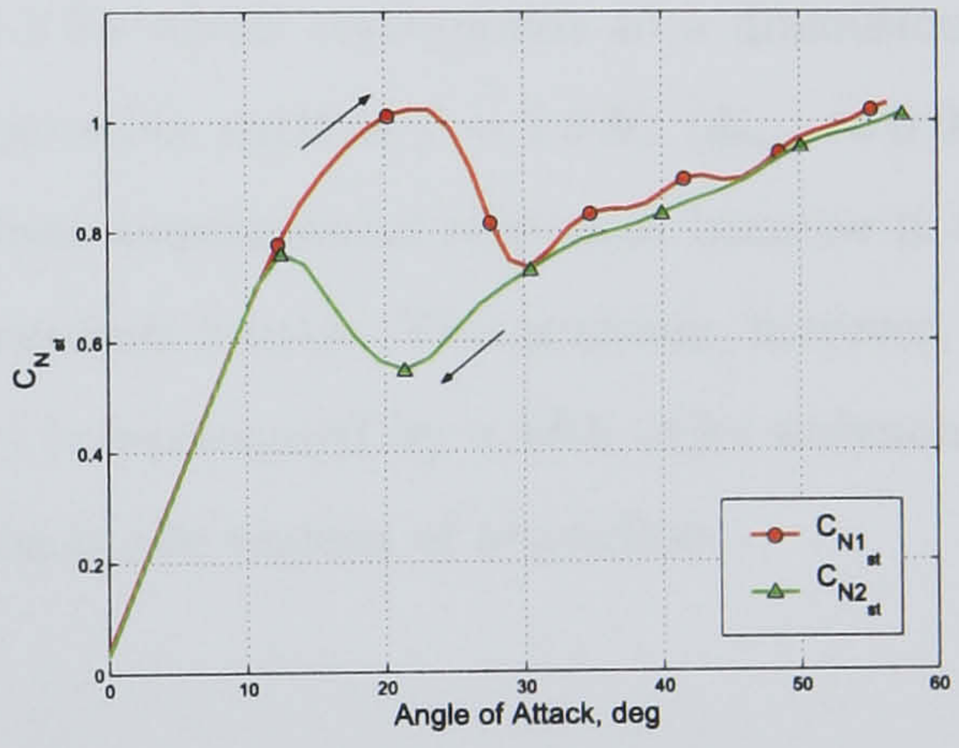

Figure 6.12: Experimental dependence of the normal force coefficient C_N during quasi-steady sweep motions ($\dot{\alpha} \approx 3^o/sec$).

of the angle of attack can significantly transform the shape of the static hysteresis due to transient dynamics after crossing the critical states points. The experimental dependence of the normal force coefficient C_N obtained during a very slow variation of angle of attack ($\dot{\alpha} = 3^o/sec$) and presented in Fig. 6.12 clearly demonstrate the transformation of the static hysteresis. It is seen that there are no clearly distinguished bifurcation points, and the critical state crossing processes are slightly tightened, as if being suspended, spreading the bifurcation points.

6.5.2 Large amplitude oscillatory motion

Analysis of the experimental aerodynamic responses obtained during a large amplitude variation of the angle of attack shows that the faster motion of the wing, the wider the hysteresis loop and the longer the transition regions after crossing the bifurcation points. The experimental aerodynamic responses and the predicted ones using the identified mathematical model are presented in Fig. 6.13. One can see a good agreement both for the aerodynamic responses placed entirely on one branch of the static hysteresis and for aerodynamic responses surrounding the static hysteresis loop at different frequencies of the pitch oscillations. It is seen that the model reproduces these dependencies very well for small and moderate oscillation frequencies ($f = 0.2 \ldots 1.2\,\mathrm{Hz}$ which corresponds to a dimensionless pitch rate up to $\bar{q}_{max} \approx 0.004$). At higher frequencies, such as $f = 1.6\,\mathrm{Hz}$ ($\bar{q}_{max} \approx 0.006$), the mathematical model fails to reproduce these experimental responses because it falls into a region of attraction of another static hysteresis branch. This problem, however, can be eliminated if the nonlinear function $F(y, \alpha)$ is represented by a fifth order polynomial, which gives more flexibility in the redistribution of the regions of attraction.

6.6 Summary

- A mathematical modelling technique for unsteady aerodynamic characteristics with static hysteresis has been developed based on the assumption that the unsteady aerodynamic loads can be split into attached and dynamic components. The technique able to tailor nonlinear differential equation governing the dynamic component according to bifurcational properties of the non-unique separated flow structure has

been developed.

- A mathematical model of the normal force coefficient $C_N(\alpha)$ of a high aspect ratio wing with a NACA-0018 aerofoil having static hysteresis has been developed and identified using experimental wind-tunnel data. A comparison of the simulated and the experimental results clearly demonstrates that the mathematical model reproduces experimental dependencies rather accurately at all ranges of the angles of attack and at a wide range of pitch rates.

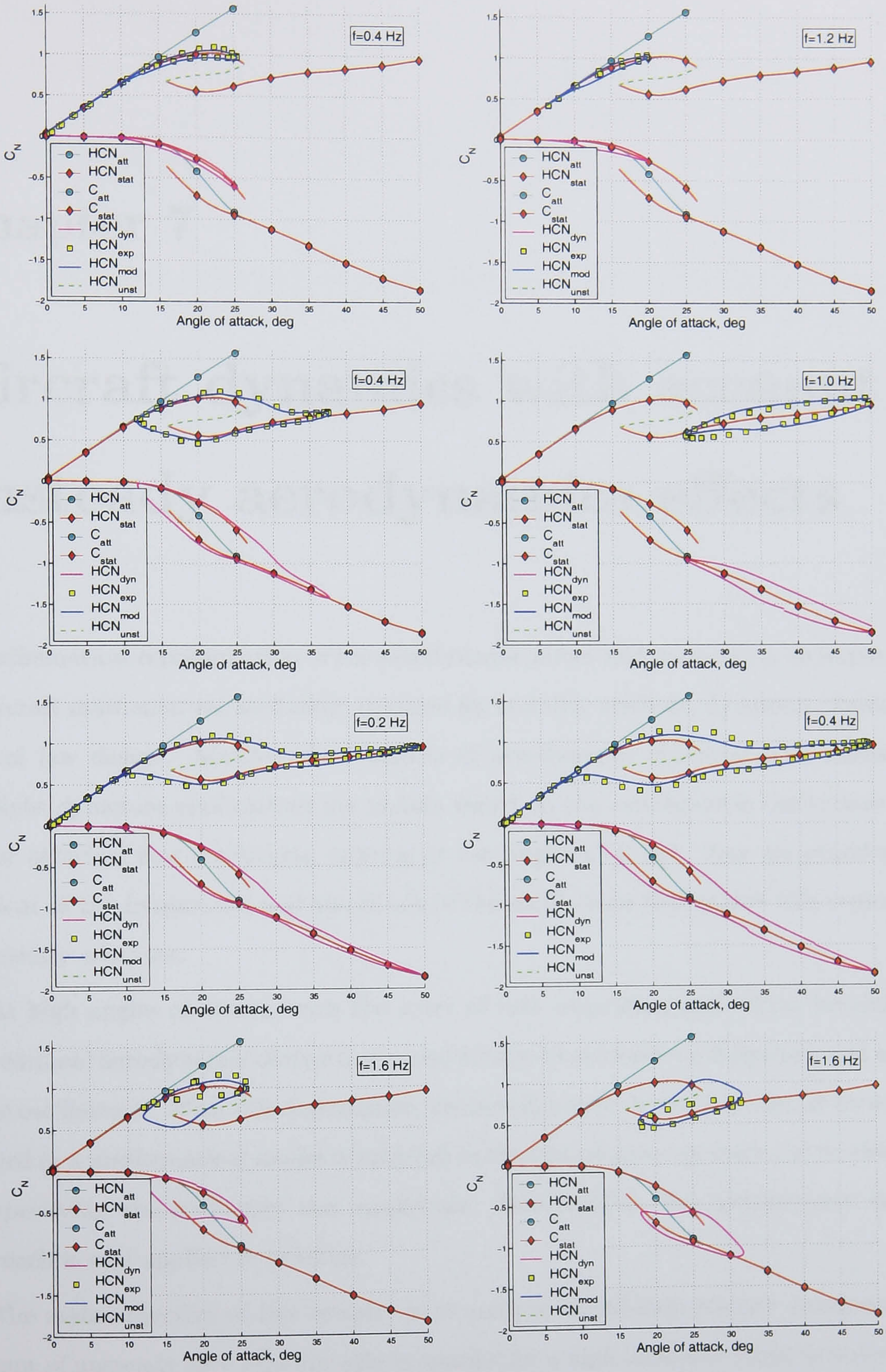

Figure 6.13: Large amplitude pitch oscillations: experimental normal force coefficient responses in comparison with predicted by nonlinear mathematical model.

Chapter 7

Aircraft dynamics with account of unsteady aerodynamics effects

A mathematical representation of the aerodynamic forces and moments is an important part of aircraft mathematical modelling required for stability analysis, dynamics simulation and control law design. Mathematical models of aerodynamic characteristics normally used for flight dynamics applications are mainly based on the aerodynamic derivatives concept. Under attached flow conditions, existing at low angles of attack, they are practically independent of the frequencies and amplitude of the oscillations that makes this representation sufficiently accurate.

At high angles of attack, with the onset of flow separation and vortex breakdown, the conventional aerodynamic derivatives reveal strong dependence on frequency and amplitude of the oscillations. With this dependence, the aerodynamic derivatives cannot be adequately applied in a mathematical model considered in the time domain as there are no clear criteria for specifying the frequency and amplitude. Nevertheless, the aerodynamic derivatives approach is still applied in practice.

The main objective of this chapter is to analyze closed-loop aircraft dynamics with an account of unsteady aerodynamic effects specific for a high incidence flight in order to reveal the impact of the two different forms of the aerodynamic load representation on the resulting aircraft dynamic properties. To do this a comparative analysis of the aircraft open-loop and closed-loop dynamics for two different forms of aerodynamic load representation is un-

dertaken. The aircraft dynamics is analysed separately with the dynamic mathematical model identified in Chapter 5 and with the traditional model based on aerodynamic derivatives. A hypothetical aircraft configuration with the 65^o delta wing is considered just to implement the developed mathematical models.

7.1 Frequency dependence effect in the time domain

Possible approaches for an aircraft dynamics analysis and control law design are discussed in this section to illustrate the peculiarities of the aerodynamic derivatives utilization in mathematical models for a high incidence flight.

The main difficulty in stability analysis, control low design or flight simulation is how to specify the frequency of oscillations in the aerodynamic model. Let us consider simplified equations of a short-period motion where the pitch moment depends on the reduced frequency parameter k:

$$\begin{aligned} \dot{\alpha} &= q \\ \dot{q} &= M(\alpha, q, k), \end{aligned} \tag{7.1}$$

where $M = \frac{\rho V^2 S\bar{c}}{2I_y} C_m(\alpha, k)$ is the aerodynamic pitch moment. Being linearized in the vicinity of the trim angle of attack α_0 system (7.1) is represented by the following linear differential equation:

$$\ddot{\alpha} - M_q(\alpha_0, k)\dot{\alpha} - M_\alpha(\alpha_0, k)\alpha = 0. \tag{7.2}$$

Parameter k in equations (7.1) and (7.2) is external, but it defines the values of the aerodynamic derivatives M_q and M_α, which affect the frequency and damping properties of the short-period motion. Unfortunately, there is no way to specify the parameter k in the time domain without preliminary physical assumptions or imposed constraints.

By definition, the reduced frequency parameter k is connected with the natural frequency of oscillations in a short-period motion ω as follows:

$$k = \frac{\bar{c}}{2V}\omega. \tag{7.3}$$

An expression for the frequency of short-period oscillations can be derived from differential equation (7.2), and with account of (7.3), the following nonlinear algebraic equation is

obtained for the definition of the parameter k:

$$\omega(k) = \sqrt{M_\alpha(k) + M_q(k)^2/4} = \frac{2Vk}{\bar{c}}. \tag{7.4}$$

This equation can be solved using, for example, Newton's method or by a direct iterative procedure. A reasonable initial value of the reduced frequency parameter $k = k_0$ is required in both cases. The Newton method requires the calculation of the M_{α_k} and M_{q_k} derivatives, while the iterative procedure can converge to the solution quite effectively without the calculation of these derivatives. Thus, equation (7.4) give us an estimate of the required value of the parameter k, which is necessary for the correct description of the aerodynamic loads and, consequently, for the adequate simulation of short-period motion dynamics. However, this approach has a weak point, namely, in order to obtain the correct values of the aerodynamic loads during a real-time flight simulation, the value of k has to be determined at each step of the integration. This can significantly slow down the calculations. Moreover, convergence of the Newton method or the iterative procedure must be ensured.

If an aircraft is equipped with a control system, the dynamic properties of the closed-loop system will depend on the control law and the feedback gains. Normally, the control system is designed to provide the required dynamic properties for the aircraft. In this case, the location of the closed-loop system eigenvalues is preset according to the requirements for the handling qualities (see [22], ch. 12), i.e. location of the "short-period" eigenvalues is used as a design criteria. Thus, the short-period motion frequency and, consequently, the parameter k can be considered as predetermined which makes possible an adequate determination of the aerodynamic loads.

At first sight it seems that the approaches described provide a regular technique for the calculation of aerodynamic loads in spite on some drawbacks. It is worth mentioning, however, that the aerodynamic derivatives concept is valid only in the vicinity of statics where linear dependence of the force/moment coefficients on the kinematic parameters can be assumed. In large amplitude motion an aircraft may pass through both the attached flow region and through the range of angles of attack where vortex breakdown and flow separation processes take place. In this case, as was shown in section 5.3, the linear mathematical model of aerodynamic loads becomes inaccurate and can result in too much uncertainty distorting the motion dynamics. Summarizing the aforesaid, one can conclude that the linear

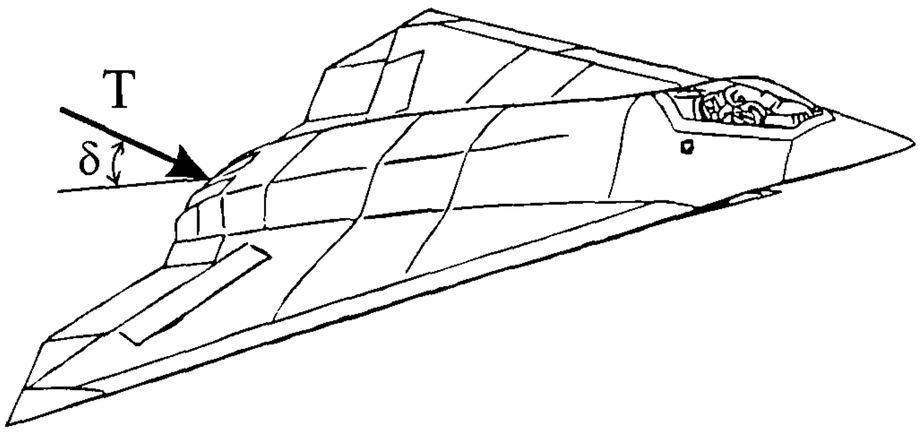

Weight, m	14865	kg
Moment of inertia, I_{yy}	106365	kg m^2
Wing area, S	75.12	m^2
Wing span, b	11.43	m
Mean aerodynamic chord, c	8.76	m
C.G. location, x_{cg}	0.40	

Table 7.1: A hypothetical 65^o delta wing aircraft with thrust vectoring control and its parameters.

aerodynamic derivative technique can be accurately used in the case of weakly disturbed motion provided that the reduced frequency parameter k is determined correctly. Some results obtained when the correct specification of the parameter k was neglected are discussed in the following sections to emphasize the importance of an adequate aerodynamic loads modelling technique.

7.2 Longitudinal motion dynamics

A hypothetical tailless aircraft with a 65^o delta wing and thrust vectoring control is considered in the chapter as a case study for the investigation of the influence of unsteady aerodynamic effects at a high incidence flight on aircraft dynamics, stability and control law design in longitudinal motion. Mass, inertia, geometric parameters and the view of a hypothetical aircraft with the 65^o delta wing and the pitch thrust vectoring considered for this comparison are given in Table 7.1. The throttle deflection $x_T \in [0,\ 2]$ and the thrust vector deflection angle in pitch δ_T are used for the speed and the angle of attack control. The aircraft is considered to be equipped with two engines with parameters similar to that used on a F-18 airplane and with thrust vectoring in pitch. The normalized maximum (T_{max}) and afterburning (T_{aft}) thrust force dependencies on the Mach number for a given altitude are shown in Fig. 7.9. Throttle positions $x_T \in [0,\ 1]$ and $x_T \in [1,\ 2]$ correspond to normal and afterburning regimes, respectively. Maximum normal and afterburning thrust forces of each engine at zero altitude are equal to $T_M = 4808\,\text{kgf}$ and $T_A = 7167\,\text{kgf}$, respectively. The thrust force produced at an intermediate throttle setting x_T is calculated

as follows:

$$T(M,H,x_T) = \begin{cases} t_{max}x_T, & 0 \le x_T \le 1 \\ t_{max} + (t_{aft} - t_{max})(x_T - 1), & 1 < x_T \le 2, \end{cases} \tag{7.5}$$

where $t_{max} = T_M T_{max}(M,H)$ and $t_{aft} = T_A T_{aft}(M,H)$.

Longitudinal aircraft dynamics is governed by the following equations:

$$\begin{aligned} \dot{V} &= \frac{T}{m}cos(\alpha + \delta_T) - (C_X \cos\alpha + C_N \sin\alpha)\frac{\rho V^2 S}{2m} - g\sin\gamma \\ \dot{\gamma} &= \frac{T}{mV}sin(\alpha + \delta_T) + (C_N \cos\alpha - C_X \sin\alpha)\frac{\rho V S}{2mV} - \frac{g}{V}\cos\gamma \\ \dot{\alpha} &= q - \dot{\gamma} \\ \dot{q} &= C_m \frac{\rho V^2 \bar{c} S}{2I_{yy}} - \frac{T l_T}{I_{yy}}\sin\delta_T, \end{aligned} \tag{7.6}$$

where V is the speed of flight, γ is the trajectory slope angle, q is the pitch rate, $T = T(H,V,x_T)$ is the engine thrust, l_T is the nozzle arm, ρ is the air density, C_N, C_m and C_X are the normal force, pitch moment and drag coefficients.

For the normal force C_N and pitch moment C_m coefficients, the following two aerodynamic models are used (here $i = N, m$):

the conventional aerodynamic derivatives model:

$$C_i = C_{i_{st}}(\alpha) + (C_{i_q} + C_{i_{\dot{\alpha}}})(\alpha,\omega)\frac{\bar{c}}{2V}q \tag{7.7}$$

the nonlinear unsteady aerodynamic model:

$$\begin{aligned} C_i(t) &= C_{i_{att}}(\alpha) + C_{i_{\dot{\alpha}_{att}}}(\alpha)\frac{\dot{\alpha}c}{2V} + C_{i_{dyn}} \\ \frac{dC_{i_{dyn}}}{dt} &= \frac{2V}{c}\sum_{m=1}^{n} k_m \left[(C_{i_{st}}(\alpha) - C_{i_{att}}(\alpha)) - C_{i_{dyn}}\right]^m \end{aligned} \tag{7.8}$$

During wind tunnel tests, the dependencies of the pitch moment coefficient were measured with respect to the axis of rotation coinciding with the model centre of gravity location $x_{cg} = 0.50$ MAC, although the CG location for the ICE prototype is 0.39 MAC. A direct application of the mathematical model identified using this data to the hypothetical aircraft would lead to an abnormally high level of instability. Therefore, to have a level of instability typical of modern combat aircraft, the pitch moment coefficient is recalculated

to $x_{cg} = 0.40$ MAC according to the following formulas:

$$\begin{aligned} C_{N_{\alpha 1}} &= C_{N_{\alpha 0}} \\ C_{m_{\alpha 1}} &= C_{m_{\alpha 0}} - \Delta x_T C_{N_{\alpha 0}} \\ (C_{N_q} + C_{N_{\dot{\alpha}}})_1 &= (C_{N_q} + C_{N_{\dot{\alpha}}})_0 + \Delta x_T C_{N_{\alpha 0}} \\ (C_{m_q} + C_{m_{\dot{\alpha}}})_1 &= (C_{m_q} + C_{m_{\dot{\alpha}}})_0 - \Delta x_T (C_{N_q} + C_{N_{\dot{\alpha}}})_0 + \Delta x_T C_{m_{\alpha 0}} - \Delta x_T^2 C_{N_{\alpha 0}}. \end{aligned} \tag{7.9}$$

The static dependencies of the pitch moment coefficient corresponding to different CG locations are presented in Fig. 7.1.

7.2.1 Trim in horizontal flight

Thrust vectoring control δ_T and throttle control x_T allow the aircraft to be trimmed in a level flight at various angles of attack. The computation of equilibrium solutions for equations (7.6) corresponding to the level flight conditions $\gamma = 0$ provides the required thrust vectoring deflection δ_T and throttle control x_T.

The speed V as well as the control variables δ_T and x_T at equilibrium level flight are presented in Fig. 7.2 for altitude $H = 1$ km as functions of the trim angle of attack α_d. The speed of flight decreases significantly at small angles of attack and above $\alpha = 25^o$ the speed varies very little $V \approx 40 \ldots 50$ m/s.

7.2.2 The open-loop system eigenvalues analysis

As discussed earlier, the aerodynamic derivatives in the conventional aerodynamic model strongly depend on the reduced frequency of oscillations in the range of angles of attack $25^o \leq \alpha \leq 48^o$. As the reduced frequency of an aircraft short-period oscillations is unknown in advance, the problem of the proper choice of the aerodynamic derivatives arises. Otherwise, significant inaccuracies in prediction of the aircraft dynamics can be produced. To evaluate these inaccuracies, some dynamic properties of the aircraft are to be compared for the cases when the conventional aerodynamic derivatives model at different values of reduced frequencies k and the unsteady aerodynamic model are used.

The root loci corresponding to a short-period motion were calculated for the aerodynamic derivatives model at frequencies $f = 0.5\,\text{Hz}$, $f = 1.0\,\text{Hz}$, $f = 1.5\,\text{Hz}$ and for the

unsteady aerodynamic model. These results are presented in Fig. 7.3. One can see that the system dynamics strongly depends on the type of aerodynamic model and sometimes demonstrates qualitatively different behavior at the same angle of attack. For example, the system responses to a five degree disturbance in the angle of attack at trim angle $\alpha = 47^o$ are shown in Fig. 7.4 for the conventional model at three different frequencies and for the unsteady aerodynamic model. The corresponding plot containing eigenvalues of the linearized system is given in Fig. 7.6. It is seen that in the case of the conventional model at $f = 0.5\,\text{Hz}$ the open-loop system is aperiodically unstable. At $f = 1.0\,\text{Hz}$ the process converges towards the limit cycle with amplitude approximately 0.5^o (note, that the linearized system has oscillatory unstable eigenvalues), and at $f = 1.5\,\text{Hz}$ the system is oscillatory stable. In the case of the unsteady aerodynamic model, the system is oscillatory unstable, and two additional real eigenvalues corresponding to the unsteady aerodynamic model appear. Thus one can see that even in the case of a relatively small disturbance, the system behaviour can strongly depend on the type of aerodynamic model, and an incorrect choice of the aerodynamic derivatives can lead to very significant changes in the dynamics.

Typical plots of the eigenvalues corresponding to a short and long period motion and unsteady aerodynamics effect are shown in Fig. 7.5 and Fig. 7.6. It is seen that the quasi-steady model based on aerodynamic derivatives provides a very broad range of results, from aperiodic instability at $f = 0.5\,\text{Hz}$ to oscillatory instability with significantly different real parts of the eigenvalues at $f = 1.0\,\text{Hz}$ and $f = 1.5\,\text{Hz}$. At the same time, the open-loop system with the unsteady aerodynamic model is oscillatory unstable both at $\alpha = 39^o$ and $\alpha = 47^o$. The same situation take place for the whole range of angles of attack $\alpha = 30^o \ldots 47^o$ (see Fig. 7.3). So, one can conclude that the quasi-steady aerodynamic model introduces very high uncertainty in the eigenvalues corresponding to a short-period motion.

7.2.3 Stabilizing control law

The aircraft configuration considered in the case study is unstable at angles of attack $\alpha < 48^o$ (see Fig. 7.3). To stabilize the aircraft short-period motion, the following PID

control law for thrust vectoring deflection is used:

$$\delta_T = k_\alpha(\alpha - \alpha_d) + k_q q + k_I \int (\alpha - \alpha_d)dt, \tag{7.10}$$

where α_d is the demanded trim angle of attack, k_α, k_q and k_I are feedback gains.

The thrust vector is deflected by the actuator, whose dynamics is approximated by the first order model:

$$\dot{\delta}_a = -Q(\delta_a - \delta_T), \tag{7.11}$$

where δ_a is a current thrust deflection angle, Q is the quality factor. The deflection limit $|\delta| \leq \delta_{max}$ and rate constraint $|\dot{\delta}| \leq \dot{\delta}_{max}$ are also implemented in the actuator model. The actuator dynamics (7.11) is taken into account only for the simulation and stability region calculation. For trimming purposes and the linearized system eigenvalues computation, the actuator transfer function is assumed equal to one.

The feedback control law (7.10) can allocate the closed-loop system eigenvalues associated with the short-period dynamics in a region with required handling quality characteristics and simultaneously maintain the equilibrium angle of attack equal to the control input α_d.

For comparison purposes, the feedback coefficients in (7.10) have been calculated for both aerodynamic models. The closed-loop system eigenvalues have been allocated in accordance with the handling qualities requirements for the short-period motion mode [22]. In Fig. 7.10 the feedback gains are presented for the unsteady aerodynamic model and quasi-steady aerodynamic model with $f = 1.0\,\mathrm{Hz}$ as function of the angle of attack in the range $\alpha \in [10^o, 60^o]$. One can see that at angles of attack corresponding to peak values of the aerodynamic derivatives ($\alpha = 38^o \ldots 45^o$) the feedback gains for the quasi-steady aerodynamic model significantly rise responding to an increase of the q-derivative while the feedback gains for the unsteady aerodynamic model are monotonic and have reasonable magnitudes. The unsteady model of the aerodynamic loads is considered as an adequate one because it is able to capture time lag effects from the flow dynamics. So, the feedback gains obtained using this model should provide the required dynamics in the closed-loop system in real flight conditions. The feedback gains obtained using the quasi-steady aerodynamic model can significantly depend on the frequency f, and the closed-loop dynamics with these gains will definitely fail to meet the formulated requirements.

7.2.4 Closed-loop system analysis

7.2.4.1 Eigenvalues analysis

The aerodynamic models (7.7) and (7.8) are compared in terms of their impact on the closed-loop system dynamics. The following scenario is considered. The system with the dynamic model of aerodynamics (7.8) is stabilized by the control law (7.10) providing the required stability and handling quality characteristics. After that the obtained eigenvalues are compared with the eigenvalues of the closed-loop system with the conventional aerodynamic model (7.7) at different frequencies f and the feedback coefficients k_α, k_q, k_I obtained with the unsteady aerodynamic model. This comparison will show the uncertainty introduced by the quasi-steady aerodynamic model in the eigenvalues of the closed-loop system.

The eigenvalues for both models under level flight conditions are presented in Fig. 7.7 for $\alpha = 20^0$. The closed-loop system eigenvalues with the dynamic aerodynamic model are shown by empty circles, while the eigenvalues for the conventional aerodynamic model at different frequencies $f = 0.5$, 1.0, 1.5 Hz are shown by dots, crosses and asterisks, respectively. Two contours confine regions of "acceptable" (external contour) and "satisfactory" (internal contour) pilot's opinion ratings [22].

The closed-loop longitudinal dynamics with the model based on aerodynamic derivatives has a fifth order because of the integral in the control law. The closed-loop system with the dynamic model of aerodynamics has two additional dimensions, and its order equals to seven. These two additional real eigenvalues located in the range $\lambda \approx -0.82 \ldots -0.25$ reflect relaxation processes in the unsteady model of aerodynamics.

The closed-loop system eigenvalues for both types of aerodynamic model at all frequencies practically coincide when $\alpha = 20^o$ (see Fig. 7.7). So, two considered aerodynamic models are practically identical in terms of the aircraft short-period dynamics, when there is no strong frequency dependence in the aerodynamic derivatives. In the range of the angle of attack with a strong dependence of the aerodynamic derivatives on frequency one can see an essential variation of the eigenvalues in the closed-loop system. For example, at $\alpha = 28^o$ the eigenvalues corresponding to the conventional model with frequencies $f = 0.5$ Hz and $f = 1.0$ Hz, move to the right semi-plane leading to oscillatory instability in the closed-loop system while eigenvalues corresponding to $f = 1.5$ Hz are still oscillatory stable (see

Fig. 7.7).

The root loci of the closed-loop system with the conventional aerodynamic model and feedback gains designed using the unsteady aerodynamic model are presented in Fig. 7.8. One can see that the root loci for the short-period eigenvalues are significantly different for various frequencies both quantitatively and qualitatively.

In another comparison scenario, the closed-loop system with the aerodynamic derivative model at $f = 1.0\,\text{Hz}$ is stabilized by the control law (7.10) with feedback coefficients providing the required handling quality (see Fig. 7.10, bottom plot). Then the obtained control law is used with the unsteady aerodynamic model and the quasi-steady aerodynamic model with frequencies $f = 0.5\,\text{Hz}$ and $1.5\,\text{Hz}$.

The closed-loop system eigenvalues for all these cases are presented in Fig. 7.11 for $\alpha = 25^o, 35^o, 40^o, 50^o$. The difference between the aerodynamic models at $\alpha = 25^o$ is not very substantial, and all short-period mode eigenvalues are located within the "satisfactory" region. At $\alpha = 35^o$ this difference becomes more significant but not resulting in qualitative changes of the closed-loop system stability. The eigenvalues for the unsteady aerodynamic model are overdamped and located out of the "acceptable" region. At $\alpha = 45^o$ the eigenvalues for the conventional aerodynamic model at different frequencies are scattered significantly from the stable overdamped ones at $f = 1.5\,\text{Hz}$ to aperiodically unstable at $f = 0.5\,\text{Hz}$. This results in a qualitatively different behavior of the closed-loop system at different frequencies f. At an angle of attack $\alpha > 49^o$ when flow dynamics is not so essential all short-period mode eigenvalues are located in the "satisfactory" region close to each other.

As the unsteady aerodynamic model is considered as an adequate model for a high incidence flight, the closed-loop system eigenvalues should provide an accurate prediction of the aircraft dynamics. At moderate angles of attack $\alpha \leq 25^o$ two aerodynamic models considered are practically identical in terms of aircraft longitudinal dynamics as there is no strong frequency dependence in the aerodynamic derivatives. At higher angles of attack $\alpha > 25^o$, the real aircraft dynamic behaviour is more stable than was expected after the control design. It is a very lucky situation as the control law was designed using an inadequate mathematical model of aerodynamics and, nevertheless, the closed-loop system remained stable, although it failed to meet the handling quality requirements.

The presented comparisons clearly demonstrate that in the case of the aerodynamic derivatives model, a level of uncertainty in the closed-loop aircraft model due to the neglected frequency dependence is very high and unacceptable for stability analysis and control law design in the time domain while the unsteady aerodynamic model is free of these drawbacks.

Note, that the closed-loop system phugoid eigenvalues do not vary significantly for the cases considered as the long-period time scale is much higher than the characteristic time scales of unsteady aerodynamics.

7.2.4.2 Stability regions analysis

The eigenvalue analysis reflects the local dynamic characteristics of the closed-loop system. The numerical simulation and stability regions analysis provides additional information about the closed-loop system dynamics. The disturbed motion with large amplitudes can reveal the effect of the aerodynamic model non-linearities.

It is well known, that stabilization of an unstable system with constraint control input needs special analysis of the controllability region for the open-loop system and analysis of the region of attraction for the closed-loop system as they can both be bounded. The size of the closed-loop system stability region specifies the critical level of the external disturbances and can be considered as an important design criteria [30].

A direct numerical simulation has been used to compute the stability regions in the plane of angle of attack and the pitch rate $\alpha - q$. The control input, i.e. the thrust vectoring deflection, was constrained both in amplitude $|\delta_T| \leq 30^o$ and the rate of deflection $|\dot{\delta}_T| \leq \dot{\delta}_{T_{max}}$. The feedback gains obtained for the unsteady aerodynamic model (see Fig. 7.10) were used in the stabilizing control law (7.10).

The computed stability regions or regions of attraction for the trimmed level flight at $\alpha = 30^o$ and $\alpha = 46^o$ are presented in Figs. 7.12–7.13. The regions of attraction for unsteady aerodynamic model at different rate saturation limits for thrust vectoring control $|\dot{\delta}_{T_{max}}| = 20,\ 40,\ 60^o/\text{sec}$ are shown in Fig. 7.12. The comparison of the regions of attraction for the closed-loop system with the unsteady aerodynamic model and the quasi-steady aerodynamic model at different frequencies $f = 0.5\,\text{Hz},\ 1.0\,\text{Hz}$ and $1.5\,\text{Hz}$ are shown in Fig. 7.13. It is seen that an increase of the rate saturation limit leads to an increase in

the size of the stability region and this effect is approximately linear.

The closed-loop system stability region is much bigger for the unsteady aerodynamic model than for the quasi-steady aerodynamic model with different values of the frequency parameter. It means that the control law design with the quasi-steady aerodynamic models provides more conservative results in terms of the closed-loop system eigenvalues and the size of stability region. If the control law designed using the quasi-steady aerodynamic model is acceptable from a stability point of view, the real dynamics will be even more stable. This fact at least could explain some successful practical applications, in particular, the design and flight tests of the control system for the X-31 aircraft.

Unfortunately, no one can guarantee that the above conclusion is true for all possible situations. The simulation results presented in Fig. 7.14 act as a counter example. The trimmed level flight at $\alpha = 48^o$ is stable for the quasi-steady model with $f = 1.0\,\text{Hz}$ and $f = 1.5\,\text{Hz}$ and unstable for the same model with $f = 0.5\,\text{Hz}$ and the unsteady aerodynamic model.

7.3 Summary

Analysis of the open- and closed- loop system eigenvalues and transient dynamics in a wide range of angles of attack for a hypothetical aircraft with the 65^o delta wing revealed that:

- at high angles of attack with the onset of the flow separation and vortex breakdown processes the conventional aerodynamic derivatives model produces a high level of uncertainty in the open- and closed-loop system eigenvalues due to a strong dependence on the frequency of oscillations and, therefore, can not be directly applied in the time domain with adequacy;

- the proposed unsteady aerodynamic model naturally incorporates frequency and amplitude dependence and can be effectively used in the time domain for dynamics simulation and control law design at high incidence flight conditions;

- at low angles of attack with the attached flow conditions, both types of aerodynamic models are equivalent in terms of their impact on the dynamic properties of an aircraft.

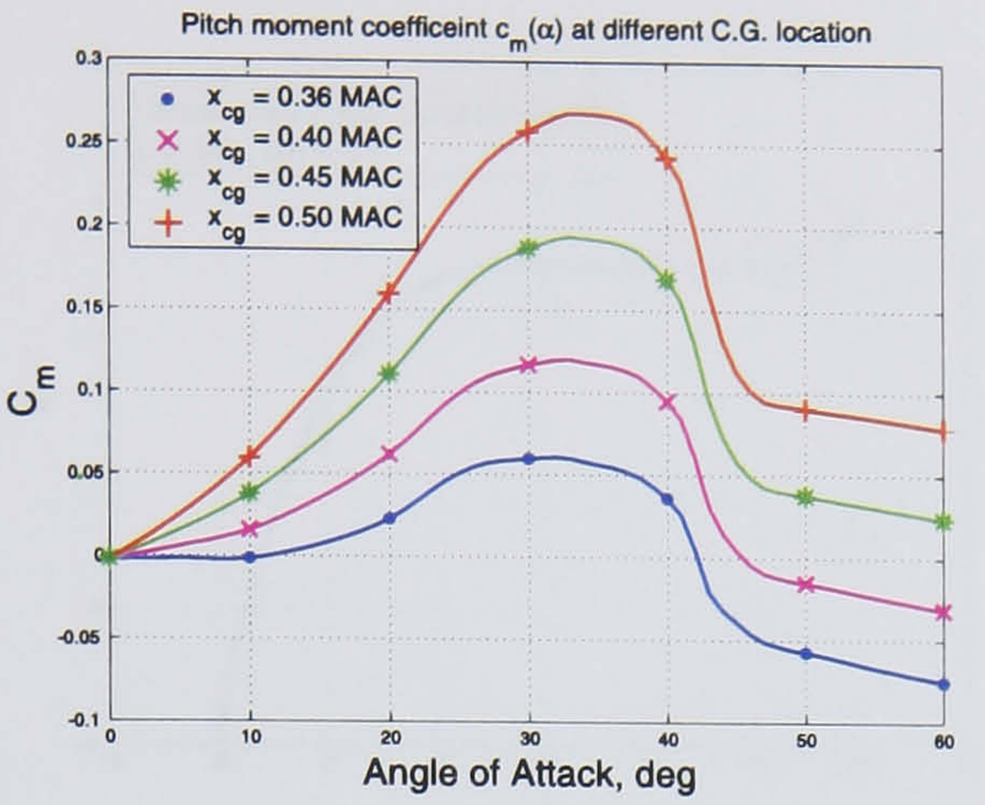

Figure 7.1: Pitch moment coefficient for different x_{cg} locations.

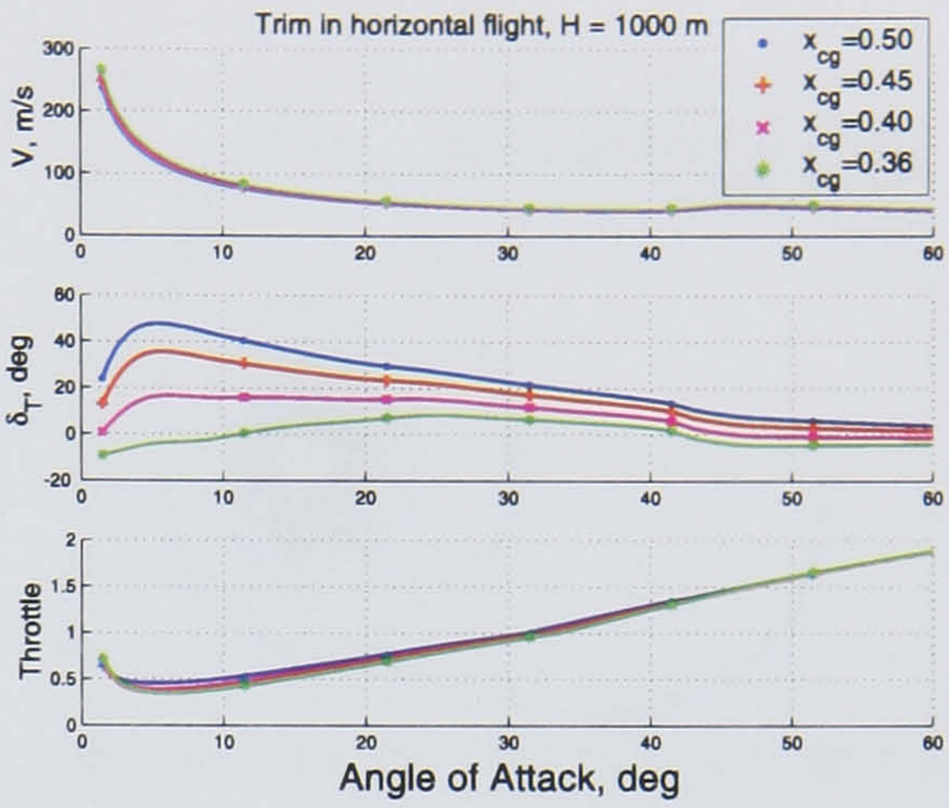

Figure 7.2: Trim speed, thrust deflection angle and throttle control at $x_{cg} = 0.40$.

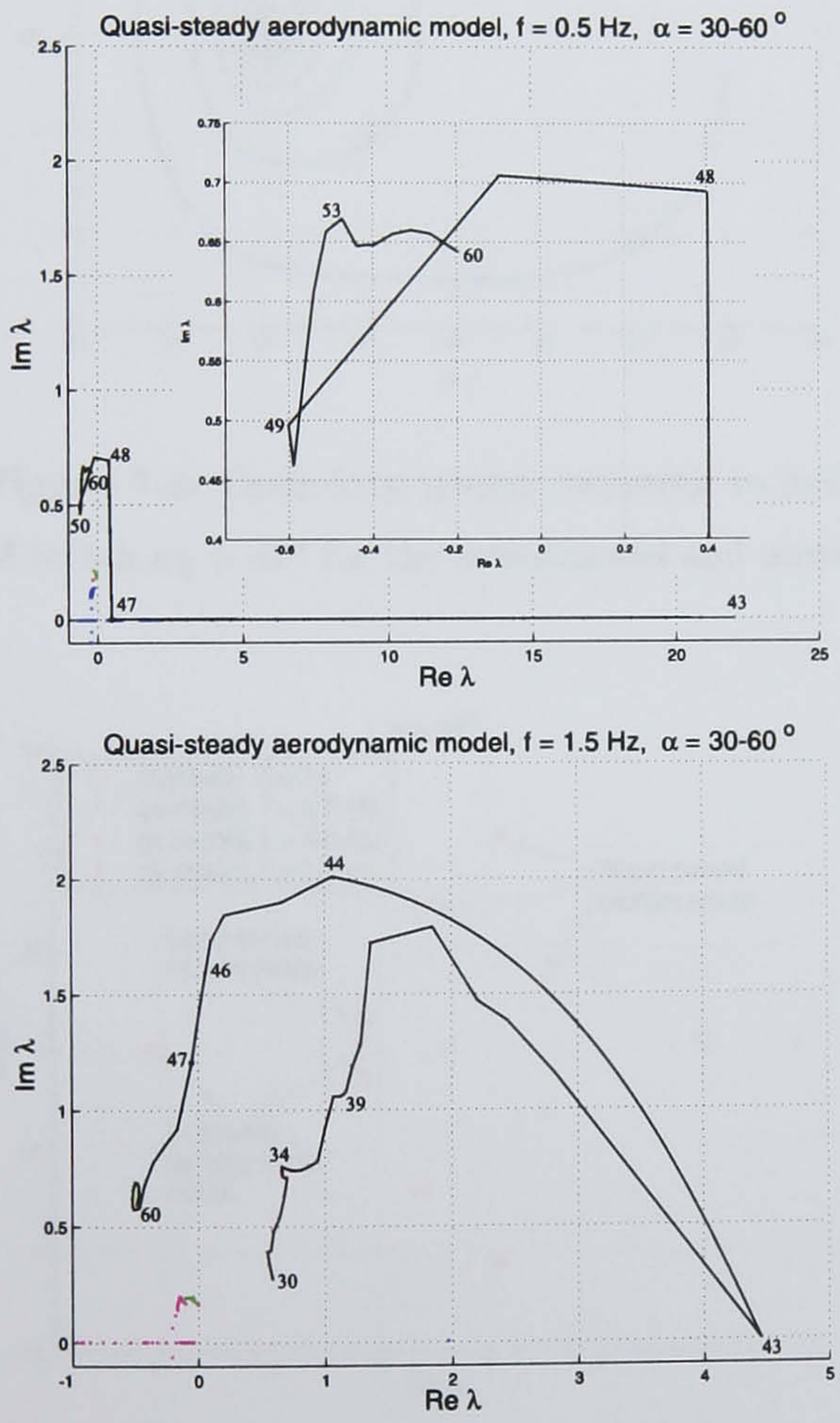

Figure 7.3: Open-loop system root loci for the quasi-steady model at $f = 0.5\,\mathrm{Hz}$, $f = 1.0\,\mathrm{Hz}$, $f = 1.5\,\mathrm{Hz}$ and the unsteady aerodynamic model.

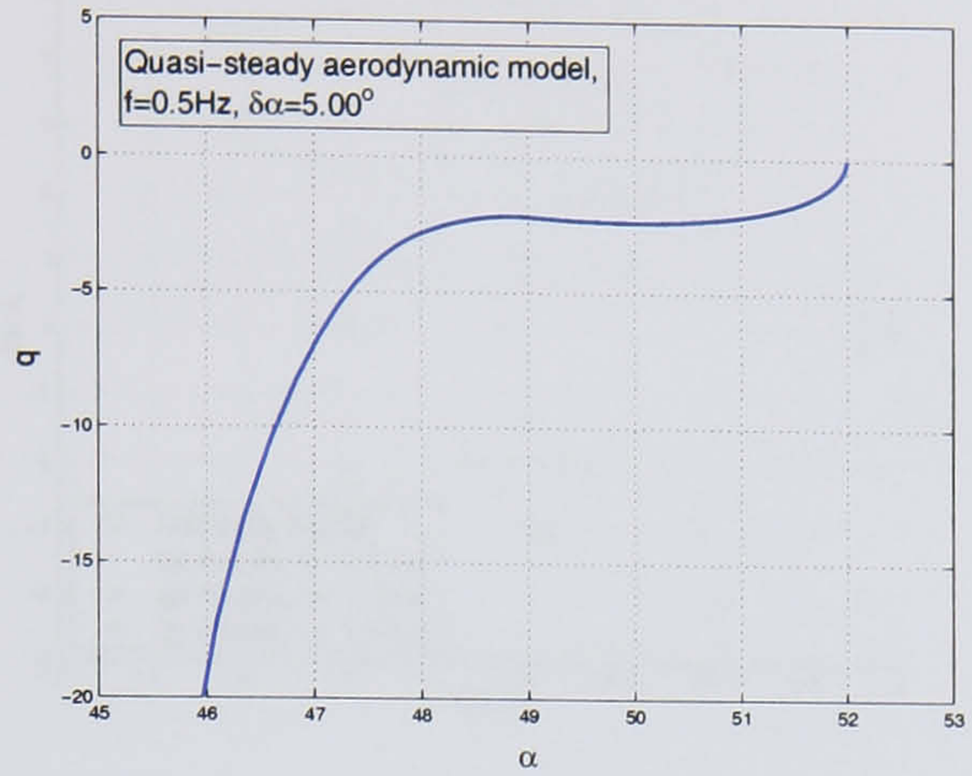

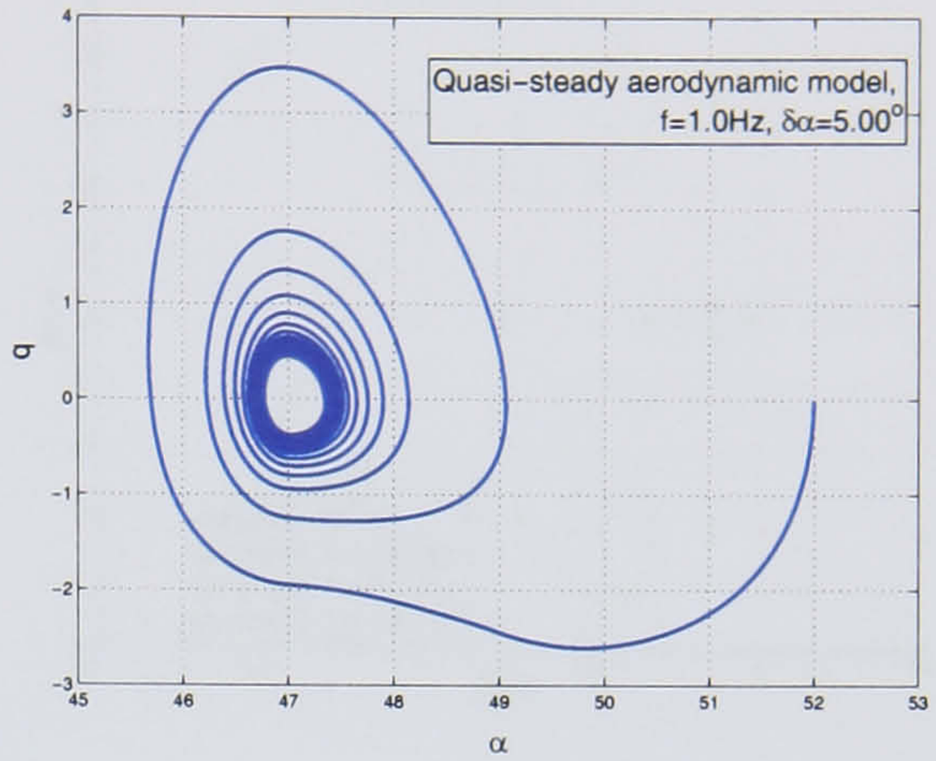

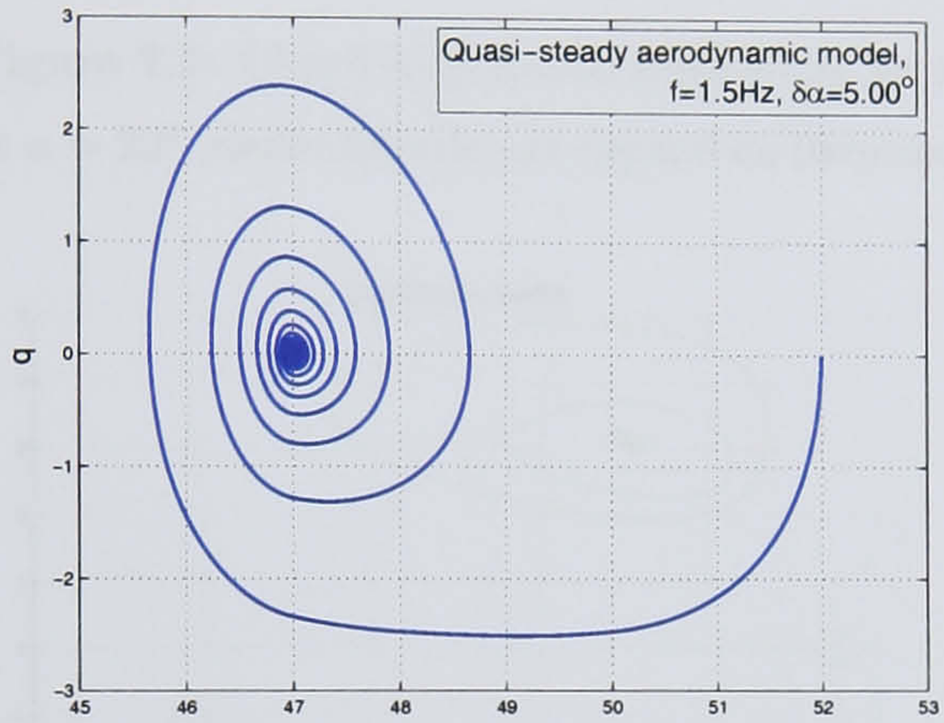

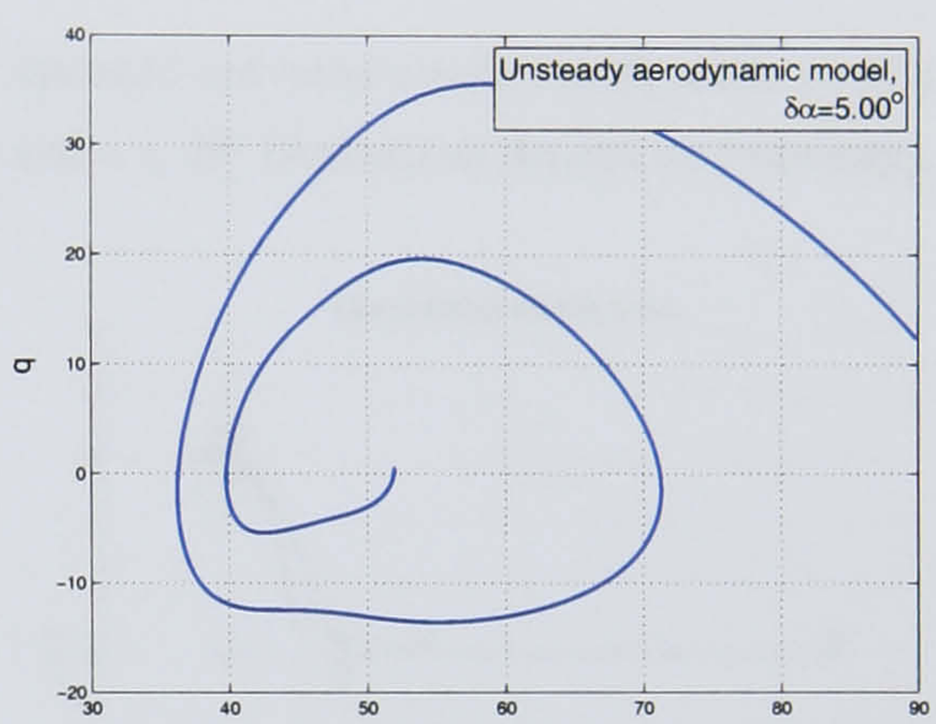

Figure 7.4: Open-loop system responses to initial disturbance $\delta\alpha = 5^o$ relative to the trim angle of attack $\alpha_0 = 47^o$ for the conventional and unsteady aerodynamic models.

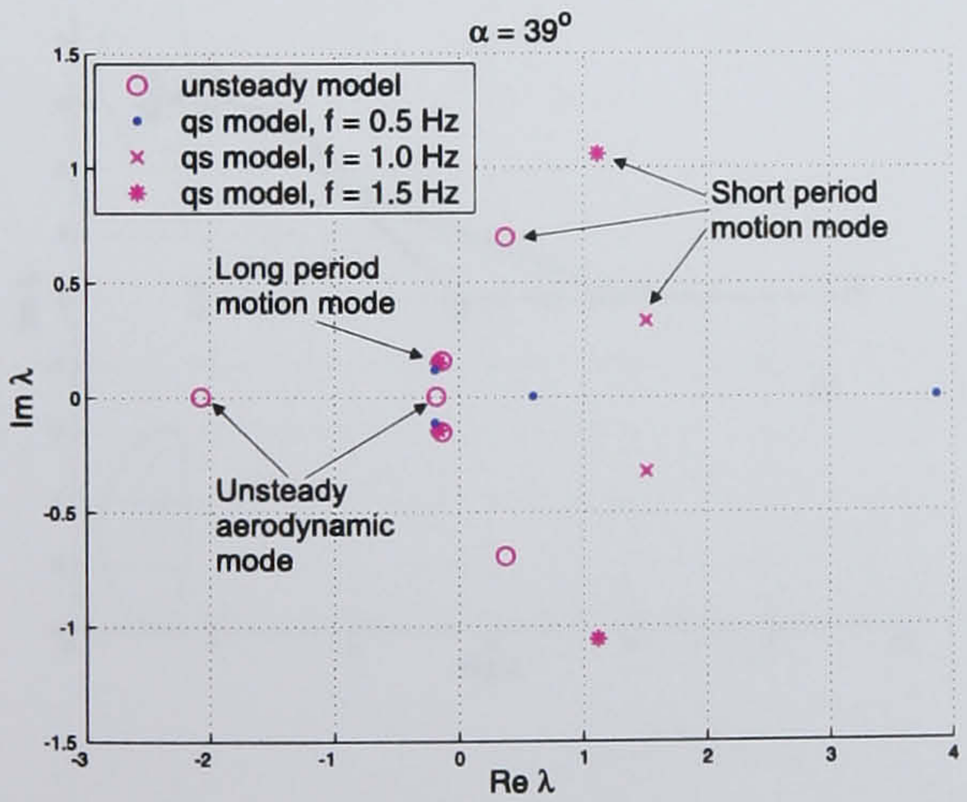

Figure 7.5: Open-loop system eigenvalues for different aerodynamic models at $\alpha = 39^o$.

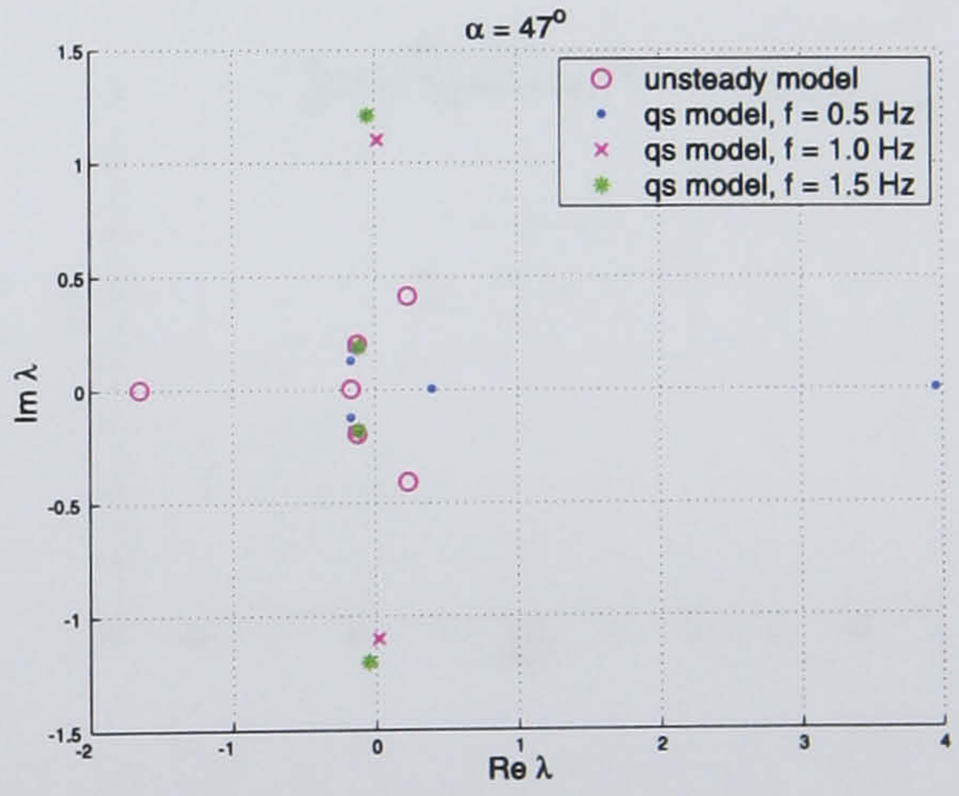

Figure 7.6: Open-loop system eigenvalues for different aerodynamic models at $\alpha = 47^o$.

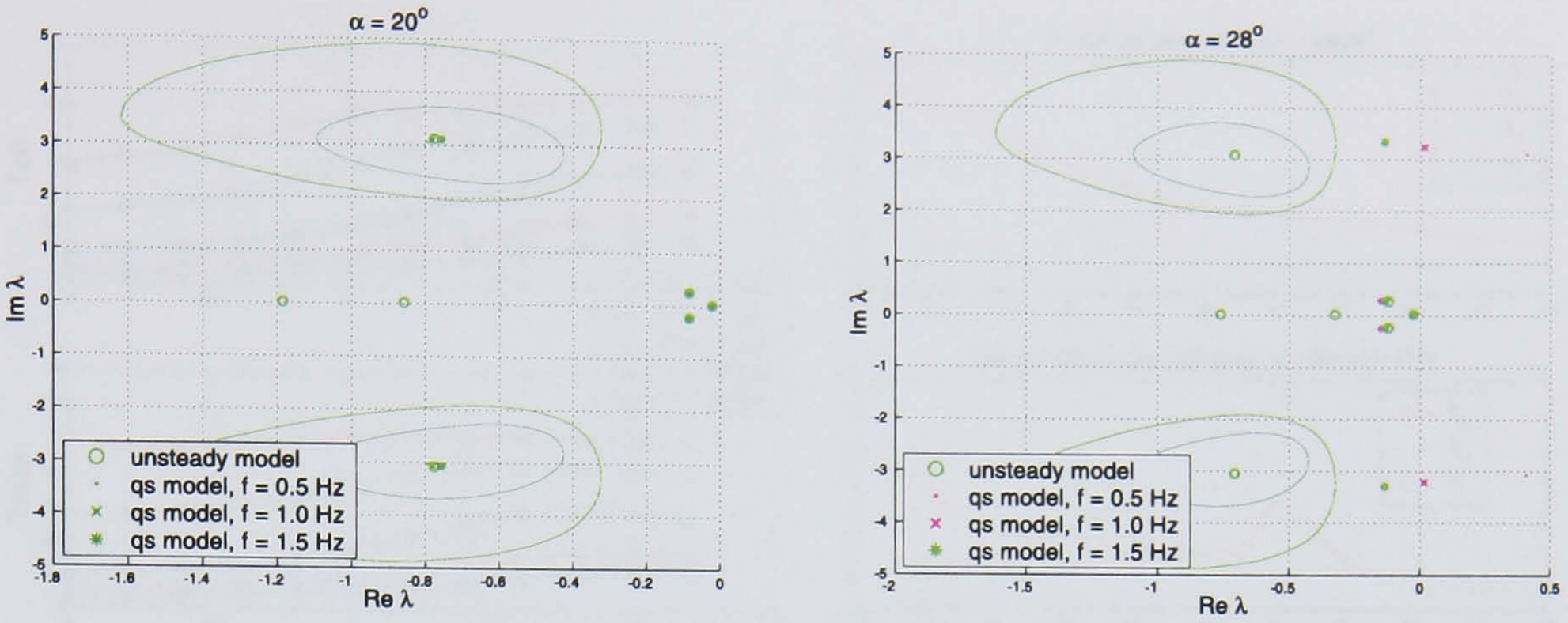

Figure 7.7: Closed-loop system eigenvalues for the dynamic and quasi-steady aerodynamic models at $\alpha = 20^o$ (derivatives do not depend on frequency) and $\alpha = 28^o$ (derivatives depend on frequency).

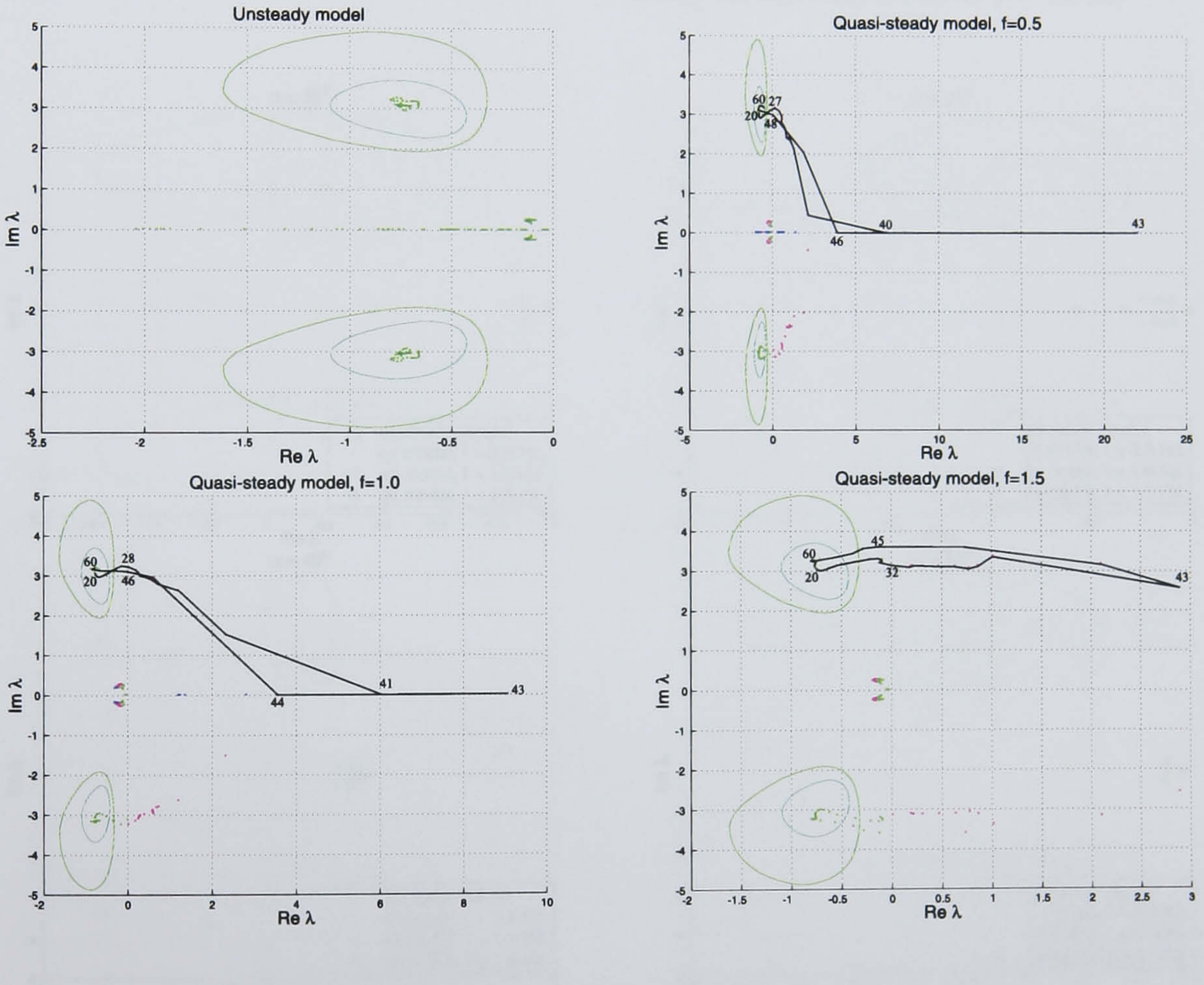

Figure 7.8: Closed-loop system eigenvalues corresponding to the quasi-steady aerodynamic model at $f = 0.5\,\mathrm{Hz}$, $f = 1.0\,\mathrm{Hz}$, $f = 1.5\,\mathrm{Hz}$ and the unsteady aerodynamic model.

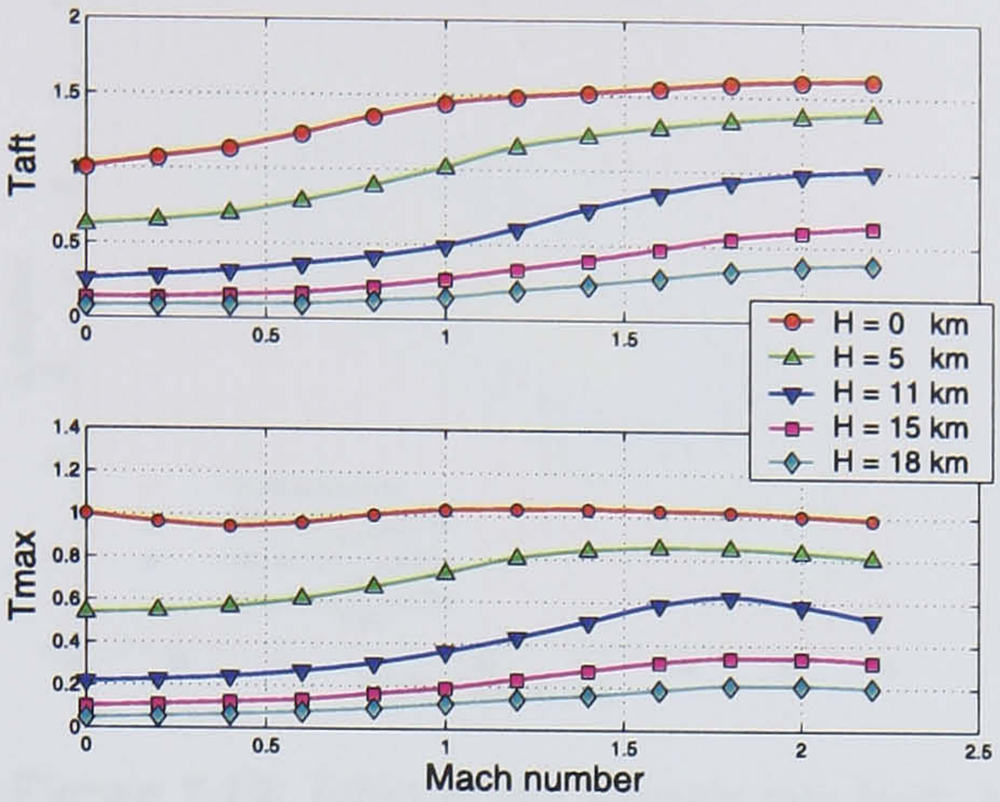

Figure 7.9: Thrust characteristics for normal (T_{max}) and afterburning (T_{aft}) regimes.

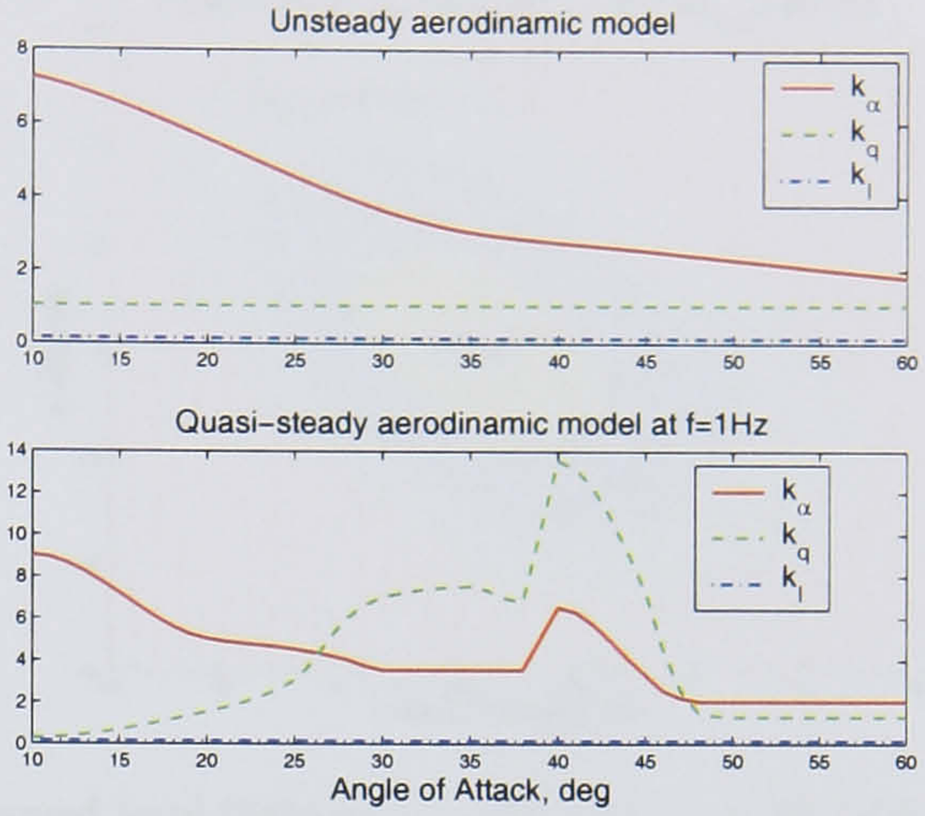

Figure 7.10: Control law feedback gains for the unsteady aerodynamic model and for the quasi-steady aerodynamic model at $f = 1.0\,\mathrm{Hz}$.

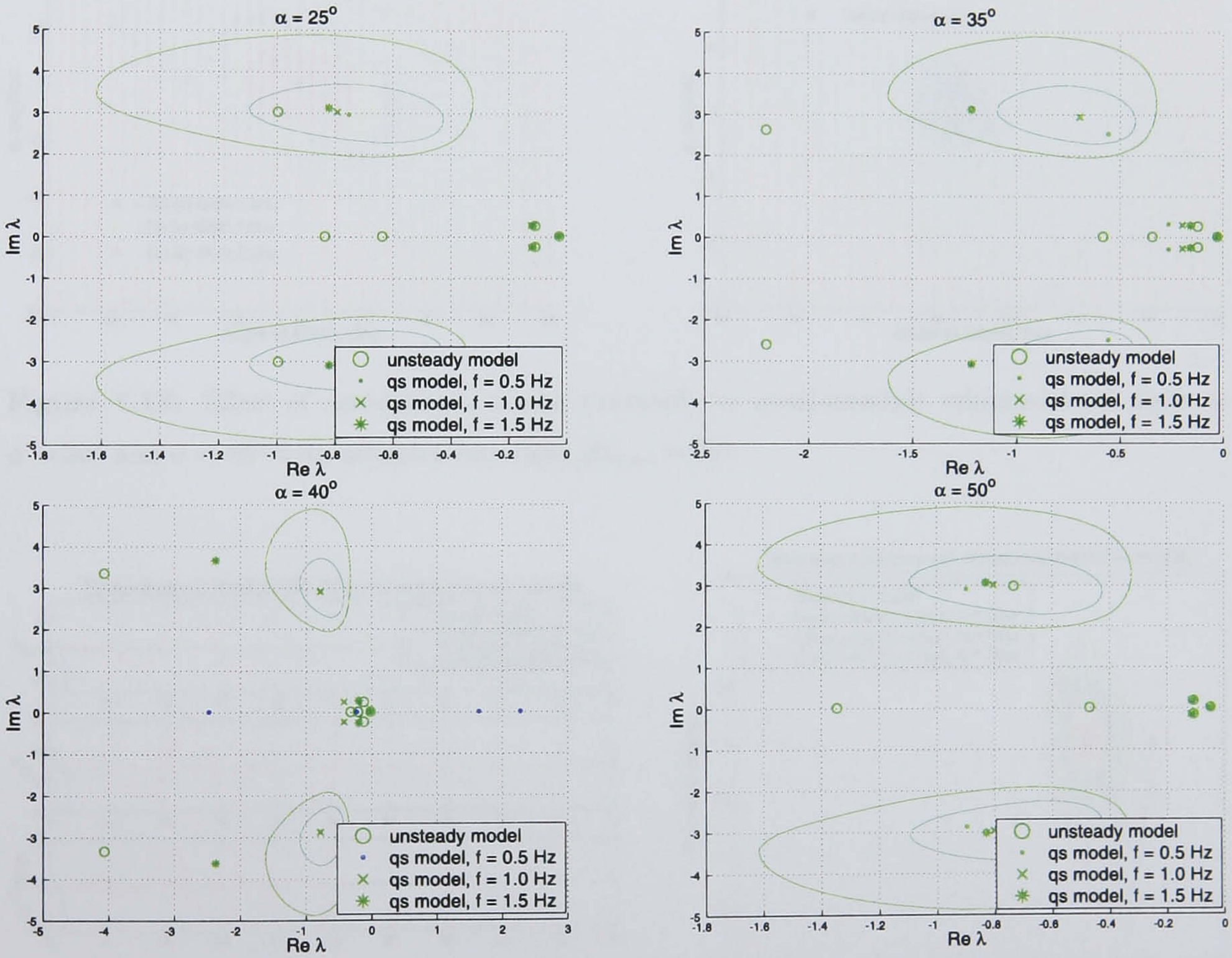

Figure 7.11: Closed-loop system eigenvalues corresponding to different aerodynamic models: quasi-steady at $f = 0.5\,\mathrm{Hz}$, $f = 1.0\,\mathrm{Hz}$, $f = 1.5\,\mathrm{Hz}$ and unsteady aerodynamic model.

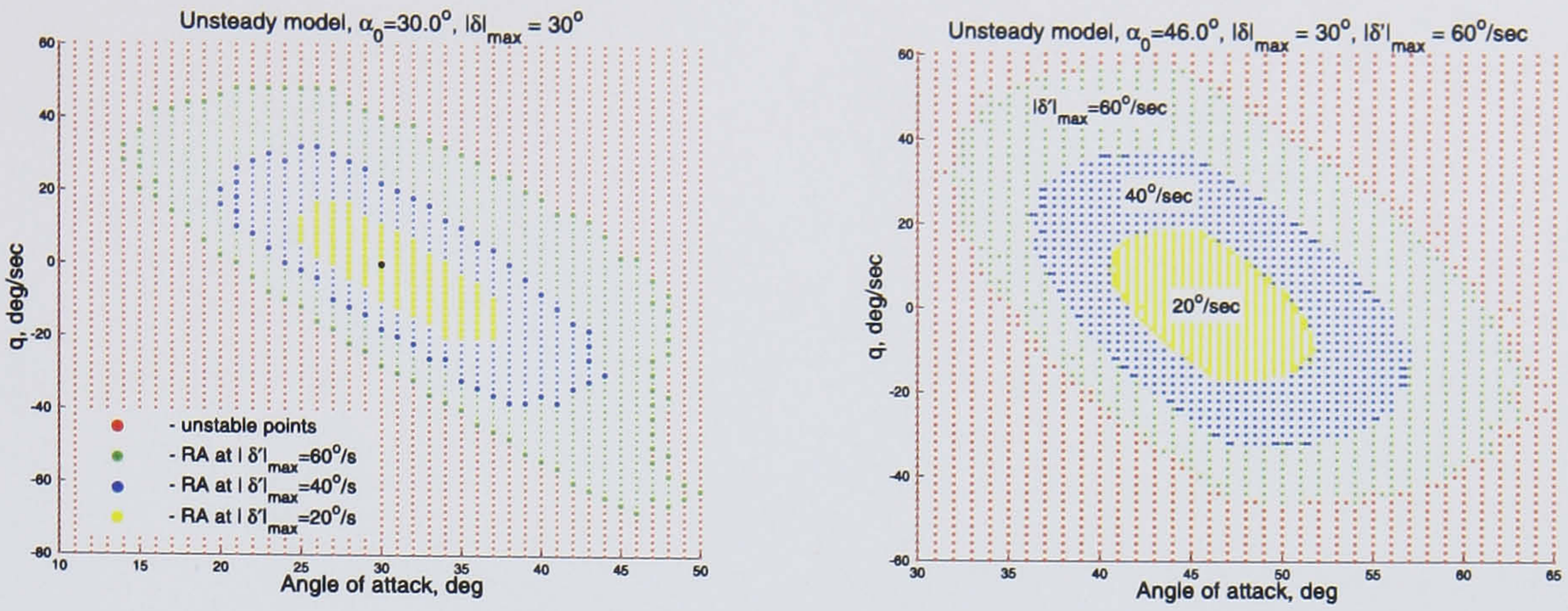

Figure 7.12: Effect of the actuator rate limit: trimmed level flight at $\alpha = 30^o$ and $\alpha = 46^o$ with the unsteady aerodynamic model.

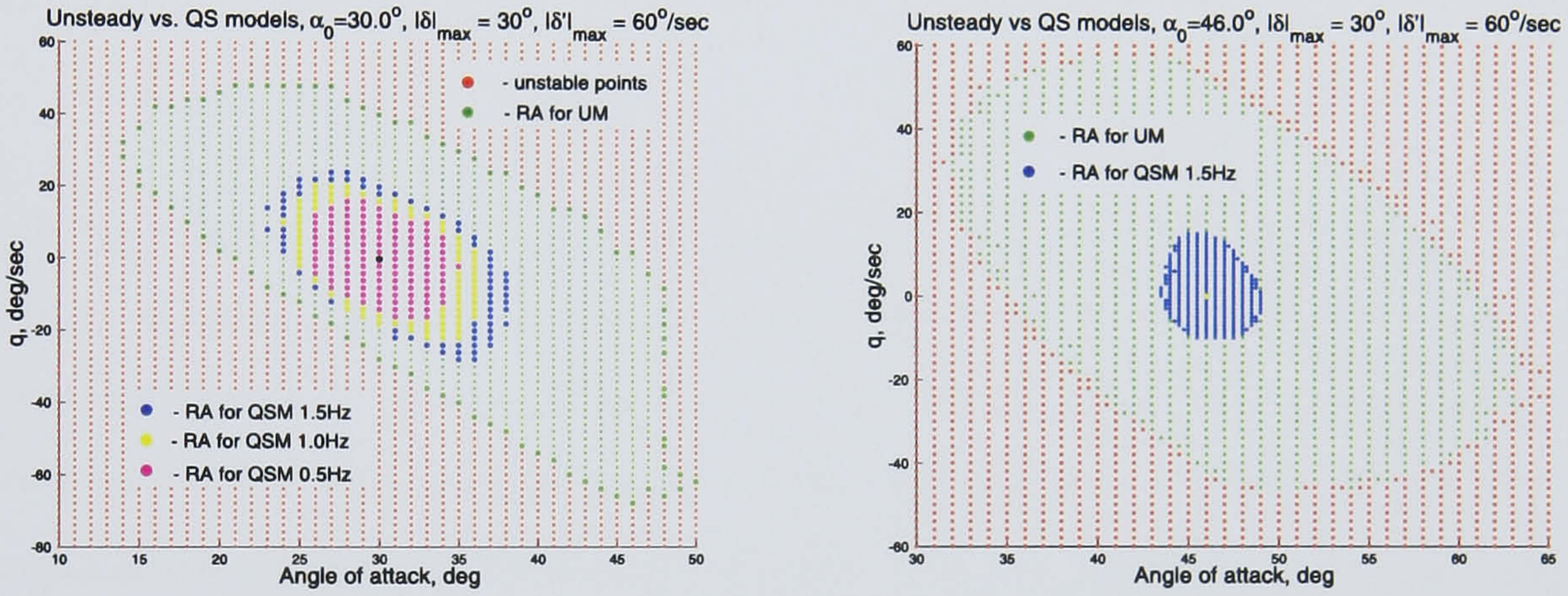

Figure 7.13: Effect of aerodynamic model (unsteady vs quasi-steady): trimmed level flight at $\alpha = 30^o$ and $\alpha = 46^o$ with actuator rate limit $|\dot{\delta}|_{max} = 60^o$.

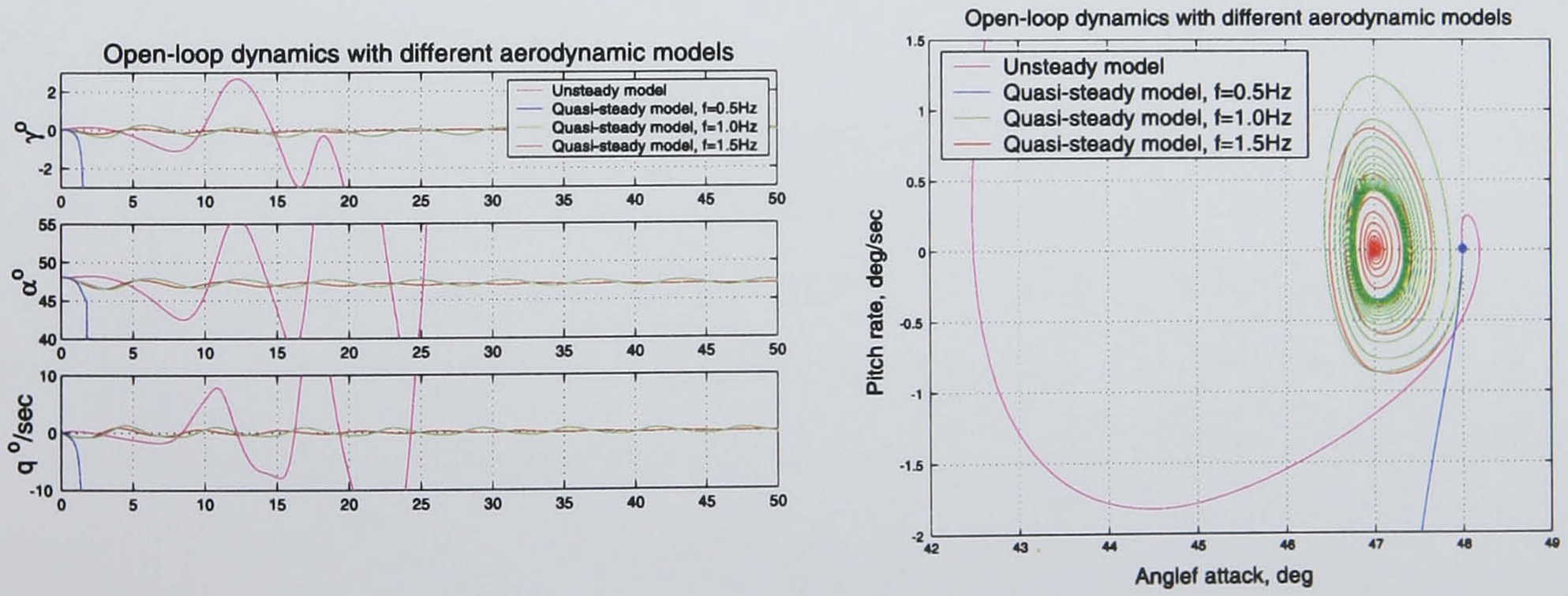

Figure 7.14: Aircraft disturbed motion from trimmed level flight at $\alpha = 48^o$ for different aerodynamic models.

Chapter 8

Aerodynamic model development tools

During the last two decades a significant number of works concerning nonlinear aircraft dynamics has been carried out [43, 75, 47, 73, 40, 38, 66, 67, 68, 65, 63]. These works complement the classical approaches to flight dynamics [22, 16, 93] and demonstrate the importance of nonlinear analysis for flight dynamics purposes but, due to complexity, the techniques are still not widely used in industry. In order to facilitate the nonlinear dynamic systems analysis for flight dynamic purposes the joint DMU-QinetiQ project "Flight Clearance Tools using Nonlinear Bifurcation Analysis Framework" [72] was initiated several years ago. This project resulted in an extensive toolset addressing a wide range of problems and having a user-friendly interface.

Since the aerodynamic model development is an essential part of the aircraft design and analysis process the special module called ADDB (AeroDynamic DataBase) supporting this process has been developed within the framework of the DMU-QinetiQ project. The ADDB program was intensively utilized for managing the experimental and computed aerodynamic data and for the development and identification of the mathematical model for the 65^o delta wing.

The ADDB toolset [10] is aimed to facilitate the development of aircraft aerodynamic models and support of these models during their life cycle and provide easy access to all aerodynamic characteristics from MATLAB. The database containing results of static and

dynamic wind tunnel tests and the results of identification has been developed in the ADDB environment and bounded together with the aircraft equations of motion implemented in MATLAB.

The PIIMTM program [34], developed in TsAGI in the middle of the 1990th, has been used for nonlinear dynamic model identification. It provides an interface and tools for a search for the unknown parameters of a dynamic model at which the best fit to the experimental time records is reached. A dynamic model is coded in the C language using a special library of macros. Then by means of a special preprocessor it is connected to the graphical environment. The conjugate gradient and the coordinate search methods are used for the parameters estimation. The graphic interface provides convenient tools for the optimization process control and assessment.

A detailed description of the software which has been developed during the work and user guides can be found in [10, 9]. This chapter gives a brief review of the original software applied during the aerodynamic models development.

8.1 ADDB - experimental data storage and processing tool

Maintenance of aerodynamic databases and development of aerodynamic models for aircraft flight dynamics and control design applications is an important and very time consuming stage of the aircraft design process. The aerodynamic data is normally obtained from different computational tools, the wind tunnel and flight tests for various aircraft configurations, and different flight conditions. Normally, results of the wind tunnel tests require special corrections to be transformed to real flight conditions. In the end, the aerodynamic database for the whole flight envelope is developed by means of processing and fusion of all computational and experimental data (Fig. 8.1). The aerodynamic characteristics in the aerodynamic database are represented in the form of multidimensional lookup tables, which are incorporated into the aerodynamic model by means of some kind of interpolation. During an aircraft development cycle, the aerodynamic database and aerodynamic model are modified and upgraded taking into account additional wind tunnel and flight test results. This makes maintenance of the aerodynamic database even more complicated (Fig. 8.2).

The ADDB program is designed to provide easy access to all aerodynamic charac-

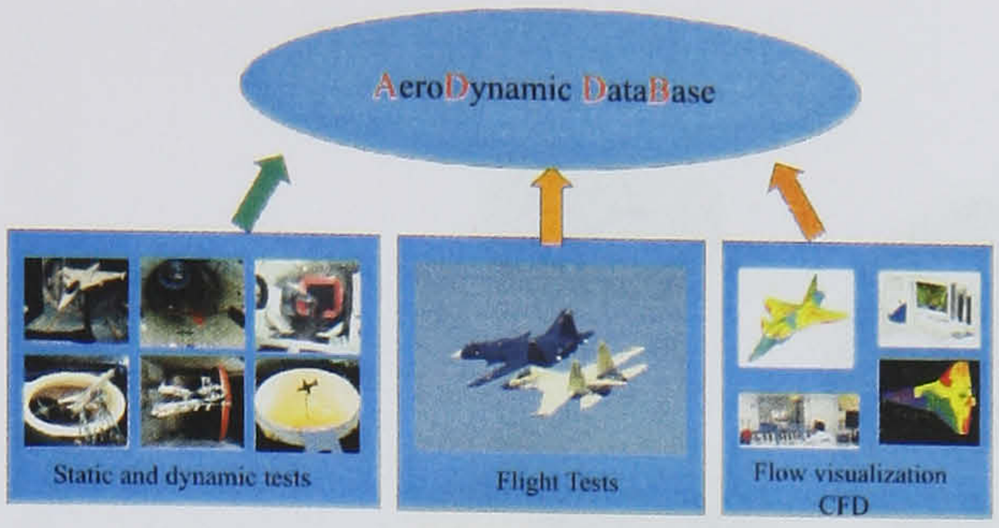

Figure 8.1: Aerodynamic data collection.

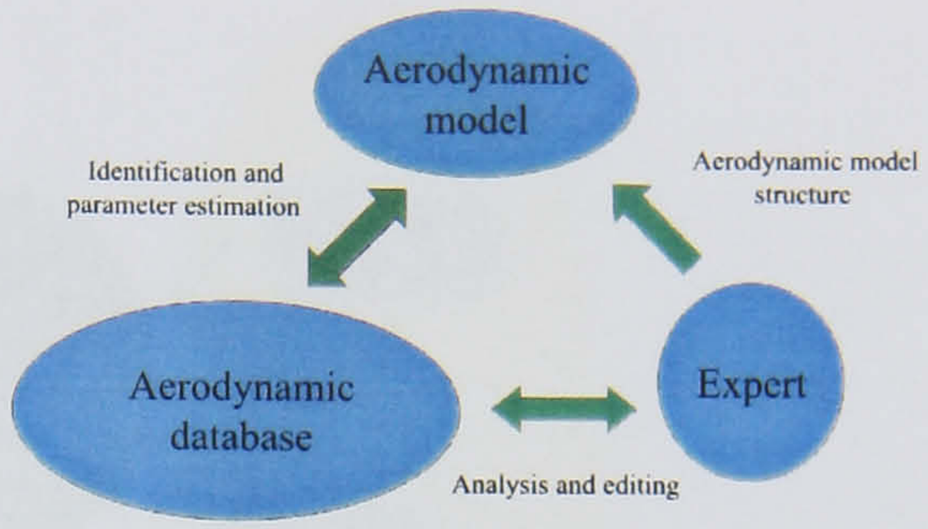

Figure 8.2: Aerodynamic model development.

teristics from different applications and may be considered as a common environment for experimental aerodynamicists, flight tests and control design engineers. The main feature of the ADDB program is that an engineer can operate with basic aerodynamic functions created on the base of lookup data tables as with simple graphical objects. The program provides an environment for the development of aerodynamic models, which are in fact composite functions depending on the aircraft configuration, flight conditions and the basic aerodynamic functions, and tools for generating different outputs for these aerodynamic models.

The ADDB contains tools for:

- managing, viewing, editing, importing and exporting aerodynamic dependencies (normally obtained in wind tunnel tests);
- representation of lookup data tables as continuous functions accessible from MATLAB command line or user's applications;
- developing a model for the total force/moment coefficients (including unsteady aerodynamic models);
- splitting or merging multidimensional arrays, fusing different data sets;
- filtering and differentiation of noisy processes;
- flight-test data conditioning;
- generation of the total aerodynamic model in Fortran, C or as SIMULINK S-function in the KRIT[1]-compatible format;
- automatic report generation.

[1]KRIT – toolbox for analysis of the nonlinear dynamic systems [72]

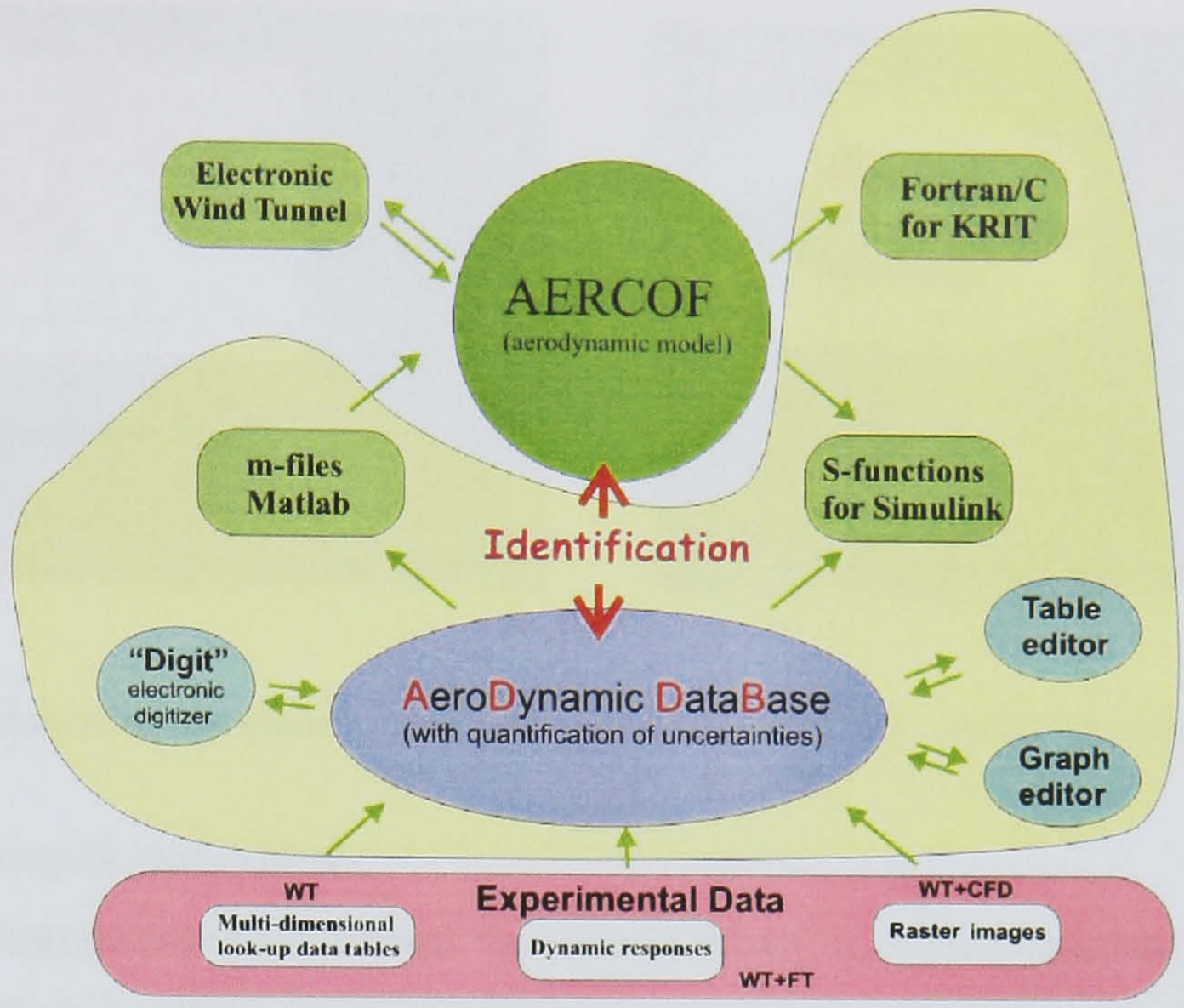

Figure 8.3: ADDB toolkit structure.

The general structure of the ADDB Toolkit is presented in Fig. 8.3.

The ADDB program has been mainly written using the MATLAB language. In addition, the C++ language has been used for the development of some complex interfaces such as the data editor in the form of a lookup data table. The current version of the ADDB program is designed for MATLAB 6.5 (Release 13) but it will also work in MATLAB 5.3 (Release 11) with some restrictions.

8.1.1 Program interface

The ADDB program is activated by calling the `addb` function without parameters. The main program window is shown in Fig. 8.4. The left part of this window shows the figure with a selected function. Control panels are placed in the right and the bottom parts of the window. A database browser contains information about opened databases and its structure. Items marked by `[-]` or `[+]` signs are groups that can be minimized or maximized by a double click of the left mouse button. The popup menu, which is called by the right mouse button and buttons at the bottom of the browser panel are used for

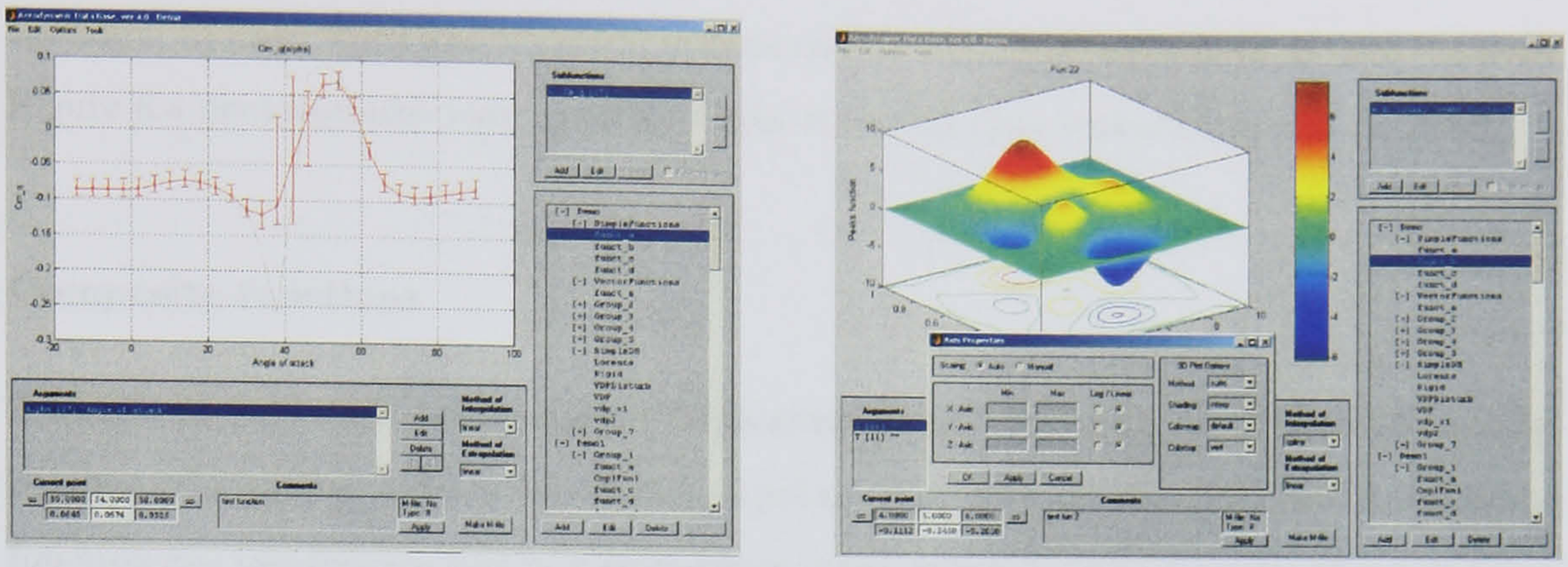

Figure 8.4: Main program window: function depending on one (left) and on two arguments (right).

database managing and control.

A list of arguments of the current function is shown in the bottom panel. It contains names of arguments, their data array length and title. To edit data array of arguments the `Edit` button opens a dialog window. Buttons `Add` and `Delete` add a new argument or delete a selected one. ⇑ and ⇓ arrows change the order of the arguments. This allows the user to plot different cross-sections of multi-argument functions.

Table "Current point" presents values of the arguments in the top row. Function values, corresponding to the current "cross-section" are given in the bottom row. The current point is marked on the figure by a bold black marker. Its coordinates are shown in the central column. ⇒ and ⇐ arrows move the bold marker along the curve.

8.1.2 Database objects

Basic functions

Objects incorporating arguments and function lookup table data sets in the ADDB database are called as Basic Functions. All these functions are organized as stand-alone `M-` and `Mat-` files with the same name and registered in a database. This approach transfers the manner of data processing from the lookup tables to a functional level. A graphical editor implemented in ADDB allows the user to operate with data arrays as with graphical objects avoiding "low-level" tables processing. Data arrays of any dimension are supported but in case of three and more arguments the selected cross-section of function data array corre-

sponding to fixed third and higher argument can be displayed and edited at each moment. Figure 8.4 demonstrates some possible forms of lookup data representation in ADDB.

Composite functions

A term composite function is used in the program for a function created by the user and depending on a number of basic functions and parameters stored in the database. A composite function can incorporate text of a subroutine, input parameters and results of calculations. The subroutine is described as a regular m-function using the MATLAB language. Parameters already defined in a database may be used in a composite function without additional definitions and values stored in a database will be set.

A composite function may be calculated at specified nodes of the arguments and plotted using a defined interpolation method. If `show tolerances` option is on and the tolerances of all basic functions involved in the composite function are correctly defined, the tolerance for the composite function will be calculated using a Monte-Carlo method. The number of iterations for the Monte-Carlo method is defined in a popup menu on the control panel. As an example of a composite function with tolerances, the coefficient of dynamic stability $C_{n_{\beta_{dyn}}} = -C_{n_\beta}(\alpha)\cos\alpha + C_{l_\beta}(\alpha)\frac{J_y}{J_x}\sin\alpha$ is shown in Fig. 8.5. Note, that the basic functions $C_{n_\beta}(\alpha)$ and $C_{l_\beta}(\alpha)$ are stored in a database with their tolerances.

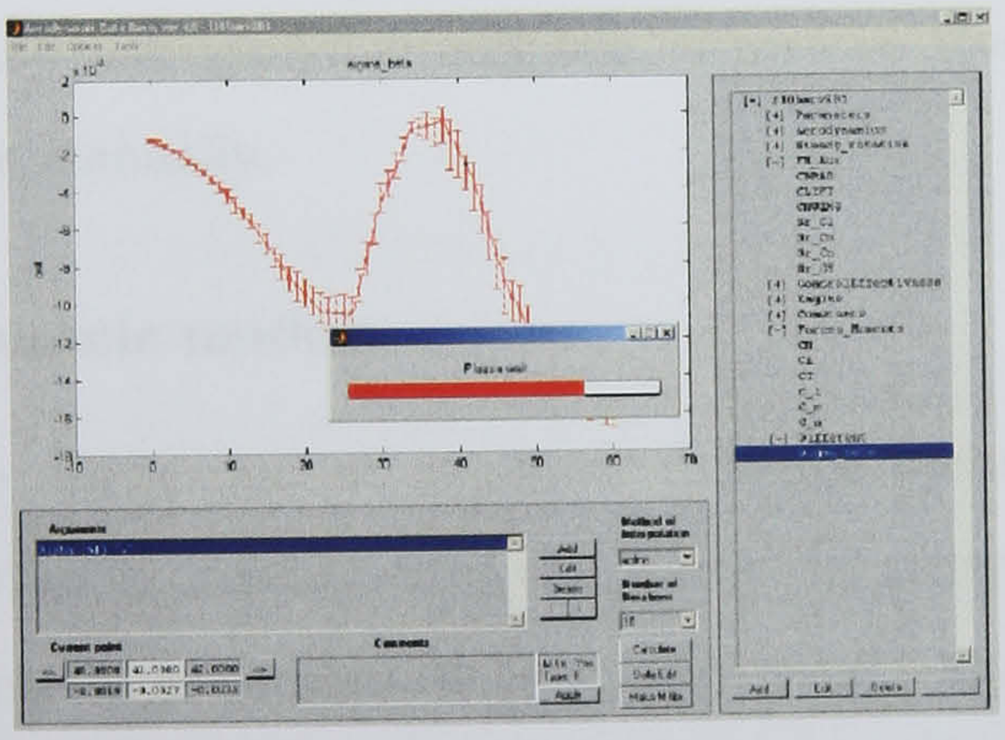

Figure 8.5: Calculation of composite function with tolerances.

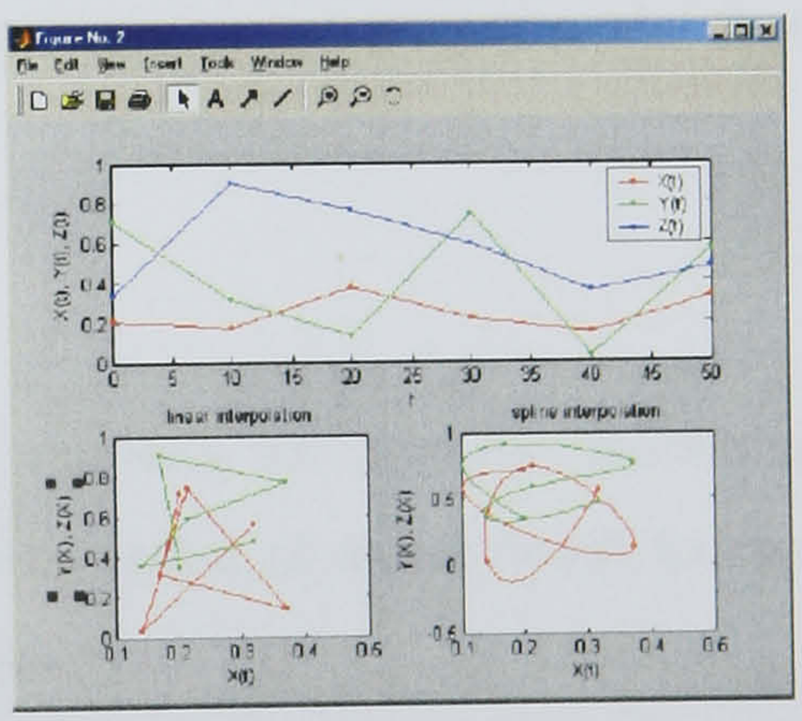

Figure 8.6: Different form of the vector-function $\{X(t),\, Y(t),\, Z(t)\}$ representation.

Vector functions

If a set of different functions of the same dimensions depends on the same arguments it can be saved in ADDB as one record. For example, wind-tunnel test protocols can be represented as vector-functions like $\mathbf{F}(\mathbf{X}) = \{f_1(x_1, \ldots, x_n), \ldots, f_m(x_1, \ldots, x_n)\}$, where aerodynamic loads f_i are considered as components depending on the kinematic parameters x_i. If vector function components are functions of the same one argument, the first subfunction in the list may be considered as an independent argument so that the remaining functions can be represented as dependencies on the first function (so called parametric plot). Different methods of presenting the vector function are given in Fig. 8.6. The upper subplot contains three components depending on time while the lower plots are their representations in a parametric form with linear and spline interpolation, respectively.

Parameters

Every aerodynamic model usually contains a set of aircraft parameters describing geometry, mass, inertia characteristics. To keep these data in the same database, a parameter type was introduced. The name, value, etc of these constants can be changed in corresponding fields of the control panel. If the prepared model is going to be converted in the Fortran and used with KRIT, the index of this parameter in the KRIT PR-Array should be specified in the corresponding edit box, otherwise these indices have to be entered in the Fortran code manually.

Dynamic models

The application of nonlinear dynamic systems for unsteady aerodynamic modelling in ADDB is considered in this thesis. In general case the vector of aerodynamic forces and moments are described by the following nonlinear system:

$$\begin{aligned} \frac{d\mathbf{x}}{dt} &= F(t, \mathbf{x}, \xi), \\ \mathbf{C} &= \mathbf{G}(\mathbf{x}, \dot{\mathbf{x}}, \xi). \end{aligned} \tag{8.1}$$

A large amount of experimental data covering the whole range of possible aircraft maneuvers is used for the identification of unsteady aerodynamic models at high angles of attack. This data are usually distributed in the form of Excel or ASCII tables. Keeping,

processing, selecting, and visualization of such an amount of experimental data is rather time consuming and cumbersome work. For more effective work with the experimental time histories for measured aerodynamic loads, the fast processing and evaluation of dynamic mathematical models, the ADDB program has been extended to support the work with dynamic experimental data and dynamic aerodynamic models of the type (8.1).

Functions **F** and **G** specifying a dynamic system are defined as regular m-functions and registered in corresponding fields of the dynamic system simulation panel. An example of the RHS-function implementing the unsteady aerodynamic model for a normal force coefficient is presented in Appendix C. Initial and final times of integration, the time sampling for output and other parameters are defined in the corresponding fields of the dialog panel, which is called by the `Options` button. In order to eliminate the influence of the initial transient process on the final result it is possible to define the time range `[t1, t2]`, in which data will be plotted. In this case, the output of a function will be a matrix `[y(t1:t2), x(t1:t2)]` instead of `[y(t_init:t_fin), x(t_init:t_fin)]`. If `t1` and `t2` are not specified, the whole time interval is used. The result of the above technique applied to the Lorentz dynamic system and a view of the dynamic system simulation panel are given in Fig. 8.7.

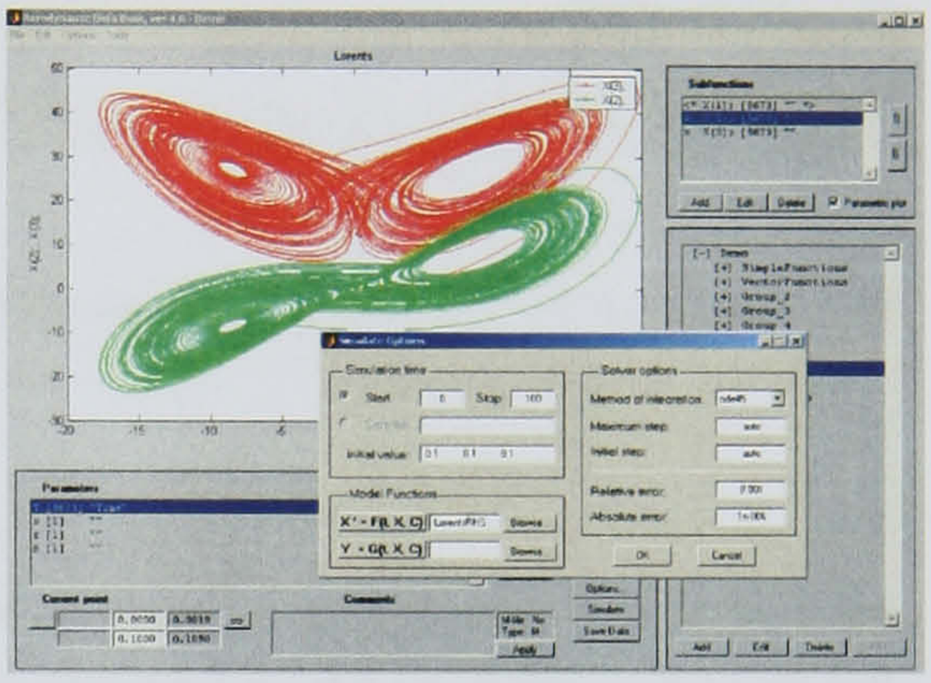

Figure 8.7: Lorentz system simulation results and view of dynamic system simulation panel.

8.1.3 Experimental data processing

The data measured in experiments are usually noisy which embarrasses such data use and analysis (Fig. 8.8). The tool for noisy processes to be filtered and differentiated is also included into ADDB. A view of the filter window is shown in Fig. 8.9. The upper part of the window contains the original (red line) and smoothed (blue line) processes. The process spectrum is plotted in the bottom figure where a cut-off frequency of the low-pass Butterworth filter can be specified using the ruler. The first derivative is calculated using special algorithm, which reduces the influence of noise.

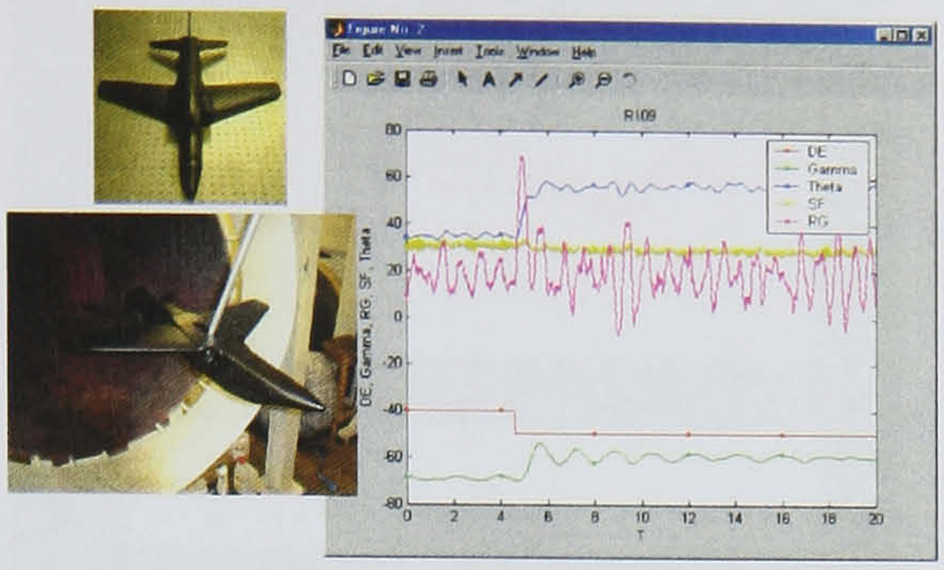

Figure 8.8: Real experimental record [17].

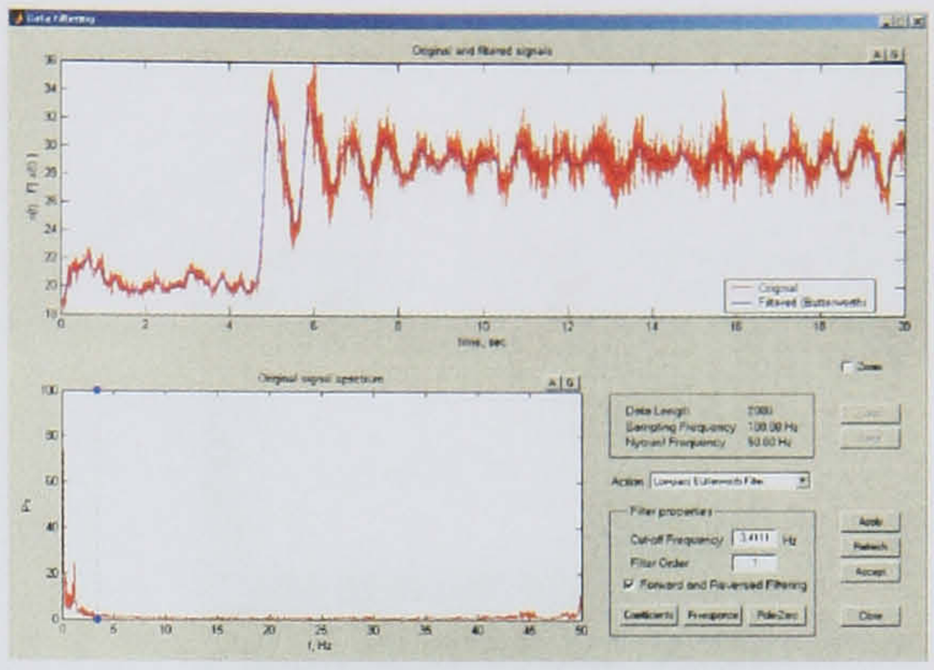

Figure 8.9: Filtering and differentiating tool.

8.1.4 Data fusion tool

A data fusion tool is designed to support the process of merging data obtained from different sources and covering different parts of the argument range. It allows the user to specify priority of certain data over others by introducing variable weights, to generate automatically "mean" values and tolerances, to fill gaps with approximate data, to edit obtained values by the mouse. The main window of the data fusion tool is shown in Fig. 8.10. It contains two plots. The top one shows the fused functions and the result of fusion. The bottom one shows the weight functions applied for fusion. All data sent from ADDB for fusion are shown together with their tolerances on the upper plot. The original data is "frozen" and cannot be modified. Only the merged function can be edited by the mouse. The solid magenta line with black dots is a mean value function calculated automatically using default weights. Dashed magenta lines represent "up" and "down" tolerances. The mean-value line and tolerances may be edited by means of the mouse in ADDB manner. The bottom plot contains the weight functions for each curve presented on the top plot with the identical colours. The weight functions may be also edited by means of the mouse in ADDB style.

8.1.5 Electronic digitizer - DIGIT

Digitizing of graphical data from different papers, reports, etc, is often an important source of information for developing aerodynamic databases. In the absence of a digitizer, this

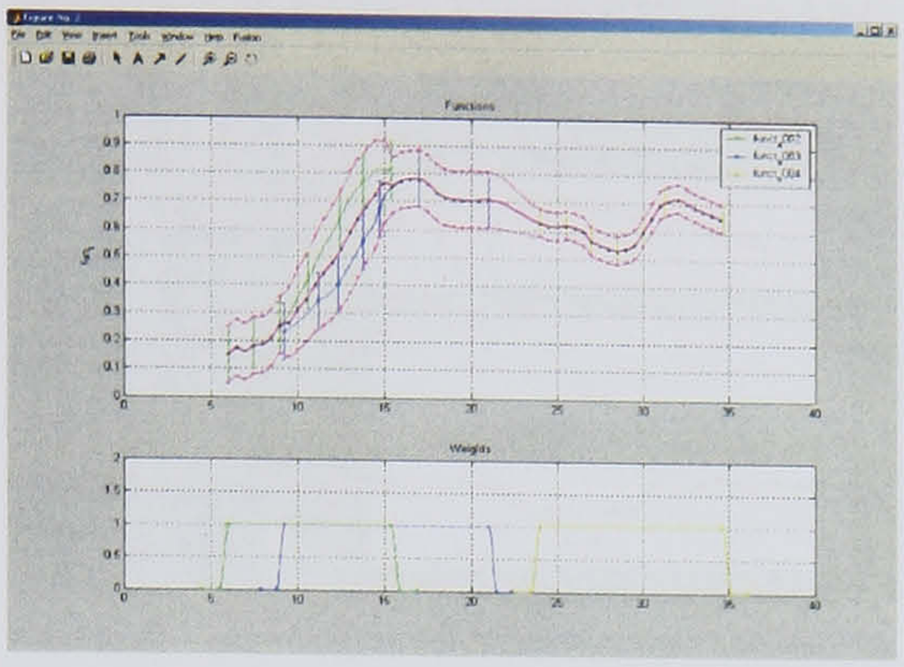

Figure 8.10: Data fusion tool.

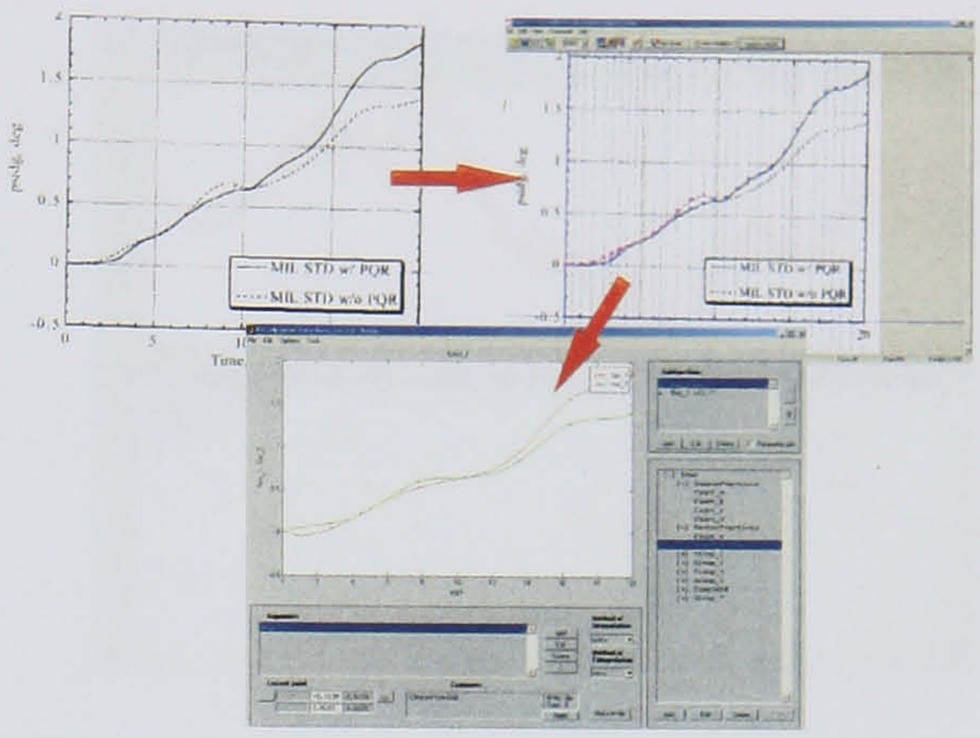

Figure 8.11: DIGIT main window.

simple program allows the user to digitize data electronically having just a scanner or downloaded image. To connect mathematical coordinates with physical points on a screen the user has to input three reference points and specify mathematical coordinates for them (the axis frame need not necessarily be orthogonal). To do this, three points must be indicated by mouse pointer. Further data are pointed by the mouse similar to a digitizer.

One can input only one curve or a family of curves. To increase accuracy a zoom tool is used. All results may be saved into a file or the ADDB database. This program has a user-friendly interface and some other functions that are very useful for work. View of the main window is given in Fig. 8.11.

8.1.6 Flight-test data processing

Correlating and correcting the data measured by onboard sensors during flight tests is a vital step in the methodology of the identification of aircraft aerodynamic parameters. The aircraft state variables recorded during flight tests differ from the genuine ones due to the random and systematic errors and noise. The magnitudes of the errors and noise intensity depend on a large number of factors. For example, atmospheric turbulence, sensor dynamics, biases in the instrumentation system, analogue to digital signal conversion and many other factors may cause noise and errors. The ADDB provides tools implementing some engineering approaches for the data compatibility check, conditioning, correlation and model regression.

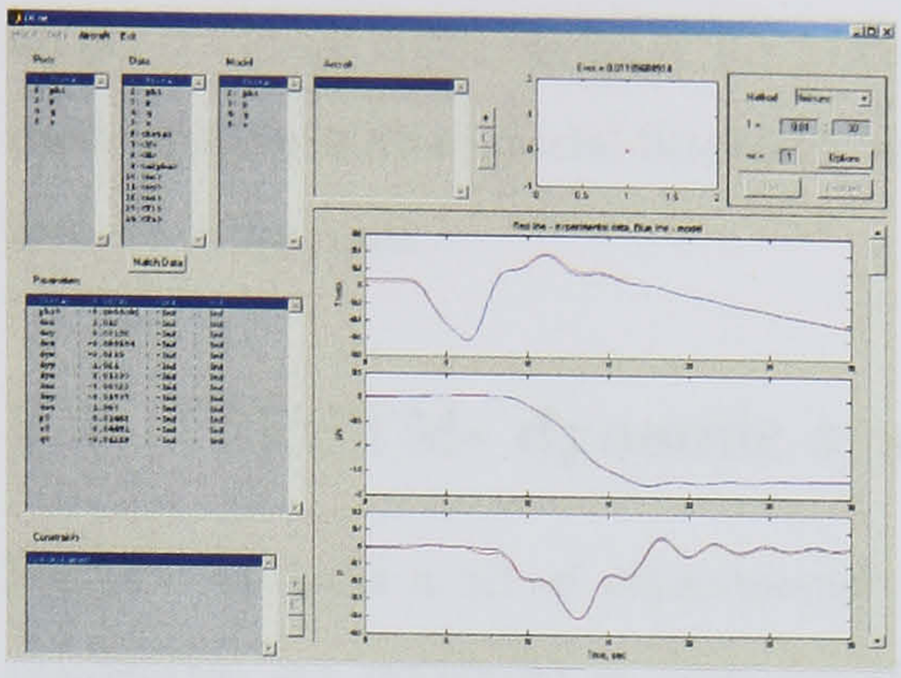

Figure 8.12: Data correlation program DCOR

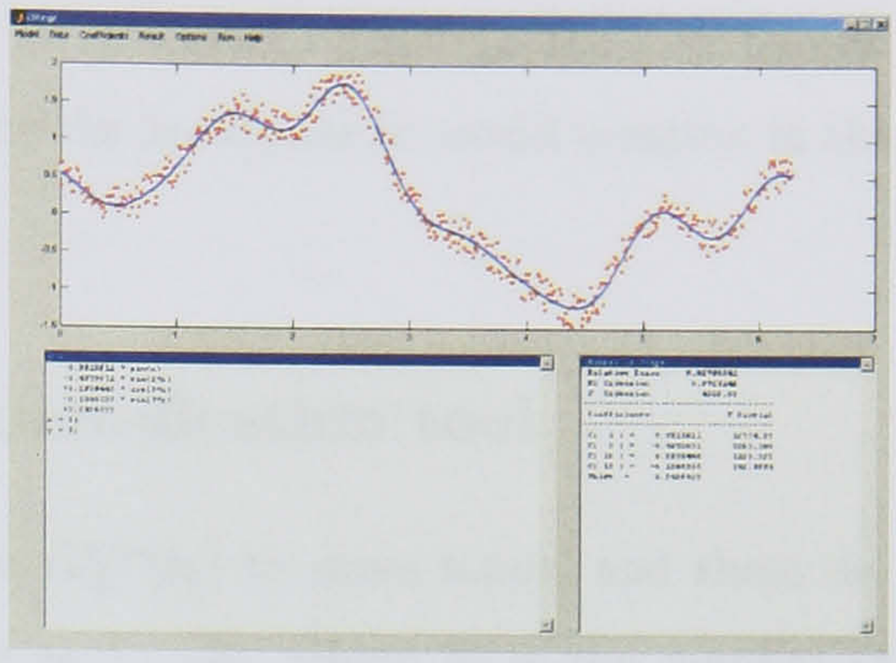

Figure 8.13: Model regression program DREGR

8.1.7 Linear regression tool

The linear regression, due to its simplicity and computational efficiency, is the most widely used technique for conventional aerodynamic model development. Linear regression analysis methods are used for assessing the structure of the mathematical model and the values of corresponding parameters. A detailed description of this technique can be found in [19]. A summary of the algorithms realized in DREGR is given in Appendix E.

The DREGR program [9] employs a linear regression technique to estimate a functional relationship of a dependent variable (process) to one or more independent variables (regressors). The structure of the mathematical model is selected interactively. Polynomials or splines are used for the approximation of aerodynamic coefficients. A user friendly interface facilitates the analysis and allow its efficiency to be enhanced.

8.1.8 Automatic generation of an aerodynamic model

After the aerodynamic database and functions for the total forces and moments have been verified it is reasonable to prepare the mex-file for further computations. The `mex`-files are more time efficient when the source code is written in Fortran or C. The KRIT-compatible Fortran or C aerodynamic module can be generated automatically on the basis of the developed database. Structure of the resulting `aercof` module is specified in `ini` file where inputs, outputs, predefined constants and the correspondence of PR elements to variables and some other parameters are described. As a result, the module containing the aerody-

namic database and a wrapper for MATLAB will be generated. This module may be also used together with a special SIMULINK wrapper for the aerodynamic model creation in the form of S-function.

8.2 PIIMTM- dynamic system identification tool

Suppose we have a set of experimental responses $G_m^{exp}(t_k)$ to some input, and these dependencies are measured in time samples t_k, $k = 1 \dots K$, where K is the number of sampling points and m is the number of response. Suppose further, these responses are described by the following mathematical model: $\dot{\mathbf{x}} = \mathbf{F}(\mathbf{x}, \mathbf{u}, \mathbf{p})$, $\mathbf{G}^{mod} = \mathbf{G}(\mathbf{x}, \mathbf{u}, \mathbf{p})$, where $\mathbf{x} \in \Re^n$ – state vector, $\mathbf{u} \in \Re^s$ – input vector, $\mathbf{p} \in \Re^q$ – vector of parameters which components satisfy the inequalities $p_{i\,min} \leq p_i \leq p_{i\,max}$, where $i \in [1, q]$. Let $\epsilon_m(\mathbf{p}) = \sum_{k=1}^{K} (G^{mod}(\mathbf{x}(t_k), \mathbf{u}_m, \mathbf{p}) - G_m^{exp}(t_k))^2$ be the error function between a simulated and experimental process. Similar to the linear regression technique (see appendix E) it is required to find a vector of parameters $\mathbf{p}$ minimizing this error function.

If a number M of experimental records which are used for the model parameters identification is more then one the following cost function is minimized:

$$\epsilon(\mathbf{p}) = \sum_{m=1}^{M} \sum_{k=1}^{K} (G^{mod}(t_{k,m}, \mathbf{u}_m, \mathbf{p}) - G_m^{exp}(t_{k,m}))^2. \tag{8.2}$$

To minimize the total cost function (8.2), direct methods such as gradient or descent are used. This approach to the identification of the dynamic systems was implemented in the very flexible and effective program PIIMTM, whose screen shot is shown in Fig. 8.14.

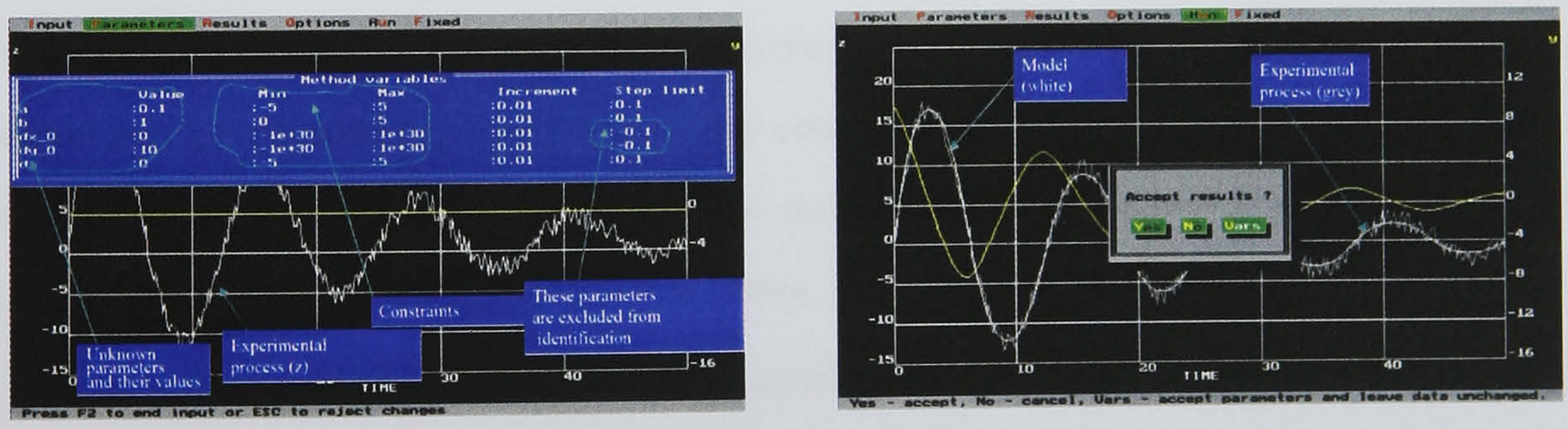

Figure 8.14: Screen shots of the dynamic system identification program PIIMTM. Identification of oscillator $\ddot{x} + 2\xi\dot{x} + \omega^2 x = 0$ parameters from the experimental response.

Chapter 9

Conclusions and suggestions for future research

9.1 Summary

This thesis presents an original technique for modelling of unsteady aerodynamic loads acting on aircraft at high incidence in the presence of vortex breakdown and flow separation. Unsteady aerodynamic characteristics are considered as a combination of two components which describe the contribution of different flow structures to the total load. The first component which would arise in the case of unburst vortical or attached flow is supposed to be inertialess. The second component represents a decrement in aerodynamic loads due to the vortex breakdown or flow separation. It is assumed that all dynamic properties of the aerodynamic characteristics are amassed in this component. To describe its dynamics specially formed nonlinear differential equations are used. Depending on the parameters of these equations either weak or strong nonlinearities (i.e. static hysteresis) can be reproduced.

The proposed model structure has an empirical nature and contains several parameters, which are identified using a large number of experimental responses to kinematic parameters variation obtained in the static and dynamic wind tunnel tests. A regular technique for the mathematical model parameters identification has been proposed both for the case of unique and non-unique (static hysteresis) static dependencies of the aerodynamic loads.

The mathematical models of the longitudinal and lateral directional aerodynamic char-

acteristics of the 65^o an 70^o delta wings have been identified using the proposed approach for the case of weak nonlinearities. The bifurcational model of the normal force coefficient for the high aspect ratio wing has been identified using the proposed approach for the case of strong nonlinearities (static hysteresis). It has been demonstrated that the developed techniques are able to reproduce aerodynamic loads taking into account bifurcational changes of the flow structure. The validation of the identified models demonstrated a very good agreement with the experimental results over a wide range of the kinematic parameters variation. It has been also shown that the proposed modelling technique can be reduced to the conventional one at low incidences i.e. the proposed approach embraces the conventional aerodynamic derivatives model under these conditions.

A coupling between aircraft dynamics and unsteady aerodynamics effects has been analyzed considering the longitudinal motion of a hypothetical aircraft with thrust vectoring control performing high incidence flight. The two different approaches to unsteady aerodynamic modelling have been considered and their impact on aircraft dynamics and control law design has been distinguished. The representation based on the aerodynamic derivative concept in the presence of a strong dependence of aerodynamic derivatives on frequency of oscillations produces a high level of uncertainty in the open- and closed-loop system eigenvalues. Therefore, this representation cannot be adequate for dynamics simulation and control law design in the time domain. The unsteady aerodynamic model approximating internal flow dynamics and represented in the form of nonlinear differential equations allows the aerodynamic responses with small and large amplitude of oscillations to be fitted accurately and naturally extrapolates these aerodynamic responses to real flight conditions. This mathematical model adequately simulates the local stability characteristics as well as the large amplitude motion dynamics and is more appropriate for the design of control laws at high incidence.

9.2 Suggestions for future research

During the research work a number of problems still remained unsolved and can be investigated in future:

- The effect of unsteady aerodynamics on the lateral-directional motion. The dynamic

properties of the lateral-directional motion at a high incidence flight can be compared when two different models are applied i.e. the conventional aerodynamic derivatives model and the unsteady aerodynamic model. One can expect that the proposed unsteady aerodynamic model will give more adequate prediction of the lateral-directional stability. The available lateral-directional departure prediction criteria can be revised with account of this unsteady aerodynamic model. The developed unsteady aerodynamic model can be also used to simulate and analyze the "Wing Rock" type motion providing an adequate basis for the active suppression of this effect.

- All mathematical models presented in this work are so called planar models, i.e. they were designed to reproduce aerodynamic responses to a separate single degree of freedom motion such as the pitch, yaw or roll. To simulate aerodynamic loads during an arbitrary spatial motion, a more complicated mathematical model is required. Such a non-planar model can be based on a multidimensional dynamic system with a set of eigenmodes excited by different types of motion. The development of such a kind of aerodynamic model could be a sequel of this work.

- Normally, due to wind tunnel walls and the presence of model support rigs, interference effects arise in the wind tunnel investigations. At high angles of attack the vortex breakdown processes are highly sensitive to minor disturbances. As a result, interaction of the vortices with the support sting or the rig struts can lead to significant variations of the aerodynamic loads. For more accurate modelling of the aerodynamic loads, the level of such interference has to be estimated and, if it is significant, taken into account. Analysis of the experimental results obtained using different rigs and aircraft models can help to eliminate the interference problem.

- The interference problem is also connected with the development of the mathematical model of aerodynamic loads for aircraft model control surfaces. Due to the strong sensitivity of the aerodynamic loads at high angles of attack to small disturbances even a small deflection of a trailing edge control surface can result in significant changes in the flow structure and, consequently, in significant changes in the aerodynamic loads. To develop an adequate unsteady aerodynamic model taking into account control surface deflections, special experimental tests have to be carried out to provide a

comprehensive set of data.

- The development of the unsteady aerodynamic model for an arbitrary non-planar motion will require experimental data obtained during multiple degree of freedom motion. For this purpose the development of multi-degree of freedom dynamic test rigs, like the pendulum suspension rig, with remotely controlled aircraft models seems to be promising.

- Mathematical models of the unsteady aerodynamic loads normally depend on a large number of parameters. In this thesis a least-squares based method was used to determine the model parameters providing the best fit to the experimental data. The non-planar mathematical model will likely contain more parameters, and a more extensive set of experimental data will be necessary for its identification. Therefore, advanced methods could be demanded for the efficient identification of such mathematical models, and further research can be focused on the development of an appropriate identification technique.

References

[1] Rotary-balance testing for aircraft dynamics. Technical report, 1990. AGARD Advisory Report No.265.

[2] Cooperative programme on dynamic wind tunnel experiments for manoeuvring aircraft. Technical report, AGARD Avisory Report 305 (Fluid Dynamics Panel Working Group 16), NATO, 1996.

[3] Abrupt wing stall - part 1. *Journal of Aircraft*, 41(3), May-June 2004.

[4] N. Abramov. Bifurcation model of aerodynamic hysteresis. *Proceedings of Moscow Institute of Physics and Technology*, 1997. (in Russian).

[5] N. Abramov. Application of nonlinear indicial response method for unsteady aerodynamics modeling at high angles of attack. In *Proceedings of Actual Problems of Aerospace Science Conference*, Zhukovsky, Russia, 26-28 May 1999. (in Russian).

[6] N. Abramov. Mathematical modelling of unsteady normal force and rolling moment coefficients for pitch and yaw motion by means of nonlinear dynamic equations. Technical report, Zhukovsky, Russia, 1999. TsAGI Technical Report 4223.

[7] N. Abramov, M. Goman, D. Greenwell, and A. Khrabrov. Two-step linear regression method for identification of high incidence unsteady aerodynamic model. In *AIAA Atmospheric Flight Mechanics Conference*, 6-9 Aug 2001.

[8] N. Abramov, M. Goman, A. Khrabrov, and K. Kolinko. Simple wings unsteady aerodynamics at high angles of attack: Experimental and modeling results. In *AIAA Atmospheric Flight Mechanics Conference*, August 9-11 1999. Portland, OR.

[9] N. Abramov, M. Goman, and A. Khramtsovsky. Aerodynamic database and programs of interactive identification: Userguide and algorithms. Technical report, De Montfort University, Leicester, UK, May 2003. Research Contract "Research on Non-Linear Bifurcation Analysis Tools", Future System Technology Division, QinetiQ Ltd, Farnborough.

[10] N. Abramov, M. Goman, and M. Sidoruck. Development of new functionality in addb software. Technical report, De Montfort University, Leicester, UK, Sept 2004. Research Contract "Flight Clearance Simulation Software Development", Future Systems Technology Division, QinetiQ Ltd, Farnborough".

[11] G.A. Addington and R.C. Nelson. The correspondence between flow-field structure and critical states on a 65-degree delta wing. Boston MA, August 1998. AIAA Atmosperic Flight Mechanics Conference. Paper AIAA-98-4520.

[12] G.A. Addington and R.C. Nelson. The correspondence between flow-field structure and critical states on a 65-degree delta wing. 1998. Paper AIAA-98-4520.

[13] S.M. Belotserkovsky, B.K. Skripach, and V.G. Tabachnikov. *Wing in unsteady flow.* Nauka, Moscow, 1971. (in Russian).

[14] R.L. Bisplinghoff, H. Ashley, and R.L. Halfman. *Aeroelaelasticity.* Addison-Wesley, Cambridge, MA, 1955.

[15] Lan E. Chin, S. Fourier functional analysis for unsteady aerodynamic modeling. *AIAA Journal*, 30(9), September 1992.

[16] M.V. Cook. *Flight Dynamics Principles.* Arnold, London, 1997.

[17] P. Davison, M. Lowenberg, and M. di Bernardo. Modelling non-linear behaviour in a single degree-of-freedom dynamic wind tunnel rig. In *AIAA Atmospheric Flight Mechanics Conference and Exhibit*, Austin, Texas, Aug. 11-14 2003.

[18] K.M. Dorsett, S.P. Fears, and H.P. Houlden. Innovative control effectors (ice), phase ii. Technical Report WL-TR-97-3059, August 1997.

[19] N. Draper and H. Smith. *Applied Regression Analysis.* Wiley, Chichester, GB, 1981.

[20] Yu.B. Dubov, V.L. Sukhanov, and A.Z. Tarasov. Mastering of a high angles of attack flight. *Polet*, 1998. (in Russian).

[21] L.E. Ericsson. Time history effects on a rolling 65 deg delta-wing-body configuration. In *AIAA Atmospheric Flight Mechanics Conference*, New Orleans, LA, August 1997. Paper 97-3645.

[22] B. Etkin. *Dynamics of atmospheric flight.* John Wiley & Sons, Inc., N.Y., 1972.

[23] Y. Fan and F.H. Lutze. Identification of an unsteady aerodynamic model at high angles of attack. In *AIAA Atmospheric Flight Mechanics Conference*, 1996. AIAA-96-3407-CP.

[24] Y. Fan and F.H. Lutze. Unsteady aerodynamic characteristics of an aircraft in harmonic pitch oscillations. In *AIAA Atmospheric Flight Mechanics Conference*, Boston, MA, August 1998. Paper AIAA-98-4457.

[25] Y. Fan and F.H. Lutze. Multiaxis unsteady aerodynamic characteristics of an aircraft. In *AIAA Atmospheric Flight Mechanics Conference*, Portland, OR, August 9-11 1999. Paper 99-4011.

[26] R. Fletcher. *Generalized Inverses for Nonlinear Equations and Optimization in: Numerical Methods for Nonlinear Algebraic Equations.* Gordon and Breach science publ., London - New York - Paris, 1970.

[27] Y.C. Fung. *An Introduction to the Theory of Aeroelasticity.* Dover, New York, 1969.

[28] M. Goman. Mathematical description of aerodynamic forces and moments at nonunique flow structure regimes. *TsAGI proceedings*, (2195), 1983.

[29] M. Goman and N. Abramov. Assessment of mathematical model for unsteady aerodynamics of 70 degree delta wing. Technical report, De Montfort University, Leicester, UK, March 2000.

[30] M. Goman and M. Demenkov. Computation of controllability regions for unstable aircraft dynamics. *Journal of Guidance, Control, and Dynamics*, 27(4), July-August 2004.

[31] M. Goman and A. Khrabrov. State-space representation of aerodynamic characteristics of an aircraft at high angles of attack. *Journal of Aircraft*, 31(5):1109–1115, Sept.-Oct. 1994.

[32] M. Goman, A. Khrabrov, and S. Usoltsev. Identification of unsteady aerodynamic model of delta wing at high angles of attack. In *10 th IFAC Symposium on System Identification, SYSID'94*, pages 3.073–3.078.

[33] M. Goman, A. Khrabrov, and S. Usoltsev. Identification of unsteady aerodynamic model for large amplitude maneuvers and its parameter identification. In *11 th IFAC Symposium on System Identification, SYSID'97*, 1997.

[34] M. Goman, A. Khramtsovsky, S. Usoltsev, Yu. Vinogradov, and S. Tyrtyshnikov. Pii scientific package. Technical report, TsAGI Report, Zhukovsky, Russia, 1994. (in Russian).

[35] M. Goman, A. Khramtsovsky, and G. Zagainov. Application of bifurcation methods to flight dynamics problems. *Progress of Aerospace Sciences*, 33:539–586, 1997. Elsevier Science Ltd.

[36] M. Goman, K. Kolinko, A. Khrabrov, and S. Usoltsev. Investigation of dynamics and unsteady aerodynamic characteristics of movable aircraft model on pendulum support in wind tunnel. In *Proceedings of the international conference "Fundamental Research in Aerospace Science*, Zhukhovsky, Russia, 1992. (in Russian).

[37] M.G. Goman, D.I. Greenwell, and A.N. Khrabrov. The characteristic time constant approach for mathematical modelling of high angle of attack aerodynamics. In *ICAS Congress*, Great Britain, September 2000.

[38] M.G. Goman and A.V. Khramtsovsky. Application of continuation and bifurcation methods to the design of control systems. *Phil. Trans. R. Soc. Lond.*, 356:2277–2295, 1998.

[39] M.G. Goman, G.I. Stolyarov, S.L. Tyrtyshnikov, S.P. Usoltsev, and A.N. Khrabrov. Mathematical description of aircraft longitudinal aerodynamic characteriastics at high

angles of attack accounting for dynamic effects of separated flow. Zhukovsky, Russia, 1990. TsAGI Preprint No.9, (in Russian).

[40] M.G. Goman, G.I. Zagainov, and A.V.Khramtsovsky. Application of bifurcation methods to nonlinear flight dynamics problems. *Prog. Aerospace Sci., Elsevier Science Ltd.*, 33:539–586, 1997.

[41] D. Greenwell. A review of unsteady aerodynamic modelling for flight dynamics of manoeuvrable aircraft. In *AIAA Atmospheric Flight Mechanics Conference and Exibit*, 16-19 August 2004.

[42] D.I. Greenwell. Difficulties in the application of stability derivatives to the manoeuvring aerodynamics of combat aircraft. In *21th ICAS Congress*, Melbourne, Australia, 13-18 September 1998.

[43] Ph. Guicheteau. Bifurcation theory in flight dynamics. an application to a real combat aircraft. In *ICAS*, 1990. Paper 116 (90-5.10.4).

[44] Alexander H. Hsia and Jerry E. Jenkins. Simplified nonlinear indicial response models of 65 degree delta wing. In *AIAA Atmospheric Flight Mechanics Conference*, Scottsdale, AZ, August 1-3 1994.

[45] C. Hu, E. Lan, and J. Brandon. Unsteady aerodynamic models for maneuvering aircraft. *AIAA Journal*, August 1993.

[46] Kenneth W. Iliff and Kon-Sheng Charles Wang. Extraction of lateral-directional stability and control derivatives for the basic f-18 aircraft at high angles of attack. Technical report, 1997. NASA-TM-4786.

[47] C.C. Jahnke and F.E.C. Culick. Application of bifurcation theory to high-angle-of-attack dynamics of the f-14 aircraft. *Journal of Aircraft*, 31:26–34, 1994.

[48] Jerry E. Jenkins. Simplification of nonlinear indicial response models: Assessment for the two-dimensional aerofoil case. *Journal of Aircraft*, 28(2), February 1991.

[49] E.A. Karavaev, Y.A. Prudnikov, and E.A. Chasovnikov. Appearance of static hysteresis of aerodynamic characteristics of high aspect ratio wing. *Scientific notes of TsAGI*, XVII(6), 1986.

[50] J. Katz. Wing/vortex interaction and wing rock. *Progress in Aerospace Sciences*, 35:727–750, 1999. Elsevier Science Ltd.

[51] A. Khrabrov, K. Kolinko, O. Miatov, and A. Zhuk. Investigation of unsteady aerodynamic characteristics during dynamic achivement of very high angles of attack and wing rock motion for the series of delta wings. Technical report, TsAGI, Zhukovsky, Russia, 2000. Final report on DERA/TsAGI Contract CU004-0000001608.

[52] A. Khrabrov, K. Kolinko, O. Miatov, and A. Zhuk. Investigations of a series delta wings unsteady aerodynamic derivatives during small amplitude forced oscillations. Technical report, TsAGI, Zhukovsky, Russia, 2000. Second progress report on DERA/TsAGI Contract CU004-0000001608.

[53] A. Khrabrov, K. Kolinko, O. Miatov, and A. Zhuk. Large amplitude pitch and yaw forced oscillations results for the series of delta wings. Technical report, TsAGI, Zhukovsky, Russia, 2000. Third progress report on DERA/TsAGI Contract CU004-0000001608.

[54] A. Khrabrov, Yu. Vinogradov, and N. Abramov. Mathematical modelling of aircraft unsteady aerodynamics at high incidence with account of wing-tail interaction. In *AIAA Atmospheric Flight Mechanics Conference and Exhibit*, Providence, Rhode Island, 19 August 2004 2004. AIAA 2004-5278.

[55] A.N. Khrabrov, K.A. Kolinko, O.L. Miatov, Yu. A. Vinogradov, and A.N. Zhuk. Unsteady aerodynamic investigations of small 70 degree delta wing and comparisons with previous experimental results. Technical report, TsAGI, Zhukovsky, Russia, 1999. Third Progress Report on DERA/TsAGI Contract No. MSS/4C3430.

[56] A.N. Khrabrov, K.A. Kolinko, O.L. Miatov, Yu.A. Vinogradov, and A.N. Zhuk. Delta wing unsteady aerodynamic characteristic at high angles of attack during small and

large amplitude forced oscillations. Technical report, TsAGI, Zhukovsky, Russia, 1998. First Progress Report on DERA/TsAGI Contract No. MSS/4C3430.

[57] V. Klein. Modeling of longitudinal unsteady aerodynamics of a wing-tail combination. Technical report, September 1999. NASA/CR-1999-209547.

[58] V. Klein and P.C. Murphy. Estimation of aircraft unsteady parameters from wind tunnel data. Technical report, NASA TM 1998-208969, December 1998.

[59] V. Klein and K.D. Noderer. Modeling of aircraft unsteady aerodynamic characteristics. Technical report, 1994. Part 1 - Postulated Models, NASA TM 109120, May 1994;
Part 2 - Parameters Estimated From Wind Tunnel Data, NASA TM 110161, April 1995;
Part 3 - Parameters Estimated From Flight Data, NASA TM 110259, May 1996.

[60] I.V. Kolin, V.L. Sukhanov, T.I. Trifonova, and D.V. Shukhovtsov. Existence and stability of the inner boundaries of the domain of multiple hysteresis of static aerodynamic forces and moments. *Fluid Dynamics, MAIK Nauka Interperiodica, Kluwer Academic Publishers*, 37(2):346–352, 2004.

[61] H. Kyle, M. Lowenberg, and D. Greenwell. Comparative evaluation of unsteady aerodynamic modelling approaches. In *AIAA Atmospheric Flight Mechanics Conference and Exibit*, 16-19 August 2004.

[62] D.J. Lesieutre, P.H. Reithenthel, and M.F.E. Dillenius. Unsteady simulation of flexible missiles flying low over the sea. *AIAA*, 1994. No. 94-0720.

[63] D. Littleboy and Y. Patel. High angle of attack control law design and analysis using bifurcation analysis. In *AIAA Guidance, Navigation and Control Conference*, Portland, US, 1998.

[64] M. Lowenberg and H. Kyle. Development of a pendulum support rig dynamic wind tunnel apparatus. In *AIAA Atmospheric Flight Mechanics Conference and Exhibit*, Monterey, California, Aug. 5-8 2002.

[65] M. Lowenberg and Y. Patel. The use of bifurcation diagrams in piloted test procedures. *The Aeronautical Journal*, pages 225–235, May 2000. Paper no 2339.

[66] M.H. Lowenberg. Bifurcation analysis as a tool for post-departure stability enchancement. In *AIAA Atmospheric Flight Mechanics Conf.*, pages 506–515, San Diego, CA, USA, 1995. Paper no. AIAA-95-3489-CP.

[67] M.H. Lowenberg. Bifurcation analysis of multiattractor flight dynamics. *Phil. Trans. R. Soc. Lond.*, (356):2297–2319, 1998.

[68] F.B. Macmillen and J.M.T. Thompson. Bifurcation analysis in the flight dynamics design process? a view from the aircraft industry. *Phil. Trans. R. Soc. Lond.*, (356):2321–2333, 1998.

[69] F.D. Marques and E.M. Belo. Identification of aircraft nonlinear dynamics using volterra series. 1998. ICAS-98-1.10.5.

[70] J.H. Myatt. Multiple time-scale effects for a pitching 65^o delta wing. In *AIAA Atmosperic Flight Mechanics Conference*, Boston MA, August 1998. Paper 98-4354.

[71] J.H. Myatt, C.J. Schumacher, P.D. McKeehen, and J.M. Buffington. Modeling and simulation of unsteady aerodynamic effects on a tailless aircraft. In *AIAA Atmospheric Flight Mechanics Conference*, Boston, MA, August 1998. Paper 98-4455.

[72] Y. Patel, M. Goman, and A. Khramstovsky. Flight clearance tools using a non-linear bifurcation analysis framework. In *AIAA Guidance, Navigation, and Control Conference and Exhibit*, Austin, Texas, Aug. 11-14 2003. AIAA-2003-5557.

[73] Y. Patel and P.R. Smith. Departure analysis of a twin-finned, high performance combat aircraft. In *AIAA Atmospheric Flight Mechanics Conference*, pages 80–87, San Diego, 1996. AIAA 96-3369-CP.

[74] Alain Pelletier and Robert C. Nelson. An experimental study of static and dynamic vortex breakdown on slender delta wing planforms. Colorado Springs, CO, June 20-22 1994. AIAA Applied Aerodynamics Conference. Technical Papers (A94-30939 10-02).

[75] J.B. Planeaux, J.A. Beck, and D.D. Baumann. Bifurcation analysis of a model fighter aircraft with control augmentation. In *AIAA Atmospheric Flight Mechanics Conf.*, Portland, OR, August 1990. AIAA Paper 90-2836.

[76] E.C. Polhamus. Prediction of vortex lift characteristics by a leading edge suction analogy. *Journal of Aircraft*, 8(4):193–199, April 1971.

[77] Patrick H. Reisenthel. Prediction of unsteady aerodynamic forces via nonlinear kernel identification. In *CEAS/AIAA/ICASE/NASA Langley International Forum on Aeroelasticity and Structural Dynamics*, Williamsburg, VA, June 22-25 1999.

[78] P.H. Reisenthel. Development of a nonlinear indicial model for maneuvering fighter aircraft. In *34th Aerospace Sciences Meeting & Exhibit*, January 1996. AIAA 96-0896.

[79] Y.A. Ryzhov, G.I Stoljarov, and V.G. Tabachnikov. Critical regimes of flow restructuring on high aspect ratio wing at unsteady subsonic stream. *Scientific notes of TsAGI*, XXVII(3-4), 1996.

[80] J. Singh and R.V. Jategoankar. Flight determination of configurational effects on aircraft stall behavior. In *AIAA Atmospheric Flight Mechanics Conference*, 1996. AIAA-96-3441-CP.

[81] Mark S. Smith. Analysis of wind tunnel oscillatory data of the x-31a aircraft. Technical report, NASA/CR-1999-208725, Feb 1999.

[82] G.I Stoljarov and V.G. Tabachnikov. Some aerodynamic characteristic properties of high aspect ratio wings at small reynolds numbers. *TsAGI proceedings*, (2290), 1985.

[83] Chapman G.T. Tobak, M. and L.B. Schiff. Mathematical modeling of the aerodynamic characteristics in flight mechanics. In *Proceedings of the Berkeley-Aimes Conference on Nonlinear Problems in Control and Fluid Dynamics*, Math Sci Press, pages 435–450, Brookline, MA, 1985.

[84] M. Tobak and G.T. Chapman. Nonlinear problems in flight dynamics involving aerodynamic bifurcations. Technical report, 1985. NASA TM 86707.

[85] M. Tobak, G.T. Chapman, and L.B. Schiff. Mathematical modeling of the aerodynamic characteristics in flight mechanics. Technical report, January 1984. NASA TM-85880.

[86] M. Tobak and L.B. Schiff. The role of time-history effects in the formulation of the aerodynamics of aircraft dynamics. *Dynamic Stability Parameters*, May 1978. Paper 26 in AGARD CP-235.

[87] M. Tobak and L.B. Schiff. Aerodynamic mathematical modelling basic concepts. *Dynamic Stability Parameters*, March 1981. paper 1 in AGARD LS-114.

[88] M. Tobak and L.B. Schiff. Some applications of aerodynamic formulations to problems in aircraft dynamics. *Dynamic Stability Parameters*, March 1981. paper 16 in AGARD LS-114.

[89] M. Tobak and A. Unal. Bifurcations in unsteady aerodynamics. Technical report, June 1986. NASA TM-88316.

[90] H. Wagner. Über die enstehung des dynamishen auftriebs von tragflüglen. *Z. angew. Math. U. Mech*, pages 17–35, 5 1925.

[91] Kolmakov Y.A., Ryzhov Y.A., Stoljarov G.I, and Tabachnikov V.G. Investigation ot flow structure of high aspect ratio wing at high angles of attack. *TsAGI proceedings*, (2290), 1985.

[92] A.N. Zhuk, K.A. Kolinko, O.L. Miatov, and A.N. Khrabrov. Experimental investigations of unsteady aerodynamic characteristics of isolated wings at separated flow regimes. *Preprint 86, TsAGI, Moscow, Russia*, 1997. (in Russian).

[93] Peter H. Zipfel. *Modeling and Simulation of aerospace vehicle dynamics.* AIAA Educational Series, 2000. ISBN 1-56347-456-5.

Appendix A

Linear regression technique

The linear regression technique is employed to estimate a functional relationship of a dependent variable to one or more independent variables. It is assumed that a dependent variable can be approximated as a linear combination of the independent variables:

$$f(t) = k_1 \cdot 1 + k_2 \cdot \varphi_2(t) + \ldots + k_n \cdot \varphi_n(t) \tag{A.1}$$

where $f(t)$ is the dependent variable, $\varphi_i(t)$ $i = 1 \ldots n$ are the independent variables or *regressors* (the first regressor is a unit function).

A.1 Least squares estimates

Suppose that the structure of (A.1) is known, and a sequence of N observations on both f and φ_i has been made at times $t_1, t_2, \ldots, t_N$. The measured data can be related by the following set of N linear equations:

$$f(i) = k_1 \cdot 1 + k_2 \cdot \varphi_2(i) + \ldots + k_n \cdot \varphi_n(i) + \varepsilon(i) \qquad i = 1, \ldots, N \tag{A.2}$$

Let $\vec{\mathbf{f}}$ be the vector of size N of measured values of $f(i)$, $\vec{\boldsymbol{\varepsilon}}$ be the vector of size N of discrepancies between measured and estimated values. The vector $\vec{\mathbf{k}}$ is a vector of size n of parameter estimates and the matrix X is an $N \times n$-matrix comprising measured values of the independent variables. Then equation (A.2) may be re-written as follows:

$$\vec{\mathbf{f}} = X\vec{\mathbf{k}} + \vec{\boldsymbol{\varepsilon}} \tag{A.3}$$

The functional Φ equals the sum of squares of the errors:

$$\Phi = \vec{\varepsilon}^T \vec{\varepsilon} \tag{A.4}$$

where the superscript T denotes the transpose matrix. Substituting (A.3) into (A.4) one can get

$$\Phi = \vec{\mathbf{f}}^T \vec{\mathbf{f}} - 2\vec{\mathbf{f}}^T X \vec{\mathbf{k}} + \vec{\mathbf{k}}^T X^T X \vec{\mathbf{k}} \tag{A.5}$$

Since $\vec{\mathbf{f}}$ and X are known, the value of $\vec{\mathbf{k}}_{min}$ the minimizing the functional ϕ can be determined analytically:

$$\left(X^T X\right) \vec{\mathbf{k}}_{min} = X^T \vec{\mathbf{f}},$$

hence

$$\vec{\mathbf{k}}_{min} = \left(X^T X\right)^+ X^T \vec{\mathbf{f}} \tag{A.6}$$

where the superscript "+" denotes the generalized inverse matrix [26]. If the matrix $X^T X$ is non-singular, equation (A.6) may be re-written as

$$\vec{\mathbf{k}}_{min} = \left(X^T X\right)^{-1} X^T \vec{\mathbf{f}} \tag{A.7}$$

Under the following assumptions:

1. $\vec{\varepsilon}$ is a stationary vector with zero mean value,
2. $\vec{\varepsilon}$ is uncorrelated with X,
3. X is the deterministic quantity i.e. the state and input variables are measured without errors,
4. $\varepsilon(i)$ is identical and uncorrelated with zero mean and variance σ_x^2,

the estimates of $\vec{\mathbf{k}}$ are unbiased, consistent and efficient. If these assumptions are extended by the assumption of a normal distribution of ε, the significance of $\vec{\mathbf{k}}_{min}$ can be evaluated using the F-criterion:

$$F = \frac{\vec{\mathbf{k}}_{min} X^T \vec{\mathbf{f}} - N \cdot \overline{f}}{(n-1)\, s^2}, \tag{A.8}$$

where $s = \Phi / (N - n)$ is the covariance matrix for $\vec{\varepsilon}$, and F is a random value which has an F-distribution with the number of degrees of freedom $\nu_1 = n - 1$ and $\nu_2 = N - n$.

The significance of individual terms in the regression (A.2) can be evaluated using the partial F-criterion:

$$F_p = \frac{k^2_{min_i}}{s^2\left(k_{min_i}\right)}, \tag{A.9}$$

where $s^2\left(k_{min_i}\right)$ is the variance estimate of k_i and F_p obeys the same distribution as F (see A.8).

A.2 Stepwise regression

Equation (A.1) represents a postulated model where the significant terms in this equation are to be found from measured data. Several techniques for the selection of the regression model have been developed [19]. One of them, the stepwise regression, has been prefered by statisticians and researchers in many applications.

The stepwise regression is a procedure which inserts independent variables into the regression model, one at a time, until the regression equation becomes satisfactory. The order of insertion is determined by using the partial correlation coefficient as a measure of the importance of variables which are not yet in the regression equation. The procedure starts with postulation of the regression model given by eq.(A.2). The first independent variable from the postulated model is chosen as one which is most closely correlated with f. The correlation coefficient is given by the expression

$$r_{jf} = \frac{S_{jf}}{\left(S_{jj}S_{ff}\right)^{1/2}}, \tag{A.10}$$

where

$$\begin{aligned}
S_{jf} &= \sum_{i=1}^{N}\left[\varphi_j(i) - \overline{\varphi}_j\right]\left[f(i) - \overline{f}\right] \\
S_{jj} &= \sum_{i=1}^{N}\left[\varphi_j(i) - \overline{\varphi}_j\right]^2 \\
S_{ff} &= \sum_{i=1}^{N}\left[f(i) - \overline{f}\right]^2 \\
\overline{\varphi}_j &= \tfrac{1}{N}\sum_{i=1}^{N}\varphi_j(i) \\
\overline{f} &= \tfrac{1}{N}\sum_{i=1}^{N} f(i)
\end{aligned}$$

If, for example, φ_2 is selected, then the model

$$f = k_1 \cdot 1 + k_2 \cdot \varphi_2 + \varepsilon \tag{A.11}$$

is used to fit the data. A new independent variable z_3 is constructed by finding the residuals of φ_3 after regressing it on φ_2, that is, the residuals from fitting the model

$$\varphi_3 = a_0 + a_1 \cdot \varphi_2 + z_3 \tag{A.12}$$

The variable z_3 is, therefore, given as

$$z_3 = \varphi_3 - \hat{a}_0 - \hat{a}_1 \cdot \varphi_2. \tag{A.13}$$

Similarly, the variables $z_4, \ldots, z_n$ are formed. A new dependent variable f^* is represented by residuals of f regressed of φ_2 using the model from (A.11); that is

$$f^* = f - \hat{k}_1 \cdot 1 - \hat{k}_2 \cdot \varphi_2. \tag{A.14}$$

In the next step, a new set of correlations which involves the variables $f^*, z_3, \ldots, z_n$ is formulated.

At every step of the regression, the variables incorporated into the model in the previous stages and a new variable entering the model are reexamined. The significance value is computed for each variable, this value is compared with a predefined value. Any variable having too low a significance value is removed from the model. The process of selecting and checking variables continues until the situation arises when there are no more variables to be added to the equation, and no more to be rejected.

A.3 Principal components regression

The development of the principal components regression starts by transforming the original regressors φ_i to the space of orthogonal regressors z_i. The transformation is accomplished by letting

$$Z = XT \tag{A.15}$$

and

$$\vec{\mathbf{k}} = T\vec{\gamma}. \tag{A.16}$$

The columns of Z, formed by the orthogonal regressors z_i, are referred to as principal components. After the transformation, the regression model becomes

$$\vec{\mathbf{f}} = Z\vec{\gamma} + \vec{\varepsilon} \tag{A.17}$$

The least squares estimates of $\vec{\gamma}$ are formed as

$$\hat{\vec{\gamma}} = \left(Z^T Z\right)^{-1} Z^T \vec{\mathbf{f}} = \Lambda^{-1} Z^T \vec{\mathbf{f}} \tag{A.18}$$

and the covariance matrix of $\hat{\vec{\gamma}}$ as

$$\text{Cov}\left\{\hat{\vec{\gamma}}\right\} = \sigma^2 \cdot \Lambda^{-1}. \tag{A.19}$$

The principal components regression "overcomes" the problem of collinearity of regressors by using less than a full set of principal components in (A.17). The principal components corresponding to very minor eigenvalues are removed from the analysis, and the least squares method is applied to the remaining components.

The principal components regression can improve the accuracy of parameter estimates over the least squares estimates when the data is ill-conditioned.

Appendix B

Aerodynamic derivatives estimation

The conventional unsteady aerodynamic modelling approach is based on the assumption that aerodynamic loads depend only on the instantaneous values of the motion parameters and are linear functions of them. For example, the normal force coefficient C_N is expressed as follows:

$$C_N(t) = C_{N_0} + C_{N_\alpha}\alpha(t) + C_{N_q}q(t)\frac{\bar{c}}{2V} + C_{N_{\dot{\bar{\alpha}}}}\dot{\alpha}\frac{\bar{c}}{2V}. \tag{B.1}$$

During small amplitude harmonic oscillations the angle of attack varies as $\alpha(t) = \alpha_0 + \Delta\alpha \sin \omega t$. Thus, taking into account the linearity of (B.1) with respect to the input parameters then an aerodynamic coefficient will be a harmonic signal with the same frequency. Output of the system may be expressed as follows

$$C_N(t) = C_{N_0} + C_{N_\alpha}\Delta\alpha \sin \omega t + (C_{N_q} + C_{N_{\dot{\bar{\alpha}}}})\frac{\Delta\alpha\omega\bar{c}}{2V}\cos \omega t. \tag{B.2}$$

Expanding the experimentally measured dependence in a Fourier series and taking into account only the first harmonic, the aerodynamic coefficient may be represented as follows

$$C(t) = A_0 + A \sin \omega t + B \cos \omega t, \tag{B.3}$$

where A_0, A, B are coefficients of the Fourier expansion. Comparing (B.2) and (B.3) one can obtain expressions for the aerodynamic derivatives via the Fourier series coefficients

$$C_{N_\alpha} = A/\Delta\alpha$$

$$C_{N_q} + C_{N_{\dot{\bar{\alpha}}}} = \frac{2VB}{\Delta\alpha\omega\bar{c}}. \tag{B.4}$$

Conducting a set of runs at several different frequencies at each tested angle of attack in the range $[\alpha_0, \alpha_1]$ with sufficiently small step one can obtain a family of aerodynamic derivatives, as shown on Figs. 2.12–2.13.

Appendix C

Example of dynamic system implementation in ADDB

This section presents an example of the dynamic system implementation in the ADDB database for the unsteady aerodynamic model of the normal force coefficient.

In the first stage, a dynamic system (Model) object has to be added to a database using the `Add` button. Then a right-hand-side function of the dynamic system is defined as a regular m-function according to the syntax required by Matlab `ode**` functions and to then registered in the `Options` dialog panel. Usually for the RHS-function $\dot{\mathbf{x}} = \mathbf{f}(t, \mathbf{x})$ at least two arguments are required.

The third and higher arguments can be any additional parameters, and they are passed into a RHS function according to the `ode**` functions syntax. The RHS-function output defines the rate vector $\dot{\mathbf{x}}$.

An example of a RHS-function `dCNvbRHS(t, CN_vb, flag, Alpha0, DelAlpha, f)` calculating the contribution of vortex breakdown dynamics in the normal force coefficient model is presented.

```
function out = dCNvbRHS(t, Cy_vb, flag, Alpha0, DelAlpha, f)
    Alpha    = AlfEx(t, Alpha0, DelAlpha, f);
    DotAlpha = DotAlfEx(t, Alpha0, DelAlpha, f);
    CN_vb_st = CN_st_1(Alpha) - CN_v_st_1(Alpha);
    dCy = Cy_vb_st - Cy_vb;
    dCyvb = (k_i_cy_1(Alpha, 1)*dCy + k_i_cy_1(Alpha, 2)*dCy.^2 + ...
             k_i_cy_1(Alpha, 3)*dCy.^3)*2*V/CBAR;
    out = dCyvb;
```

```
    %# dCN_vb
return
```

The second step is to develop function **G** calculating the full model. Any number of arguments can be passed into and returned from this function. The following function `ModCN(t, CNvb)` and the RHS function form the full dynamic model of the normal force coefficient for the longitudinal motion.

```
function CN = ModCN(t, CNvb, Alpha0, DelAlpha, f)
    D2R = pi/180;
    Alpha = AlfEx(t, Alpha0, DelAlpha, f);
    DotAlpha = DotAlfEx(t, Alpha0, DelAlpha, f);
    CN = CN_v_st_1(Alpha) + CNvb + CN_DotAlpDL*DotAlpha*CBAR/V*D2R;
    %# CN
return
```

Appendix D

Example of the model implementation in PII

```
/* Include C libraries */
#include <stdio.h>
#include <math.h>
#include "PIIMath.h"

/* Model description */
$PERIODIC       /* Periodic input */
$TASK
    65 deg Delta Wing, Rolling moment coefficient in yaw
    Beta = variable, Alpha = const
    Version  15.03.2002
$END

/* Model data structure description */
$DATA           /* Input data (experimental records) */
    TIME
  $INDEP        /* Independent variables */
    Alpha Psi DotPsi
  $DEP          /* Dependent variable */
    Cl
$END

$INTERNAL       /* Internal state variable */
    Cl_dyn
$END

$CALCULATED     /* Auxiliary variables */
   D ClSt ClDelta ClAtt ClrAtt TAU DotPsiDl
$END

$FIXED          /* Model parameters (constants) */
```

```
    SysOrd b V Weight
$END

$PARAMETER      /* Model parameters to be identified */
    psi0 kclb1 clb3 psi1 psi2 K11 k1_psi2 k2_psi1 k2_psi2 k3_psi1 k3_psi2
$END

/* Functions and variables declaration */
float fCl_st  (float alpha, float psi);
float fClDelta(float alpha, float psi);
float fCl_att (float alpha, float psi);
float fClr_att(float alpha);
float fki     (float alpha, float psi, int i);

static float dim  = 61;
static float DIMa = 13;
static float DIMb = 73;

static float alpha0 [61];
static float Clb_att[61];
static float Clr_att[61];
static float k1     [61];
static float Alpha_i[13];
static float Psi_i  [73];
static float Clst_i [949];

/* Model body, begin */
$SYSTEM
   float Delta, rhs, b_2V, DotPsi_dl, tau, fk1, fk2, fk3;
   int i;
   FILE *fp;
   static int flag = 1;

   if (flag)
   {
      flag = 0;
      if (!(fp = fopen("Cl0dat.d","r"))) exit(0);

for(i=0;i<dim;i++)
{
   fscanf(fp, "%f %f %f %f", &alpha0[i],&tau,&Clb_att[i],&Clr_att[i]);
   k1[i] = 1./tau;
}

for(i=0;i<DIMa*DIMb;i++)
   fscanf(fp, "%f", &Clst_i[i]);

for(i=0;i<DIMa;i++)
   fscanf(fp, "%f", &Alpha_i[i]);

for(i=0;i<DIMb;i++)
   fscanf(fp, "%f", &Psi_i[i]);
```

```
   fclose(fp);
}

fk1        = fki(@Alpha,@Psi,1);
b_2V       = @b/(2.*@V);
DotPsi_dl = @DotPsi*DTOR*b_2V;

@ClSt     = fCl_st(@Alpha,@Psi);
@ClDelta = fClDelta(@Alpha,@Psi);

@ClAtt   = fCl_att(@Alpha,@Psi);
@ClrAtt = fClr_att(@Alpha);

@TAU       = 1./fk1;
@DotPsiDl = DotPsi_dl;
   Delta = @ClDelta-@Cl_dyn;
   if (int(@SysOrd)==1)
      rhs = fk1*Delta;
   else if (int(@SysOrd)==3)
   {
      fk2 = fki(@Alpha,@Psi,2);
      fk3 = fki(@Alpha,@Psi,3);
      rhs = Delta*(fk1 + Delta*(fk2 + fk3*Delta));
      @D   = fk2*fk2-4*fk1*fk3;
   }
   else
      exit(0);

   @Cl_dyn' = rhs/b_2V;
   @Cl = @ClAtt + @Cl_dyn + @ClrAtt*DotPsi_dl;

$END
/* Model body, end */

/* Constraint violation penalty */
$FUNCTIONAL
   if(@D > 0)
      FUNCT = @Weight;
   else
      FUNCT = 0;
$END

/* Attached flow component calculation */
float fCl_att(float alpha, float psi)
{
    float bt = (psi-@psi0)*cos(alpha*DTOR)*DTOR;
    float clb1 = MatInterpolate(dim, alpha0, Clb_att, alpha);

    return (clb1*@kclb1 + @clb3*bt*bt)*bt;
}
```

```
/* Attached flow yaw derivative calculation */
float fClr_att(float alpha)
{
    return MatInterpolate(dim, alpha0, Clr_att, alpha);
}

/* Calculation of difference between attached component and statics */
float fClDelta(float alpha, float psi)
{
    return fCl_st(alpha,psi)-fCl_att(alpha,psi);
}

/* Static dependence */
float fCl_st(float alpha, float psi)
{
    return MatInterpolate3d(DIMb, DIMa, Psi_i, Alpha_i, Clst_i, psi, alpha);
}

/* Calculation of parameters k1, k2 and k3 */
float fki(float alpha, float psi, int n)
{
   float  k1_psi1;
   if(n == 1)
   {
      k1_psi1 = MatInterpolateLin(dim, alpha0, k1, alpha);
      return MatDdspl(@psi1,@psi2,@K11*k1_psi1,@k1_psi2,fabs(psi));
   }
   else if(n == 2)
      return MatDdspl(@psi1,@psi2,@k2_psi1,@k2_psi2,fabs(psi));
   else if(n == 3)
      return MatDdspl(@psi1,@psi2,@k3_psi1,@k3_psi2,fabs(psi));
   else
      return 0;
}
```

Appendix E

Experimental and predicted aerodynamic responses

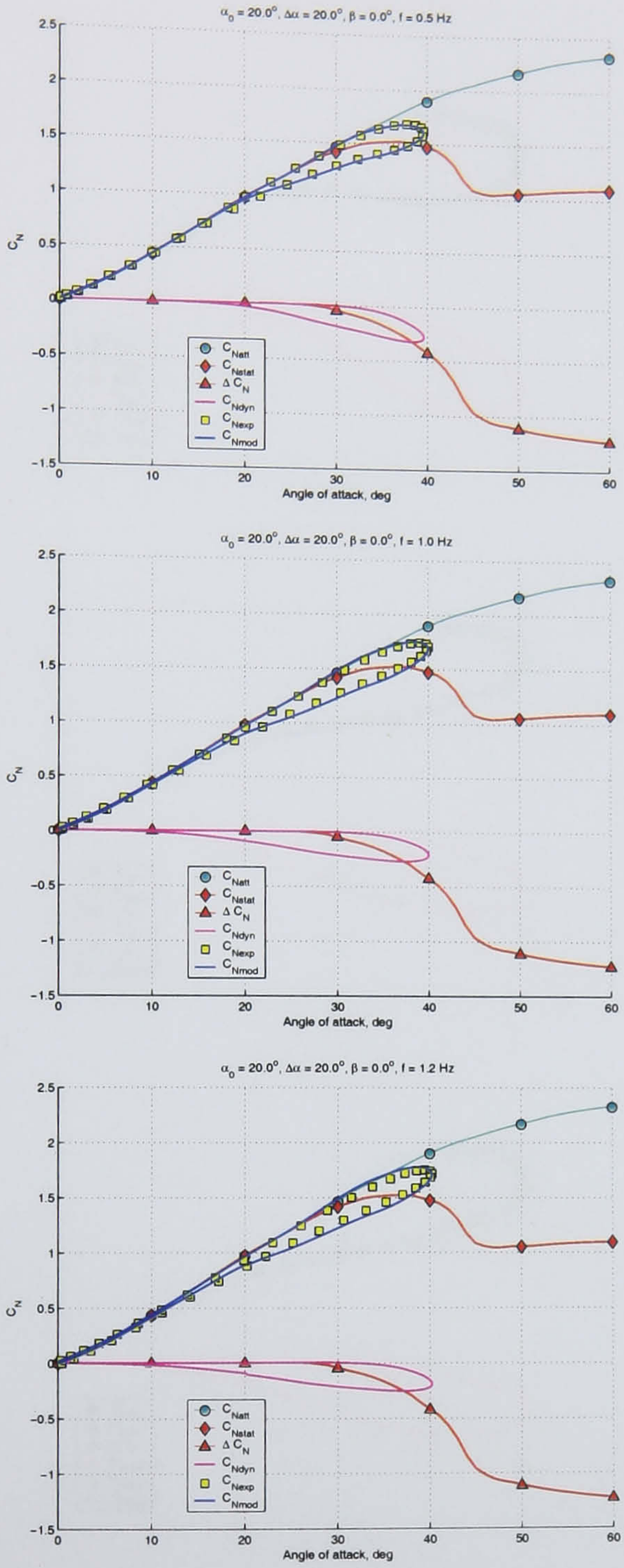

Figure E.1: Large amplitude pitch oscillations: the experimental normal force coefficient responses in comparison with predicted ones using the nonlinear mathematical model; other components of the mathematical model.

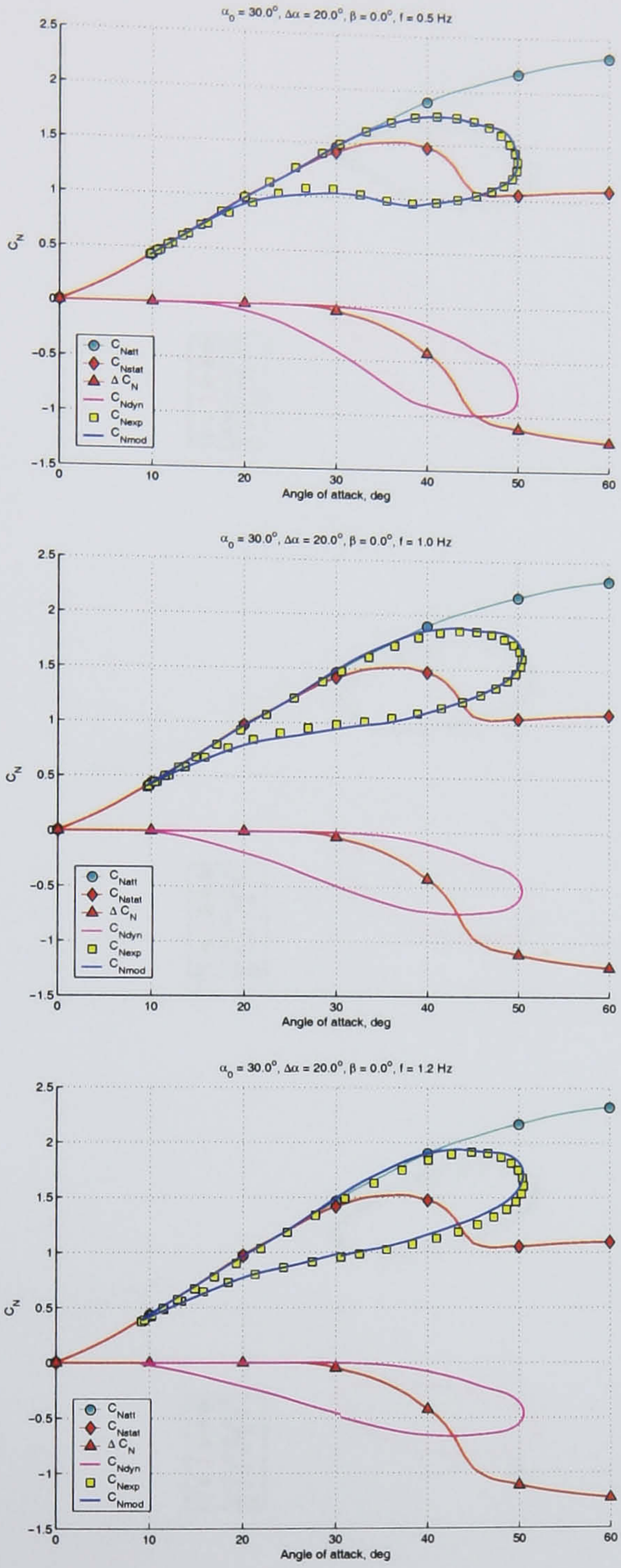

Figure E.2: Large amplitude pitch oscillations: the experimental normal force coefficient responses in comparison with predicted ones using the nonlinear mathematical model; other components of the mathematical model.

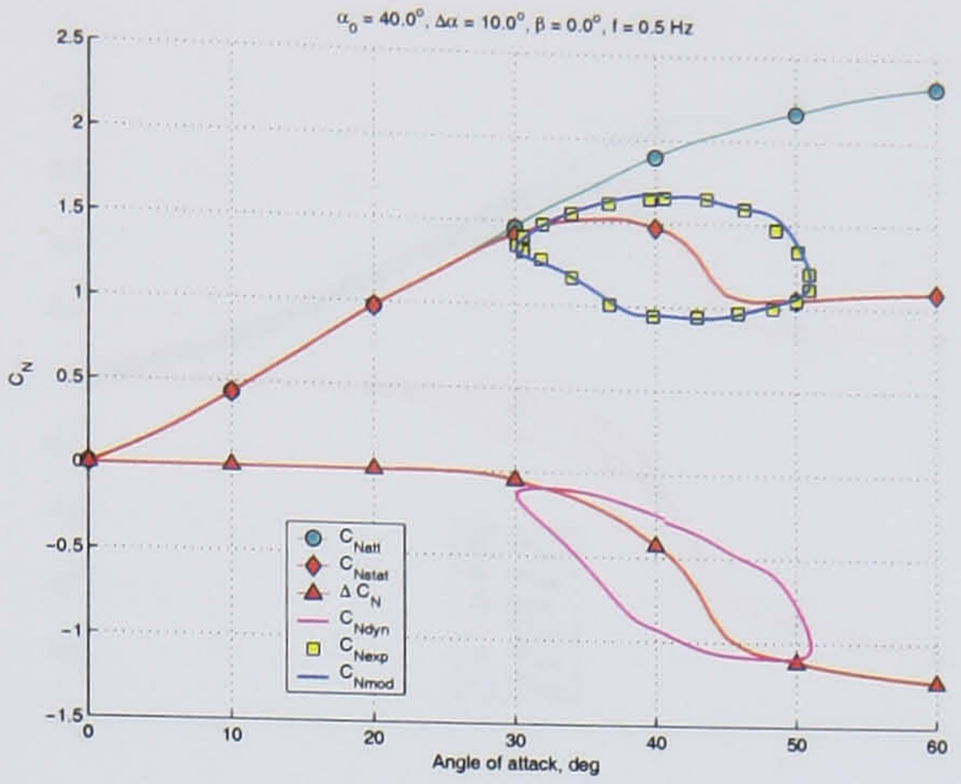

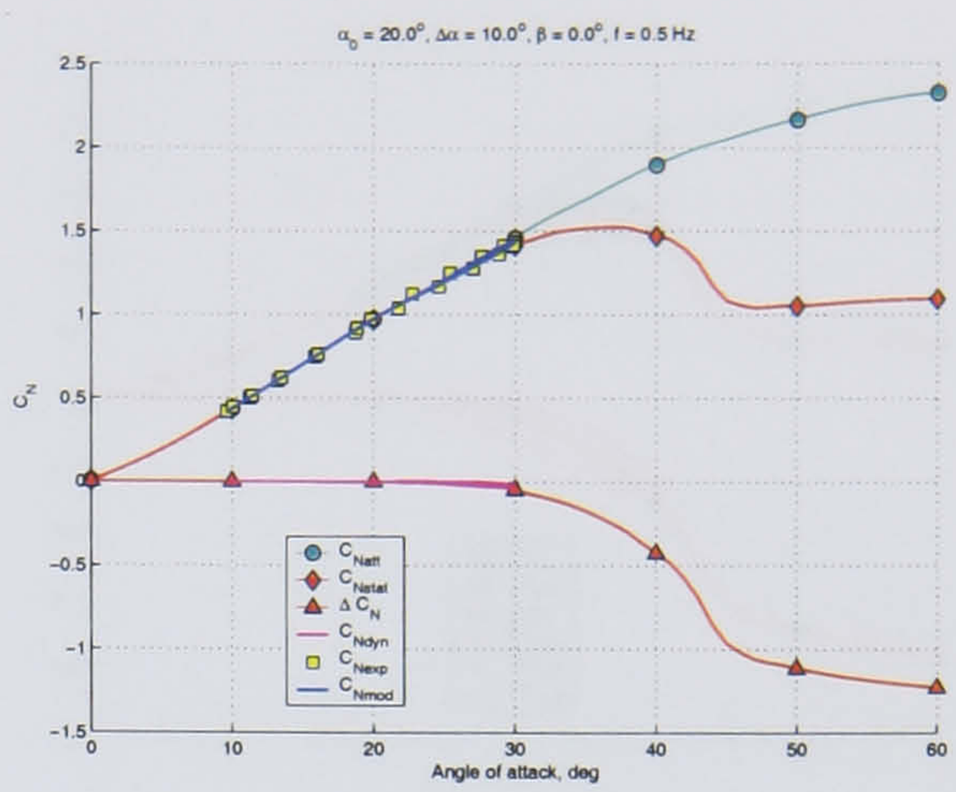

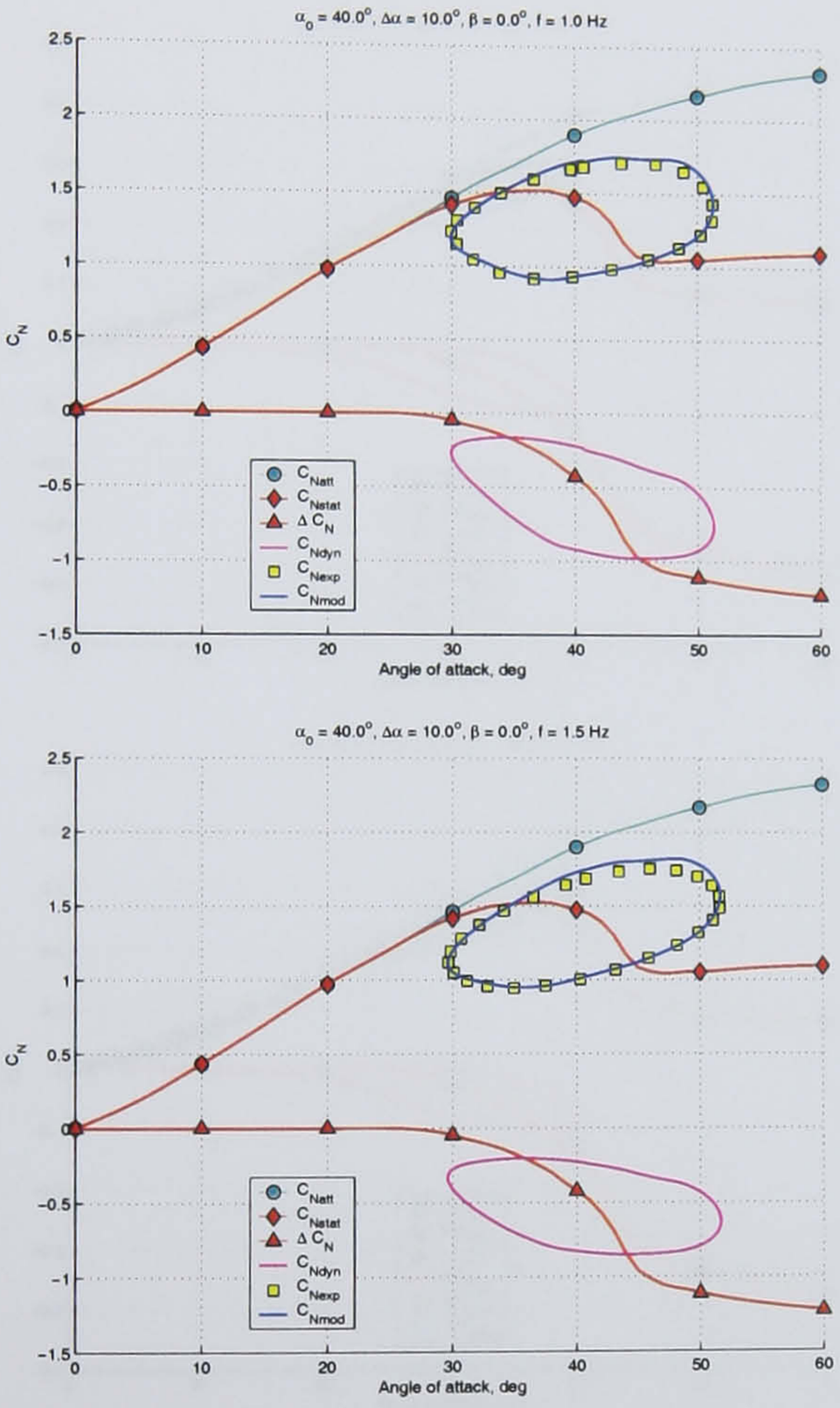

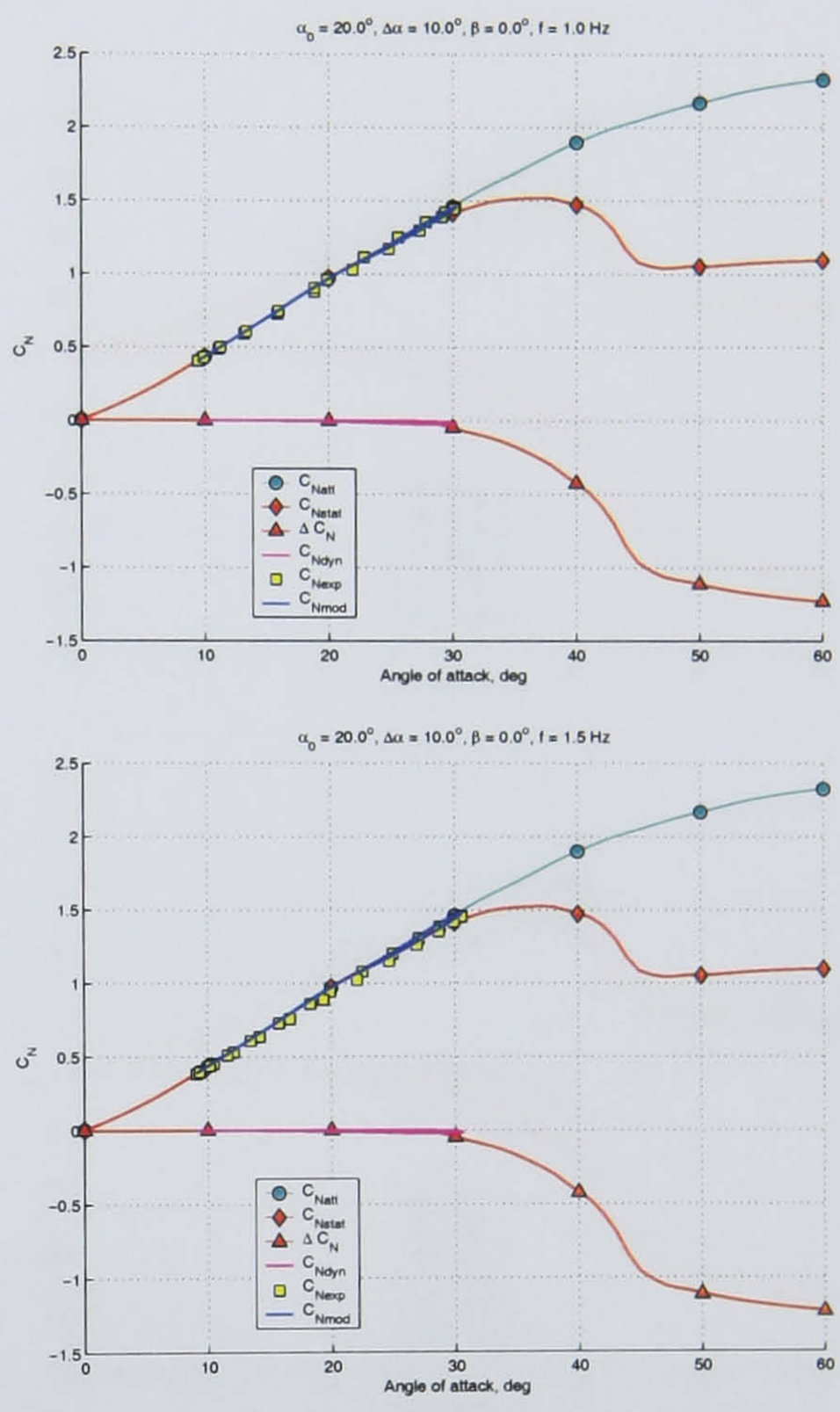

Figure E.3: Large amplitude pitch oscillations: the experimental normal force coefficient responses in comparison with predicted ones using the nonlinear mathematical model; other components of the mathematical model.

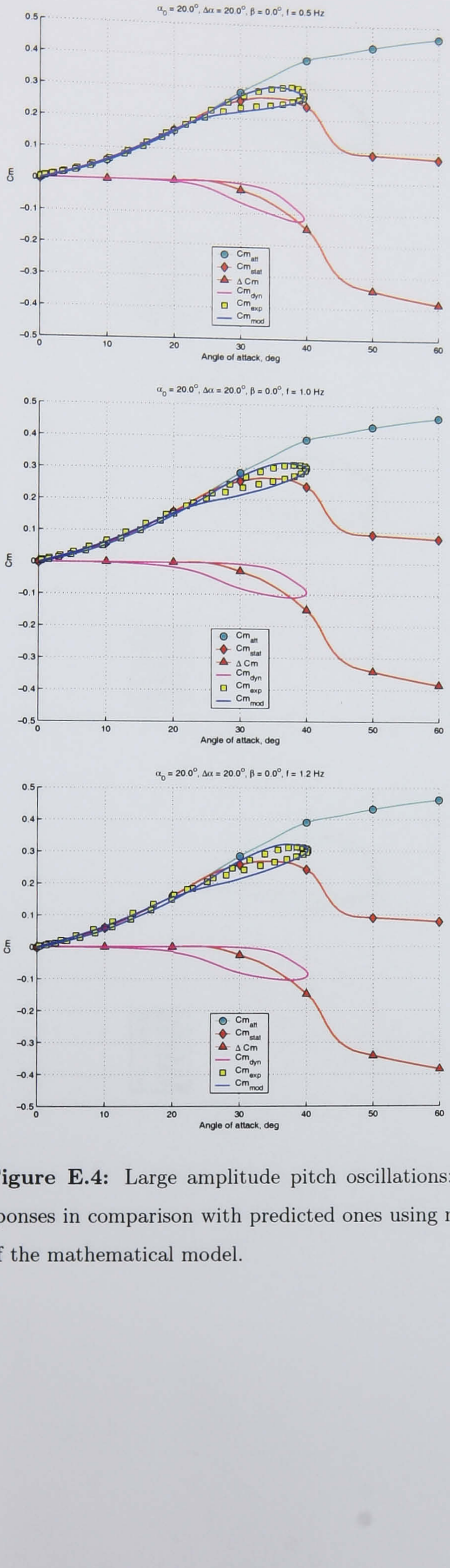

Figure E.4: Large amplitude pitch oscillations: the experimental pitch moment coefficient responses in comparison with predicted ones using nonlinear mathematical model; other components of the mathematical model.

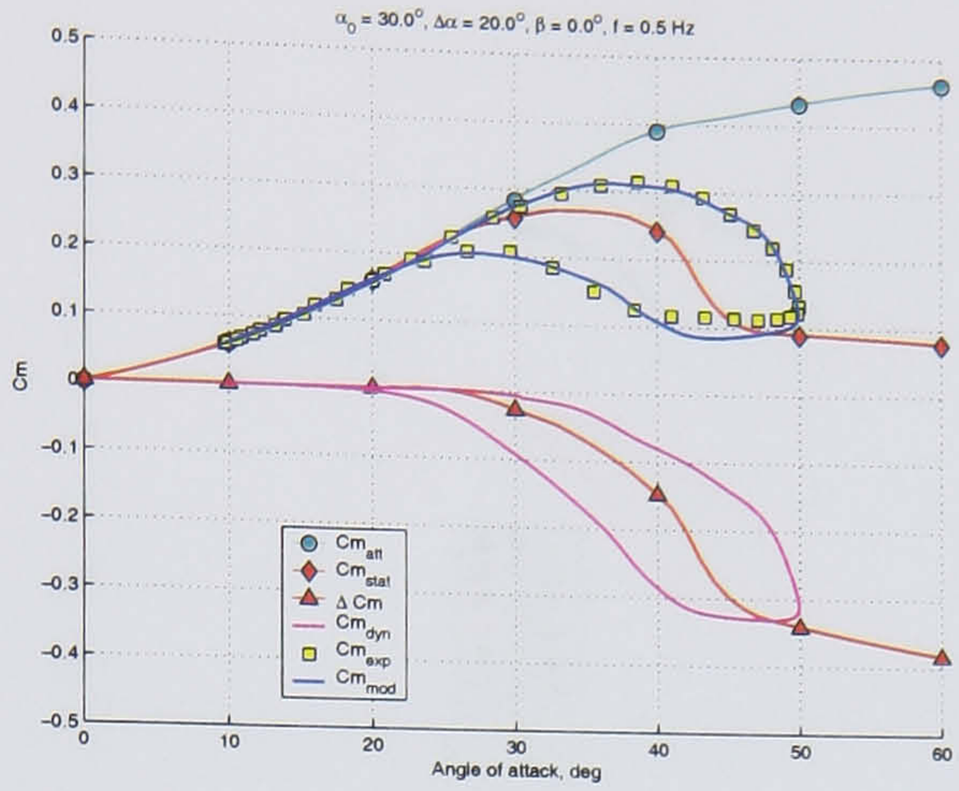

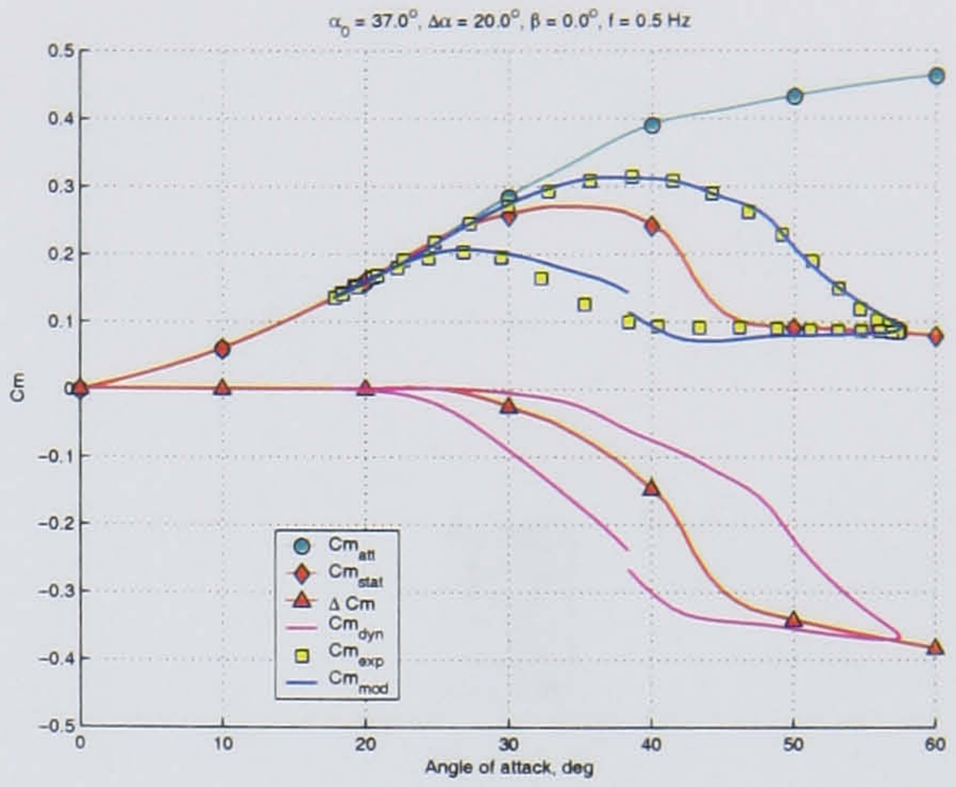

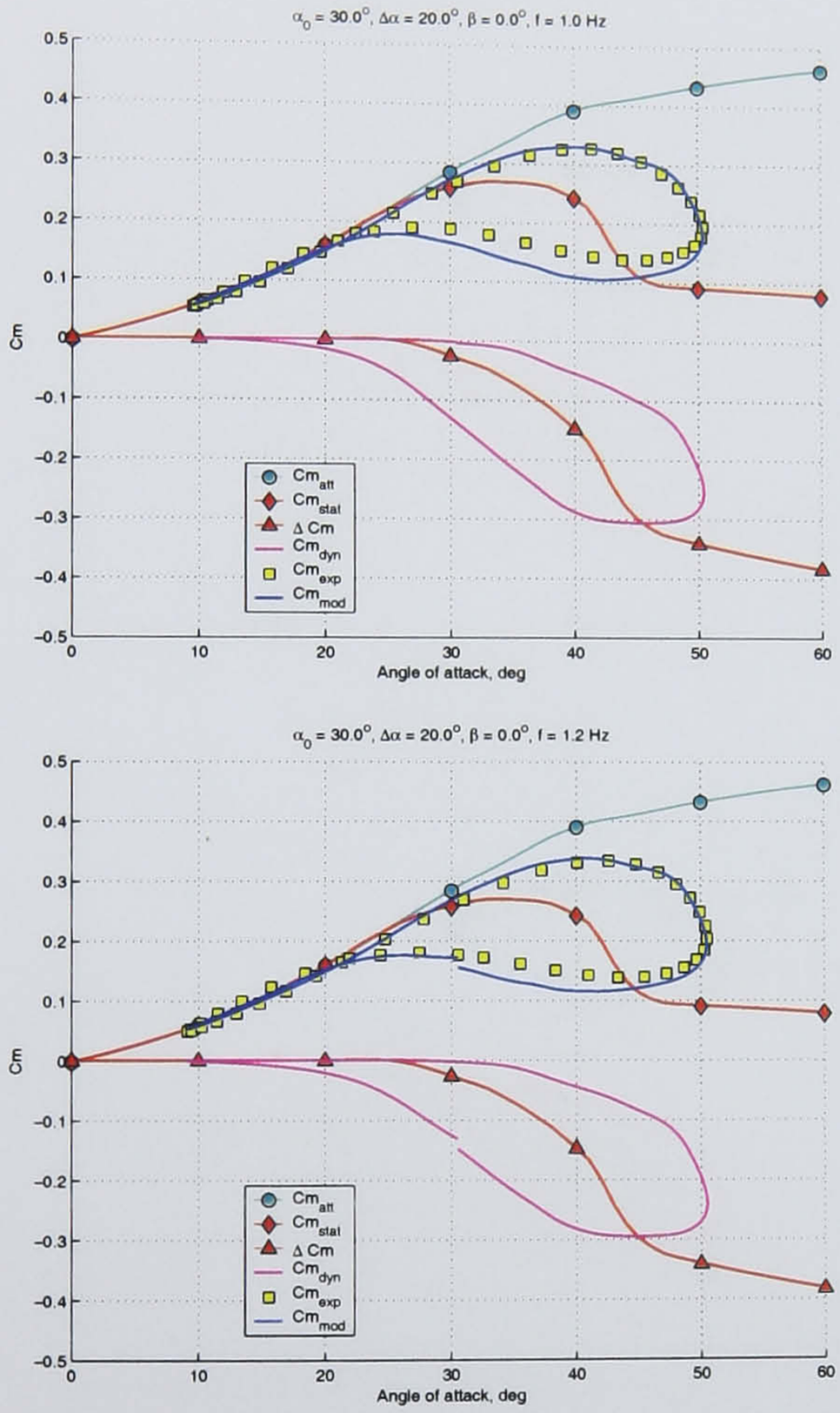

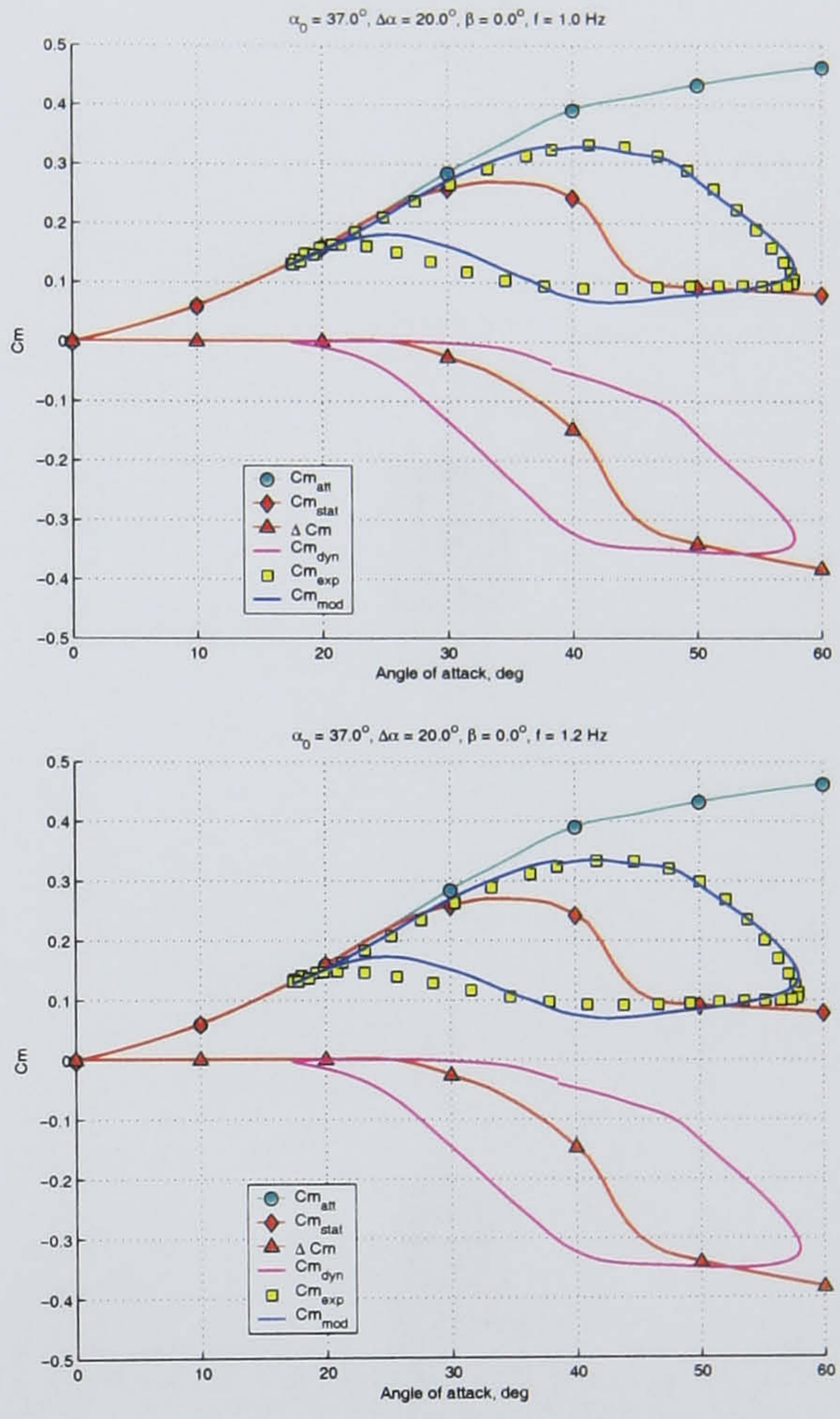

Figure E.5: Large amplitude pitch oscillations: the experimental pitch moment coefficient responses in comparison with predicted ones using nonlinear mathematical model; other components of the mathematical model.

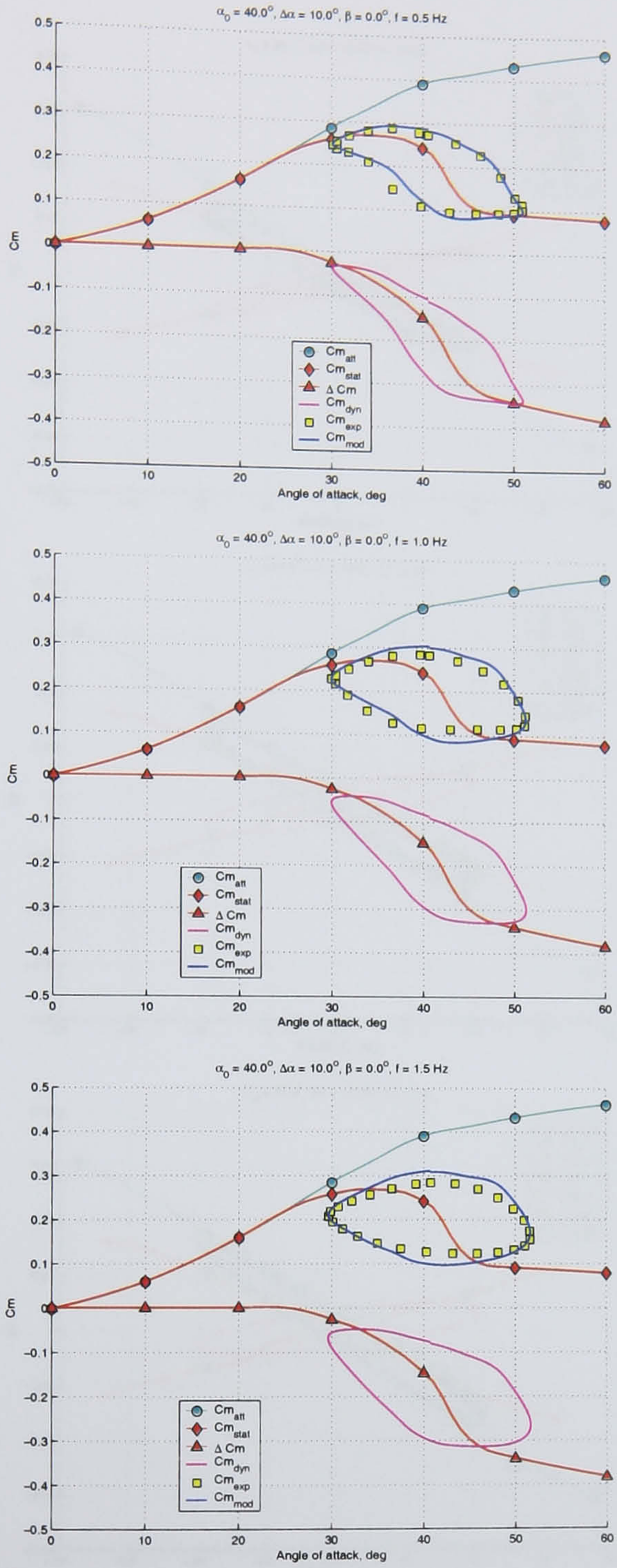

Figure E.6: Large amplitude pitch oscillations: the experimental pitch moment coefficient responses in comparison with predicted ones using nonlinear mathematical model; other components of the mathematical model.

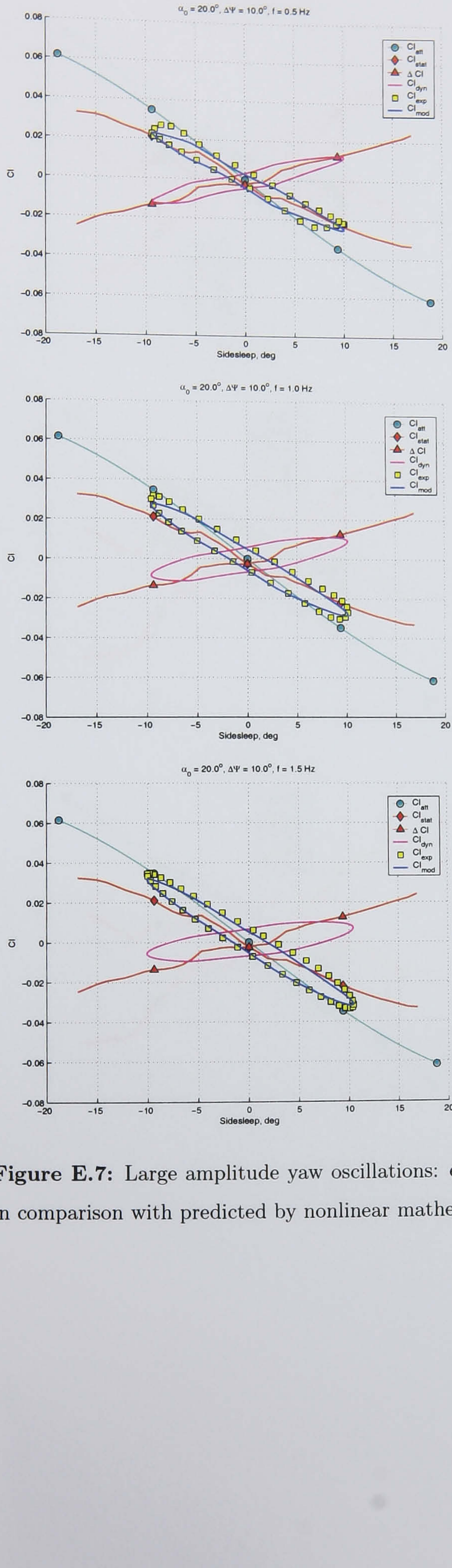

Figure E.7: Large amplitude yaw oscillations: experimental rolling moment coefficient responses in comparison with predicted by nonlinear mathematical model and other model components.

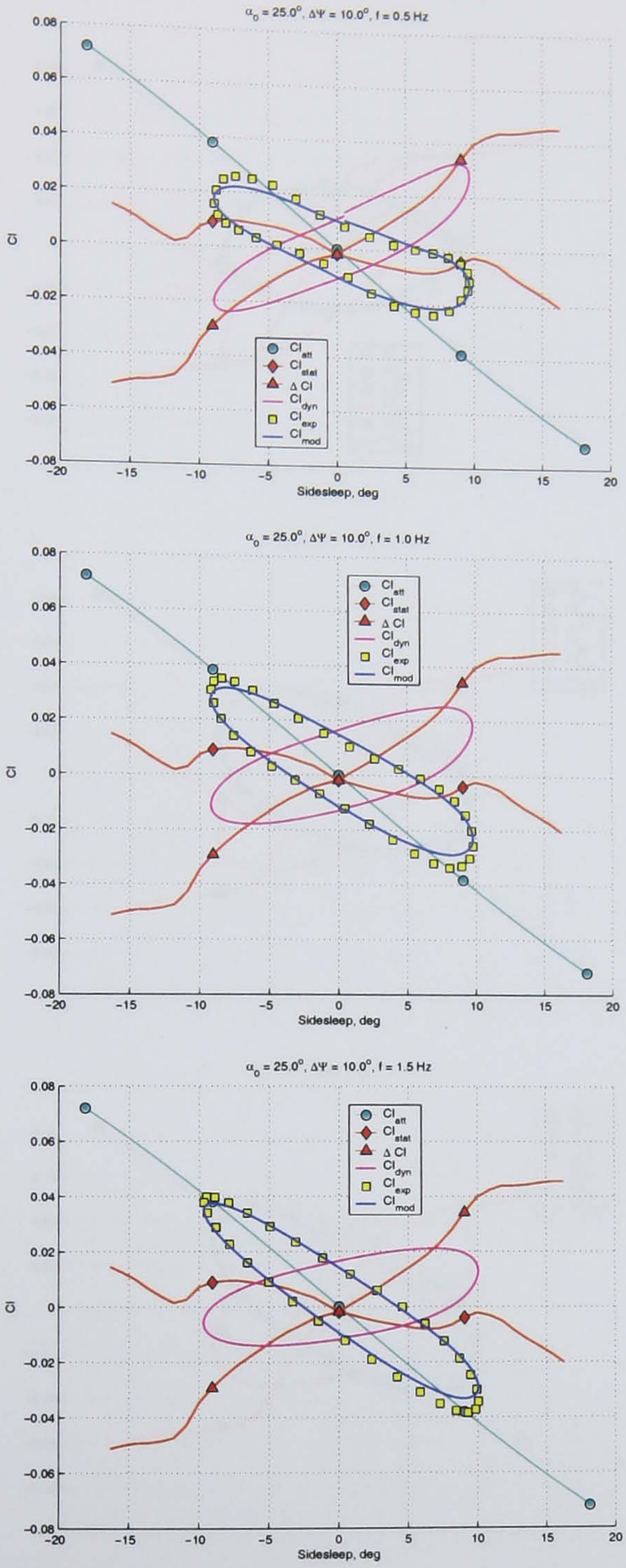

Figure E.8: Large amplitude yaw oscillations: experimental rolling moment coefficient responses in comparison with predicted by nonlinear mathematical model and other model components.

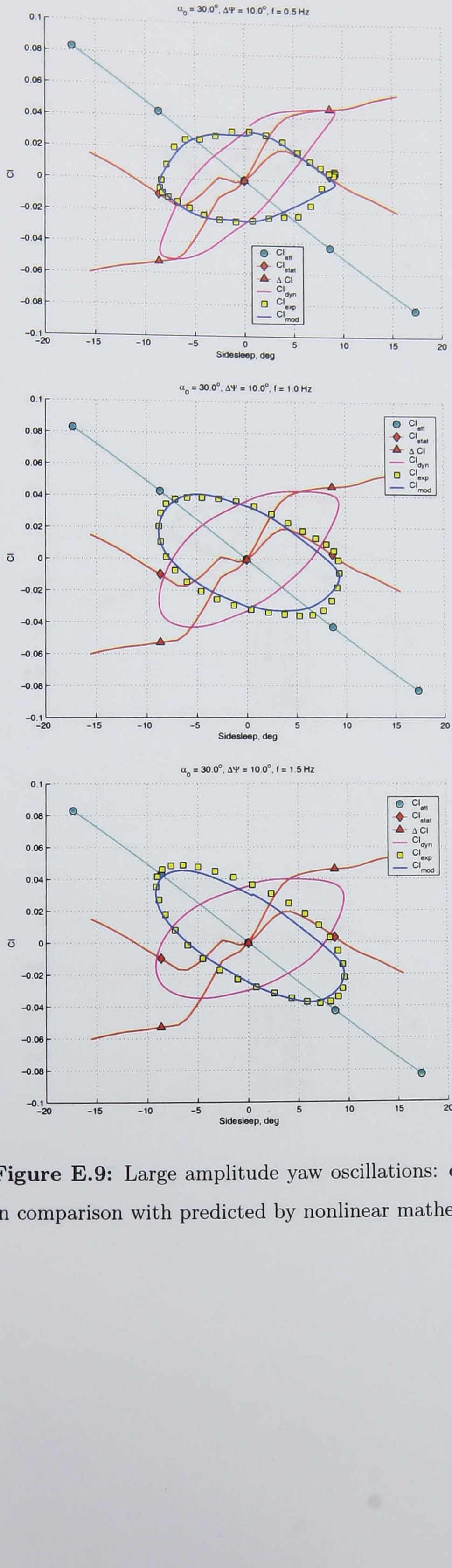

Figure E.9: Large amplitude yaw oscillations: experimental rolling moment coefficient responses in comparison with predicted by nonlinear mathematical model and other model components.

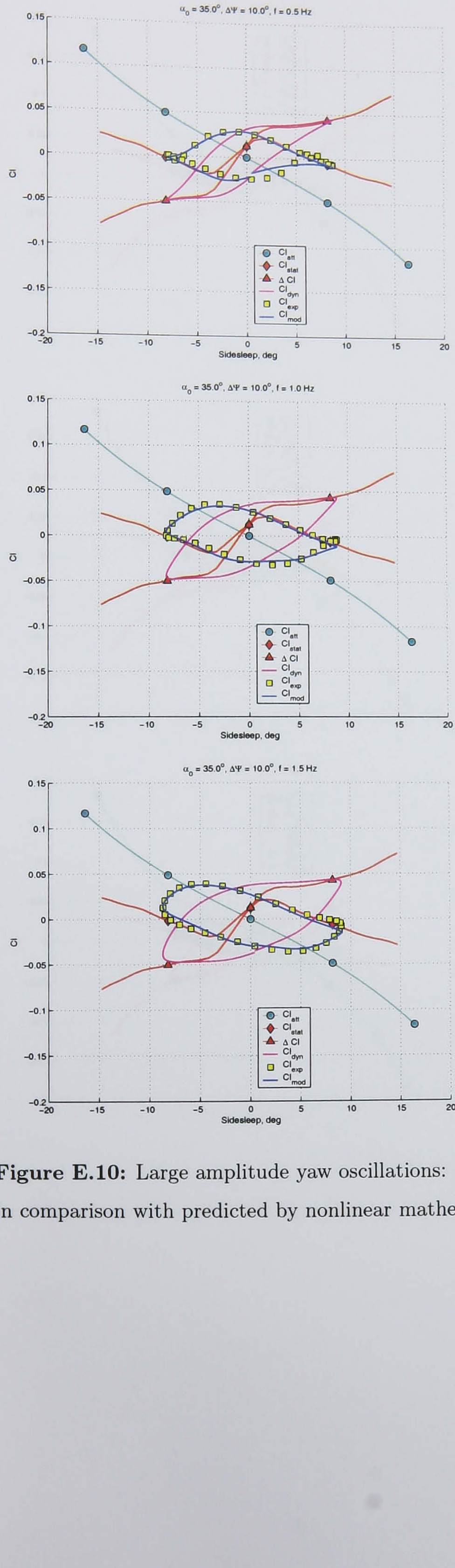

Figure E.10: Large amplitude yaw oscillations: experimental rolling moment coefficient responses in comparison with predicted by nonlinear mathematical model and other model components.

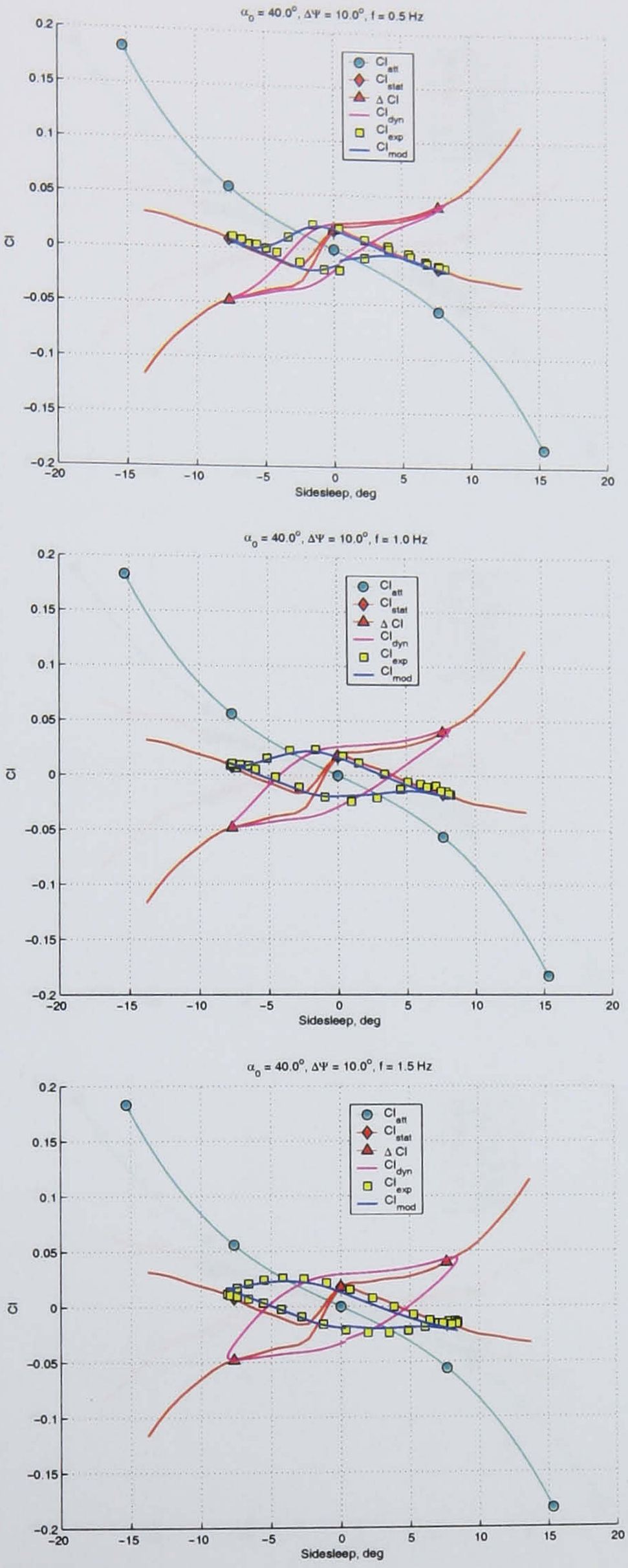

Figure E.11: Large amplitude yaw oscillations: experimental rolling moment coefficient responses in comparison with predicted by nonlinear mathematical model and other model components.

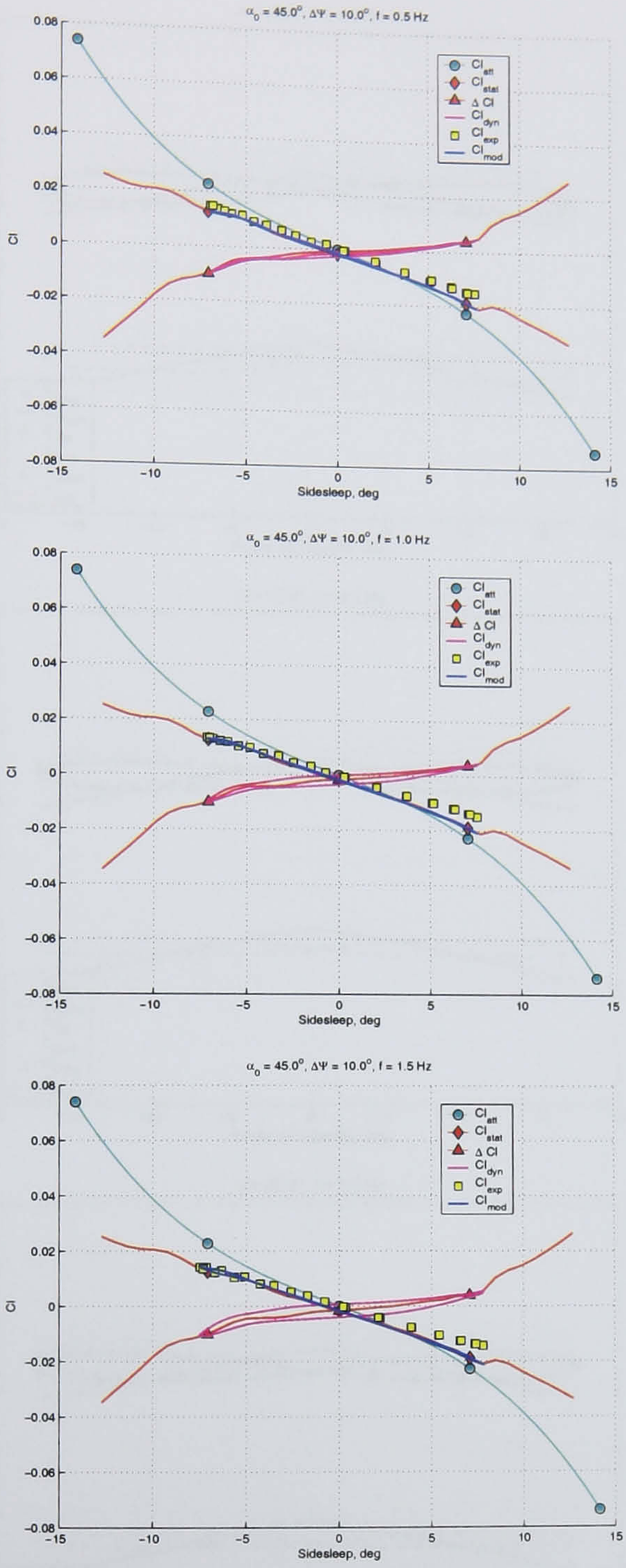

Figure E.12: Large amplitude yaw oscillations: experimental rolling moment coefficient responses in comparison with predicted by nonlinear mathematical model and other model components.

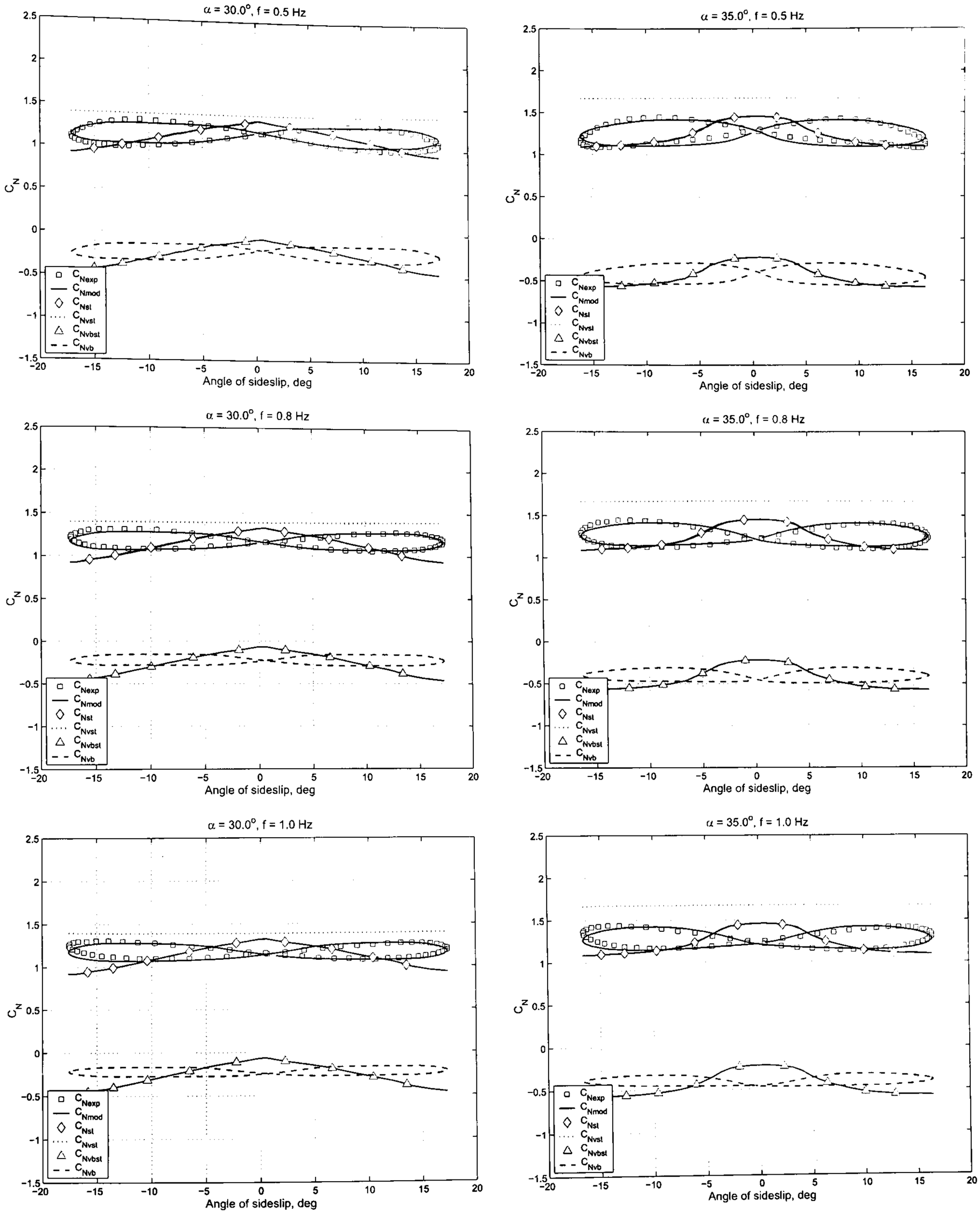

Figure E.13: Predicted and experimental responses of the normal force coefficient $C_N(\alpha, \beta)$ for the 70° delta wing at different fixed angle of attack.

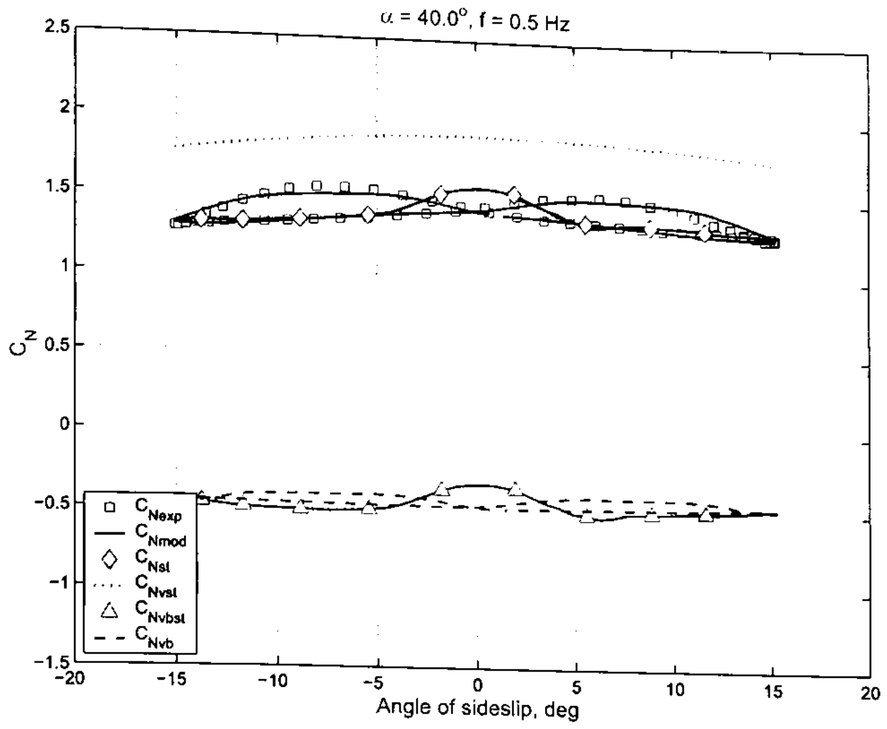

Figure E.14: Predicted and experimental responses of the normal force coefficient $C_N(\alpha, \beta)$ for the 70° delta wing at different fixed angle of attack.

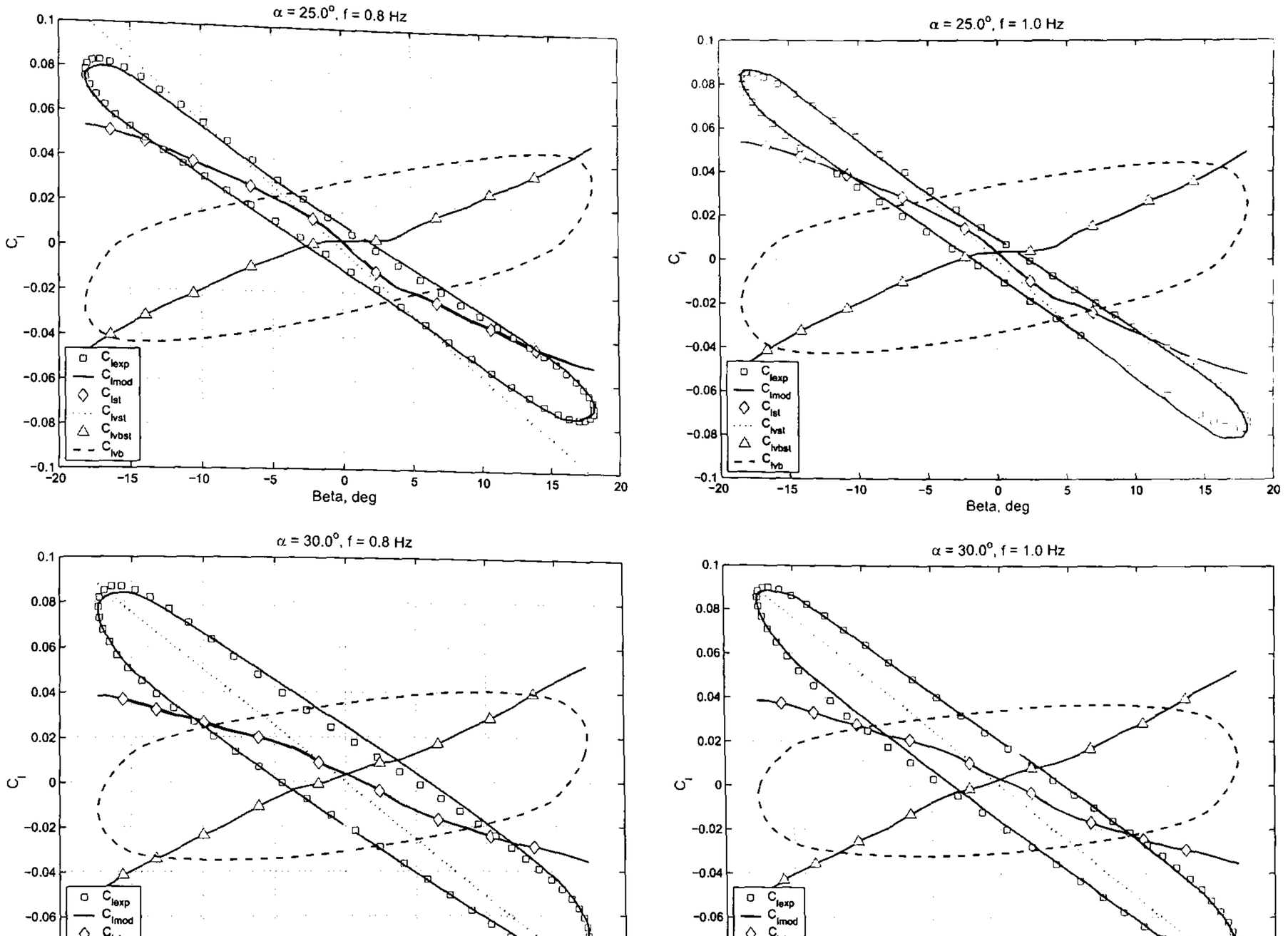

Figure E.15: Predicted and experimental responses of the rolling moment coefficient $C_l(\alpha, \beta)$ for the 70^o delta wing at different fixed angle of attack.

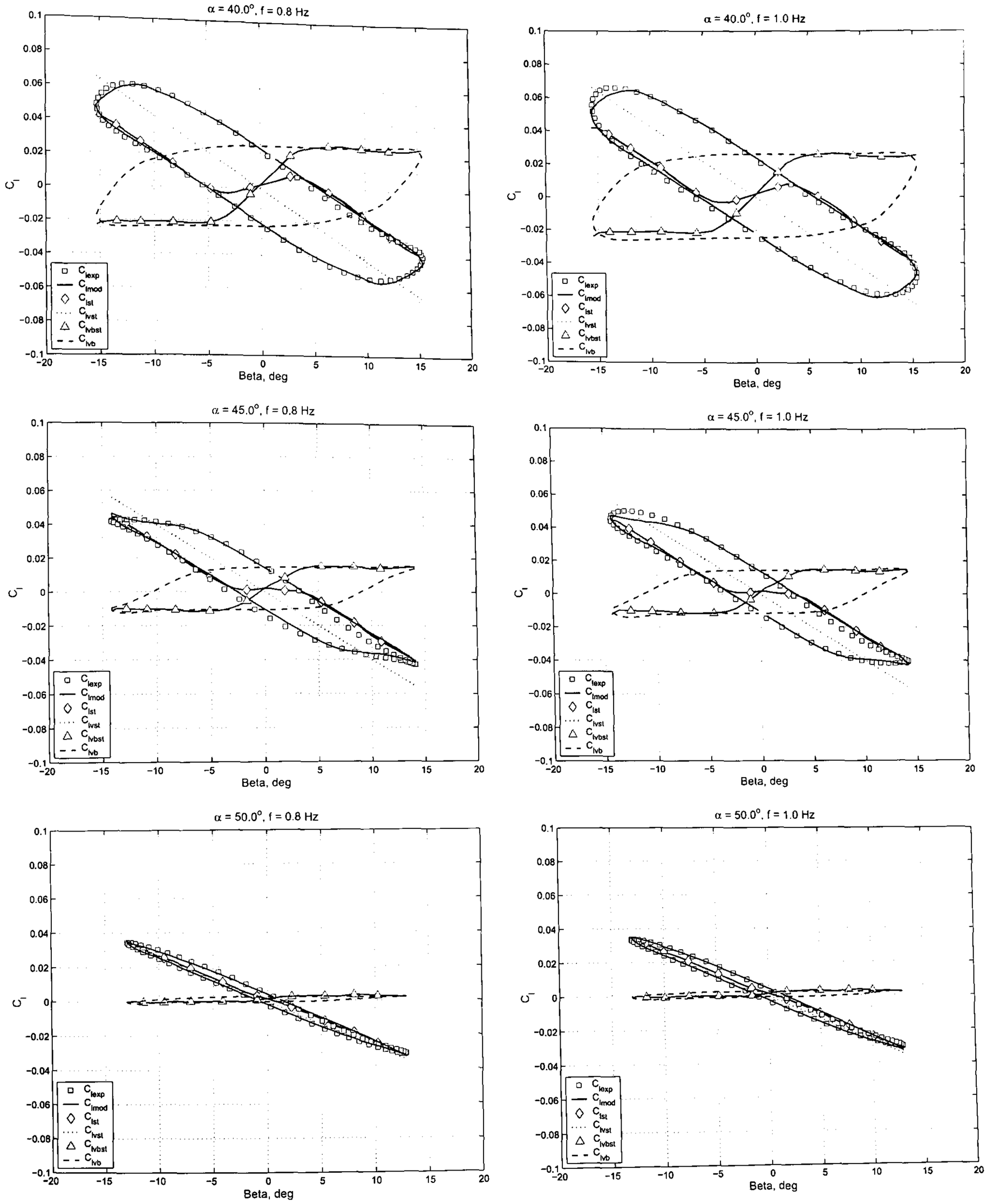

Figure E.16: Predicted and experimental responses of the rolling moment coefficient $C_l(\alpha, \beta)$ for the 70^o delta wing at different fixed angle of attack.

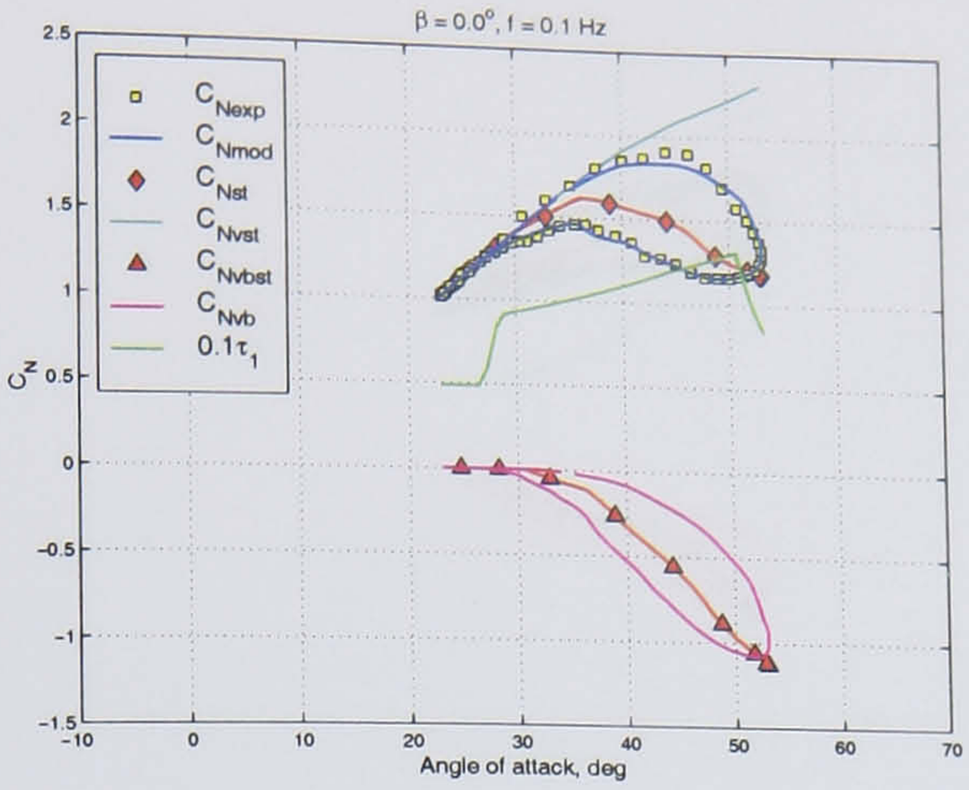

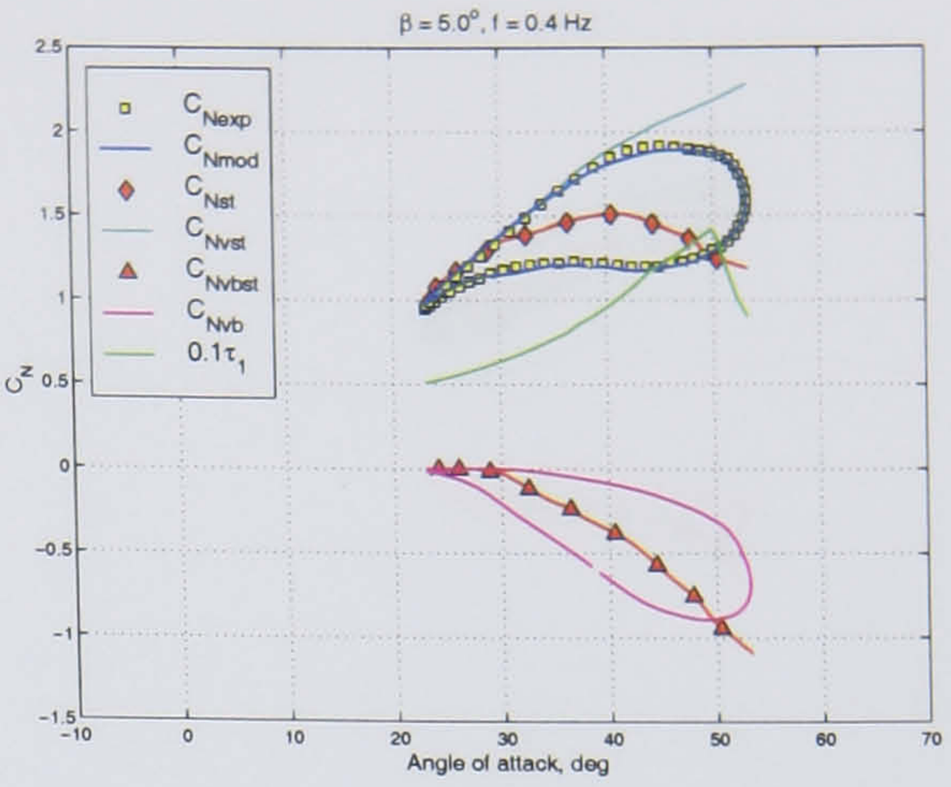

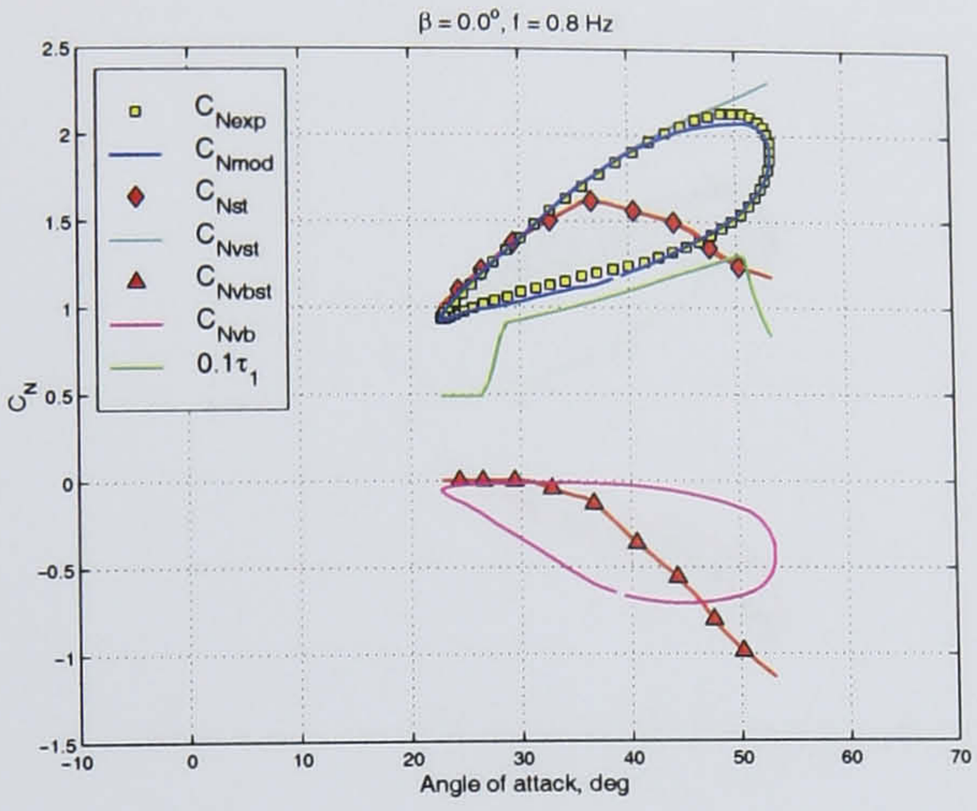

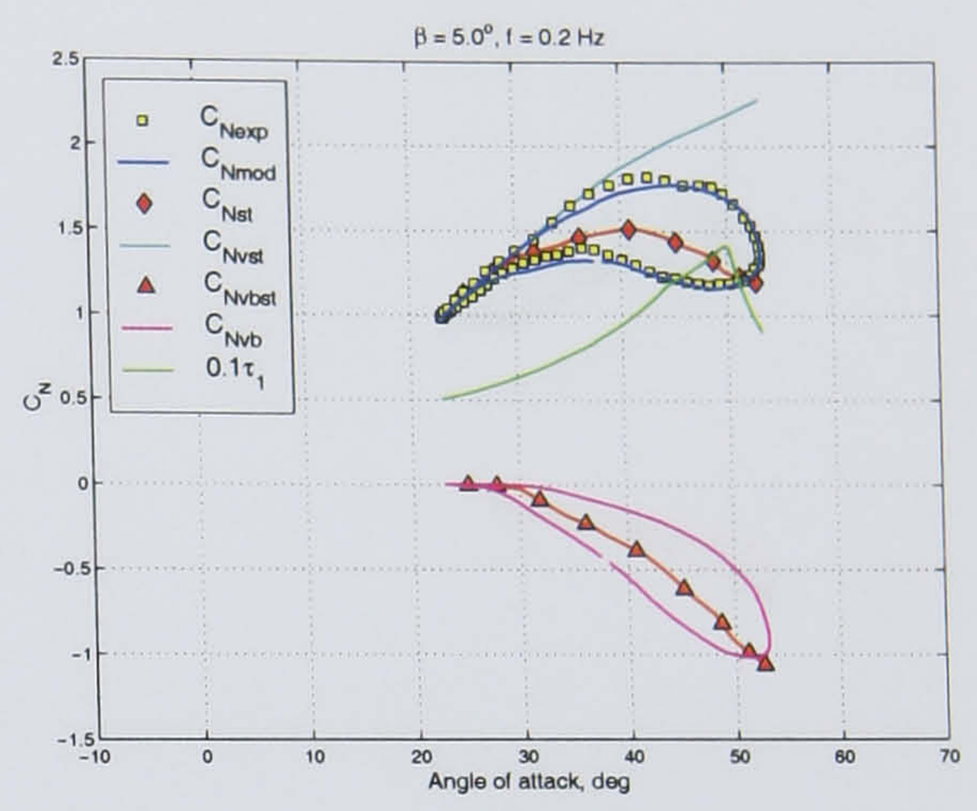

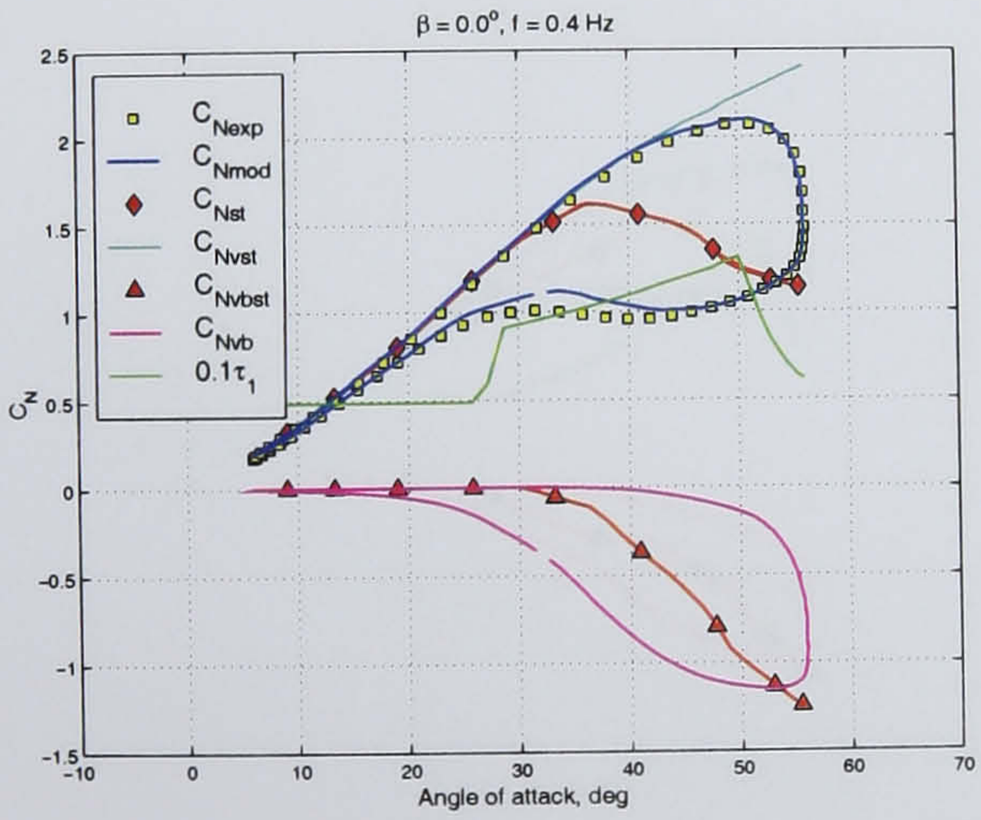

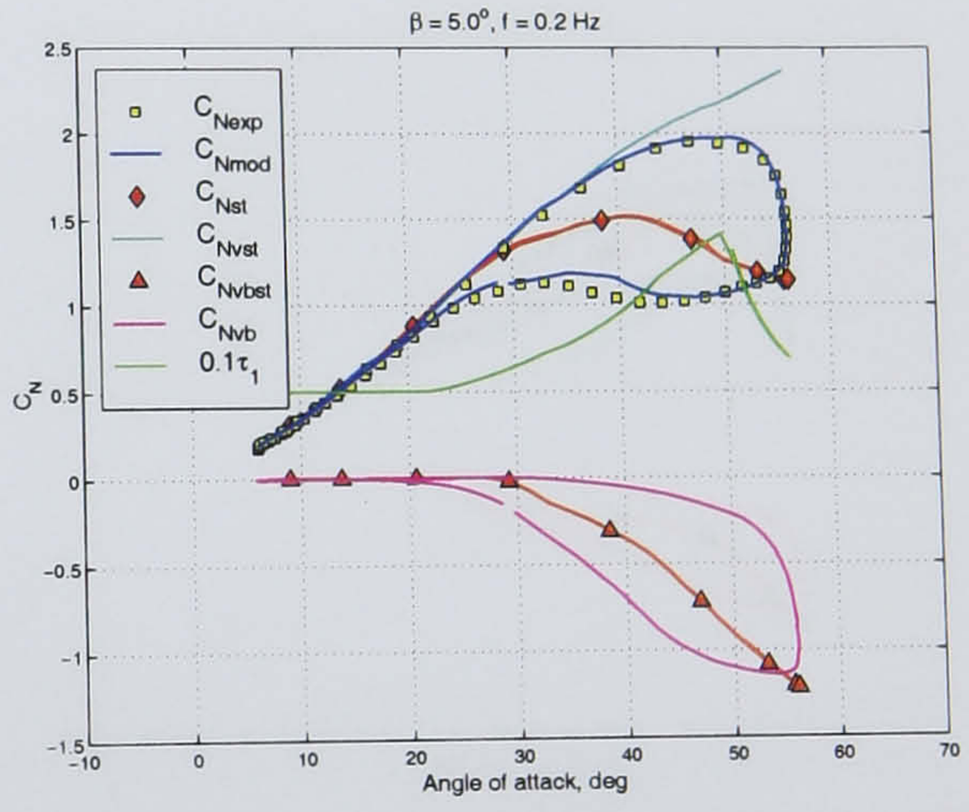

Figure E.17: Predicted and experimental responses of the normal force coefficient $C_N(\alpha, \beta)$ for the 70^o delta wing at different fixed sideslip angles.

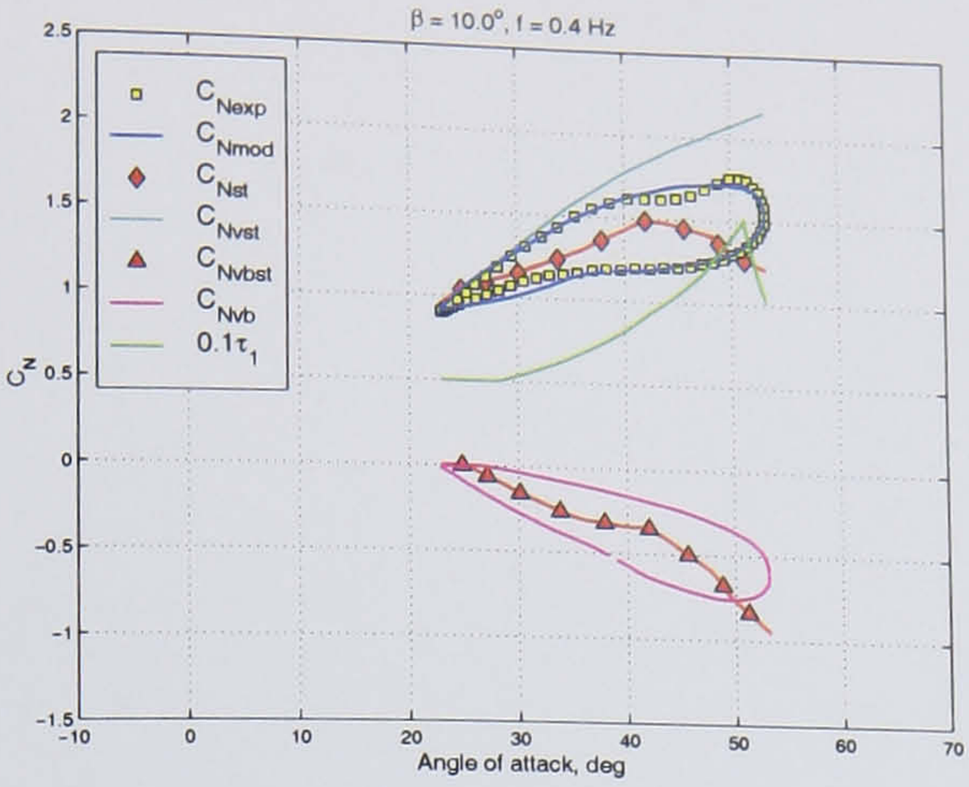

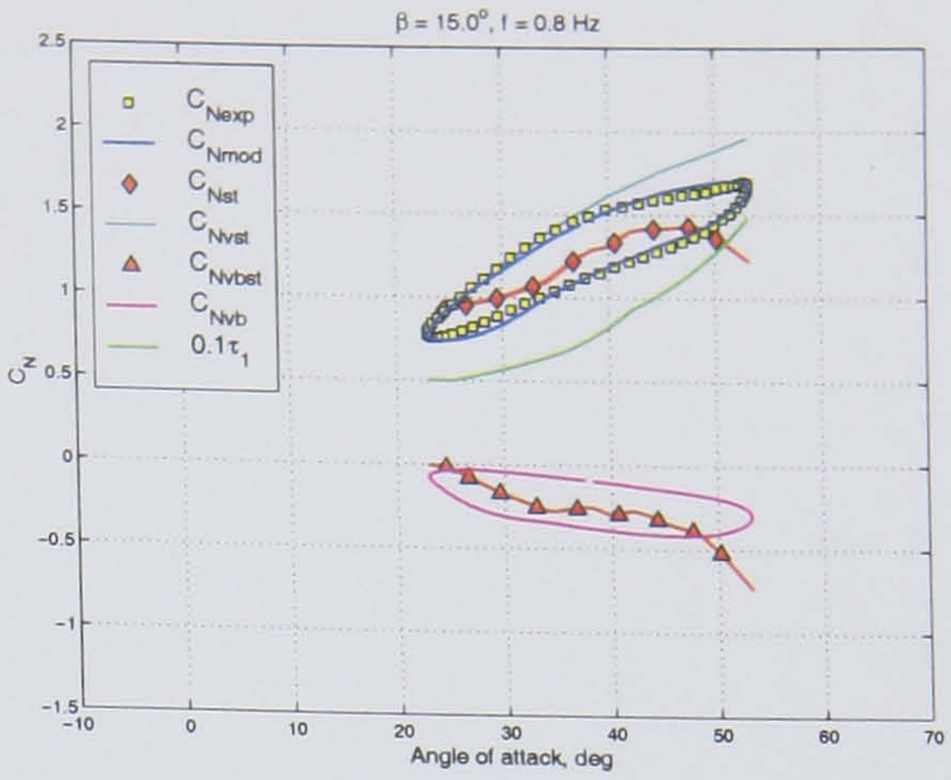

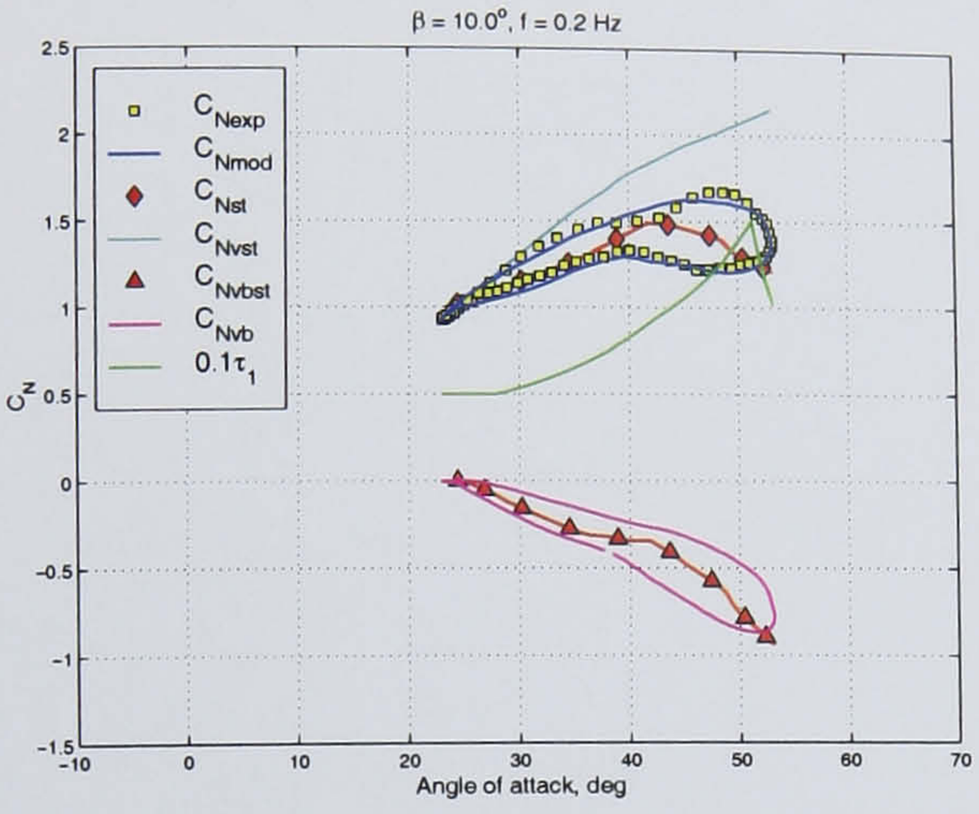

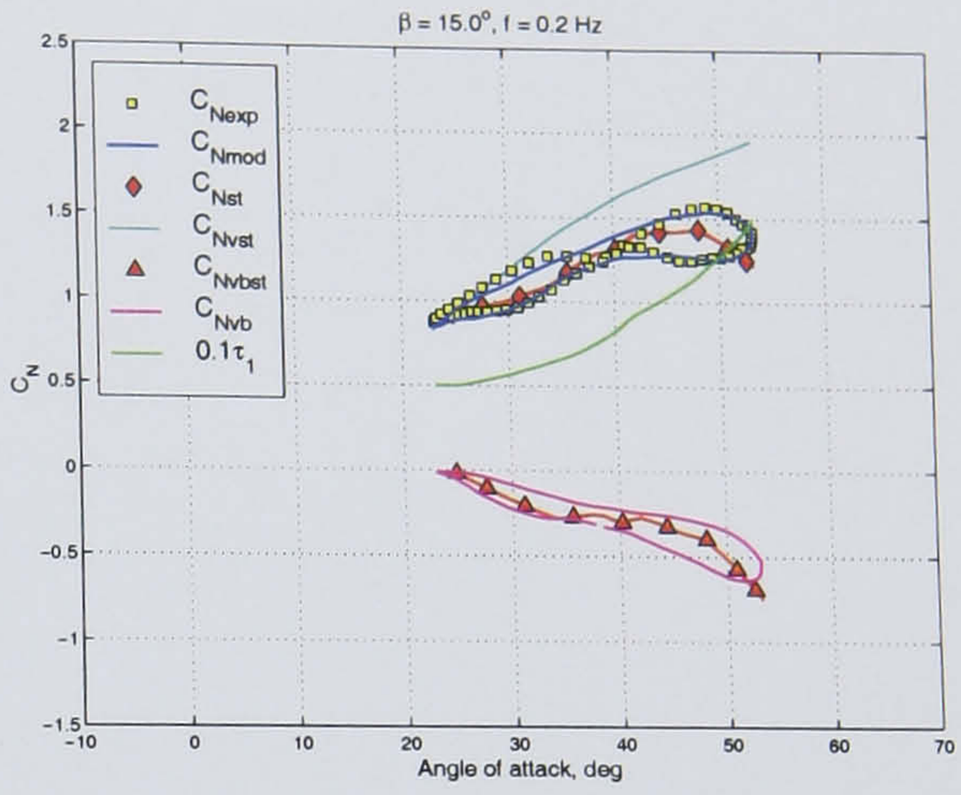

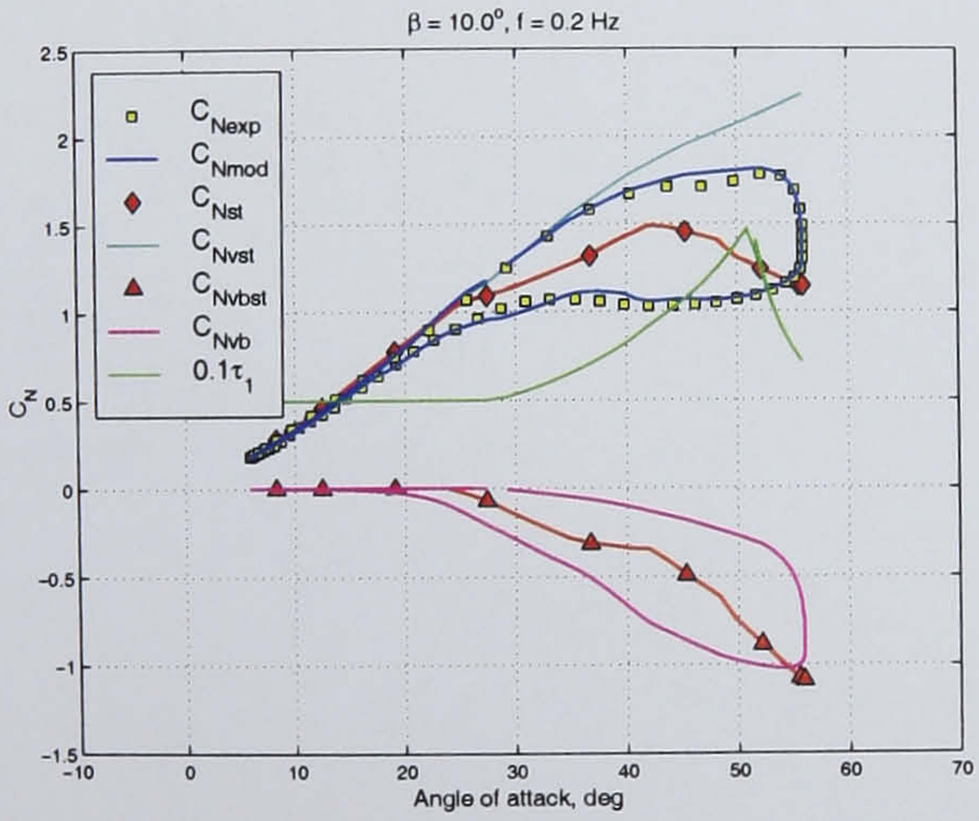

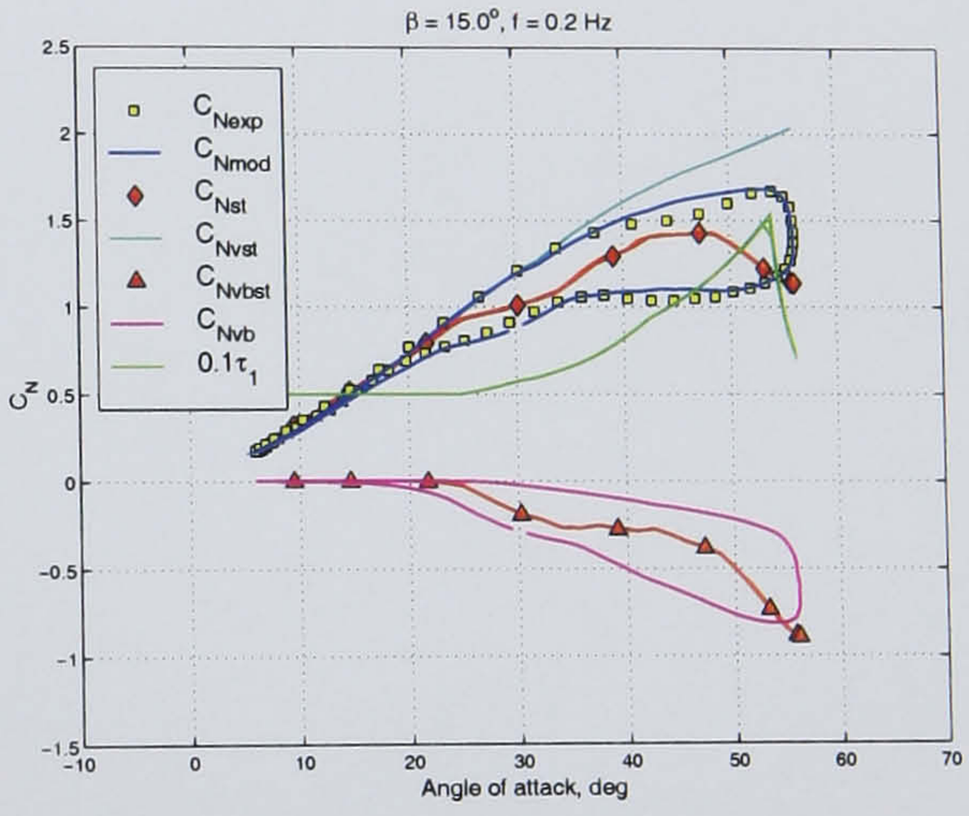

Figure E.18: Predicted and experimental responses of the normal force coefficient $C_N(\alpha, \beta)$ for the 70^o delta wing at different fixed sideslip angles.